

University of Nevada, Reno

TERNARY PHASE EQUILIBRIA OF POLYALCOHOL AND  
AMINE “PLASTIC CRYSTALS”

A DISSERTATION SUBMITTED IN PARTIAL FULFILLMENT OF THE  
REQUIREMENTS FOR THE DEGREE OF DOCTOR OF PHILOSOPHY IN

Materials Science and Engineering

by

Amrita Mishra

Dr. Dhanesh Chandra / Dissertation Advisor

December, 2011



University of Nevada, Reno  
Statewide • Worldwide

THE GRADUATE SCHOOL

We recommend that the dissertation  
prepared under our supervision by

**AMRITA MISHRA**

entitled

**Ternary Phase Equilibria of Polyalcohol and Amine "Plastic Crystals"**

be accepted in partial fulfillment of the  
requirements for the degree of

**DOCTOR OF PHILOSOPHY**

Dr. Dhanesh Chandra, Advisor

Dr. Jeffrey Lacombe, Committee Member

Dr. Qizhen Li, Committee Member

Dr. Wen-Ming Chien, Committee Member

Dr. Jaak Daemen, Graduate School Representative

Marsha H. Read, Ph. D., Associate Dean, Graduate School

December, 2011

# Abstract

Solid-solid phase change materials are considered to be potential candidates for thermal energy storage (TES). Amongst the solid-solid heat storage materials, the most promising heat storage materials are organic polyalcohol globular molecular crystals (with orientational disorder in the energy storing phase). Studies on CALPHAD modeling of binary and ternary phase diagrams of these organic plastic crystals are limited, in fact to our knowledge, there are no *ternary* phase diagram reported in the literature for these systems, leading to the motivation for the this study. Binary systems of organic plastic crystals have been analyzed to lower or adjust the transition temperature for thermal energy storage applications. In this study, binary phase diagrams of 6 systems (PE-PG, PG-NPG, PE-NPG, PE-AMPL, PG-AMPL, NPG-AMPL) were first modeled to determine interaction parameters; in effect self consistent data base used to generate 4 ternary phase diagrams (PE-PG-NPG, PE-NPG-AMPL, PG-NPG-AMPL, PE-PG-AMPL). Several isothermal sections were developed, and isopleths were generated for each of the above four system; these isopleths are key to understanding the nature of phase transitions. The solution phases are modeled as substitutional solution model, in which the excess Gibbs energies are expressed by the Redlich-Kister-Muggianu polynomial. Experimental data from literature has been used for optimization of the *binary* phase diagrams to calculate the excess Gibbs energy parameters. The phase diagrams are calculated from room temperature to the liquid phase. A set of self consistent thermodynamic parameters formulating the Gibbs

energies of various phases in the ternary systems are obtained in the present work. Activities and enthalpies of mixing for the binary systems are calculated from the excess Gibbs energy parameters. Activities for ternary phase diagrams are extrapolated from the binary data by the application of Krupkowski's formalism. In this dissertation, the above mentioned six binaries and four ternaries along with their isopleths are presented. The results of these studies allowed us to better understand the complex phase transition mechanisms and gave us more latitude for adjustment of phase transition temperatures.

---

PE- Pentaerythritol ( $C_5H_{12}O_4$ ), PG- Pentaglycerine ( $C_5H_{12}O_3$ ),

NPG- Neopentylglycol ( $C_5H_{12}O_2$ ), AMPL - 2 amino,2 methyl, 1,3 propanediol ( $C_5H_{11}O_2N$ )

## Acknowledgements

First of all I would like to thank Dr. Dhanesh Chandra for the guidance and support he has afforded me throughout the period of my Doctoral degree. He has been a constant source of encouragement and I am grateful to him for the time he spent with me.

I would like to thank Dr. Wen-Ming Chien and Dr. Anjali Talekar for giving me for being infinitely patient while answering numerous questions.

I am thankful to my advisory committee members for the motivation and guidance for my research work. Without their guidance this dissertation would not have been complete. Their kind attention and suggestions helped me a lot in improving this dissertation.

Thank you to all the staff members of the Department of Chemical and Materials Engineering for their help. Thank you to all my group members for their unwavering support and friendship which has made my time at UNR wonderful and unforgettable.

Finally, I would like to thank my family and dear ones for their love and support and for being with me through everything. Their efforts have made me what I am today. I thank them for everything.

## Table of Contents

Abstract.....	i
Acknowledgement.....	iii
Table of Contents.....	iv
List of Figures.....	vii
List of Tables.....	xi
1. Chapter I Introduction.....	1
1.1. Energy storage methods.....	2
1.1.1. Sensible heat storage.....	2
1.1.2. Latent heat storage.....	3
1.1.3. Thermochemical energy storage.....	4
1.2. Latent heat storage materials.....	6
1.3. Types of Phase Change Materials.....	7
1.4. Organic Plastic Crystals.....	12
1.4.1. Pentaerythritol (PE).....	16
1.4.2. Pentaglycerine (PG).....	19
1.4.3. Neopentylglycol (NPG).....	21
1.4.4. 2-Amino-2-Methyl-1,3-Propanediol (AMPL).....	23
1.5. Binary phase diagrams of polyalcohols.....	27
1.5.1. Pentaerythritol (PE)-neopentylglycol (NPG) binary phase diagram.....	28
1.5.2. 2-amino,2-methyl-1,3-propanediol (AMPL)-neopentylglycol (NPG) binary phase diagram.....	33
1.5.3. PG-AMPL binary phase diagram.....	36
1.5.4. Pentaglycerine (PG)-Pentaerythritol (PE) Phase Diagram.....	39
1.5.5. Pentaglycerine (PG)-Neopentylglycol (NPG) Phase Diagram.....	43
2. Chapter II CALPHAD Modeling.....	51

2.1.	Determination of the coefficients.....	57
2.2.	Higher component systems.....	57
2.3.	Improved Capabilities.....	58
2.4.	Computer software tools and databases.....	62
2.4.1.	The Lukas program.....	62
2.4.2.	Thermo-Calc.....	64
2.4.3.	Modules in Thermo-Calc.....	66
2.5.	Assessment Technique.....	67
2.5.1.	Literature search.....	68
2.5.2.	Analysis of experimental data.....	68
2.6.	The PARROT program.....	70
2.6.1.	The use of PARROT.....	71
2.6.2.	The POP file.....	73
2.7.	Thermodynamic Models for Solution Phases.....	73
2.7.1.	Stoichiometric compounds.....	74
2.7.2.	Random Substitutional Models.....	75
2.7.3.	Simple mixtures.....	75
2.7.3.1.	Dilute solutions.....	75
2.7.3.2.	Ideal solutions.....	76
2.7.3.3.	Non-ideal solutions; regular and non-regular solution models.....	78
2.8.	The extrapolation of Gibbs excess energy to multi-component systems.....	80
2.9.	References.....	82
3.	Chapter III (Results and discussion-Part I) Ternary phase diagram calculations of pentaerythritol(PE)-pentaglycerine(PG)-neopentylglycol(NPG) system.....	83
	Summary.....	83

3.1.	Introduction.....	84
3.2.	Experimental data from literature.....	87
3.2.1.	Thermodynamic properties of pure PE, PG and NPG.....	87
3.2.2.	Binary Phase Diagram Data.....	87
3.3.	Thermodynamic Modeling.....	88
3.4.	Optimization of Binary Phase Diagrams.....	95
3.5.	Results and Discussion.....	97
3.6.	Conclusions.....	112
3.7.	References.....	113
4.	Chapter IV (Results and discussion-Part II) Thermodynamic assessment of pentaerythritol-neopentylglycol-2-amino-2methyl-1,3,propanediol (PE-NPG-AMPL) ternary phase diagram.....	115
	Summary.....	115
4.1.	Introduction.....	115
4.2.	Computational Procedure.....	119
4.2.1.	Calculation of thermodynamic properties.....	120
4.2.2.	Thermodynamic Modeling of Solution Phases.....	121
4.2.3.	Metastable Phase Calculations.....	125
4.3.	Experimental Data.....	128
4.3.1.	Phase Equilibria.....	128
4.3.2.	AMPL-NPG binary phase diagram.....	129
4.3.3.	PE-AMPL binary phase diagram.....	129
4.3.4.	PE-NPG binary phase diagram.....	130
4.4.	Results and Discussion.....	131
4.4.1.	Thermodynamic Analysis.....	131
4.4.2.	AMPL-NPG binary system.....	131

4.4.3. PE–AMPL binary system.....	135
4.4.4. PE–NPG binary system.....	140
4.4.5. Ternary PE-NPG-AMPL.....	144
4.4.6. Activity Calculations.....	150
4.5. Conclusions.....	152
4.6. References.....	154
5. Chapter V (Results and discussion-Part III) Phase diagram calculations of pentaglycerine-neopentylglycol-2-amino-2methyl-1,3, propanediol (PG-NPG-AMPL) ternary system.....	157
5.1. Computational Procedure.....	158
5.1.1. Thermodynamic Modeling of Solution Phases.....	158
5.1.2. Metastable Phase Calculations.....	161
5.2. PG-AMPL binary phase diagram.....	162
5.3. AMPL-NPG binary phase diagram.....	165
5.4. PG-NPG binary phase diagram.....	165
5.5. PG-NPG-AMPL ternary phase diagram.....	166
5.6. References.....	171
6. Chapter VI (Results and discussion-Part IV) The equilibrium phase diagram of the pentaerythritol-pentaglycerine-2-amino-2methyl-1,3,propanediol(PE-PG-AMPL) system.....	172
6.1. Computational Procedure.....	172
6.1.1. Thermodynamic Modeling of Solution Phases.....	172
6.1.2. Metastable Phase Calculations.....	175
6.2. Experimental Data.....	176
6.2.1. Phase Equilibria.....	176
6.3. PE-PG-AMPL ternary phase diagram.....	177

6.4. References.....184

7. Conclusions.....187

## List of Figures

Figure 1-1	Different types of thermal storage of solar energy [3] .....	3
Figure 1-2	Classification of PCMs [3] .....	8
Figure 1-3	Comparison of energy densities per unit mass (a) and energy densities per unit volume (b) of solid-solid, solid-liquid and solid-gas systems [13].....	11
Figure 1-4	Hydrogen bonds in the binary system of NPG/PE after PE is added into NPG [42].....	15
Figure 1-5	(001) Layer of the crystal structure of pentaerythritol at ambient conditions space group I-4). (Grey circles, large black circles and small black circles represent carbon, oxygen and hydrogen, respectively. The dashed lines represent the intra-layer hydrogen bonds.) [48].....	17
Figure 1-6	Crystal structure of the low temperature phase of pentaerythritol [50].....	18
Figure 1-7	Molecular structure of pentaglycerine.....	20
Figure 1-8	Molecular structure of NPG.....	22
Figure 1-9	The molecule of AMPL [C <sub>4</sub> H <sub>11</sub> NO <sub>3</sub> ] with non-hydrogen atoms represented by thermal vibration ellipsoids drawn to encompass 50% of their electron density; hydrogen atoms are represented by arbitrarily small spheres. [64].....	26
Figure 1-10	Orientation of O—H and N—H bonded molecules in the unit cell of AMPL[65].....	27
Figure 1-11	Experimental phase diagram of PE-NPG system by Tesseire et al.[72]....	31
Figure 1-12	Experimental PE-NPG phase diagram by Barrio et al. [59].....	32
Figure 1-13	AMPL-NPG binary phase diagram by Barrio et al. [66].....	35
Figure 1-14	AMPL-NPG binary phase diagram by Salud et al. [73].....	37
Figure 1-15	PG-AMPL binary phase diagram reported by Salud et al. [68].....	40
Figure 1-16	PE-PG experimental phase diagram [79].....	42

Figure 1-17	PG-NPG experimental phase diagram [86].....	46
Figure 2-1	Different assessments of the Al-Ni system showing the progress made with the CALPHAD method: (2a) a 1978 assessment by Kaufman and Nesor, [20] (2b) a 1988 assessment by Ansara et al. [11] (2c) a 1997 assessment by Ansara et al. [12] and (2d) the evaluated experimental diagram [21].....	60
Figure 2-2	Schematic of CALPHAD assessment methodology [35].....	70
Figure 2-3.	Geometrical constructions of (a) Muggianu, (b) Kohler and (c) Toop models.....	82
Figure 3-1	Molecular structures of PE, PG and NPG.....	86
Figure 3-2	Calculated PE-PG phase diagram from this study (data points from Barrio et al. [37]).....	99
Figure 3-3.	Calculated PE-NPG phase diagram from this study (data points from Chandra et al. [18, 35]).....	101
Figure 3-4.	Calculated PG-NPG phase diagram from this study (data points from Barrio et al. [36]).....	103
Figure 3-5	Enthalpy of mixing of (a) PG-NPG and (b) PE-NPG liquid at 450K (calculated, this work).....	105
Figure 3-6	Activity of (a) PE and NPG in PE-NPG liquid and, (b) PG and NPG in PG-NPG liquid at 440K (calculated, this work) .....	106
Figure 3-7	Binary phases projecting into PE-PG-NPG ternary. Two-phase regions are shown hatched by tie-lines (green in color); Red (in color) lines represent invariant equilibria.....	108
Figure 3-8	Isotherms for ternary PE-PG-NPG (a) 313K, (b) 333K, (c) 353K, (d) 380K, (e), 413K, (f) 450K, (g) 463K, (h) 480K and (i) 513K.....	109
Figure 3-9.	Isopleths along the line on the PE-PG-NPG isotherm at 413K.....	110
Figure 4-1	Structure of PE, NPG and AMPL.....	118
Figure 4-2	Optimized binary phase diagram of AMPL-NPG.....	134
Figure 4-3	Activities of AMPL and NPG at 340K.....	136
Figure 4-4a	Binary phase diagram of PE-AMPL (optimized).....	138

Figure 4-4b	Activities of PE and AMPL at 340K.....	140
Figure 4-5a	Optimized binary phase diagram for PE-NPG system.....	143
Figure 4-5b	Activities of PE and NPG at 340K.....	144
Figure 4-5c	Binary phases projecting on to ternary isotherm at 400K.....	146
Figure 4-6	Isotherms for PE-NPG-AMPL ternary system.....	148
Figure 4-7	Isopleths at 0.5AMPL/0.5PE-NPG and 0.2AMPL/0.8PE-NPG and isotherm at 300K.....	149
Figure5-1	PG-AMPL phase diagram (optimized).....	165
Figure 5-2	AMPL-NPG binary system (calculated, this work).....	166
Figure 5-3	PG-NPG phase diagram.....	167
Figure 5-4	Binary phases projecting on to ternary (PG-NPG-AMPL) phase diagram.....	169
Figure 5-5	Isotherms of PG-NPG-AMPL over a temperature range showing phase transitions from room temperature to liquid phase.....	170
Figure 5-6	Isopleths of PG-NPG-AMPL and an isotherm at 300K.....	171
Figure 6-1	PE-PG-AMPL isotherms at 335K and 340K.....	181
Figure 6-2	PE-PG-AMPL isotherms at 360K and 415K.....	182
Figure 6-3	PE-PG-AMPL isotherms at 430K and 450K.....	183
Figure 6-4	PE-PG-AMPL isopleths and an isotherm at 390K.....	184

## List of Tables

Table 1-1	Lattice Parameters of Pure PG and PE at Elevated Temperatures Along with Lattice Expansions [51].....	21
Table 1-2	Lattice Parameters for NPG [51].....	22
Table 1-3	Bond Lengths of non-Hydrogen Atoms in AMPL [64].....	24
Table 1-4	Lattice parameters and the volume occupied by the average molecule for the pure substances as a function of the mole fraction of NPG [71].....	33
Table 1-5	Characteristic temperatures and corresponding mole fractions of the invariant points in the NPG/AMP phase diagram [71].....	34
Table 1-6	Comparison between Experimental (E) and Calculated (C) Invariant Equilibria .....	39
Table 3-1	Crystal structure, transition temperatures and thermal properties of NPG, AMPL and PE [14].....	88
Table 3-2	List of symbols to denote the phases in the ternary PE-PG-NPG system.....	90
Table 3-3	Expressions of Gibbs energy equations for PE-PG-NPG ternary system.....	95
Table 3-4	Invariant equilibria for PE-NPG binary system (this work).....	102
Table 3-5	Phase transitions in PE-PG-NPG system.....	112
Table 4-1	List of symbols denoting phases in PE-NPG-AMPL system.....	123
Table 4-2	Crystal structure, transition temperatures and thermal properties of NPG, AMPL and PE [42].....	129
Table 4-3	Expressions for Gibbs energies of pure components (NPG-AMPL).....	133
Table 4-4	Comparison of calculated and experimental invariant equilibria.....	135
Table 4-5	Experimental invariant equilibria.....	137
Table 4-6	Expressions for Gibbs energies of pure components (PE -AMPL).....	139
Table 4-7	Expressions for Gibbs energies of pure components (PE-NPG).....	142

Table 4-8	Phase transitions occurring in the PE-NPG-AMPL ternary system.....	150
Table 4-9	Activity of PE (at 0.06 $X_{PE}$ ) at 460, 500 and 640K.....	153
Table 5-1	List of symbols for PG-NPG-AMPL ternary system.....	159
Table 5-2	Gibbs energy expressions for PG-NPG-AMPL.....	168
Table 5-3	Phase transitions in PG-NPG-AMPL system.....	172
Table 6-1	List of symbols for denoting phases in PE-PG-AMPL system.....	174
Table 6-2	Crystal structure, transition temperatures and thermal properties of PG, AMPL and PE [8].....	179
Table 6-3	Gibbs energy expressions for PE-PG-AMPL system.....	180
Table 6-4	Phase transitions in PE-PG-AMPL.....	185

## Chapter I ∞ Introduction

---

Due to increasing global energy demands, and depletion of available energy resources, the need for alternate energy solutions has become an imminent necessity. Possible options are solar, wind, nuclear, geothermal, tidal, and hydrogen energy. Direct solar energy radiation is considered to be one of the most potential sources of energy. Since solar energy is available only during the day, its application involves effective thermal energy storage, so that the excess heat accumulated can be stored for use at night. Heat recovery systems have the same problem, where the surplus heat availability and consumption periods are different, which necessitates thermal energy storage. Additionally, electrical energy consumption fluctuates considerably during the day, especially in extreme climates, where most of the variation is used to space heating and air conditioning. This variation leads to periods of uneven power distributions. Power stations have to be designed with very efficient power distribution system. This can be achieved if some of the load during peak hours can be shifted to off peak hours. This can be achieved by thermal storage. Hence, the successful application of load distribution depends on the method of storage used.

The storage of energy in forms, which can be converted to the required form, poses a present day challenge to scientists. Besides reducing mismatch between supply and demand, it also improves energy system performance and plays an important role in conserving energy [1]. One technique for storing thermal energy is the application of phase change materials (PCMs).

## **1.1. Energy storage methods**

Different forms of energy that can be stored include mechanical, electrical and thermal energy [2].

Mechanical energy storage involves gravitational energy storage or pumped hydropower storage (PHPS), compressed air energy storage (CAES) and flywheels. The PHPS and CAES technologies can be used for large scale energy storage while flywheels are more suitable for intermediate storage. Storage is carried out when inexpensive off-peak power is available, e.g., at night or weekends. Stored power is discharged when power is needed.

Electrical energy is stored using batteries. The battery is charged by connecting a source of electric current, and releases the energy when discharged. Batteries are potentially applicable for utilization of off-peak power, load leveling and photovoltaic plants.

Thermal energy storage can be stored as a change in internal energy of a material as sensible heat, latent heat and thermochemical or combination of these. An overview of major technique of storage of solar thermal energy is shown in figure 1-1 [3].

### ***1.1.1. Sensible heat storage***

Thermal energy is stored in sensible heat storage materials by increasing the temperature of a solid or liquid. These materials use the heat capacity and temperature difference while charging and discharging. The amount of heat stored depends on the heat capacity, temperature change and the quantity of storage materials [4].

$$Q = \int_{T_i}^{T_f} mC_p dT$$

$$= mC_p(T_f - T_i)$$

Water is considered as the best sensible heat storage material as it is inexpensive and has a high specific heat. Although, molten salts and liquid metals, etc. are used at high temperatures (100°C).

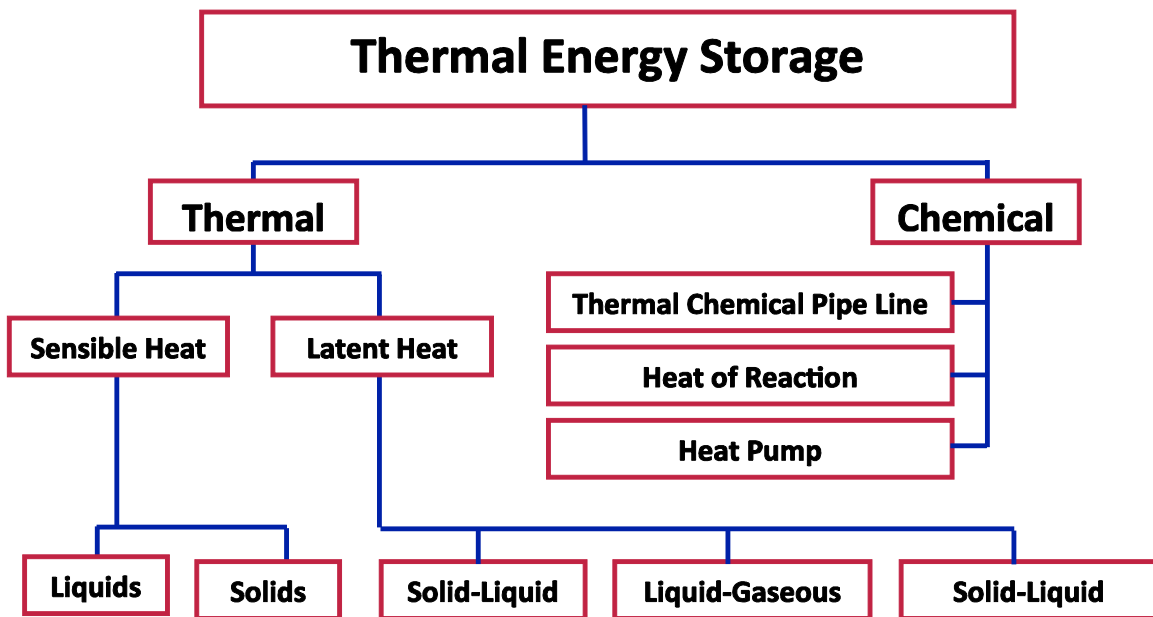


Figure 1-1 Different types of thermal storage of solar energy [3].

### 1.1.2. Latent heat storage

Latent heat storage is based on the principle of heat release or absorption when the material undergoes a phase change (solid-liquid/liquid-gas). The storage capacity of latent heat storage system with a PCM medium [5] is given by

$$Q = \int_{T_i}^{T_m} mC_p dT + ma_m \Delta h_m + \int_{T_m}^{T_f} mC_p dT$$

$$Q = m[C_{sp}(T_m - T_i) + a_m \Delta h_m + C_{lp}(T_f - T_m)]$$

### 1.1.3. Thermochemical energy storage

Thermochemical systems rely on the energy absorbed and released in breaking and reforming molecular bonds in a completely reversible chemical reaction. In this case, the heat stored depends on the amount of storage material, the endothermic heat of reaction, and the extent of conversion.

$$Q = a_r m \Delta h_r$$

Amongst all the above mentioned heat storage methods, latent heat storage is the most attractive due to its high-energy storage density and its capability to store heat at constant temperature equivalent to the phase transition temperature of materials. Phase change can be described as a material undergoing phase transformation from solid-solid, solid-liquid, solid-gas, liquid-gas and vice-versa. In solid-solid phase transitions, heat is stored as the material transforms from one crystalline phase to another. Solid-solid phase transitions have small latent heat and small volume changes, as compared to solid-liquid transitions. These phase change materials are advantageous because of the need of less severe container requirements and greater design flexibility [6]. Most of the solid-solid phase change materials are organic solid solutions of pentaerythritol with a melting point of 188°C, and latent heat of fusion 323kJ/kg. Other examples belonging to this class of materials are pentaglycerine, Li<sub>2</sub>SO<sub>4</sub>, etc.

The most promising materials are organic solid solutions of pentaerythritol (m.p. 188 8C, latent heat of fusion 323 kJ/kg), pentaglycerine (m.p. 81 8C, latent heat of fusion 216

kJ/kg),  $\text{Li}_2\text{SO}_4$  (m.p. 578, latent heat of fusion 214 kJ/kg) and  $\text{KHF}_2$  (m.p. 196 °C, latent heat of fusion 135 kJ/kg) [1]. Trombe wall with these materials could provide better performance than a plain concrete Trombe wall. Solid–gas and liquid–gas transition through have higher latent heat of phase transition but their large volume changes on phase transition are associated with the containment problems and rule out their potential utility in thermal-storage systems. Large changes in volume make the system complex and impractical [7]. Solid–liquid transformations have comparatively smaller latent heat than liquid–gas. However, these transformations involve only a small change (of order of 10% or less) in volume. Solid–liquid transitions have proved to be economically attractive for use in thermal energy storage systems. PCMs themselves cannot be used as heat transfer medium. A separate heat transfer medium must be employed with heat exchanger in between to transfer energy from the source to the PCM and from PCM to the load. The heat exchanger to be used has to be designed specially, in view of the low thermal diffusivity of PCMs in general. The volume changes of the PCMs on melting would also necessitate special volume design of the containers to hold PCM. It should be able to absorb these volume changes and should also be compatible with the PCM used. Any latent heat energy storage system therefore, possess at least following three components:

- (i) a suitable PCM with its melting point in the desired temperature range,
- (ii) a suitable heat exchange surface, and
- (iii) a suitable container compatible with the PCM.

The development of a latent heat thermal energy storage system hence, involves the understanding of three essential subjects: phase change materials, containers materials and heat exchangers.

## **1.2. Latent heat storage materials**

Phase change materials (PCM) are “Latent” heat storage materials. The thermal energy transfer occurs when a material changes from solid to liquid, or liquid to solid. This is called a change in state, or “Phase.” Initially, these solid–liquid PCMs perform like conventional storage materials; their temperature rises as they absorb heat. Unlike conventional (sensible) storage materials, PCMs absorb and release heat at a nearly constant temperature. A large number of PCMs are known to melt with a heat of fusion in any required range. However, for their employment as latent heat storage materials these materials must exhibit certain desirable thermodynamic, kinetic and chemical properties. Moreover, economic considerations and easy availability of these materials has to be kept in mind. The PCMs to be used in the design of thermal-storage systems should pass desirable thermophysical, kinetics and chemical properties follows [8,9].

Selecting a PCM for a particular application, the operating temperature of the heating or cooling should be matched to the transition temperature of the PCM. The latent heat should be as high as possible, especially on a volumetric basis, to minimize the physical size of the heat store. High thermal conductivity would assist the charging and discharging of the energy storage. Phase stability during freezing melting would help towards setting heat storage and high density is desirable to allow a smaller size of

storage container. Small volume changes on phase transformation and small vapor pressure at operating temperatures reduce containment problem.

Supercooling has been a troublesome aspect of PCM development, particularly for salt hydrates. Supercooling of more than a few degrees will interfere with proper heat extraction from the store.

PCMs can suffer from degradation by loss of water of hydration, chemical decomposition or incompatibility with materials of construction. PCMs should be non-toxic, nonflammable and non-explosive. Low cost and large-scale availability of the phase change materials is also very important.

### **1.3. Types of Phase Change Materials**

A large number of phase change materials (organic, inorganic and eutectic) are available in any required temperature range. A classification of PCMs is given in figure 1-2. There are a large number of organic and inorganic chemical materials, which can be identified as PCM from the point of view melting temperature and latent heat of fusion. However, except for the melting point in the operating range, majority of phase change materials does not satisfy the criteria required for an adequate storage media as discussed earlier.

As no single material can have all the required properties for an ideal thermal-storage media, one has to use the available materials and try to make up for the poor physical property by an adequate system design. For example metallic fins can be used to increase the thermal conductivity of PCMs, supercooling may be suppressed by introducing a nucleating agent or a 'cold finger' in the storage material and incongruent melting can be inhibited by use of suitable thickness. In general inorganic compounds have almost

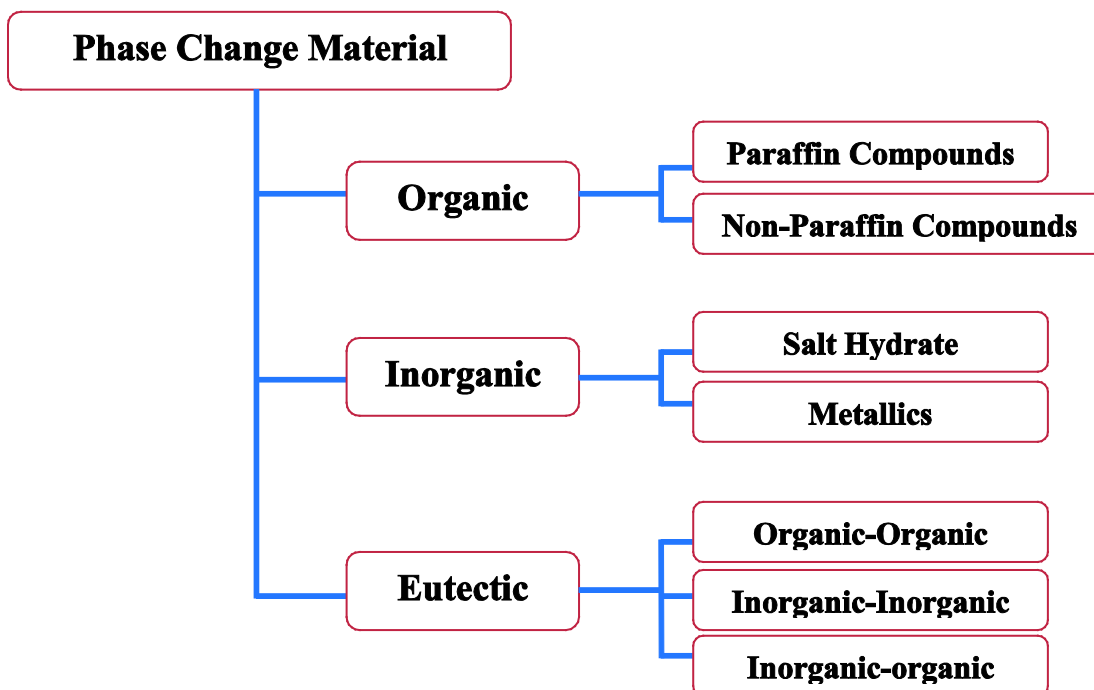


Figure 1- 2 Classification of PCMs [3]

double volumetric latent heat storage capacity (250–400 kg/dm<sup>3</sup>) than the organic compounds (128–200 kg/dm<sup>3</sup>). For their very different thermal and chemical behavior, the properties of each subgroup affect the design of latent heat thermal energy storage systems using PCMs of that subgroup.

The solid-gas phase change materials, specifically metal hydrides, have also been considered for thermal energy storage. The phase change is the absorption of hydrogen into the lattice of the metal alloy, during a reaction of the following form:  $M + H_2 \rightarrow MH_2$  generate heat during transformation [10]. Substituted  $LaNi_5 - xMx$ , where  $M = Sn, Gd$ ,

Al, or excess Ni, is a potential candidate for this type of storage medium. In a unique experimental lab configuration [11], hydrogen at pressures exceeding 150 psi is allowed to saturate the host alloy. Once the compound is depressurized the temperature of the metal can exceed 125 °C. Through a series of chambers and valves, a metal hydride heat pump can be used for —on demand— heat release. A typical enthalpy of hydrogen reaction with the alloy is -35 KJ/mol. For cold weather applications, a charged MHHP containing -220 grams of an alloy at 0 °C upon discharge will increase in temperature to 35 °C. This thermal energy storage system is being considered for space exploration situations. The obvious disadvantage to this system is pressurized hydrogen and the possibility of leakage but the metal hydride heat pump is a promising new approach to specific thermal energy needs. Other metal hydrides systems are being suggested for heating and air conditioning applications in commercial buildings. The third class of phase change materials is which undergo solid-solid phase transitions. In particular, certain class of organic molecular crystals called polyalcohols is currently being developed for thermal storage applications. These polyalcohols are currently being developed for thermal energy storage applications. Polyalcohols such as pentaerythritol, pentaglycerine, neopentylglycol, and tris exhibit crystalline transformations which reversibly absorb and emit large amounts of heat [12]. Thermal storage of latent heat occurs with the change in crystal structure at a fixed transition temperature ( $T_c$ ). The low temperature structure is a low symmetry type which transforms to a symmetric crystalline form but disordered when these crystals are heated above the transition point. The thermal energy storage capacities of the different systems are compared on a volumetric and gravimetric basis as shown in figures below. In Figure 1-3(a) energy densities per

unit mass for PCMs are plotted against their respective transition temperature. The calculated volumetric energy densities for the same materials are plotted as a function of transition temperature are shown in Figure 1-3(b) [13]. Volumetric energy densities are of significant importance for designing compact thermal energy storage systems. When compared to polyalcohols, salt hydrates or other eutectic salts, the hydrides have the highest volumetric densities.

The polyalcohols, amines, and other families of compounds have two crystallographic forms. The high temperature crystalline phases have been designated as—phase I and the low temperature phase had been designated as —phase II, by Timmermann [14], Nitta [15], and others. The early studies on thermal energy store were mainly concentrated on the structure and thermodynamic properties of pure polyalcohols. Murrill and Breed [16] evaluated the feasibility of thermal applications of selected SSPCMs on passive temperature control of satellites. With the potential for an excellent energy storage resource in mind, investigators were initiated for passive energy storage in solar buildings. Benson et al. [17] conducted studied various polyalcohols using thermal analysis methods. From the preliminary tests, they realized that in order for the polyalcohols to be effective thermal energy storage mediums the phase transition temperatures would have to be adjusted. They covered that my mixing PE-PG, PE-NPG, and PE-NPG to form solid solutions, the transition temperature could be changed.

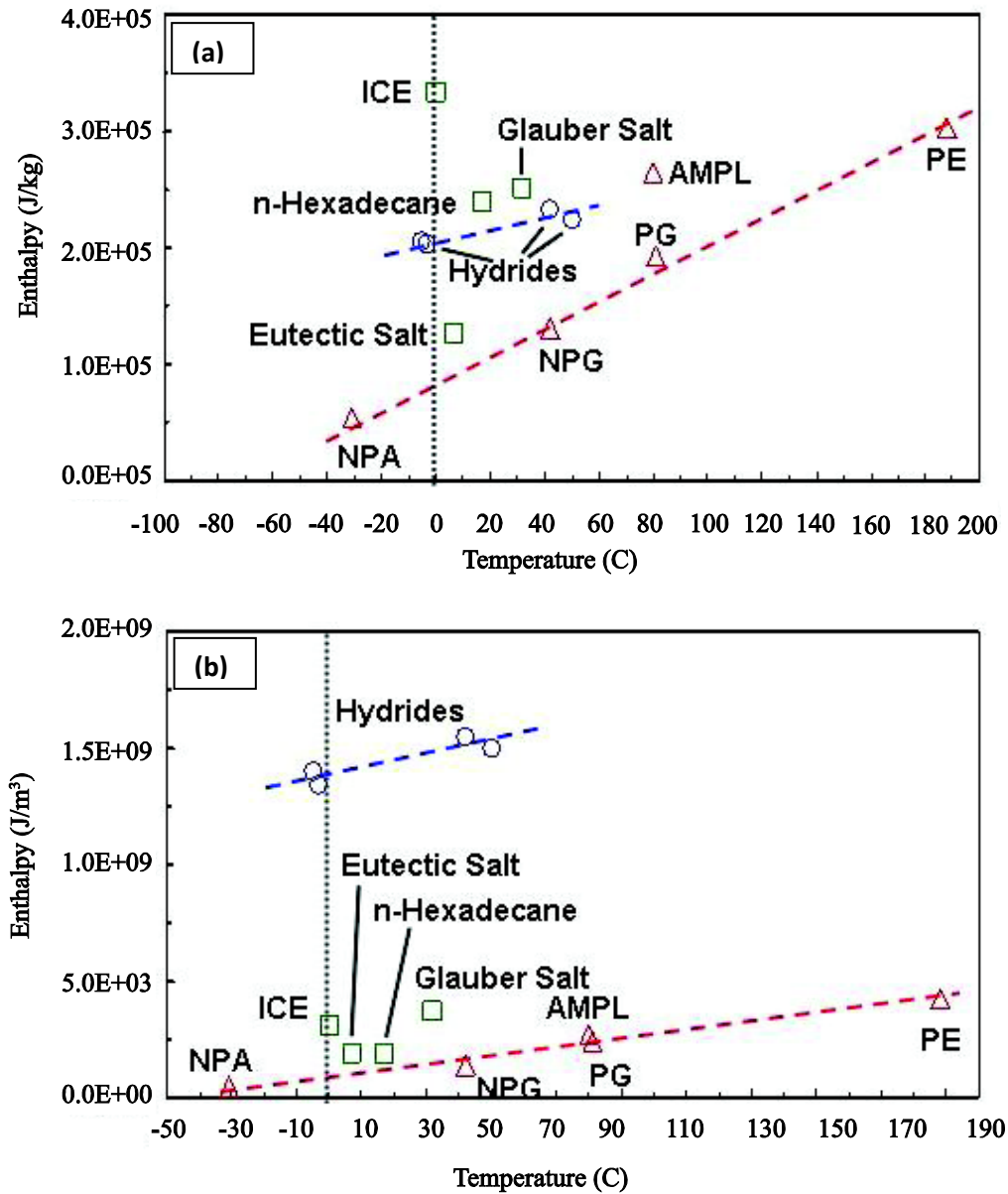


Figure 1- 3 Comparison of energy densities per unit mass (a) and energy densities per unit volume (b) of solid-solid, solid -liquid and solid- gas systems [13].

Thermal energy storage materials are becoming increasingly important as a renewable energy resource. Several types of phase change material (PCM) have been evaluated for thermal energy storage applications [18,19,20,21,22]. The solid-liquid PCM including

paraffin and salt hydrates [23,24,25] have been extensively studied and solid-gas PCM in the form of metal hydrides have also been investigated [26,27].

Solid-solid phase change materials involve a process in which some solid materials adsorb a significant amount of heat at a fixed temperature when they transform from a low symmetry crystal structure to a high symmetry one. In the process, these materials store a large amount of heat, and this heat can be removed reciprocally for use. Compared to solid-liquid phase change materials, solid-solid phase change materials have the advantages of smaller volume changes during the phase change process, no leakage problems, smaller erosion to the device and longer service life among others, although they also have the drawbacks of smaller latent heat and higher phase change temperatures which are undesirable for low temperature applications. In addition, some crystalline solids with carbon and hydrogen elements can reciprocally absorb and remove a large amount of heat when they transform from one crystal structure to another, which makes these solid-solid phase change materials potentially efficient and promising heat storage materials.

#### **1.4. Organic Plastic Crystals**

A special class of organic molecular crystals exhibits polymorphisms that are characterized by high enthalpies of solid-solid transitions and a low enthalpy of fusion. Such organic —plastic crystals are potential thermal energy storage materials that undergo solid-solid phase transitions storing a significant amount of thermal energy and can be incorporated in practical applications such as dry-wall and thrombi walls in passive solar buildings. Timmermann [28] identified this group of molecules as globular molecules. An important characteristic of these molecules is that they undergo phase

transition from a layered or chained low temperature structure (for example: tetragonal, monoclinic, orthorhombic etc.) to a disordered but isotropic high temperature cubic phase (FCC or BCC). This high temperature phase is referred to as orientationally disordered crystal (ODIC) or plastic crystal phase. Alcohol derivatives of neopentane are examples of these —plastic crystals. These materials are proposed for use in passive solar buildings, and can potentially be incorporated in building materials.

These materials are far superior as compared to conventional sensible heat storage materials.

At present, the potential solid-solid phase change materials are polyalcohols, amines, polyethylenes, layered perovskites, etc. The polyalcohols include pentaerythritol [PE:  $(\text{CH}_2\text{OH})_2\text{C}(\text{CH}_2\text{OH})_2$ ], pentaglycerine [PG:  $(\text{CH}_3)\text{C}(\text{CH}_2\text{OH})_3$ ], neopentylglycol [NPG:  $(\text{CH}_3)_2\text{C}(\text{CH}_2\text{OH})_2$ ], and neopentylalcohol [NPA:  $(\text{CH}_3)_3\text{C}(\text{CH}_2\text{OH})$ ]. Examples of amine derivatives include 2-amino-2-methyl-1,3-propanediol [AMPL:  $(\text{NH}_2)\text{C}(\text{CH}_3)(\text{CH}_2\text{OH})_2$ ], and tris(hydroxymethyl) aminomethane [Tris:  $(\text{NH}_2)\text{C}(\text{CH}_2\text{OH})_3$ ]. [29,30,31,32,33,34,35,36,37,38,39]

It is found that these polyalcohols are heterogeneous at low temperatures, but when the temperature rises to the solid-solid phase change temperatures, their molecules become homogeneously face-centered cubic crystals with high symmetry and absorb a great deal of hydrogen bonds and among these square-bridge type molecules break. Experiments show that the phase change of polyalcohols is first order and their Gibbs changes are zero [40]. Benson et al. [31,32] believe that the solid-solid phase change enthalpy in NPG or PE should be as follows

$$\Delta H = T_s \Delta S = nB_h + \Delta H_0$$

where  $\Delta H_0$  is the contribution from the non-hydrogen bond to the enthalpy which can be estimated from the solid-solid phase change enthalpy of neopentane which does not contain OH (about 2.6 kJ/mol),  $B_h$  is the average hydrogen bond energy which is about 9.7 kJ/mol for the polyalcohols NPG and PE and  $n$  is the average hydrogen bond number in every molecule which is related to  $N$ , the number of OHs in every molecule, by the following equation

$$n = \frac{fN^2}{4}$$

For NPG and PE,  $N$  is 4 and 2 respectively, and  $f=1$ , therefore,

$$\Delta H = \Delta H_0 + \frac{N^2 B_h}{4}$$

To obtain solid-solid phase change materials which have a larger range of phase change temperatures, which are beneficial for low temperature utilizations of solar energy, it is reasonable to combine, at a fixed molecule fraction, two or more polyalcohols together to form an alloy type mixture whose phase change temperature can then be adjusted to meet the application requirements [41]. Figure 1-4 shows the hydrogen bonds in PE-NPG after NPG is added to PE [42]. Benson et al., Zhang et al., and Ruan et al. examined experimentally the solid-solid phase change temperatures and enthalpy of the binary system consisting of NPG and PE [29,31]. Benson et al. believed that the mechanism of the solid-solid phase change in the binary system of polyalcohols is similar to that in the monophyletic system, which is governed by the crystal structure change.

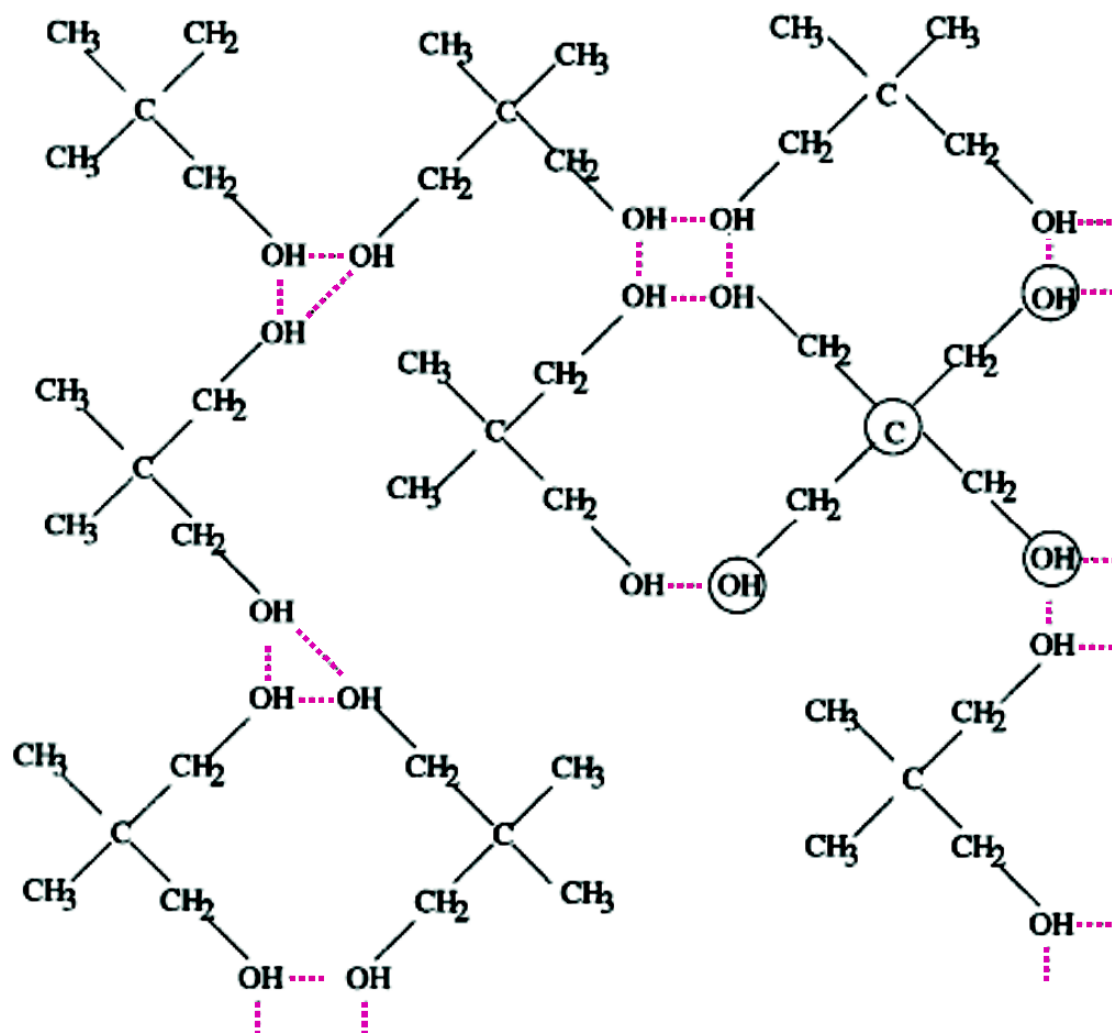


Figure1- 4 Hydrogen bonds in the binary system of NPG/PE after PE is added into NPG [42].

### ***1.4.1. Pentaerythritol (PE)***

Pentaerythritol ( $C(CH_2OH)_4$ ), is one of the simplest molecular solids, as it may be viewed as formed by replacing each H in methane by  $(CH_2OH)$  units. At ambient conditions, pentaerythritol (PE) has a simple layered structure [43] (space group  $I_4$ ). In this phase, the intralayer molecules (parallel to the a–b crystallographic plane) interact through cooperative hydrogen bonding as shown in figure 1-5 [44]. In contrast the interlayer bonding (along the c-axis) is weak van der Waals type (closest distance of approach of layers 3.5 Å). Thus PE is a model compound to study the properties of hydrogen bonds and the phase transformations in cyclic and acyclic alcohols under high pressures. In addition, its structure is closely related to that of pentaerythritol nitrate (PEN) which is used as an initiating explosive, the explosive sensitivity of which seems to be related to its structural features [45].

Nitta and Watanbe [46] were the first to determine the crystal structure of PE. Later on, Eilerman and Rudman [47] refined the PE structure and determined atom positions in the unit cell.

The important features of the determined tetragonal structure may be summarized as follows: If the hydrogen atoms of the OH groups are not taken into consideration, the molecule  $C(CH_2OH)_4$  in the crystal possesses approximately the symmetry of  $D_{2d-42m}$ , precisely  $S_4-4$ , with one pair of primary alcohol radicals puckered upwards and the other downwards, namely, all the bond angles of these atoms being approximately tetrahedral

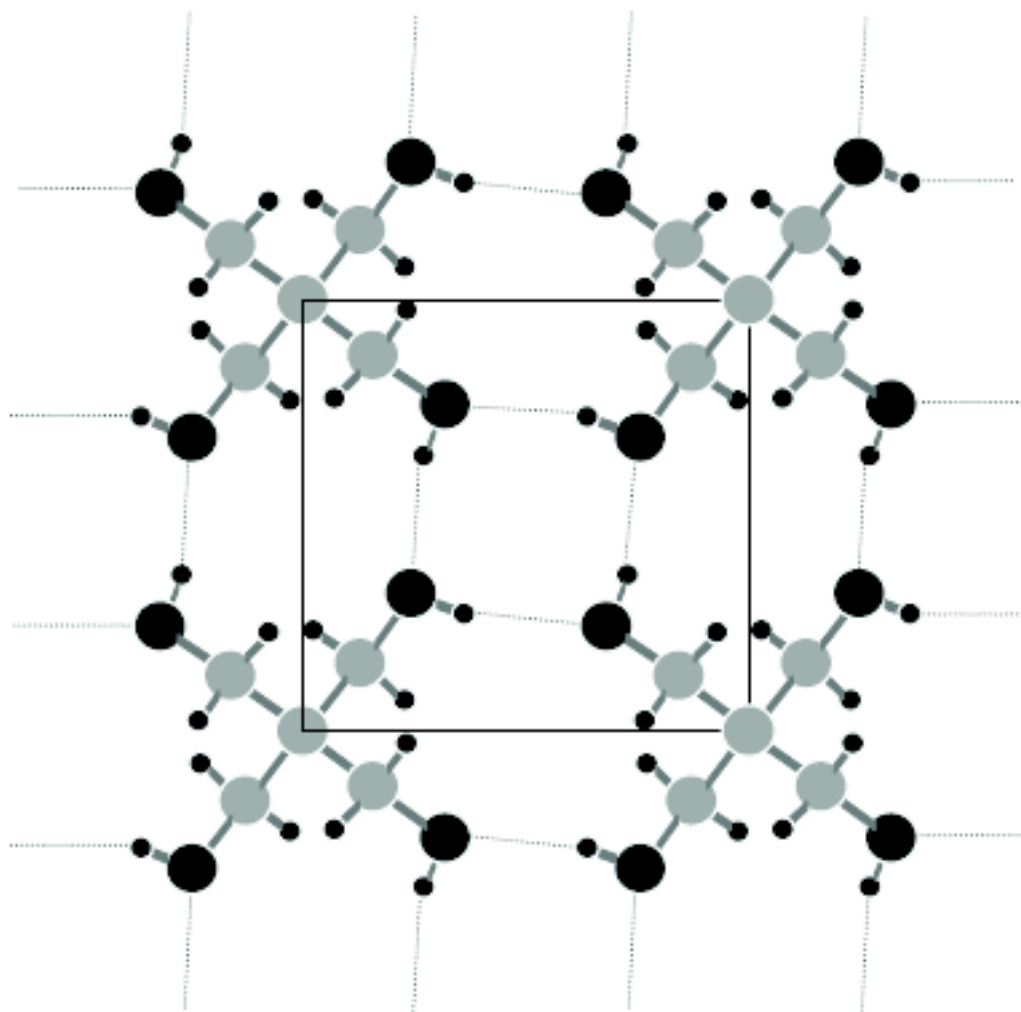


Figure 1-5 (001)Layer of the crystal structure of pentaerythritol at ambient conditions space group  $I_{-4}$ . (Grey circles, large black circles and small black circles represent carbon, oxygen and hydrogen, respectively. The dashed lines represent the intra-layer hydrogen bonds.) [48]

The molecules are arranged flat in a sheet parallel to the crystallographic  $c$ -plane, and the whole crystal is made up of such molecular layers. The linkage between neighboring molecules in a layer is more or less firm by the interaction of the hydroxyl groups. The geometrical aspect of this linkage is such that four hydroxyl oxygen atoms, one out of each adjoining molecule, constitute a square, of which every side is presumably bridged

over by a hydrogen atom [49]. The crystal structure of low temperature phase of PE is shown in figure 1-6 [50].

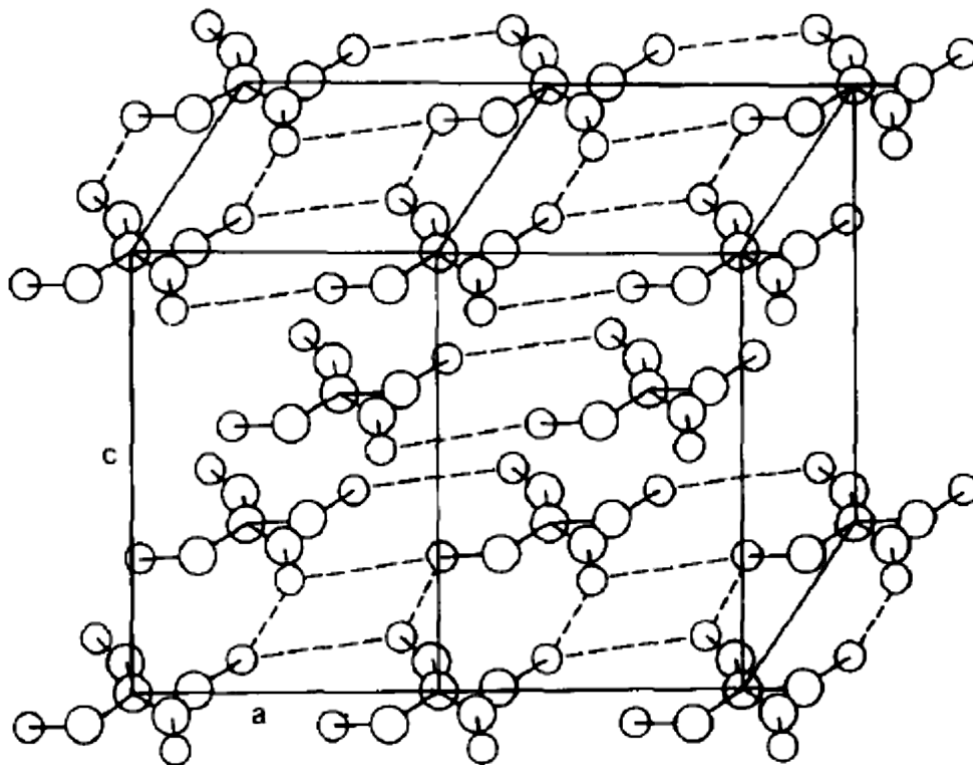


Figure 1-6 Crystal structure of the low temperature phase of pentaerythritol [50]

Polyalcohol crystals undergo  $\alpha\gamma$  transitions from a lower symmetry to a higher symmetry structure, when heated. Pentaglycerine and pentaerythritol have similar layered body centered tetragonal (BCT) low temperature ( $\alpha$ ) phases. The high temperature ( $\gamma$ ) plastic phases for both PG and PE are FCC. The lattice expansions on PG have been determined by Chandra et al. [51] using high temperature Guinier X-ray diffraction. Chandra et al. [51] provide a detailed evaluation of the XRD patterns, which revealed that

the two  $\gamma$  peaks were superimposed along with those of the  $\alpha$  phase. They also observed a single  $\gamma$  phase region above 91°C, and measured the position of the low and high temperature phases and lattice parameters based on several d-spacings using least square fit. The complexity of liberation and translation movements of molecules is undoubtedly very large in the cubic phase compared with those of the tetragonal phase. As a result, layering is not maintained, cubic phase is “plastic”, “not layered” and evidence indicated that the molecules are not rigid. The question of statistical preference of molecular orientation in the cubic cell was addressed by Nitta and Watanbe [52] attempted to match the intensities of the reflection from powder sample to ten different models, and with very few Debye rings that are available at such high temperatures (because of the extremely high x-ray temperature factor).

#### ***1.4.2. Pentaglycerine (PG)***

The crystal structure of PG at room temperature was studied by Rudman et al. in 1983 [53]. They showed that the crystal structure is body centered tetragonal with  $Z=2$  (phase II). When heated, PG undergoes a phase transition leading to an orientationally disordered face centered cubic lattice (phase I) at about 353K [53]. This phase is stable up to the melting point (about 460K).

The low temperature phases held together by hydrogen bonds between OH groups of neighboring molecules. The FCC phase transition is accompanied with large enthalpy [54] related to breaking of hydrogen bonds. This takes place as the molecule is going from an ordered phase to disordered phase.

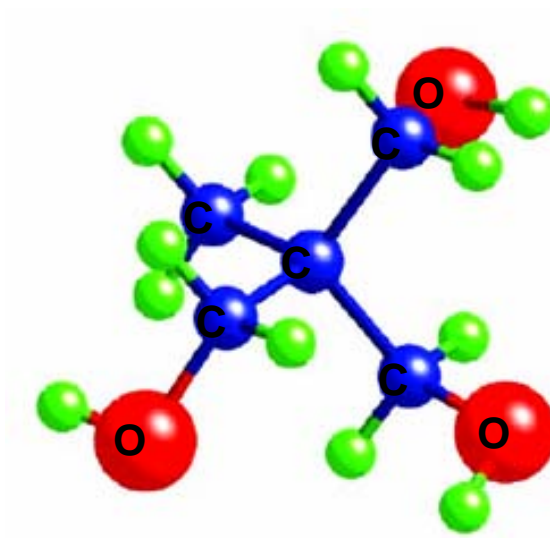


Figure 1-7 Molecular structure of pentaglycerine

The changes in the lattice parameters in the  $\alpha$  phase reported by Chandra et al [51] is reported in Table 1-1.

The transition entropy is the measure of the disorder in the high temperature phase. The entropy corresponding to this orientational disorder is  $R \ln(48) = 32.2 \text{ JK}^{-1}\text{mol}^{-1}$ . This is supplemented by conformational disorder which does not depend on symmetry. Assuming the molecule has tetrahedral shape, the total entropy of  $59.6 \text{ JK}^{-1}\text{mol}^{-1}$  calculated matches well with the experimentally determined entropy of  $59.3 \text{ JK}^{-1}\text{mol}^{-1}$  [51].

Suenaga et al. [54] reported the dependence of thermo physical properties of the homologous polyols on number of  $-\text{OH}$  groups. As the number of  $-\text{OH}$  groups increases in each molecule, the molar volume of the high temperature phase decreases and that of

Table 1-1 Lattice Parameters of Pure PG and PE at Elevated Temperatures Along with Lattice Expansions [51].

No.	Temp. (°C)	Lattice Parameters		Lattice Expansions	
		a (Å)	b (Å)	$\Delta a/a$	$\Delta c/c$
$\alpha$ -Phase (BCT)					
1.	32	6.1672(0.0026)	8.5477 (0.0037)		
2.	38	6.1634 (0.0014)	8.5542 (0.0015)	0.007	0.020
3.	43	6.1708 (0.0030)	8.5524 (0.0033)	0.132	0.013
4.	52	6.1681 (0.0029)	8.5600 (0.0031)	0.185	0.072
5.	56	6.1693 (0.0040)	8.5547 (0.0043)	0.259	-0.023
6.	62	6.1678 (0.0055)	8.5619 (0.0058)	0.336	0.037
7.	66	6.1790 (0.0041)	8.5553 (0.0044)	0.391	-0.019
8.	72	6.1740 (0.0028)	8.5614 (0.0029)	0.398	0.010
9.	78	6.1790 (0.0022)	8.5638 (0.0024)	0.514	0.040
$\gamma$ -Phase (FCC)					
10.	84		8.8656 (0.0006)		4.200
11.	91		8.8772 (0.0003)		4.337
12.	98		8.8800 (0.0015)		4.448
13.	103		8.8937 (0.0052)		4.531
14.	109		8.9090 (0.0066)		4.711

low temperature phase increases. The temperature, enthalpy and entropy of transition also depend systematically on the number of OH groups. Dissociation of hydrogen bonds and the intermolecular motional degrees of freedom thereby enhanced would play an essential role in the phase transition.

#### 1.4.3. Neopenylglycol (NPG)

The unit cell and space group of the solid crystal phase at room temperature were reported by Zannetti [55] as monoclinic with systematic absences corresponding to space group  $P2_1/c$  with  $Z=4$ .

The crystal structure was settled by Nakano et al. [56] who indicated the same unit cell and assigned the space group to be  $P2_1/n$ . The monoclinic structure is stable up to about 313K. Between this temperature and the melting point about (398K) the NPG exists a plastic crystal phase the structure of which is face centered cubic ( $Z=4$ ). The previously reported data and results are reported in Table 1-2.

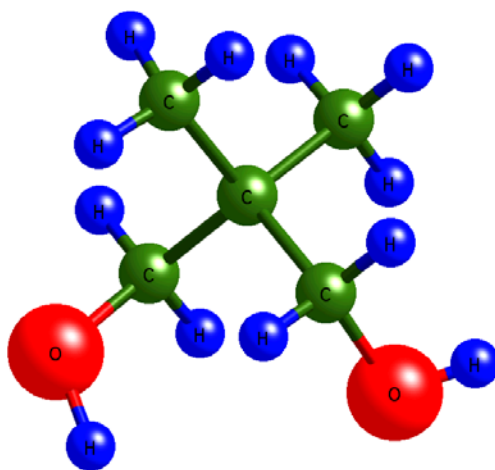


Figure 1-8 Molecular structure of NPG

X-ray diffraction studies by Barrio et al. at [57] room temperature gave lattice parameters:  $a=6.019(3)$  Å;  $b=10.881(4)$  Å;  $c=10.132(4)$  Å  $\beta=100.61(1^\circ)$ . Their studies revealed that at  $313.2 \pm 1.0$ K NPG becomes cubic (f.c.c., phase I), with lattice parameter  $a=8.860(8)$  Å at 356K. This phase I remains until the melting point at  $398 \pm 1.0$ K. The enthalpy variations for phase II to phase I and for the phase I to liquid transitions are  $14.1 \pm 0.5$  and  $4.0 \pm 0.1$  kJmol<sup>-1</sup>, respectively.

The NPG compound may be considered as a derivative of the pentaerythritol (PE) compound. NPG is obtained from PE by substituting two CH<sub>2</sub>OH groups to two CH<sub>3</sub> groups.

Table 1-2 Lattice Parameters for NPG [57]

Phase	Parameters				Temperature (K)	Reference
	a(Å)	b(Å)	c(Å)	$\beta$ (°)		
II	5.98(2)	11.00(3)	10.81(3)	112.4(3)	Room	
	6.01	10.91	10.18	100.0	Room	
	6.0773	10.9642	10.1125	99.68	294	
	5.985(3)	10.877(4)	10.101(4)	99.75(1)	288	
I	8.82				348	
	8.838				320	
	8.860(8)				356	

Infrared absorption studies [58] indicated that the –OH stretching band corresponding to hydrogen bond is present in PE, PG and NPG for the low temperature phases. On heating, the frequency of the absorption band of –OH increases at temperature close to the transition temperature. These shifts are characteristic of hydrogen bond breakage.

#### 1.4.4. 2-Amino-2-Methyl-1,3-Propanediol (AMPL)

The unit cell of the low-temperature phase (denoted as M,) at room temperature was earlier determined as monoclinic, the results being  $a=8.62$  &  $b=11.00$  Å,  $c=10$  Å and  $\beta=93.53(1)$ ,  $Y = 579.4(6)$  and  $Z = 4$  [59]. X-ray diffraction results are:  $a = 6.105(2)$  Å,  $b = 11.037(4)$  Å,  $c = 8.613(3)$  and  $\beta = 93.57(1)$ . In spite of the 45 reflections used in the refinement process of lattice parameters no systematic absences were detected and hence the space group remains still undetermined.

The monoclinic phase is stable up to  $(352.6 + 1.0)$  K. At higher temperatures AMPL is cubic (phase 1, body centred cubic (bee.), with  $Z = 2$ , and called C, ). The lattice parameter of this phase is  $6.753(7)$  Å at  $353.2$  K [59].

AMPL has large entropy of solid-solid phase transition and very low entropy of fusion [60]. Rose and Van Camp [61] reported the powder data on AMPL and concluded the structure to be monoclinic with lattice parameters;  $a = 8.62 \text{ \AA}$ ,  $b = 11.00 \text{ \AA}$ ,  $c = 6.1(3) \text{ \AA}$ ,  $\beta = 93.32(1)^\circ$ ,  $V = 580.3(5) \text{ \AA}^3$  at  $20 (\pm 1)^\circ\text{C}$ ,  $D_x = 1.211 \text{ g. cm}^{-3}$  for  $z = 4$  from the JCPDS card. In 1991, Chandra, Ding, and Lynch [62] reported powder diffraction patterns of binary solid-solutions with other organic compounds such as neopentylglycol and AMPL [63] which are indexed based on the JCPDS card 12-1111. Chandra, Ding and Lynch [63] have shown that AMPL has a propensity to undercool with substitutional doping of this organic plastic crystal. The bond lengths of non-hydrogen atoms are listed in Table 1-3.

Table 1-3 Bond Lengths of non-Hydrogen Atoms in AMPL. [64]

**Type Length (Å) Type Length (Å)**

O<sub>1</sub>—C<sub>1</sub> 1.425(4) O<sub>2</sub>—C<sub>3</sub> 1.410(4)

C<sub>1</sub>—C<sub>2</sub> 1.534(4) C<sub>2</sub>—N 1.477(4)

C<sub>2</sub>—C<sub>3</sub> 1.525(4) N—H<sub>1a</sub> 0.93(5)

C<sub>2</sub>—C<sub>4</sub> 1.529(5) N—H<sub>2a</sub> 0.89(5)

O<sub>1</sub>—H<sub>10</sub> 0.82(6) O<sub>2</sub>—H<sub>2o</sub> 0.86(5)

The monoclinic structure of the  $\alpha$  phase of AMPL has a tetrahedral molecular chain joined via O...H and N...H bonds. The molecules have intermolecular O...H—O bonds along the linear chains and the chains are interconnected by alternating O...H—O and O...H—N bonds leaving unbounded periodic hydrogen atom sites in the structure.

The molecular arrangement may be explained by showing the bonds between four molecules in Figure 4. Computer generated projections of the molecules in the a-b, b-c, and a-c planes in the space group  $P2_1/n$  are given in Figure 4 with the unit cell outlined.

There are inversion centers at the midpoints of each unit cell edge, at the corners of the unit cell, and at  $\frac{1}{2}$ ,  $\frac{1}{2}$ , and  $\frac{1}{2}$ . Bonding between the four AMPL molecules in Figure 4 can be viewed as follows; the central AMPL molecule is bonded to the right hand molecule (b) with hydrogen bonds, namely O2-H2o...O1b AND O1b-H2o-O1 bonds. The other two molecules, a and c, to the left are bonded alternately by O1-H1o...H2na-O2 and NH2n... O2c, respectively. The average nitrogen acceptor (N) contact distance with donor oxygen is 2.725 Å and the average hydrogen distance, shown by the double dashed line, is 1.89 Å. The O—H bonds, however, involve two types of interactions. The first is donor O-H2o and the acceptor O1 distance is 1.86 Å. The second donor O—H2n and the acceptor is O2 bond with a distance of 3.068 Å, and the hydrogen to acceptor O2 bond with a distance of 2.18 Å. Figure 5 shows the orientation of O—H and N—H bonded molecules in the unit cell of AMPL. Figures 1-9 and 1-10 show the orientation of alternating bimolecular chains in the Y-Z and X-y planes, respectively. In Figure 6, the atom positions are projected on the a-c plane. The molecules are bonded along the length of the chain with O—H bonds and alternate chains are joined by O—H and N—H bonds. In 1991, Chandra, Ding, and Lynch [60] reported the phase structure BCC  $a = 6.7$  Å above approximately 84°C at which the hydrogen/nitrogen bond configuration changes and an isotropic but orientationally disordered BCC phase is obtained unlike most of the other plastic crystals which have FCC structure [60].

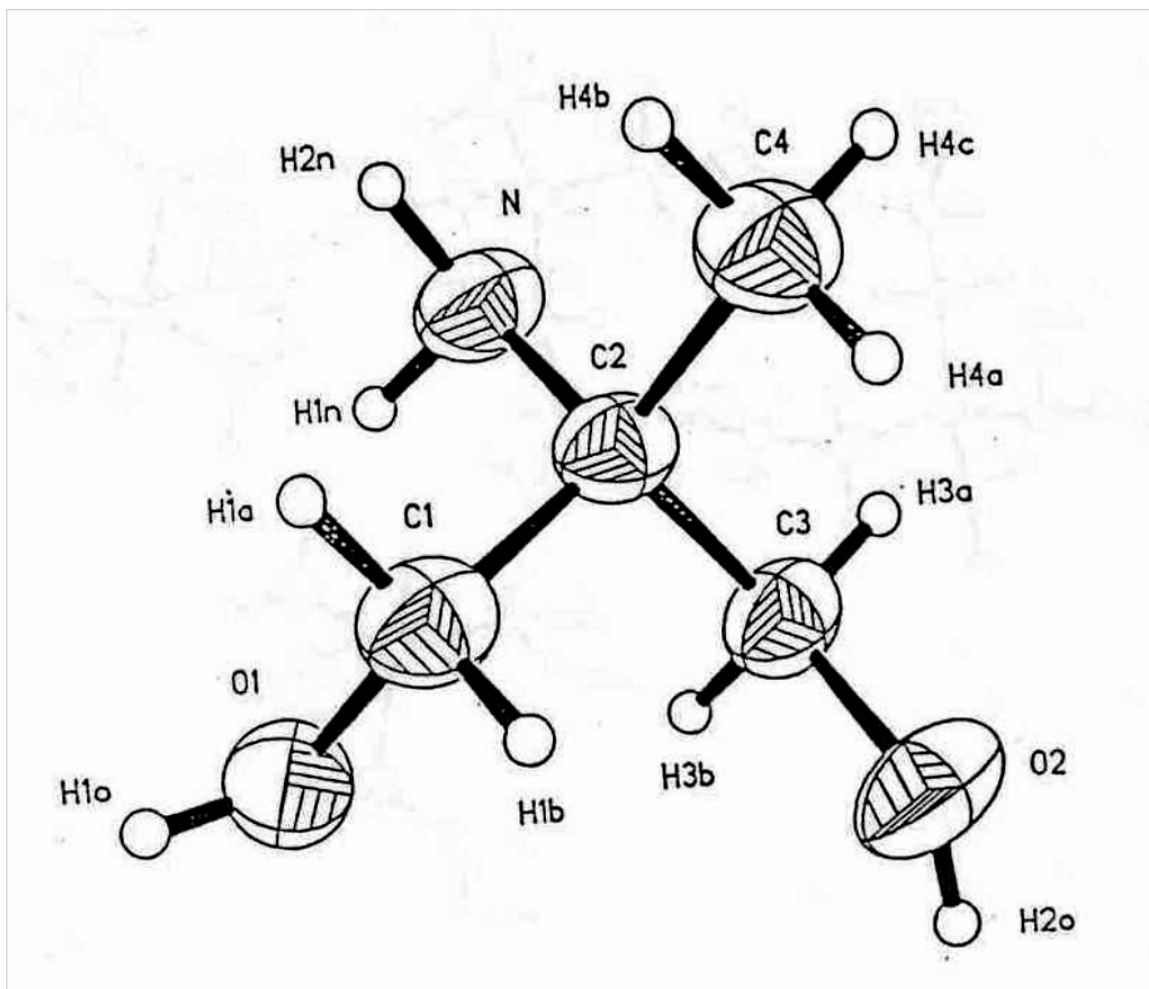


Figure1- 9The molecule of AMPL [C<sub>4</sub>H<sub>11</sub>NO<sub>3</sub>] with non-hydrogen atoms represented by thermal vibration ellipsoids drawn to encompass 50% of their electron density; hydrogen atoms are represented by arbitrarily small spheres. [64]

Thermal energy storage materials are crucial elements for the effective utilization of solar thermal energy. Phase change heat storage has larger energy storage density, smaller volume expansion requirement of the storage device, higher efficiency, and fixed temperature for heat absorption and removal cycle and is advantageous compared to

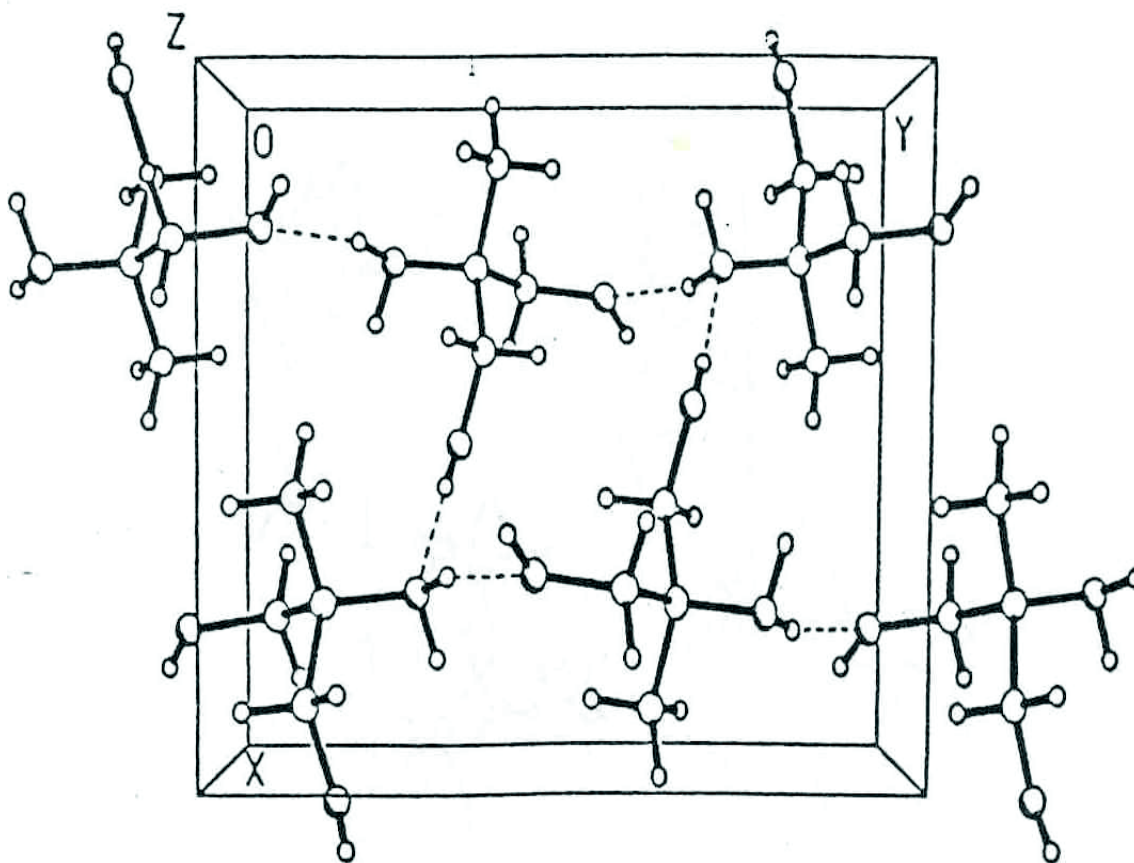


Figure1- 6Orientation of O—H and N—H bonded molecules in the unit cell of AMPL.  
[Hansen's Thesis]

sensible heat storage. Unlike the sensible heat storage method, the latent heat storage method provides much higher storage density, with a smaller temperature difference between storing and releasing heat.

### 1.5. Binary phase diagrams of polyalcohols

Pure organic polyalcohols, so called "Plastic Crystals", undergo crystallographic changes absorbing or releasing large amounts of latent heat at constant transition temperature well

below their melting points. There are relatively few known pure polyalcohols which undergo energetic solid-solid phase transitions and have high transition temperatures. Therefore, lowering of transition temperatures is important for development of practical thermal energy storage materials. Binary polyalcohols allow adjustment of transition temperatures to near or below room temperature.

The transition temperatures for polyalcohols range from room temperature to 188°C with the flexibility to vary the transition temperature by changing the composition of a particular binary. There is great potential for passive heating as well as other high temperature heat storage systems such as a water heater application.

#### ***1.5.1. Pentaerythritol (PE)-neopentylglycol (NPG) binary phase diagram***

PE and NPG have hydrogen-bonded lattices with layered and chain type low temperature structures, respectively are known as model materials. The phase diagram and the transition mechanisms were not known. This led researchers to study and develop the PE-NPG binary phase diagram. Chandra et al. developed a PE-NPG binary phase diagram based on X-ray diffraction and using the “FACT” program. They reported thermodynamic properties such as free energies for solid-solid transformations and excess energy for the binaries. This binary system was shown to exhibit a complex behavior with one than one solid-solid phase transition. Chandra et al [65] observed that the  $\beta$  phase (NPG rich side-PE system) transforms to  $\gamma$  at a constant temperature but the transition of PE-rich  $\alpha$  to  $\gamma$  varies as a function of temperature. Their DSC results of the NPG rich binaries showed two normal endotherms  $\alpha \rightarrow \beta$  and  $\beta \rightarrow \gamma$  and another continuous broad endotherm for the  $\alpha \rightarrow \gamma$  transition in the two phase region. They

proposed that these  $\beta \rightarrow \alpha$  transitions are due to changes in the compositions and the amounts of phases in this binary. In the PE(rich)-NPG binary,  $\alpha \rightarrow \gamma$  and  $\beta \rightarrow \gamma$  transitions occur as expected but the energy stored in the  $\beta$  phase at low temperatures is continuously released at a higher temperature due to the  $\alpha \rightarrow \gamma$  transformation. Thus simple heating of PE-rich binaries results in “Heat Pump” action. By choosing appropriate binary compositions one can select a desirable transition temperature for heat storage.

Barrio et al. [67] developed PE-NPG binary phase diagram in 1990. They noticed an intermediate cubic phase by using x-ray diffraction. They had developed a They showed the existence of two endothermic effects between these temperatures and for molar fractions ranging between  $X=0.05$  and  $X=0.9$ . They also found an intermediate cubic phase in the PE-NPG binary system. The invariant temperature (at 343.6K) produced by the existence of the new phase was determined by x-ray powder diffraction and thermal analysis. They determined the solubility boundaries between the intermediate cubic phase and the adjacent biphasic domains by means of the evolution of the lattice cubic parameters with temperatures and, from the study of the thermal expansion coefficients of the cubic alloys. Between 343.6K and about 373K the concentration range of the cubic phase was predicted to be very narrow (ranging between 0.12 and 0.13 molar fraction of PE at 353K). When the temperature rises, the concentration domain increases and displaces to higher concentrations.

The PE-NPG binary phase diagram is reported by different groups with significant differences in their observations [66, 67, 68]. Barrio et al. [64] reported the existence of an intermediate cubic phase. They reported an invariant temperature as 70.6°C (343.6K),

produced by the presence of a new phase. Tesseire et al. [6868] also developed the PE-NPG binary phase diagram using calorimetry and x-ray diffraction but they did not notice the presence of an intermediate cubic phase as reported by Barrio et al. [64].

Tesseire et al. [6868] noted a solid-liquid phase at 165°C (438K) in the PE-NPG system, whereas Chandra et al. [69] showed a two phase region consisting of two individual high temperature phase regions. Barrio et al. [64] proposed a PE-NPG phase in the temperature range from room temperature to 393K. They observed invariant equilibria at 343.6K which does not correspond to the phase diagrams proposed by Tesseire et al. and Chandra et al. [67,68]. The PE-NPG phase diagram by Chandra et al. [70] was calculated using the FACT Sage program. There is good agreement between the phase diagrams calculated by Chandra et al. and proposed by Tesseire et al. [67,68]. According to Tesseire et al. a two phase region exists from room temperature to 36°C (309K), and a small region on the NPG rich side consisting of a low temperature NPG single phase and a high temperature NPG phase [68]. The major difference between the two above mentioned phase diagrams are that Tesseire et al. [68] predicted a two phase (solid-liquid) region at about 163°C (436K), shown in figure 1-11, whereas Chandra et al. predicted the presence of a two phase region consisting of two high temperature solid phases belonging to PE and NPG each at the same temperature. Barrio et al. pointed out that since the two substances are isomorphic at high temperatures a new phase might appear. The experimental phase diagram developed by Barrio et al. is shown in figure 1-12 [64].

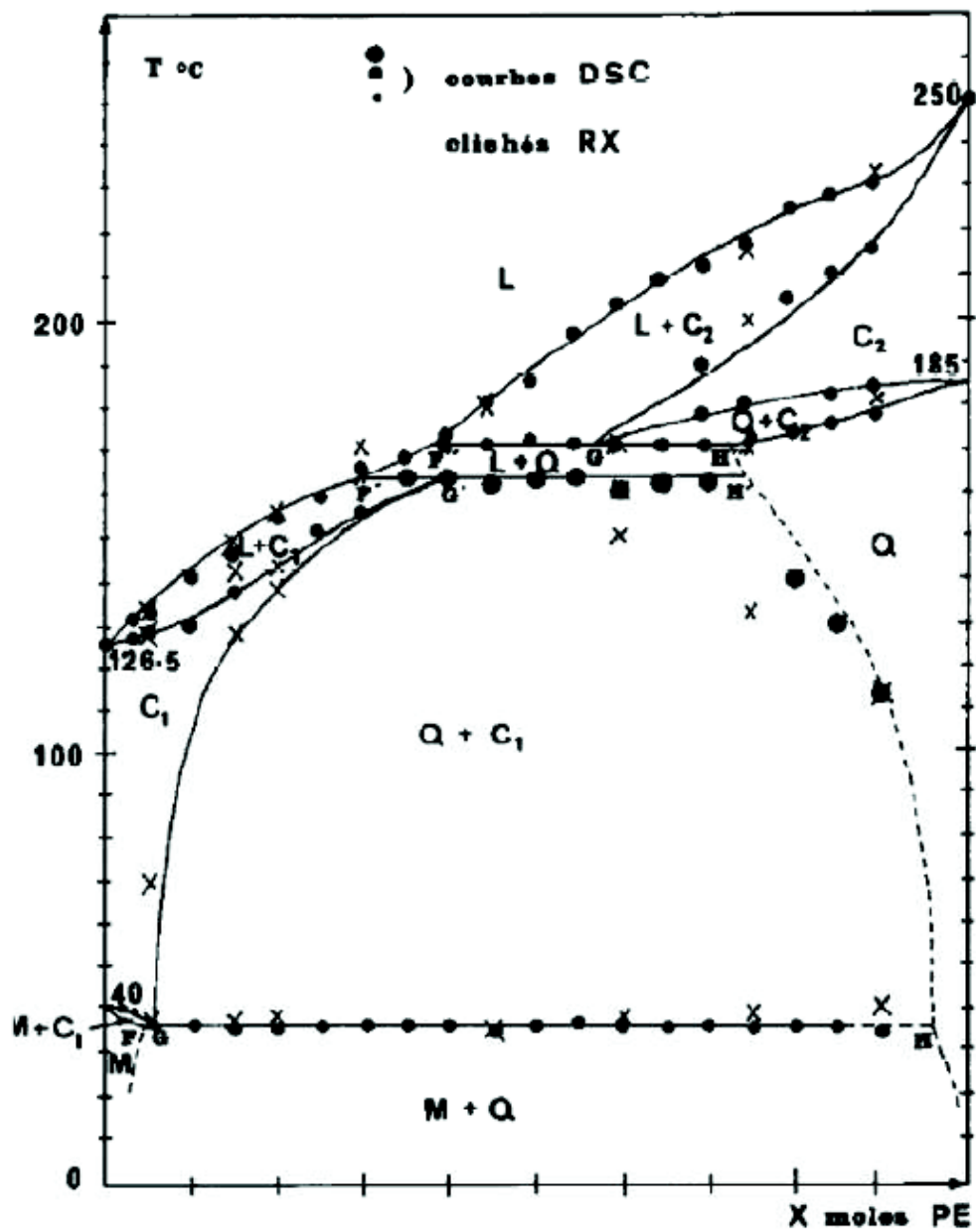


Figure 1-7 Experimental phase diagram of PE-NPG system by Tesseire et al.[68]

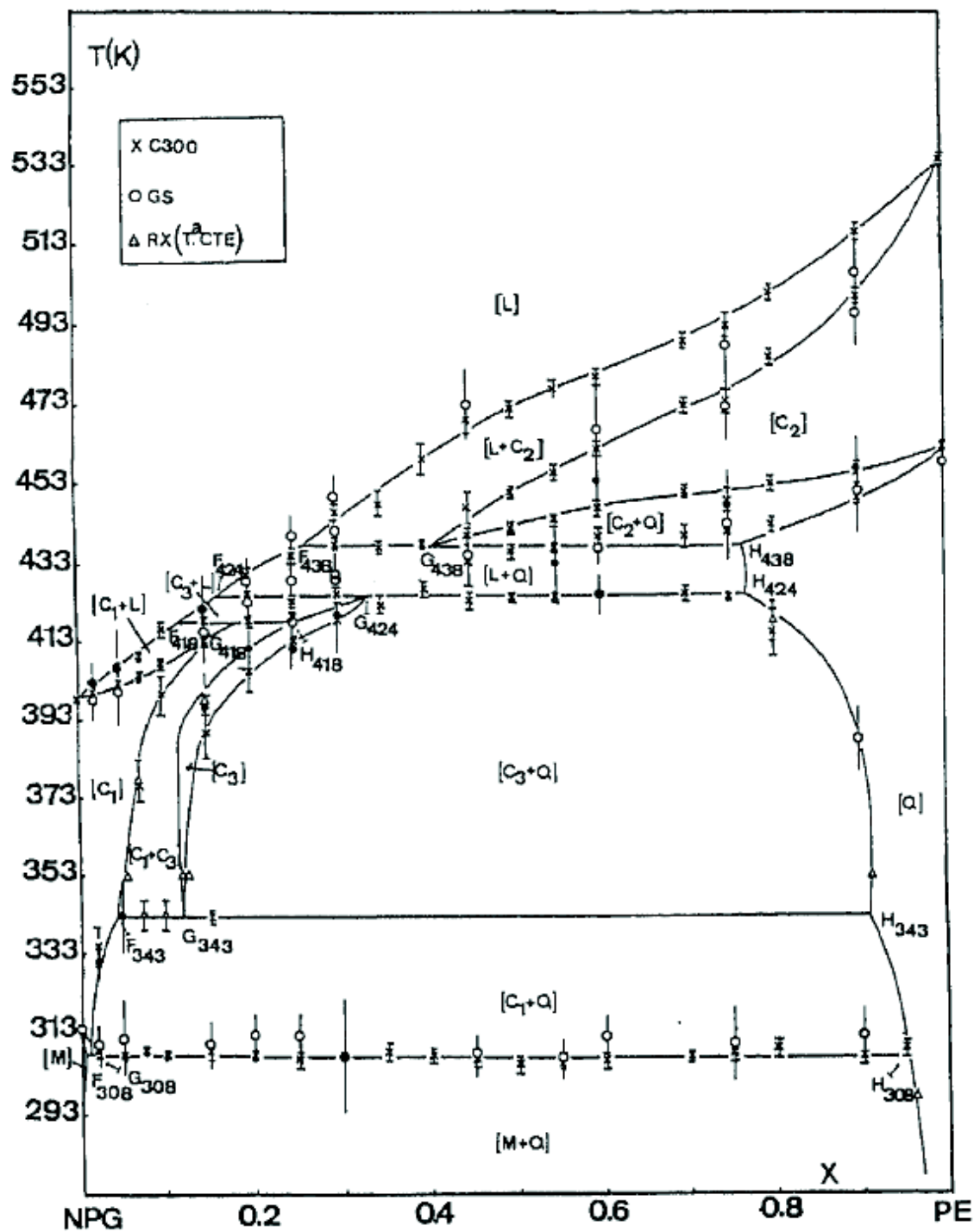


Figure 1-8 Experimental PE-NPG phase diagram by Barrio et al. [64]

**1.5.2. 2-amino,2-methyl-1,3-propanediol (AMPL)-neopentylglycol (NPG) binary phase diagram**

Barrio et al. [71] determined the AMPL-NPG binary phase diagram by using crystallographic and thermodynamic methods. The phase diagram showed an extensive difference in the two phase regions, due to the polymorphism of the two substances. The AMPL-NPG system is characterized by an invariant at 293K, below which a two phase region  $M_1+M_2$  coexist. In order to determine the limits of the de-mixing regions for the AMPL-NPG, Barrio et al. studied the binary system by X-ray powder diffraction at 318K and 353K. At 318K they observed a de-mixing region. They determined the cubic parameter for phase  $C_2$  as a function of mole fraction which is represented in table x. The table also shows the volume occupied by the average molecule ( $V/Z$ ) in each lattice.

Table 1-4 Lattice parameters and the volume occupied by the average molecule for the pure substances as a function of the mole fraction of NPG [71]

X	Form	Parameters			$\beta(\text{\AA})$	$V/Z(\text{\AA}^3)$
		a( $\text{\AA}$ )	b( $\text{\AA}$ )	c( $\text{\AA}$ )		
0(AMP)	$M_1$	8.617(5)	11.058(5)	6.108(3)	93.56(2)	145.2(7)
0.02	$M_1$	8.615(6)	11.065(7)	6.115(4)	93.47(2)	145.5(9)
0.05	$M_1$	8.620(6)	11.065(7)	6.121(4)	93.52(2)	145.7(9)
$S_A=0.06$	$M_1$	8.622(6)	11.065(5)	6.118(3)	93.49(2)	145.7(7)
$S_B=0.52$	$C_2$	8.735(11)				166.6(5)
0.55	$C_2$	8.750(10)				167.5(5)
0.60	$C_2$	8.768(10)				168.5(5)
0.70	$C_2$	8.790(10)				169.8(5)
0.80	$C_2$	8.805(10)				170.7(5)
0.90	$C_2$	8.815(10)				171.2(6)
1 (NPG)	$C_2$	8.812(8)				171.0(4)

At 353K Barrio et al. [71] noticed a de-mixing region since the pure substances do not belong to the same group. They did the thermal analysis using a differential heat flux

calorimeter. The characteristic temperatures of the transitions were determined using the “shape factor method” [72]. The AMPL-NPG phase diagram was created using thermal analysis data along with the solubility boundaries from X-ray diffraction. The main characteristics of the phase diagram are the existence of two eutectoids and one eutectic invariant. The motivation for this work for Barrio et al. [71] was to contribute to the establishment of the conditions ruling the solubility in organic binary systems which are characterized by the ODIC state. The first step to determine this is the geometrical approach. This approach requires analysis of the size and shape of the molecules of the constituent pure substances. They calculated the molecular size using the Van der Waals radii of the individual atoms and assumed that the molecular distortions due to the intermolecular interactions in the lattice are absent. They suggested that the difference in size between NPG and AMPL is about 5%, and that the molecular shape in the formation of the molecular alloys plays an important part. The difference in shape between the AMPL and NPG molecules is caused by an  $\text{NH}_2$  group in AMPL where NPG has a  $\text{CH}_3$  group. Table 1-5 shows the invariant equilibria for AMPL-NPG system developed by Barrio et al. [71]. Figure 1-13 shows the AMPL-NPG binary diagram developed by Barrio et al. [71].

Table 1-5 Characteristic temperatures and corresponding mole fractions of the invariant points in the NPG/AMP phase diagram [71]

Invariant	<u>X(mole fraction NPG)</u>			Temperature (K)
	M	E	N	
Eutectoid	0.06	0.54	0.92	293.7
Eutectoid	0.07	0.46	0.51	325.0
Eutectic	0.39	0.42	0.44	363.9

AMPL and NPG are not isomorphic in the high temperature phase, thus implying that the miscibility in this phase can only be partial. Barrio et al. [71] observed the monophasic domains corresponding to BCC and FCC molecular plastic alloys are quite large.

Salud et al. also published an AMPL-NPG phase diagram in 1997 [73]. They analyzed the phase diagram thermodynamically and concluded that there were some incoherencies

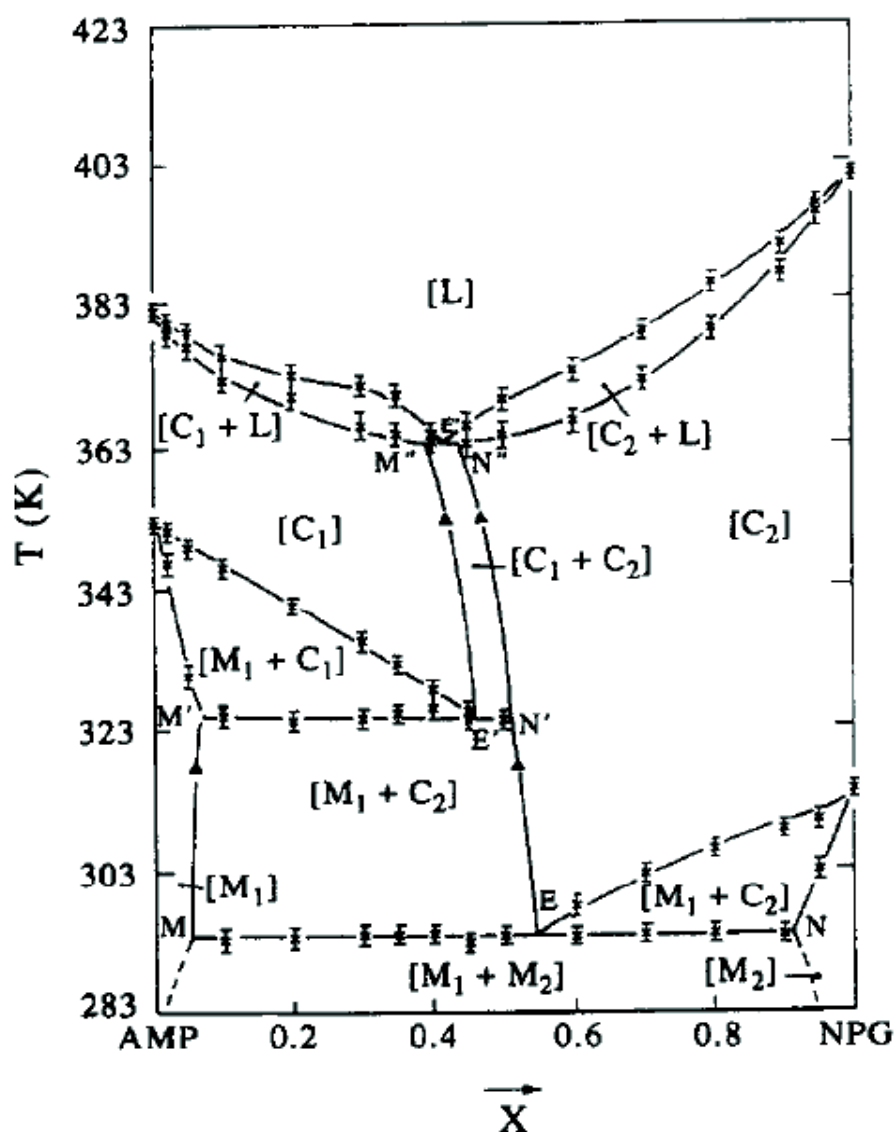


Figure 1-9 AMPL-NPG binary phase diagram by Barrio et al. [71]

with the phase diagram published by previous authors [71,74]. According to Salud et al. [73] these discrepancies arise from the difficulty of accounting for the one and two phase low-temperature domains by means of the Gibbs energy functions calculated from the high temperature equilibria. The temperature of the re-established eutectoid invariants are 293.7 and 325.0K. Figure 1-14 shows the AMPL-NPG phase diagram developed by Salud et al. [73].

### ***1.5.3. PG-AMPL binary phase diagram***

The experimental PG-AMPL binary phase diagram was reported by Salud et al. in 1997 [73]. They established the phase diagram from room temperature to the liquid state using thermal analysis and X-ray powder diffraction techniques. They discussed the intermolecular interactions in the orientationally disordered mixed crystals by analyzing the evolution of the packing coefficient as a function of the composition. They analyzed the phase diagram thermodynamically using the enthalpy-entropy compensation theory. From the Guinier-Simon patterns, they determined the existence of a two-phase domain  $[M_1+Q]$ , the disappearance of the cubic  $C_1$  phase, and giving rise to a  $[M_1 + C_1]$  domain. At 330K, they noticed the disappearance of the  $M_1$  phase. At  $X=0.55$  (mole fraction PG), as the temperature increased, they noticed the transition from  $[M_1+Q]$  to  $[Q+C_1]$  at 321K. At the same composition in the mixture the  $C_1$  phase disappeared and  $C_F$  appeared at 326-328K, giving rise to a  $[Q+C_F]$  two-phase domain.

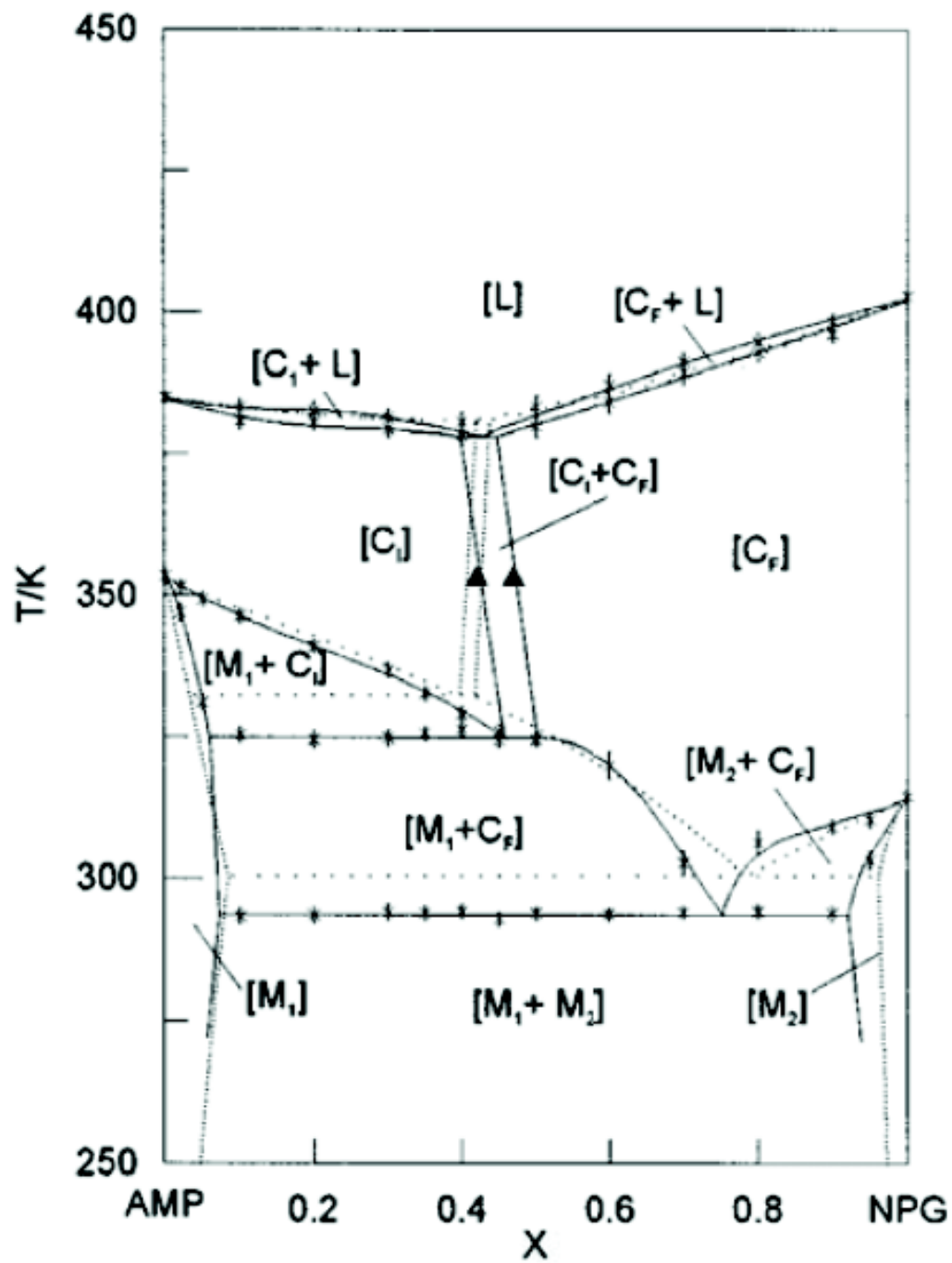


Figure 1-14 AMPL-NPG binary phase diagram by Salud et al. [73]

At higher temperatures, transformations of the  $[Q+C_F]$  domain to  $[C_F]$  on-phase domain (to an orientationally disordered molecular alloy). They were not able to make a proper determination of the transition from plastic crystalline solid to liquid. Salud et al. [73] attribute this to the large differences in vapor pressure. Determination of these characteristics of the phase diagram were made by diffraction as a function of temperature. They also did diffraction at constant temperature because, they wanted to determine the existence of close eutectoid invariants, and to delimit the range of the  $[M_1+Q]$  and  $[C_1+C_F]$  two-phase region.

Tamarit et al. [75] showed that the intermolecular interactions by hydrogen bonds play an important role in the orientationally disordered phases. Salud et al. [73] studied the packing coefficient evolution for PG-AMPL and observed that the total number of groups able to form hydrogen bonds are equal; two  $CH_2OH$  groups and one  $NH_2$  group in the AMPL molecule and three  $CH_2OH$  groups in the PG molecule. They also showed that the substitution of the molecules did not produce any significant changes in the intermolecular interaction scheme. They also emphasized the relatively high values of the packing parameter for the pure compounds as well as for their alloys, which ruled out incompatibility between high packing and the existence of orientational [76]. Salud et al. [73] used the enthalpy-entropy compensation theory [77] to thermodynamically analyze the phase diagram. Since excess enthalpy data are hard to obtain, they measured the heat of melting as a function of the mol fraction for the PG-AMPL system in each solid solution domain. They assumed temperature independent enthalpy form and nonexistence of excess values for the liquid solution. The excess enthalpy for each solid solution was obtained by fitting a second-order polynomial to the experimental data.

They calculated the phase diagram using the Pro Phase program [78]. The resulting phase diagram is shown in figure 1-15. Comparison between calculated and experimental invariant equilibria is shown in table 1-6.

Table 1-6 Comparison between Experimental (E) and Calculated (C) Invariant Equilibria [73]

Invariant		T(K)	X <sub>M</sub>	X <sub>N</sub>	X <sub>P</sub>
Eutectoid	E	323.0	0.09	0.43	0.92
	C	330.0	0.09	0.47	0.92
Eutectoid	E	330.2	0.44	0.53	0.93
	C	333.5	0.51	0.54	0.96
Peritectic	E	413.6	0.40	0.47	0.57
	C	418.4	0.48	0.53	0.56

#### ***1.5.4. Pentaglycerine (PG)-Pentaerythritol (PE) Phase Diagram***

Pentaerythritol (PE) and Pentaglycerine (PG) phase was investigated by Barrio et al.[79]. Thermal analysis and X-ray Guinier-Simon method was used by the authors to characterize PE-PG alloys from room temperature to liquid phase. The alloys were prepared by melting the desired composition in a furnace and slow cooling to room temperature. PE and PG are iso-structural, both at room temperature (body centered tetragonal) [80] and high temperature phases (FCC). Figure 1-16 shows the PE-PG experimental phase diagram developed by Barrio et al. [79]. Low temperature phase of PE is

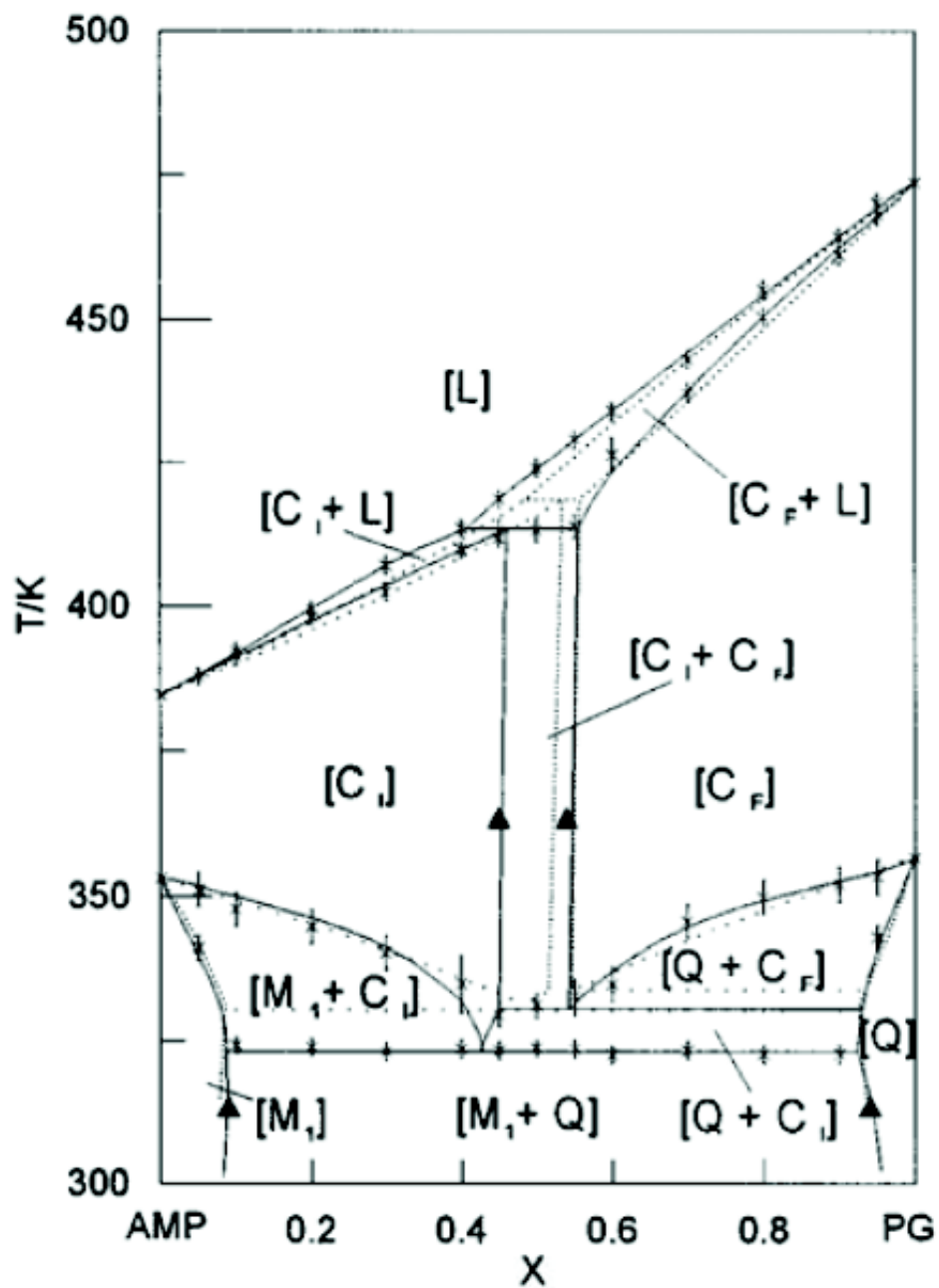


Figure 1-10 PG-AMPL binary phase diagram reported by Salud et al. [73]

characterized by strong intermolecular hydroxyl hydrogen bonding between molecule and eight of its neighbors in a layer parallel to the (001) plane. The interlayer bonds are weak and due to Van der Waals forces. PG has similar bonding scheme to PE except that one link is open, due to substitution by  $-\text{CH}_2\text{OH}$  group in the PE molecule for a  $-\text{CH}_3$  group in the PG molecule. Symmetry of PG requires the presence of a statically disordered molecule since the required site symmetry, 4, is not present in PG molecule as in PE. As reported previously, the crystal to plastic transformation in PE and PG are first order transitions. Nitta [81] suggested correlation between the hydrogen bond breaking at higher temperatures permitting rotation and molecular vibration leading to plastic phase. Benson et al. [82] measured infrared absorption for PE and indicated that all the hydrogen bonds are broken at the transition temperature. Taking into account the enthalpy variations for the crystalplastic phase transition in PE in which there are four hydrogen bonds for each molecule, the maximum energy value for one bond is about  $10 \text{ kJmol}^{-1}$ . This result also matches the enthalpy variation for the crystal to plastic phase transition in PG, in which there are two hydrogen bonds for each molecule on average. Figure 1-16 shows the experimental phase diagram of PE-PG [79].

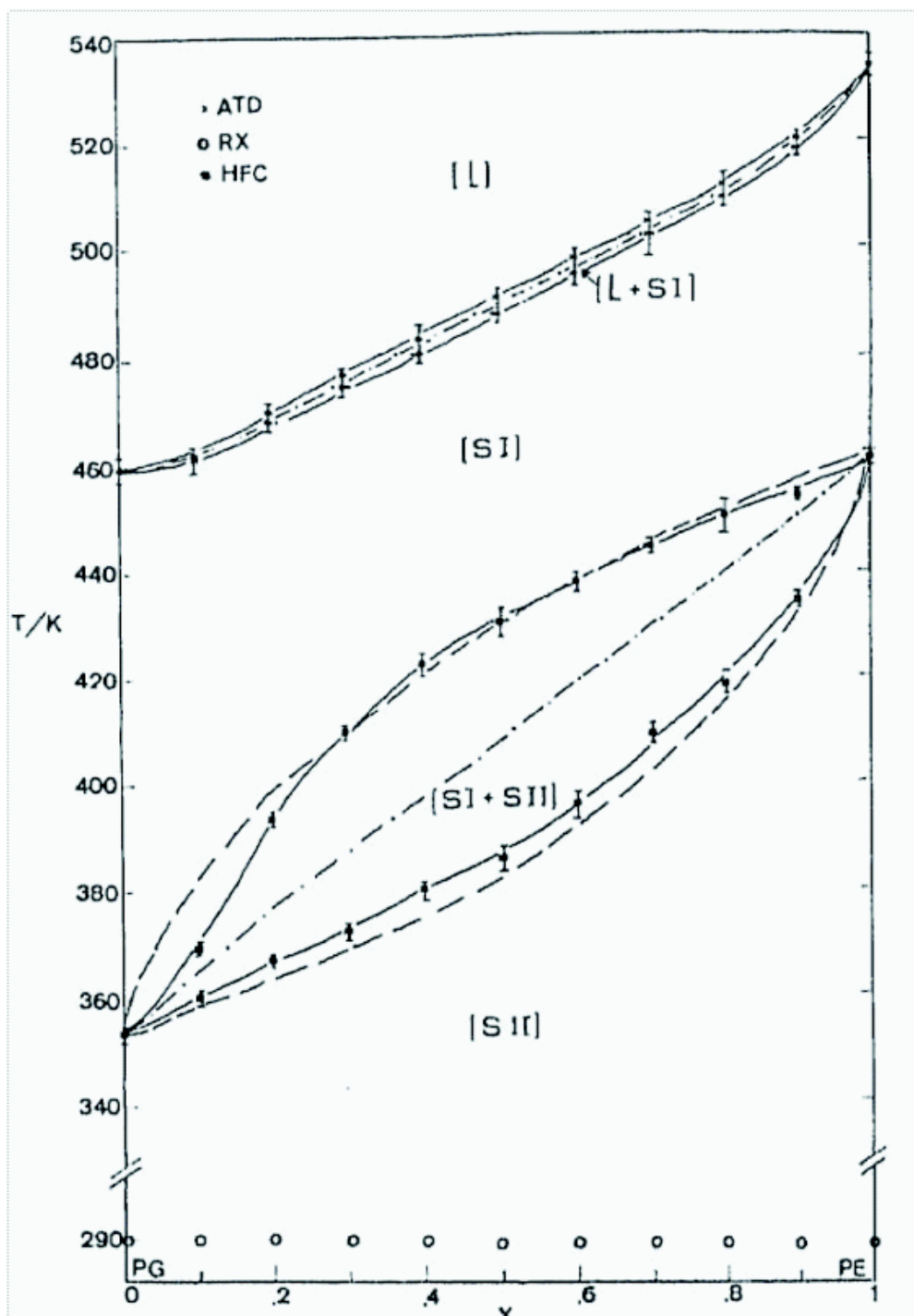


Figure 1-16 PE-PG experimental phase diagram [79]

The absence of splitting in these reflections (002) and the continuous variation of Bragg's angles with composition suggest total miscibility at 293 K. It was found that 'a' parameter of PE showed 0.55% expansion and 'c' parameter showed a contraction of 1.45% throughout the system. Thus, it was concluded that taking into account the estimated error, the system behave as quasi-ideal from a crystallographic point of view. The difference in evolution of 'a' and 'c' is due to strong hydrogen bonds in (001) plane and weak interlayer Van de Waals forces. PE-PG phase diagram is characterized by a very narrow plastic to liquid domain, which has a maximum width of about 3 K and a wide crystal to plastic equilibrium domain with a maximum width of 43 about 44 K for the central compositions. Calculated phase diagram is based on Oonk's method [83] which uses the concept of Equal Gibbs Curve (EGC). The phase diagram shows two domains of complete miscibility; one at lower temperature with tetragonal structure and another one at higher temperature plastic phase with cubic structure. Finally, the authors concluded that the plastic alloys behavior can be considered as ideal

#### ***1.5.5. Pentaglycerine (PG)-Neopentylglycol (NPG) Phase Diagram***

Pentaglycerine (PG) and neopentylglycol (NPG) exhibit plastic crystal phases at high temperatures in which there is relative loss of order and thus these phases are also known as orientationally disordered crystals (ODIC). The low temperature PG and NPG rearrange their molecules into a cubic phase at higher temperatures, where some hydrogen bonding which is responsible for the rigid low temperature structure are broken. Barrio et al.[84] was the first to propose a phase diagram for the binary mixture

of PG-NPG system. In their work, they used thermal analysis and X-ray powder diffraction techniques to characterize the changes taking place in the mixtures. PG and NPG, both may be considered a derivative of pentaerythritol (PE). PG is obtained by substituting one  $-CH_2OH$  group with a methyl ( $-CH_3$ ) group. In a similar manner, NPG involves substitution of two  $-CH_2OH$  groups with two methyl groups. Phase transitions in PG and NPG have been characterized as first order transitions [85,86]. The first hypothesis for crystal to plastic transition was made by Nitta [81] for PE, where he proposed that hydrogen bonds which maintain the molecules rigidly in the ordered solid crystal phase are broken at the transition temperature permitting the molecular vibration and rotation, so that the molecules can be considered as spherical in the plastic form. Infrared absorption studies done by Benson et al. [85] further strengthen this argument that the  $-OH$  stretching vibrations corresponding to hydrogen bond is present in PE, PG, and NPG for the low temperature phase. Upon heating, the vibration frequency band of  $-OH$  increases at temperature close to the transition temperature. These shifts are known to be characteristic of hydrogen bond breakage. Based on these facts, same phase transformation mechanism can be applied to PG and NPG compounds. Because of chemical bond similarity of PG and NPG with PE, structural studies done on PE can be used to investigate these molecules. PG is isostructural with PE (body centered tetragonal structure with  $I_4$  space group) and same hydrogen bonding is found except one link is open in the PG structure. This means that PG has strong intermolecular hydroxyl hydrogen bonding in the layers parallel to the (001) plane [85]. The interlayer bonds are weak Van der Waals forces. The same structural study of NPG also indicates that the arrangement of hydrogen bonds around the center of symmetry is similar to that of PE.

For example, the hydrogen bond distance O...O is 2.710 Å in PE 1; 2.714 Å in PG [87] and between 2.65 Å and 2.75 Å in NPG [88]. The phase diagram solubility boundaries/limits at room temperature were determined from Bragg's angles variation with the concentration of PG. (021) and (011) reflections of monoclinic phase were studied. Using this method, solubility boundary of PG in NPG was established – 0.07 mol fraction of PG; NPG 0.83PG 0.07 In the same manner, evolution of (002) and (110) reflections corresponding to body centered tetragonal phase with respect to concentration established the NPG solubility in PG at 0.58 mol fraction of PG; NPG 0.42PG 0.58. At 356 K, just above the crystal to plastic phase transition temperature of PG, only cubic reflections were recorded. The DSC pattern at such a point only shows melting which signifies complete miscibility. Figure 1-17 shows the experimental PG-NPG phase diagram developed by Barrio et al. [86]

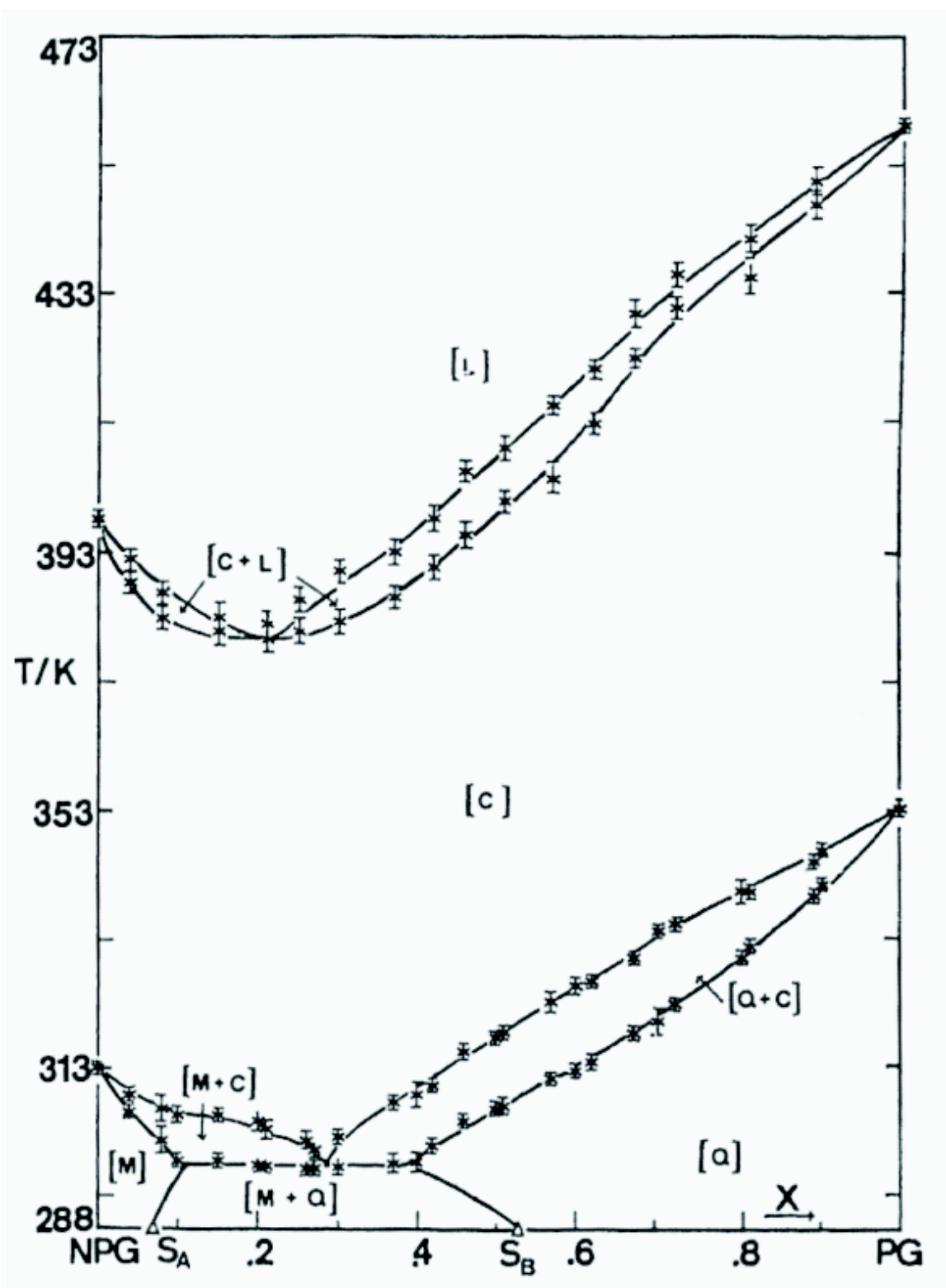


Figure 1-17 PG-NPG experimental phase diagram [86]

## References:

- 
- 1 Garg HP, Mullick SC, Bhargava AK. Solar thermal energy storage. D. Reidel Publishing Co; 1985.
  - 2 Khartchenko NV. Advanced energy systems. Berlin: Institute of Energy Engineering & Technology University; 1997.
  - 3 Kauranen P., Peippo K. and Lund P. D., Solar Energy, 46, 275-278 (1991)
  - 4 Lane GA. Solar heat storage—latent heat materials, vol. I. Boca Raton, FL: CRC Press, Inc.; 1983.
  - 5 Ruan D, Zhang T, Zhang D, Liang S, Hu Q. Acta Energiæ Solaris Sinica 1994;15(1):19.
  - 6 Pillai KK, Brinkwarth BJ. The storage of low grade thermal energy using phase change materials. Appl Energy 1976;2:205–16.
  - 7 Abhat A. Low temperature latent heat thermal energy storage. In: Beghi C, editor. Thermal energy storage. Dordrecht, Holland: D. Reidel Publication Co.; 1981.
  - 8 Abhat A. Low temperature latent heat thermal energy storage: heat storage materials. Solar Energy 1981;30(4):313–32.
  - 9 Buddhi D, Sawhney RL. In: Proceedings on thermal energy storage and energy conversion; 1994.
  - 10 A. Ter-Gazarian, Energy Storage For Power Systems, Peter Peregrinus L.T.D, p1-10, p57-73, 1994.
  - 11 D. Chandra, H. Mandalia, and J. Hansen, Thermal Energy Storage in Phase Change Materials with On-Demand Heat Release, Final Report DOE Contract No. 19X-SL974V, Jan. 1994.
  - 12 D. Chandra, Crystal Structure Changes in the Solid-Solutions of Pentaglycerineneopentylglycol, Final Report to Solar Energy Research Institute, Midwest Research Institute, Golden Colorado, 1986.
  - 13 Hemley, R. J.; Ashcroft, N. W. *Physics Today* 1998, 51, 26.
  - 14 J. Timmermanns, J.Phys.Chem.Solids, Pergamon Press, 1961, Vol. 18, No. 1239, 1961, 1-8
  - 15 I. Nitta and T. watanabe, Bull.Chem. Soc. Japan, 13, No. 28, 1938.
  - 16 E. Murrill, and L. Breed, Thermochemica Acta, 1, 1970, 239.
  - 17 A. Ter-Gazarian, Energy Storage For Power Systems, Peter Peregrinus L.T.D, p1-10, p57-73, 1994.
  - 18 D. Mondieig, Y. Haget, M. Labrador, M.A. Cuevas-Diatre, P.R. Vander Linde, H.A.J. OOnk, Mat. Res. Bull. 26 (1991) 1091-1099.
  - 19 D.L. Bushnell, M. Sohi, Sol. Energy 49 (4) (1992) 235-244.
  - 20 J. Font, J. Muntasell, F. Cardoner, Sol. Energy Mater. Sol. Cells 33 (1994) 169-176
  - 21 H. Suga, Tthermochim. Acta 328 (1999) 9-17.
  - 22 X. Wang, E. Lu, W. Lin, T. Liu, Z. Shi, R. Tang, C. Wang, Energy Convers.
  - 23 C.J. Swet, in: Proceedings of the Fifth National Passive Conference, Amherst, MA, 19-26 October, (1980), pp. 282-286.
  - 24 G.A. Lane, P.J. Moses, in: Proceedings of Thermal Energy Storage Workshop, Palo Alto, CA, EPRI, January, (1983).

- 
- 25 K. Nagno, K. Ogawa, T. Mochida, K. Hayashi, H. Ogoshi, *Appl. Therm. Eng* 24 (2004) 209-220.
  - 26 S. Suda, *Int. J. Hydrog. Energy* 10 (11) (1985) 757-765.
  - 27 B. Bogdanovic, A. Reiser, K. Schlichte, B. Spliethoff, B. Tesche, *J. Alloys Compounds* 245 (2002) 77-89.
  - 28 J. Timmermanns, *J. Phys. Chem. Solids* 18 (1) (1961) 1-8.
  - 29 Ruan D, Zhang T, Zhang D, Liang S, Hu Q. *Acta Energiae Solaris Sinica* 1994;15(1):19.
  - 30 Xing D, Shi G, Ruan D, Huo L, Li D, Zhang T, Zhang D. *Acta Energiae Solaris Sinica* 1994;16(2):131.
  - 31 Benson DK, Burrows RW, Webb JD. *Solar Energy Materials* 1986;13:133.
  - 32 Benson DK, Chandra D. Solid-state phase-change materials for thermal energy storage. US DOE Contract No. DE-AC02-83CH10093, 1985.
  - 33 Son CH. Solid±solid phase-change materials as a space-suit battery heat storage medium. Ph.D. Thesis, University of South Carolina, 1989.
  - 34 Son CH, Morehouse JH. *ASME Journal of Solar Energy Engineering* 1991;113:244.
  - 35 Zhang ZY, Yang ML. *Thermochimica Acta* 1990;169:263.
  - 36 Murrill E, Breed L. *Thermochimica Acta* 1970;1:239.
  - 37 Nakano E, Hirotsu K, Shimada A. *Chem Soc Jap* 1969;42:3367.
  - 38 Zhang ZY. *Thermochimica Acta* 1992;202:105.
  - 39 Font J, Muntasell J, Navarro J, Tamarit JL, Lloveras J. *Solar Energy Materials* 1987;15:299.
  - 40 Wang Q. *Hydrogen bonds in organic chemistry*. Tianjin: Tianjin University Press, 1993.
  - 41 Wang X. Study on the heat storage performance of the monophyletic and binary systems of NPG, PE and TAM. M.Sc. thesis, Yunnan Normal University, Kunming, 1997.
  - 42 Xiaowu Wang, Enrong Lu, Wenxian Lin, Caizhang Wang, *Energy Conversion & Management* 41 (2000) 135-144
  - 43 F.J. Llewellyn, E.G. Cox, T.H. Goodwin, *J. Chem. Soc.* (1937) 883–894.
  - 44 Nandini Garga,, Surinder M. Sharma, S.K. Sikka, *Solid State Communications* 136 (2005) 56–61
  - 45 Y.A. Gruzdkov, Y.M. Gupta, *J. Phys. Chem. A* 104 (2000) 11169.
  - 46 I. Nitta and T. Watanabe, *Bull. Chem. Soc. Japan*, 13, N0. 28 (1938)
  - 47 D. Eilerman, R. Rudman, *Acta Cryst. B* 35 (1979) 2458.
  - 48 Nandini Garga,, Surinder M. Sharma, S.K. Sikka, *Solid State Communications* 136 (2005) 56–61
  - 49 W.F.Pergner, S. Vutukuri, Z.A.Dreger, Y.M.Gupta and K.Flurchick, *Chem. Phys. Lett.*, 422, 397-401 (2006)
  - 50 P. Alonso et al., *Soc. Espan. Hist. Nat.* 46 (1959) 379.

- 
- 51 D. Chandra and C. S. Barrett, Effect of interstitial dopants on the Thermophysical properties of solid-state phase change materials., DOE report, DE-AC03-84SF-12205 (1986)
- 52 I. Nitta and T. Watanabe, Bull. Chem. Soc. Japan, 13, NO. 28 (1938)
- 53 D. Eilerman, R. Lippman, and R. Rudman, Acta Cryst. B 39, 263 (1983)
- 54 K. Suenaga, T. Matsuo and H. Suga, Thermochemica Acta, 163, 263-270 (1990)
- 55 R. Zannetti, Unit Cell and Space Group of 2,2 Dimethyl-1,3 Propanediol, Acta Cryst., 14, 203 (1961).
- 56 E. Nakano, K. Hirotsu and A. Shimada, the Crystal Structure of Pentaglycol and Neopentylglycol, Bull. Chem. Soc. of Japan, 42, 3367 (1969).
- 57 M. Barrio, J. Font, D. O. Lopez, J. Muntasell, J. Ll. Tamarit, N. B. Chanh, Y. Haget, J. Chim. Ohys., 87, 1835 (1990).
- 58 D. K. Benson, R. W. Burrows and J. D. Webb, Solar energy Mater., 13, 133, (1986).
- 59 J. Font, J. Muntasell, F. Cardoner, Sol. Energy Mater. Sol. Cells 33 (1994) 169-176
- 60 D.Chandra, Crystal Structure and Thermal studies on Solid-Solid Energy Storage Materials, Final Report DOE Contract No. 19X-SC644V, 1990.
- 61 H. A. Rose and A. Van Camp, Anal. Chem., 28(11), 1790-1791, 1956.
- 62 D. Chandra, R. A. Lynch, W. Ding and J. J. Tomlinson, —Advances in X-Ray Barrio, J. Font, D. O. Lopez, J. Muntasell and J. LL. Tamarit, N. B. Chanh and Y. Haget, *I. Phys. Chem. So/i&* Vol. 52, No. 5, Analysis, Plenum Publishing, 32, 609-615, 1989.
- 63 D. Chandra, W. Ding, R. A. Lynch, and J. J. Tomlinson, J. Less Common Metals, 168, 159-167, 1991.
- 64 R. Russell, M.S. Thesis, University of Nevada, Reno, 1995
- 65 D. Chandra, Crystal Structure and Thermal Studies On solid –State Energy Storage Materials, Final Report, Contract number:19X-SC644V/DE-AC05-84 OR21400, 1990.
- 66 M. Barrio, J. Font, J. Muntasell, J. Navarro, J.Ll. Tamarit, Sol. Energy Mater. 18 (1–2) (1998) 109.
- 67 D. Chandra, Crystal Structure and Thermal Studies On solid –State Energy Storage Materials, Final Report, Contract number:19X-SC644V/DE-AC05-84 OR21400, 1990
- 68 M.Teisseire, N.B. Chanh, M.A. Cuevas-Diarte, J. Guion, Y. Haget, D. Lopez and J. Muntasell Thermochemica Acta 181 (1991) 1.
- 69 D. Chandra, C.S. Barrett, Final Report to DOE, Contract No. DEAC03- 84SF12205, January, 1986.
- 70 Chandra, C.S. Barrett and D.K.Benson Advances in X-ray Analysis. 32 (1989) 609.
- 71 M. Barrio, J. Font, D.O. Lopez, J. Muntasell, J. Ll. Tamarit, P. Negrier and Y. Haget, J. Phys. Chem. Solids 55, 1994, 1295-1302.
- 72 R. Courchinoux, N. B. Chanh, Y. Haget, T. Cavet, E. Estop and M. A. Cuevas Dirte, J. Chim. Phys, 86 (1989) 561.
- 73 J. Salud, D. O. Lopez, M. Barrio, J. Li. Tamarit, H. A. Oonk, P. Negrier and Y. Hager, Journal of Solid State chemistry 133, (1977) 536-544.
- 74 D. Chandra, W. Ding and R. A. Lynch, J. Less Common Metals 168, (1991) 159.
- 75 J. Ll Tamarit, M. Barrio, D.O. Lopez and Y. Haget, J. Appl. Crystallogr. 30, 118 (1997).
- 76 S. Urban, J. Domoslawski and Z. Tomkowiz, Mater. Sci., IV/3, 91 (1978).

- 
- 77 H. M. Boots and P. K. de Bokx. *J. Phys. Chem.* 93, 8240 (1989).
- 78 L. Robe ls-Beneyt, Doctoral thesis, Bordeaux, 1995.
- 79 M. Barrio, J. Font, J. Muntasell, J Li Tamarit, N.B. Chanh, and Y. Haget, *J. Chim. Phys.*, 87 255-270 (1990)
- 80 D. Eilerman, R. Rudman, *Acta Cryst. B* 35 (1979) 2458.
- 81 I. Nitta and S. Seki, M. Momotani, *Proc. Japan Acad.*,26, 25 (1950)
- 82 E. Murrill and L. Breed, *Thermochimica Acta*,1, 239 (1970)
- 83 H.A.J. Oonk, "Phase Theory. The thermodynamics of heterogenous Equilibria", Elsevier Scientific Publ. Company, Amsterdam (1981)
- 84 M. Barrio, J. Font, D. O. Lopez, J. Muntasell, J Li Tamarit, N.B. Chanh, and Y. Haget, *J. Chim. Phys.*, 87 1835-1851 (1990)
- 85 D.K.Benson, J.D.Webb, R.W.Burrows, *Solar Energy Materials*,13 133-152 (1986)
- 86 M. Barrio, J. Font, J. Muntasell, J Li Tamarit, N.B. Chanh, and Y. Haget, *J. Chim. Phys.*, 87 255-270 (1990)
- 87 D. Eilerman, R. Lippman, and R. Rudman, *Acta Cryst. B* 39, 263 (1983)
- 88 D. Eilerman, R. Lippman, and R. Rudman, *Acta Cryst. B* 39, 263 (1983)

## Chapter II CALPHAD Modeling

---

In recent years thermodynamic modeling via the CALPHAD method has been extensively applied to industrial alloys of many types. Although pertaining to equilibrium conditions, use has shown that valuable information can be gained for a variety of practical applications. In essence, the issues involved in computational methods are less diverse and mainly revolve around Gibbs energy minimization. In addition there are “optimization” codes which are used for thermodynamic assessment of phase equilibria, thermodynamic properties and the equivalent experimentally measured quantities.

CALPHAD methods attempt to provide a true equilibrium calculation by considering the Gibbs energy of all phases and minimizing the total Gibbs energy of the system (G).

To calculate phase equilibria in a multicomponent system, it is essential to minimize the total Gibbs energy of all the phases involved in the equilibrium,

$$G = \sum_{i=1}^p n_i G_i^\phi = \text{minimum} \quad (1)$$

where  $n_i$  is the number of moles, and is  $G_i^\phi$  the Gibbs energy of phase  $i$ .

Describing a system thermodynamically requires the assignment of thermodynamic functions for each phase. The CALPHAD approach utilizes a variety of models to portray the temperature, pressure, and composition dependencies of the free-energy functions of the numerous phases. The Gibbs energy of a phase  $j$  is,

$$G^\phi = G_T^\phi(T, x) + G_p^\phi(p, T, x) + G_m^\phi(T_C, \beta_0, T, x) \quad (2)$$

where  $G_T^\phi(T, x)$  is the contribution to the Gibbs energy by the temperature ( $T$ ) and the composition ( $x$ ),  $G_p^\phi(p, T, x)$  is the contribution of the pressure ( $p$ ), and  $G_m^\phi(T_C, \beta_0, T, x)$  is the magnetic contribution of the Curie or Néel temperature ( $TC$ ) and the average magnetic moment per atom ( $\beta_0$ ).

The temperature dependence of the concentration term of  $G_T^\phi$  is usually expressed as a power series of  $T$ .

$$G = a + b \cdot T \cdot c \cdot T \cdot \ln(T) + \sum d_n \cdot T^n \quad (3)$$

where  $a$ ,  $b$ ,  $c$ , and  $d_n$  are coefficients, and  $n$  are integers. To represent the pure elements, the  $n$  are typically 2, 3, -1, and 7 or -9 [1]. This function is valid for temperatures above the Debye temperature; in each of the equations in the following models describing the concentration dependence, the  $G$  coefficients on the right-hand side can have such temperature dependence. Frequently, only the first two terms are used for the representation of the excess Gibbs energy. Dinsdale [1] also gives expressions for the effects of pressure and magnetism on the Gibbs energy; however, pressure dependence for condensed systems at normal pressures is usually ignored.

For multicomponent systems, it is useful to distinguish three contributions from the concentration dependence to the Gibbs energy of a phase,  $G^\phi$ .

$$G^\phi = G^0 + G^{ideal} + G^{xs} \quad (4)$$

The first term,  $G^0$ , corresponds to the Gibbs energy of a mechanical mixture of the constituents of the phase; the second term,  $G^{ideal}$ , corresponds to the entropy of mixing for an ideal solution, and the third term,  $G^{xs}$ , is the so-called excess term. Since Hildebrand [2] introduced the term "regular solution" to describe interactions of different elements in a random solution, a series of models have been proposed for phases that deviate from this regularity (i.e., show a strong compositional variation in their thermodynamic properties) to describe the excess Gibbs energy. For example, an ionic liquid model [3] or associate model [4], among others, have been proposed for liquid phases. For ordered solid phases, Wagner and Schottky [5] introduced the concept of defects on the crystal lattice in order to describe deviations from stoichiometry.

A description of order/disorder transformations was proposed by Bragg and Williams [6]. Since then, many other models have been proposed. Today, the most commonly used models for disordered phases, and sublattice models for ordered phases having a range of solubility or exhibiting an order/disorder transformation. The following examples give descriptions of models for binary phases and can easily be expanded for ternary and higher order phases.

The Gibbs energy of a binary stoichiometric phase is given by

$$G^\phi = x_A^0 G_A^0 + x_B^0 G_B^0 + \Delta G^f \quad (5)$$

where  $x_A^0$  and  $x_B^0$  are mole fractions of elements A and B and are given by the stoichiometry of the compound,  $G_A^0$  and  $G_B^0$  are the respective reference states of

elements A and B, and  $\Delta G^f$  is the Gibbs energy of formation. The first two terms correspond to  $G^0$ , and the third term corresponds to  $G^{xs}$ .  $G^{ideal}$  of Equation 4 is zero for a stoichiometric phase, since there is no random mixing.

Binary solution phases, such as liquid and disordered solid solutions, are described as random mixtures of the elements by a regular-solution type model

$$G^\phi = x_A G_A^0 + x_B G_B^0 + RT\{x_A \ln x_A + x_B \ln x_B\} + x_A x_B \sum_{i=0}^n G_i (x_A - x_B)^i \quad (6)$$

where  $x_A$  and  $x_B$  are the mole fractions, and  $G_A^0$  and  $G_B^0$  are the reference states of elements A and B, respectively. The first two terms correspond to  $G^0$  and the third term, from random mixing, to  $G^{ideal}$  in Equation 4. The  $G_i$  of the fourth term are coefficients of the excess Gibbs energy term,  $G^{xs}$ , in Equation 4. The sum of the terms  $(x_A - x_B)^i$  is the so-called Redlich-Kister polynomial [7], which is the most commonly used polynomial in regular-solution type descriptions. Although other polynomials have been used in the past, in most cases they can be converted to Redlich-Kister polynomials [8].

The most complex and general model is the sublattice model frequently used to describe ordered binary solution phases. The basic premise for this model is that a sublattice is assigned for each distinct site in the crystal structure. For example, the CsCl (B2) structure consists of two sublattices, one of which is occupied predominantly by Cs atoms and the other by Cl atoms. An ordered binary solution phase with two sublattices that exhibits substitutional deviation from stoichiometry can be described by the expression

$$\begin{aligned}
G^\phi &= x_A G_A^0 + x_B G_B^0 + RTa^1(y_A^1 \ln y_A^1 + y_B^1 \ln y_B^1) + a^2(y_A^2 \ln y_A^2 + y_B^2 \ln y_B^2)y_A^1 y_A^2 G_{AA}^0 + y_A^1 y_B^2 G_{BB}^0 \\
&+ y_B^1 y_A^2 G_{BA}^0 + y_B^1 y_B^2 G_{BB}^0 + y_A^1 y_B^1 y_A^2 \sum_{i=0}^{n_{2A}} G_i^{2A} (y_A^1 - y_B^2)^i + y_A^1 y_B^2 y_B^2 \sum_{i=0}^{n_{2B}} G_i^{2B} (y_A^1 - y_B^1)^i \\
&y_A^1 y_A^2 y_B^2 \sum_{i=0}^{n_{1A}} G_i^{1A} (y_A^2 - y_B^2)^i + y_B^1 y_A^2 y_B^2 \sum_{i=1}^{n_{1B}} G_i^{1B} (y_A^2 - y_B^2)^i + y_A^1 y_B^1 y_A^2 y_B^2 G^{hp}
\end{aligned}$$

(7)

where  $y_A^1$ ,  $y_B^1$ ,  $y_A^2$ , and  $y_B^2$  are the species concentrations of element A and B on sublattices 1 and 2 with  $a^1 y_A^1 + a^2 y_A^2 = x_A$ ,  $a^1 y_B^1 + a^2 y_B^2 = x_B$ ,  $y_A^1 + y_B^1 = 1$  and  $y_A^2 + y_B^2 = 1$ .  $a^1$  and  $a^2$  are the site fractions of the sublattices 1 and 2 and are given by the number of sites in the unit cell. The first two terms correspond to  $G^0$ , and the third term corresponds to  $G^{ideal}$  in. The remaining terms are the excess Gibbs energy term,  $G^{xs}$ . The coefficients  $G_{AA}^0$ ,  $G_{AB}^0$ ,  $G_{BA}^0$ , and  $G_{BB}^0$ , can be visualized as the Gibbs energies of the end-member phases. The end-member phases are formed when each sublattice is occupied only by one kind of species and can be either real ( $A_a^1 B_a^1$ : A atoms on sublattice 1 and B atoms on sublattice 2) or hypothetical ( $A_a^1 A_a^2$ ,  $B_a^1 A_a^2$ , and  $B_a^1 B_a^2$ ). The remaining terms of  $G^{xs}$  describes interactions between the atoms on one sublattice similar to regular-solution type models for disordered solution phases. This model description was first introduced by Sundman and Ågren [9] and later refined by Andersson et al. [10].

For the treatment of order/disorder transformations with this model, the coefficients in  $G^{xs}$  are not independent of each other. For example, Ansara et al. [11] derived dependencies for the order/disorder transformation of fcc/L12. This model was later

modified by Ansara et al. [12] to allow independent evaluation of the thermodynamic properties of the disordered phase. Chen et al. [13] have proposed another model for the treatment of ordered phases.

The generality of the sublattice description allows the formulation of a general description for multicomponent phases that can easily be computerized. Lukas et al. [8] give an example of a description.

From the condition that the Gibbs energy at thermodynamic equilibrium reveals a minimum for given temperature, pressure, and composition, J.W. Gibbs derived the well-known equilibrium conditions that the chemical potential,  $\mu_n^\phi$ , of each component, n, is the same in all phases,  $\phi$

$$\begin{aligned} \mu_1^{\dot{}} &= \mu_1^{\ddot{}} = \dots \mu_1^\phi \\ \mu_2^{\dot{}} &= \mu_2^{\ddot{}} = \dots \mu_2^\phi \\ &\dots \\ \mu_n^{\dot{}} &= \mu_n^{\ddot{}} = \dots \mu_n^\phi \end{aligned} \quad (8)$$

The chemical potentials are related to the Gibbs energy by the well known equation

$$G = \sum_{i=1}^n \mu_i x_i \quad (9)$$

Equation 8 results in n nonlinear equations that can be used in numerical calculations. All of the CALPHAD-type software tools use methods like the two-step method of Hillert [14] or the one-step method of Lukas et al. [8] to minimize the Gibbs energy. The equations obtained from these methods are usually nonlinear and are solved numerically using a Newton-Raphson technique.

## **2.1. Determination of the coefficients**

The coefficients of the Gibbs energy functions are determined from experimental data for each system. In order to obtain an optimized set of coefficients, it is desirable to take into account all types of experimental data (e.g., phase diagram, chemical potential, and enthalpy data). The coefficients can be determined from the experimental data by a trial-and-error method or mathematical methods. The trial-and-error method is only feasible if few different data types are available. This method becomes increasingly cumbersome as the number of components and/or the number of data types increases. In this case, mathematical methods, such as the least squares method of Gauss [15], the Marquardt method [16], or Bayesian estimation method [17], are more efficient. The determination of the coefficients is frequently called assessment or optimization of a system.

## **2.2. Higher component systems**

A higher component system can be calculated from thermodynamic extrapolation of the thermodynamic excess quantities of the constituent subsystems. Several methods exist to determine the weighting terms used in such an extrapolation formula.

Hillert [18] analyzed various extrapolation methods and recommended the use of Muggianu's method [19] since it can easily be generalized. The Gibbs energy of a ternary-solution phase determined by extrapolation of the binary energies using Muggianu's method is given by

$$G^\phi = x_A G_A^0 + x_B G_B^0 + x_C G_C^0 + RT \{ x_A \ln x_A + x_B \ln x_B + x_C \ln x_C \} \\ + x_A x_B \sum_{i=0}^{n_{AB}} G_i^{AB} (x_A - x_B)^i + x_A x_C \sum_{i=0}^{n_{AC}} G_i^{AC} (x_A - x_C)^i + x_B x_C \sum_{i=0}^{n_{BC}} G_i^{BC} (x_B - x_C)^i \quad (10)$$

where the parameters  $G_i^{ik}$  have the same values as in Equation 6 for each of the binary systems. If necessary, a ternary term  $x_A, x_B, x_C, G^{ABC}(T, x)$  can be added in order to describe the contribution of three element interactions to the Gibbs energy.

The usual strategy for assessment of a multicomponent system is shown in Figure 1. First, the thermodynamic descriptions of the constituent binary systems are derived. Thermodynamic extrapolation methods are then used to extend the thermodynamic functions of the binaries into ternary and higher order systems. The results of such extrapolations can then be used to design critical experiments. The results of the experiments are compared to the extrapolation, and if necessary, interaction functions are added to the thermodynamic description of the higher order system. As mentioned previously, the coefficients of the interaction functions are optimized on the basis of these data. In principle, this strategy is followed until all 2, 3,... n constituent systems of an n-component system have been assessed. However, experience has shown that, in most cases, no corrections or very minor corrections are necessary for reasonable prediction of quaternary or higher component systems. Since true quaternary phases are rare in metallic systems, assessment of most of the ternary constituent systems is often sufficient to describe an n-component system.

### **2.3. Improved Capabilities**

One goal of the CALPHAD group is to generate descriptions of binary, ternary, and quaternary systems that can be used for the construction of thermodynamic databases. Thermodynamic databases of multicomponent systems require consistency in the model

descriptions and the parameters used. With the constant improvement of computational technology, the use of more realistic models, such as the sublattice model description, becomes feasible. This allows more accurate descriptions of complex systems and makes it desirable to reassess systems that have been previously assessed.

The progress that has been made with these reassessments is shown in Figure 2-1 for the Al-Ni system, a basic system for superalloys. In the first assessment of Kaufman and Nesor, [20] the phases were either described as disordered solution phases [liquid, (Al), (Ni), and AlNi] or as stoichiometric compounds ( $\text{Al}_3\text{Ni}$ ,  $\text{Al}_3\text{Ni}_2$ , and  $\text{AlNi}_3$ ). The (Al) and (Ni) phases were described as one phase since they both have the fcc structure. Although the general topology of the experimentally determined phase diagram [21] is reproduced, major differences occur for the equilibria involving the  $\text{Al}_3\text{Ni}_2$  and AlNi phases. These differences are at least partially a result of ignoring the homogeneity range of the  $\text{Al}_3\text{Ni}_2$  phase and not considering the fact that AlNi is an ordered phase with CsCl structure.

In the second assessment by Ansara et al., [11] the sublattice-model description was introduced for the ordered phases with noticeable homogeneity ranges ( $\text{Al}_3\text{Ni}_2$ , AlNi, and  $\text{AlNi}_3$ ).

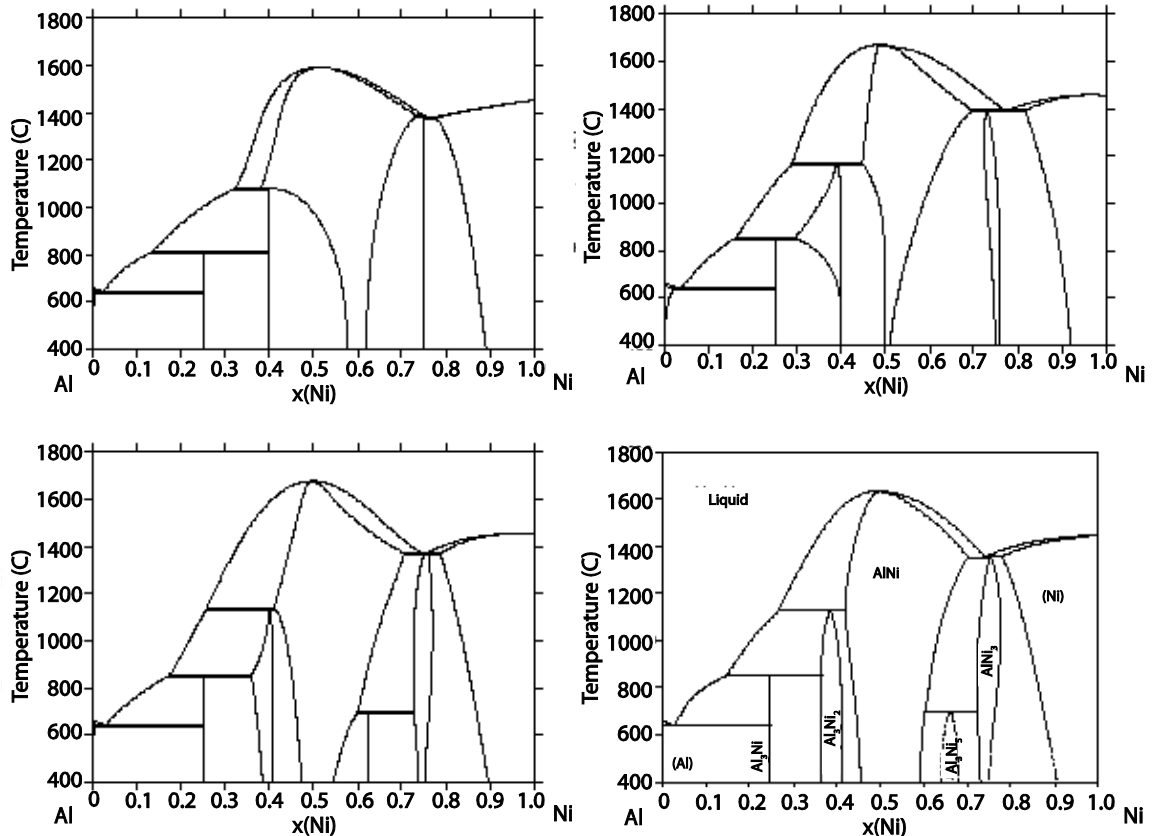


Figure 2-1 Different assessments of the Al-Ni system showing the progress made with the CALPHAD method: (2a) a 1978 assessment by Kaufman and Nesor, [20] (2b) a 1988 assessment by Ansara et al. [11] (2c) a 1997 assessment by Ansara et al. [12] and (2d) the evaluated experimental diagram [21].

The disordered fcc phase [(Al) and (Ni)] and the ordered L12 phase ( $\text{AlNi}_3$ ) were described with a single free-energy function as one phase that undergoes an order/disorder transformation. While the phase diagram calculated from these improved analytical descriptions shows better agreement with the observed diagram, some noticeable disagreement still remains. The range of the (Al) solid solution is overestimated, and the region of single-phase  $\text{AlNi}_3$  slants to the nickel-rich side at lower temperatures. Both problems likely result from describing all of these phases with the single function. It should be also noted that the region of single-phase  $\text{Al}_3\text{Ni}_2$  is overestimated at higher temperatures and underestimated at lower temperatures. This

may be caused by the substitutional sublattice model description used in this assessment. It has been experimentally observed that on the nickel-rich side of the nominal stoichiometry, nickel atoms fill structural vacancies; on the aluminum-rich side, nickel atoms are substituted by aluminum.

This has been considered in the most recent assessment by Ansara et al., [12] who also modified the model for the description of the order/disorder transformation mentioned above. This assessment also includes a description of the  $\text{Al}_3\text{Ni}_5$  phase as a stoichiometric compound, though its homogeneity range has been ignored. The phase diagram obtained from this assessment is in very good agreement with the observed diagram. It should be noted that the calculated phase diagram not only reproduces the experimentally observed phase diagram, but also provides the thermodynamic functions for extrapolation into higher order systems or use in the modeling of, for example, casting solidification.

A disadvantage of this iterative process with improved descriptions is that the descriptions used in previous assessments may be incompatible with newer assessments that are based on recently developed model descriptions. Despite this, significant progress has been made in recent years, and an increasing number of databases have become available for use with multicomponent systems.

#### **2.4. Computer software tools and databases**

A variety of software packages can be used for the calculation of phase diagrams, making it impossible to list all of them here. Frequently used software packages are ChemSage

[22], the so-called *Lukas* programs [8,15] , *MTDATA* [23] and *Thermo-Calc* [24]. Although all of these software packages can be used for the calculation of phase equilibria, their features and user interfaces differ. Most of the model descriptions used for alloy and ceramic systems are common to all these programs; however, not every package has other specific model descriptions (e.g., models for aqueous or polymer solutions). Another important feature of these software packages is the availability of a module for the optimization of the Gibbs energy functions. Such optimizing modules are available with *ChemSage* [25], the *Lukas* programs [15], and *Thermo-Calc* [26].

For the incorporation of phase-equilibria calculations into micromodeling (e.g., the modeling of diffusion processes), an interface must be created in which the important variables are transferred from one computer code segment to another. For the simulation of diffusional reactions, *Thermo-Calc* [26] has been interfaced with the package DICTRA [27]. A general interface (TQ interface) is available for *Thermo-Calc* and *ChemSage* [28].

#### **2.4.1. The Lukas program**

The Lukas program is one of the first dedicated optimizing programs for use by CALPHAD users. The two main forms of the program available are BINGSS and TERGSS, which are applicable to binary and ternary systems respectively. The original code involved the use of a Gaussian least-squares method (Zimmerman 1976) but later versions also include a method used by Marquardt (1963). The program separates the experimental measurements into three distinct types: calorimetric measurements (usually enthalpies), EMF and vapor pressure measurements (partial Gibbs energies), and phase diagram information.

For calorimetric measurements these equations are governed by the number of phases involved and the temperature of the measurement. If one phase only is programmed, the measured value describes the heat of formation of a phase from its pure components. As the enthalpy of the pure components is defined before the optimization takes place, there is only one unknown. The equation of error for two phases applies to enthalpies of melting and transformation. In such a case there are two unknowns; which are the enthalpies of the phases involved in the transformation. Enthalpy changes involving three phases can also be considered. For example, the enthalpy changes on mixing two liquids of different compositions. In this case the enthalpy of the two original liquids and the final liquid are needed.

For phase diagrams, a phase boundary is one end of a tie-line and, therefore, is dependent on the phase which exists at the other end of the tie-line. In a binary system, two independent measurements are therefore needed to define the tie-line. Ideally it would be desirable to have two compositions as independent variables giving rise to two independent equations of error. The Lukas program does this by making two equations but where the dependence of error on one of the measurements is weak. This is important if two concentrations have different accuracies.

EMF and vapor pressure measurements are dependent on the temperature, the number of phases involved and, importantly, the reference state of the component. The problem with the reference state is important as experimentally stated values of partial Gibbs energies will be dependent on this value.

Once the equations of errors are defined, “weighing factors”, in terms of estimated accuracy of the experiment, are included. These are either taken as the accuracy of the corresponding measurement estimated by the person doing the optimization. The error is then divided by these weighting factors to provide a dimensionless relative error for all types of experimental measurement. In addition to this, the sensitivity of the, measured value of changes in temperature and composition are considered.

If the Lukas program is run with all experimental data, including reasonable estimates for accuracy, it performs its fitting operation by assuming that errors arise from random effects rather than systematic inaccuracies. Systematic errors can be taken into account in at least two ways. Firstly, it is possible to ignore the particular experiments completely, and there is a command in the program which allows this to be done. Secondly, the estimated experimental error can be increased by increasing the corresponding value in the data file which contains the experimental information. Both routes emphasize that a purely mathematical approach to optimization is usually not possible and some form of personal judgement is required.

#### ***2.4.2. Thermo-Calc***

Thermo-Calc is a powerful and flexible software and database package for all kinds of phase equilibrium, phase diagram and phase transformation calculations and thermodynamic assessments; with its application-oriented interface, many types of process simulations can also be performed. It has been developed for complex heterogeneous interaction systems with strongly non-ideal solution phases [29,30] and can be applied to any thermodynamic system in the fields of chemistry, metallurgy,

material science, alloy development, geochemistry, semiconductors etc. depending on the kind of database it is connected to. It is based on the work of Mats Hillert [31] and makes use of a very general algorithm to find the equilibrium state of a system. The implementation of these ideas was made by Bo Jansson and is described in his thesis [32]. This technique allows much more flexibility for the user setting the external conditions for his equilibrium state than any other thermodynamic software. Thermo-Calc is for example the only software that allows explicit conditions on individual phase compositions or configuration whereas most software can handle conditions on the overall composition only. For example, activities and chemical potentials of the components, volumes, enthalpies, entropies etc can also be set as conditions. Many quantities that must be calculated by so called “target calculations”, i.e. a double minimization procedure, with other software can be calculated directly and much faster with Thermo-Calc. The flexible way to set conditions is particularly useful when Thermo-Calc is used as a subroutine package in application programs, for example in microstructure evolution or process simulations.

For diagram calculations the facility that each condition is set separately and that any condition can be used as axis variable means that Thermo-Calc can calculate innumerable types of diagrams. Thermo-Calc was designed originally for multi-component systems and all its facilities are available for systems with up to 40 components.

Thermo-Calc can use many different thermodynamic databases, especially those developed by SGTE.

General Databases with data for compounds and solutions include:

- SSUB: SGTE Substances database. Data for 5000 condensed compounds or gaseous species.
- SSOL: SGTE Solutions database. A general database with data for many different systems covering 78 elements and 600 solution phases.
- BIN: SGTE Binary Alloy Solutions database.

There are also other commercially available databases for specific alloy systems, eg. TTAI (aluminium), TTMg (magnesium), TTNi (Ni-based superalloys), TCFE (steels and ferritic alloys), TTTi (titanium) and SNOB (Spencer's Nobel Metals database).

#### ***2.4.3. Modules in Thermo-Calc***

Thermo-Calc consists of several modules for specific purposes and the various tasks the user may be interested to perform. The TDB module is used for retrieving databases or data files. The GES module is used for listing system information and thermodynamic/kinetic data, or interactively manipulating and entering such data. The POLY module can calculate various complex heterogeneous equilibria, and its post processor, the POST module; makes it possible to plot many kinds of phase diagrams and property diagrams. The PARROT module provides a useful and flexible tool for data evaluation and assessment of experimental data. The TAB module tabulates various properties for pure substances or mixtures or chemical reactions. Some special easy-to-use modules are also available within Thermo-Calc, which just require rather simple responses to some questions for performing certain types of calculation or simulation. The BIN and TERN modules are designed to plot phase diagrams and property diagrams for various binary and ternary systems respectively.

The POT module is used to illustrate gas speciation and partial pressures in gas-bearing interaction systems. The POURBAIX module is used to plot pH-Eh and other aqueous property diagrams for heterogeneous interactions involving complex aqueous solutions. The SCHEIL module is designed to simulate solidification processes where no kinetic description is needed, using the Scheil-Gulliver model. The REACTOR module is used to simulate mass transfer and energy transport in multi-staged steady-state processes. Thermo-Calc employs many comprehensive thermodynamic models for various materials and interfaces with a wide spectrum of assessed and validated databases for specific material systems. Thermo-Calc forms the basis for some other thermodynamic/kinetic software systems. The DICTRA program [33,34] described later on, is specially designed for simulating various diffusion-controlled phase transformation process

### **2.5. Assessment Technique**

The assessment methodology involves a critical assessment of the available literature. Since a system may be reassessed several times by the same user, it is very important to document the decisions made to optimize the work. The process of reassessing a system becomes easier if an assessment logbook is maintained. By combining the data available in literature with thermodynamic models, an analytical description is created and determination of adjustable model parameters is often done using the least-squares method. This technique is called an optimization. However, the least-squares method works well only if the scatter of experimental data is completely random. Non-randomly distributed deviations of some data may completely destroy the utility of the least-square method. They must be classified as systematic errors and excluded from the

optimization. Therefore subjective judgements are required and decisions have to be taken on the selection of data during the optimization. A schematic of an assessment procedure is shown in figure 2-2 [35].

### ***2.5.1. Literature search***

The first step of the optimization process is the literature search. It is very important to consider all the data that are available, so as to contribute to the optimization. Sometimes original data may contain more information than reported in tables and curves. The additional information can, however, still be extracted from the reported data, if the experimental method is well described in the publication. Experimental data here can be described as thermodynamic data; which include enthalpies, chemical potential measurements obtained by vapor pressure methods, etc., or phase diagram data (thermal analysis, metallography, X-ray diffraction, solidification-path experiments), crystal structure data, etc.

### ***2.5.2. Analysis of experimental data***

After data collection from literature, a good review of the system must be made. At this stage contradictory data sets may be noticed. These are most obvious when different values are reported for the same quantity (e.g. contradictory points of a solvus line of a binary system). It is impossible to give a general rule on how to select the best one of several contradictory sets of measurements. Contradictions between quantities obtained from different data sets maybe undetectable before running an optimization, but found after the first trials. For values such as temperature of invariant equilibria and standard enthalpies of formation, the best value for each of these quantities should be selected.

## **2.6. The PARROT program**

The PARROT program is integrated into the Thermo-Calc software package. With the PARROT program, it is possible to fit thermodynamic model parameters to all kinds of experimental information that can be measured at equilibrium, stable or metastable. Any kind of model parameter can be optimized, including magnetic and pressure-dependent parameters, in all models that have been implemented in the Gibbs Energy System (GES), which is also a part of Thermo-Calc. A special version of PARROT, can also optimize mobilities and activation energies for diffusion.

PARROT is not limited to binary systems but can handle experimental information for systems with up to twenty components. In practice systems with more than five components have never been used in an assessment and in most of these cases binary and ternary parameters only were adjusted to fit the multicomponent information. PARROT is a fully interactive program. It is possible to give all information about the system to be assessed directly from the keyboard to the program, but it is recommended that the user start by creating a number of text files for data and commands, of which the most important are the *setup file* and the *experimental file*. PARROT has a main module for manipulating the optimizing conditions and a special EDIT-EXPERIMENT module for

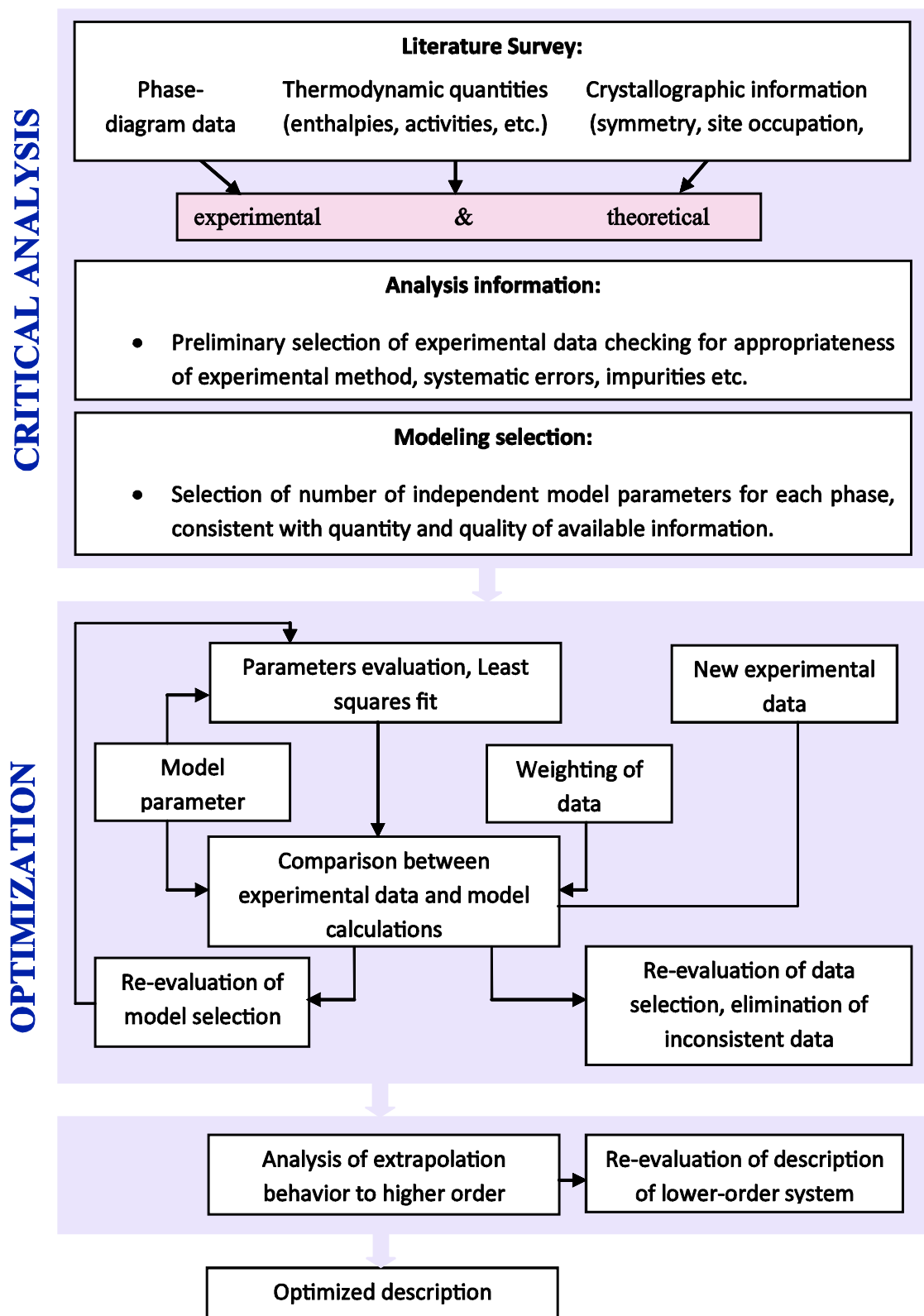


Figure 2-2 Schematic of CALPHAD assessment methodology [35].

manipulating each individual experimental equilibrium.

### ***2.6.1. The use of PARROT***

The assessor has to prepare a number of files that will be used during the assessment:

- POP file with experimental data,
- SETUP file with models and known and unknown parameters,
- EXP file with experimental data to be plotted, and
- MACRO files for quick calculation of various diagrams.

A simple description of the assessment can be described as follows:

1. Preparation of SETUP and POP and EXP file with a text editor
2. Starting PARROT and running the SETUP file once to create the work file usually called the PAR since its extension is “.PAR”. The PAR file is machine-dependent and cannot be read by a text editor. It can be manipulated only through the PARROT module. The PAR file always contains the last results and is automatically updated whenever it is used in PARROT. Whenever a user wants to “freeze” a reasonable set of model parameters but perhaps continue trying to change the weightings or set of model parameters, it is advisable to make a copy of the PAR file.
3. Compilation (COMPILE) of the POP file inside the PARROT module. The experiment data will be stored on the PAR file.
4. Selection of variables to optimize.

5. SET-ALTERNATE-MODE ON and optimize all equilibria until they have converged.
6. RESCALE the variables to set the start values to the final values.
7. Optimization and rescaling until no more changes occur.
8. SET-ALTERNATE-MODE OFF.
9. Calculation of diagrams and comparing the results with experimental data. This should be done whenever needed. The sum of errors is not a sufficient measure of the overall fit. A MACRO file should be used to calculate several diagrams.
10. Using the EDIT-EXPERIMENT module to COMPUTE-ALL equilibria. Some equilibria might not converge or may converge to results far away from the experimental data. Experimental data that cannot be calculated should have SET-WEIGHT zero. SAVE when finished with EDIT module.
11. Optimizing the variables zero times and checking the errors, using the LIST-RESULT command. This output will provide an overview of the current fit to all experimental data.
12. Optimizing and rescaling the variables until the calculation have converged. Some variables may be very large or very small. This may be due to lack of experimental information. The number of optimized variable may have to be increased or decreased.
13. Optimization may have to be carried out in “parts”, keeping the variables for some phases fixed and optimizing others with respect to selected sets of experimental data. The selections of experiments can be made in the EDIT module.

14. Several iterations might be necessary before the user is satisfied with the results. Various models have to be tried out for the phases and various numbers of variables for each phase.
15. A final optimization has to be carried out with all variables and all experiments with selected weightings.

### ***2.6.2. The POP file***

Experimental data on a system, taken from literature or measured by the assessor, should be written onto a file called “POP file”. The experimental equilibria and measurements are described with POLY commands, with some additional features.

The POP file is a very important form of documenting experimental data for a system. The POP file is intended to be self documenting and readable both to a human and to the computer. The experimental data are described independently of the models selected for the phases. It is possible to use the same POP file to assess a system using different models for the phases. It is not uncommon that a system must be reassessed some years later when new information is available. Since, the reassessment may be done by someone other than the original user; the POP file should be informative and well documented.

## **2.7. Thermodynamic Models for Solution Phases**

Thermodynamic modeling of solution phases is the crux of CALPHAD method. Calculations involving purely stoichiometric phases are very rare. Solution phases are defined as any phase in which there is solubility of more than component, and can be broken down to : (1) random substitutional, (2) sublattice, (3) ionic, and aqueous. These are the four major types which are currently available in CALPHAD software programs. For all solution phases the Gibbs energy is given by the general formula

$$G = G^0 + G_{mix}^{ideal} + G_{mix}^{xs} \quad (11)$$

where  $G^0$  is the contribution of the pure components of the phase to the Gibbs energy,  $G_{mix}^{ideal}$  is the ideal mixing contribution and  $G_{mix}^{xs}$  is the contribution due to non-ideal interactions between the components (Gibbs energy of mixing).

The random substitutional and sublattice models are closely related, as a phase with randomly occupied atoms on all sites can technically be considered as a phase containing a single sublattice and mathematically the same general equations used in both cases.

### ***2.7.1. Stoichiometric compounds***

The internal Gibbs energy of a pure species or stoichiometric compound is given by

$$G_{(T,P)} = H_{(T,P)} - TS_{(T,P)} \quad (12)$$

where  $H_{(T,P)}$  and  $S_{(T,P)}$  are the enthalpy and entropy as a function of temperature and pressure. Thermodynamic information is usually held in the databases using some polynomial function for the Gibbs energy which, for the case of the Scientific Group Thermodata Europe, is of the form

$$G_m(T) - H_m^{SER} = a + bT + cT \ln(T) + \sum_2^n d_n T^n \quad (13)$$

The left hand side of the equation is defined as the Gibbs energy relative to a standard element reference state (SER) where  $H_m^{SER}$  is the enthalpy of the element or substance in its defined reference state at 298.15K,  $a$ ,  $b$ ,  $c$ ,  $d_n$  are coefficients and  $n$  represents a set of integers, typically taking the values of 2, 3 and -1.

### ***2.7.2. Random Substitutional Models***

Random substitutional models are used for phases such as the gas phase or simple metallic liquid and solid solutions where components can mix on any spatial position which is available to the phase. For example, in a simple body-centered cubic phase any of the components could occupy any of the atomic sites which define the cubic structure.

In a gas or liquid phase the crystallographic structure is lost, but otherwise positional occupation of the various components relies on random substitution rather than any preferential occupation of site by any particular component.

### ***2.7.3. Simple mixtures***

#### ***2.7.3.1. Dilute solutions***

There are a number of areas in materials processing where low levels of alloying are important, for example in refining and some agehardening processes. In such cases it is possible to deal with solution phases by dilute solution models. These have the

advantage that there is a substantial experimental literature which deals with the thermodynamics of impurity additions, particularly for established materials such as ferrous and copper based alloys.

In a highly dilute solution, the solute activity coefficient ( $a_i$ ) is found to closely match a linear function of its concentration ( $x_i$ ). In its simplest form the activity can be defined as

$$a_i = \gamma_i^o x_i \quad (14)$$

where  $\gamma_i^o$  is the value of the activity coefficient of  $i$  at infinite dilution. This is known as Henry's law. The partial free energies can be depicted as

$$\bar{G} = \bar{G}_i^{xs} + RT \log_e x_i \quad (15)$$

where  $\bar{G}_i^{xs}$  has a constant value in the Henrian concentration range and can be obtained directly from  $\gamma_i^o$ . The expression can also be modified to take into account interactions between the solute elements and the above equation can be written as

$$\bar{G}_i = \bar{G}_i^{xs} + RT \log_e x_i + RT \sum_j \varepsilon_i^j x_j \quad (16)$$

where  $x_i$  is the concentration of solute  $i$  and  $\varepsilon_i^j$  is an interaction parameter taking into account the effect of mixing of component  $i$  and  $j$  in the solvent.

### 2.7.3.2. Ideal solutions

An ideal substitutional solution is characterized by the random distribution of components on a lattice with an interchange energy equal to zero. The entropy due to

configuration is easily calculated and is related to the probability of interchange of the components. The configurational entropy  $S^{conf}$  is given by

$$S^{conf} = k \log_e W_p \quad (17)$$

where  $k$  is Boltzmann's constant and  $W_p$  is the number of components in the system. For one of the components  $N$  is equal to Avogadro's number. From Stirling's formula,  $S^{conf}$  can be

$$S^{conf} = -k \sum_i n_i \log_e \frac{n_i}{N} \quad (18)$$

The ideal molar entropy of mixing is then given by

$$S_{mix}^{ideal} = -Nk \sum_i x_i \log_e x_i \quad (19)$$

where  $x_i$  is the mole fraction of component  $i$ . With the assumption that the interchange energy is zero it is possible to substitute the atoms without changing the energy of that state and ideal mixing can be described as

$$G_{mix}^{ideal} = -TS_{mix}^{ideal} = RT \sum_i x_i \log_e x_i \quad (20)$$

where  $R$  is the gas constant. The Gibbs energy of an ideal solution phase will then be

$$G_m = \sum_i x_i G_i^o + RT \sum_i x_i \log_e x_i \quad (21)$$

where  $G_i^o$  is the Gibbs energy of the phase containing the pure component  $i$ .

### 2.7.3.3. Non-ideal solutions; regular and non-regular solution models

The regular solution model is the simplest of the non-ideal models and basically considers that the magnitude and sign of interactions between the components in a phase are independent of composition. Assuming the total energy of the solution ( $E_o$ ) arises from only nearest-neighbors bond energies  $E_0$  in a system  $A$ - $B$  then

$$E_0 = \omega_{AA}E_{AA} + \omega_{BB}E_{BB} + \omega_{AB}E_{AB} \quad (22)$$

where  $\omega_{AA}$ ,  $\omega_{BB}$ ,  $\omega_{AB}$ ,  $E_{AA}$ ,  $E_{BB}$  and  $E_{AB}$  are the number of bonds and energies associated with the formation of different bond types  $AA$ ,  $BB$  and  $AB$ . If there are  $N$  atoms in solution and the co-ordination number of the nearest neighboring atoms in the crystal structure is  $z$ , the number of bond types being formed in a random solution is

$$\begin{aligned} \omega_{AA} &= \frac{1}{2}Nzx_A^2 \\ \omega_{BB} &= \frac{1}{2}Nzx_B^2 \\ \omega_{AB} &= Nzx_Ax_B \end{aligned} \quad (23)$$

where  $x_A$  and  $x_B$  are the mole fractions of  $A$  and  $B$ .

If the reference states are taken as  $A$  and  $B$ , then enthalpy of mixing is given by

$$H_{mix} = \frac{Nz}{2} x_A x_B (2E_{AB} - E_{AA} - E_{BB}) \quad (24)$$

If the bond energies are temperature dependent there will also be excess entropy of mixing leading to the regular solution model for the Gibbs excess energy of mixing

$$G_{mix}^{xs} = x_A x_B \Omega \quad (25)$$

where  $\Omega$  is temperature dependent interaction parameter. When added to Gibbs energy of an ideal solution phase the equation becomes;

$$G_m = \sum_i x_i G_i^o + RT \sum_i x_i \log_e x_i + \sum_i \sum_{j>1} x_i x_j \Omega_{ij} \quad (26)$$

However, the assumption of composition-independent interactions is too simplistic. This led to the development of the sub-regular solution model, where interaction energies are considered to change linearly with composition. The following expression for  $G_{mix}^{xs}$  is then obtained as (Kaufman and Bernstein 1970).

$$G_{mix}^{xs} = x_i x_j (\Omega_{ij}^i x_i + \Omega_{ij}^j x_j) \quad (27)$$

A general formula in terms of a power series provides the capability to account for most types of composition dependence (Tomiska 1980). The most method is based on the Redlich-Kister equation, and the above equation can be expanded to

$$G_m = \sum_i x_i G_i^o + RT \sum_i x_i \log_e x_i + \sum_i \sum_{j>1} x_i x_j \sum_v \Omega_{ij}^v (x_i - x_j)^v \quad (28)$$

where  $\Omega_{ij}^v$  is a binary interaction parameter dependent on the value of  $v$ . The above equation for  $G_{mix}^{xs}$  becomes regular when  $v=0$  and sub-regular when  $v=1$ . In practice the value of  $v$  does not rise above 2.

The above equation assumes ternary interactions to be small in comparison to those which arise from the binary terms. This may not always be the case and where evidence

for higher-order interactions is evident these can be taken into account by a further term of the type  $G_{ijk} = x_i x_j x_k L_{ijk}$  where  $L_{ijk}$  an excess ternary interaction parameter.

## **2.8. The extrapolation of Gibbs excess energy to multi-component systems**

Most methods of extrapolating the thermodynamic properties of alloys into multi-component systems are based on the summation of the binary and ternary excess parameters. Three main methods are proposed to demonstrate this principle.

### *Muggianu's equation*

In this circumstance the excess energy in a multi-component system expands to

$$G_{mix}^{xs} = x_A x_B (L_{AB}^0 + L_{AB}^1 (x_A - x_B)) + x_B x_C (L_{BC}^0 + L_{BC}^1 (x_B - x_C)) + x_A x_C (L_{AC}^0 + L_{AC}^1 (x_A - x_C))$$

### *Kohler's equation*

In the Kohler equation (Kohler 1960)  $G_{mix}^{xs}$  is described by

$$\begin{aligned} G_{mix}^{xs} = & (x_A + x_B)^2 \frac{x_A}{x_A + x_B} \cdot \frac{x_B}{x_A + x_B} \left( L_{AB}^0 + L_{AB}^1 \left( \frac{x_A - x_B}{x_A + x_B} \right) \right) \\ & + (x_B + x_C)^2 \frac{x_B}{x_B + x_C} \cdot \frac{x_C}{x_B + x_C} \left( L_{BC}^0 + L_{BC}^1 \left( \frac{x_B - x_C}{x_B + x_C} \right) \right) \\ & + (x_A + x_C)^2 \frac{x_A}{x_A + x_C} \cdot \frac{x_C}{x_A + x_C} \left( L_{AC}^0 + L_{AC}^1 \left( \frac{x_A - x_C}{x_A + x_C} \right) \right) \end{aligned} \quad (29)$$

*Toop's equation*

Both the Muggianu and Kohler equations can be considered symmetrical as they treat the components in the same way and do not differentiate between them. Toop's equation is essentially different in that it considers one of the binary systems does not behave the same way as the others and the extrapolation is based essentially on two of the binaries having identical mole-fraction products with the mole-fraction products of the third being different. For a sub-regular solution Toop's equation breaks down to

$$G_{mix}^{xs} = x_A x_B (L_{AB}^0 + L_{AB}^1 (x_A - x_B - x_C)) + x_A x_C (L_{AC}^0 + L_{AC}^1 (x_A - x_C - x_B)) + x_B x_C \left( L_{BC}^0 + L_{BC}^1 \left( x_B - x_C + \frac{x_B - x_C}{x_B + x_C} x_A \right) \right) \quad (31)$$

The geometrical representation of the Muggianu, Kohler and Toop equations is best summarized using the figure 2-3.

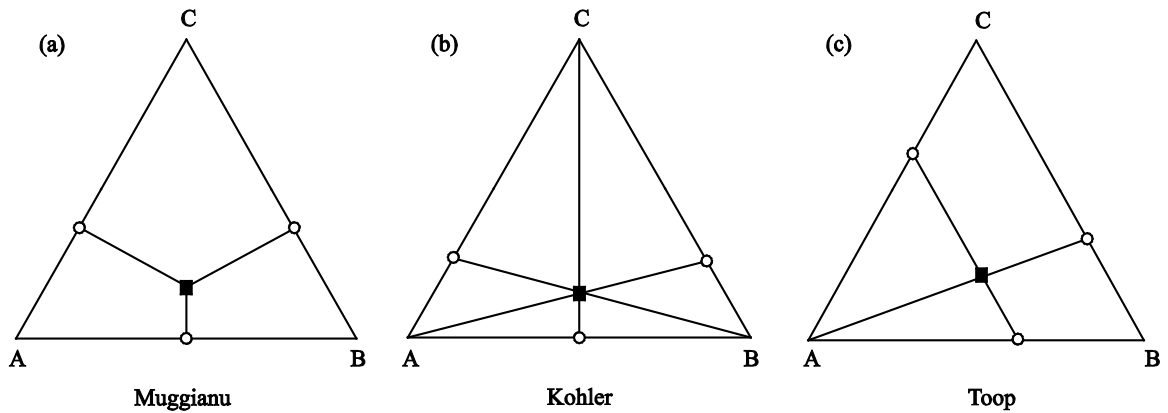


Figure 2-3. Geometrical constructions of (a) Muggianu, (b) Kohler and (c) Toop models

## References:

- 
- 1 A.T. Dinsdale, *CALPHAD*, 15 (1991), pp. 317-425.
  - 2 J.H. Hildebrand, *J. Amer. Chem. Soc.*, 51 (1929), pp. 66-80.
  - 3 M. Hillert and L.-I. Staffansson, *Acta Chem. Scand.*, 24 (1970), pp. 3618-3626.
  - 4 F. Sommer, *Z. Metallkd.*, 73 (1982), pp. 72-76.
  - 5 C. Wagner und W. Schottky, *Z. Phys. Chem.*, B11 (1930), pp. 163-210.
  - 6 W.L. Bragg and E.J. Williams, *Proc. Royal Soc. A, London*, 145 (1934), pp. 699-730; 151 (1935), pp. 540-566.
  - 7 O. Redlich and A.T. Kister, *Indust. Eng. Chem.*, 40 (1948), pp. 345-348.
  - 8 H.L. Lukas, J. Weiss, and E.-Th. Henig, *CALPHAD*, 6 (1982), pp. 229-251.
  - 9 B. Sundman and J. Ågren, *J. Phys. Chem. Solids*, 42 (1981), pp. 297-301.
  - 10 J.-O. Andersson et al., *Acta Metall.*, 34 (1986), pp. 437-445.
  - 11 I. Ansara, B. Sundman, and P. Willemin, *Acta Metall.*, 36 (1988), pp. 977-982.
  - 12 I. Ansara et al., *J. Alloys Compd.*, 247 (1997), pp. 20-30.
  - 13 S.-L. Chen, C.R. Kao, and Y.A. Chang, *Intermetallics*, 3 (1995), pp. 233-242.
  - 14 M. Hillert, *Physica*, 103B (1981), pp. 31-40.
  - 15 H.L. Lukas, E.-Th. Henig, and B. Zimmermann, *CALPHAD*, 1 (1977), pp. 225-236.
  - 16 D.W. Marquardt, *J. Soc. Indust. Appl. Math.*, 11 (1963), pp. 431-441.
  - 17 E. Königsberger, *CALPHAD*, 15 (1991), pp. 69-78.
  - 18 M. Hillert, *CALPHAD*, 4 (1980), pp. 1-12.
  - 19 Y.-M. Muggianu, M. Gambino, and L.P. Bros, *J. Chim. Phys.*, 72 (1975), pp. 85-88.
  - 20 L. Kaufman and H. Nesor, *CALPHAD*, 2 (1978), pp. 325-348.
  - 21 H. Okamoto, *J. Phase Equilibria*, 14 (1993), pp. 257-259.
  - 22 G. Eriksson and K. Hack, *Metall. Mater. Trans. B*, 21B (1990), pp. 1013-1023.
  - 23 R.H. Davies et al., *Applications of Thermodynamics in the Synthesis and Processing of Materials*, eds. P. Nash and B. Sundman (Warrendale, PA: TMS, 1995), pp. 371-384.
  - 24 B. Sundman, B. Jansson, and J.-O. Andersson, *CALPHAD*, 9 (1985), pp. 153-190.
  - 25 E. Königsberger and G. Eriksson, *CALPHAD*, 19 (1995), pp. 207-214.
  - 26 B. Sundman, *User Aspects of Phase Diagrams*, ed. F.H. Hayes (London, UK: Institute of Metals, 1991), pp. 130-139.
  - 27 J. Ågren, *ISIJ International*, 32 (1992), pp. 291-296.
  - 28 G. Eriksson, H. Sippola, and B. Sundman, *CALPHAD*, 18 (1994), pp. 345-345.
  - 29 B. Sundman, B. Jansson and J.-O. Andersson, *CALPHAD*, 9 (1985) 153.
  - 30 B. Sundman, *Anales de Fisica, Serie B*, 86 (1990) 69.
  - 31 M. Hillert *Phase Equilibria Phase Diagrams and Phase Transformations*, (1999) Cambridge Univ. Press ISBN 0-521-56270-8.
  - 32 B. Jansson, Thesis (1984) Royal Institute of Technology, Stockholm, Sweden.
  - 33 J.-O. Andersson, L. Hoglund, B. Jonsson, J. Ågren in *Fundamentals and Applications of Ternary Diffusion*, G.R. Purdy, Editor, Pergamon Press, New York (1990) 153.
  - 34 T. Helander and J. Ågren, *Metall. Mater. Trans. A*, 28A, (1997) 303
  - 35 H.L. Lukas, S.G. Fries, B. Sundman, "Computational Thermodynamics", Cambridge University Press, 2007.

## Chapter III $\infty$ Ternary phase diagram calculations of pentaerythritol(PE)-pentaglycerine(PG)-neopentylglycol(NPG) system

---

### **Summary**

The pentaerythritol(PE)-pentaglycerine(PG)-neopentylglycol(NPG) ternary system has been thermodynamically assessed using the CALPHAD method and Thermo-Calc software. The PE-PG, PG-NPG, PE-NPG binary systems have also been calculated using CALPHAD on the basis of reported binary experimental data. The solution phases are modeled as substitutional solutions, in which the excess Gibbs energies are expressed by the Redlich-Kister-Muggianu polynomial. The PE-NPG binary phase diagram was modeled using Henrian solution model, and the liquid phase was assumed ideal. The PG-NPG system was optimized using regular and sub-regular solution models and show invariant equilibria at 298K. The PE-NPG binary system was calculated from room temperature to the liquid phase temperatures. The modeled phase diagrams and the experimental data are in good agreement. A set of self consistent thermodynamic parameters formulating the Gibbs energies of various phases in the PE-PG-NPG ternary system are obtained in the present work. Thermodynamic properties, several vertical and isopleth sections have been calculated and are in good agreement with experimental data.

### **3.1. Introduction**

Increasing global energy demands, and depletion of available energy resources, warrant the need for alternate energy solutions. In many parts of the world, direct solar radiation is considered to be one of the most prospective sources of energy. Solar energy is available only during the day, and hence, its accrual requires efficient thermal energy storage so that the excess heat collected during sunshine hours may be stored for later use during the night. Amongst the solid-solid heat storage materials, the most promising heat storage materials are organic polyalcohol globular molecular crystals (with orientational disorder in the energy storing phase) that are being studied as potential passive thermal energy storage materials. These are sometimes referred to as “plastic crystals” and undergo crystallographic changes, absorbing or releasing large amounts of solid state latent heat at temperatures well below their melting points. The main property of these advanced materials is energetic solid-solid phase transitions, rather than solid-liquid phase transitions, which make them potential candidates for dry walls and Trombe walls and other thermal energy storage applications. There are relatively few known polyalcohols that have energetic solid-solid transitions typically well above room temperature. To develop practical thermal energy storage materials, adjustment of phase transition temperatures is achieved by using binary and ternary combinations of these materials. In the past binaries have been used to lower the solid-solid phase transition temperatures, more recently ternaries are being explored for this purpose. NPG

(neopentylglycol,  $C_5H_{12}O_2$ ), PE (pentaerythritol,  $C_5H_{12}O_4$ ), TAM (trihydroxymethylaminomethane,  $C_4H_{11}O_3N$ ) etc. are extensively studied among the polyalcohols [1-9].

Timmermans [10] reported observing very small entropy of fusion in these organic crystals, and classified them as globular molecules with symmetry around the center of rotation, similar to a sphere of rotation around an axis in cyclohexane. These molecules undergo phase transformations from a layered or chained low temperature structure to orientationally disordered isotropic high temperature cubic phase (plastic phase) [10-12]. Examples of these 'plastic crystals' include pentaerythritol [PE:  $C(CH_2OH)_4$ ], pentaglycerine [PG:  $(CH_3)C(CH_2OH)_3$ ], neopentylglycol [NPG:  $(CH_3)_2C(CH_2OH)_2$ ], tris(hydroxymethyl)aminomethane [TRIS:  $(NH_2)C(CH_2OH)_3$ ], and 2-amino-2-methyl-1,3-propanediol [AMPL:  $(NH_2)(CH_3)C(CH_2OH)_2$ ].

The molecular structures of PE, PG and NPG are shown in Figure 3-1. Nita et al. determined crystallographic properties of PE in 1938 [13]. Eilerman et al. [14] also reported several important crystallographic details. Chandra et al. determined high temperature structural details of PE and NPG using Guinier diffraction system [15, 16].

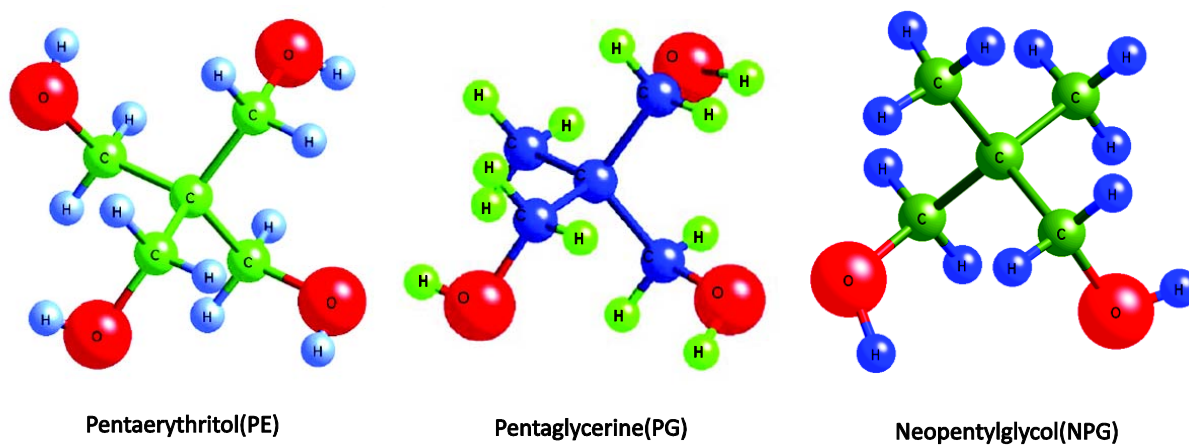


Figure 3-1. Molecular structures of PE, PG and NPG

To adjust the phase transition temperature to suit particular applications binary or ternary solid solutions of these compounds are required [8]. Mixtures of polyalcohols undergoing solid-solid phase transitions have been studied by Benson et al. [3] primarily to determine the effect of mixing on the transition temperatures. A comparative study of thermal energy storage capacity of PE-PG, PG-NPG, and PE-NPG binary systems has been conducted by Barrio et al [17]. Chandra et al. [17, 18] also reported significant decreases in the transition temperature of PE (to room temperature) by using binary PG-NPG materials. Experimental phase diagrams started appearing in the early 1990s for various binary polyalcohol systems. Various groups, including our group, have reported partial and complete phase diagrams of PE-PG, PE-NPG, PG-NPG, PG-AMPL, NPG-AMPL, TRIS-AMPL, NPG-TRIS, PG-TRIS, and PE-TRIS [17, 19-34]. Chandra et al. [34] determined the phase diagram for the PG-NPG binary from DSC and XRD studies in 1989. In 1990 Barrio et al. [36] also reported a phase diagram on the PG-NPG binary. The PE-PG binary was also reported by Barrio et al. in 1990 [37]. In 2011 Singh [35], ternary polyalcohol calorimetric and x-ray diffraction experimental studies were carried out on the PE-PG-NPG system. To our knowledge, PE-PG-NPG ternary phase diagrams have never been calculated using the CALPHAD method. This work aims at creating a calculated PE-PG-NPG ternary phase diagrams.

As part of this study the phase diagram of the PE-NPG, PG-NPG and PE- PG binary systems have been calculated from available experimental data in the literature. These calculated binary phase diagrams are then used to calculate thermodynamic parameters of the PE-PG-NPG ternary system. Ternary phase diagrams as well as selected isopleths are presented in this paper.

## **3.2. Experimental data from literature**

### ***3.2.1. Thermodynamic properties of pure PE, PG and NPG***

Enthalpies and phase transition temperatures for pure PE, PG and NPG used for calculations were taken from Eilerman et. al. [14]. The melting temperature of pure NPG used in the calculations is 126°C (399K) [39]. This value is lower than that reported in recent literature 129.8°C (402.8K) [39], but the value is close to that reported by Sigma-Aldrich Company. Table 1 shows the thermodynamic properties of PE, PG and NPG [14].

### ***3.2.2. Binary Phase Diagram Data***

The PE-NPG binary phase diagram is reported by different groups with significant differences in their observations [17, 40, 41]. Barrio et al. [42] reported the existence of an intermediate cubic phase. They reported an invariant temperature as 70.6°C (343.6K), produced by the presence of a new phase. Teisseire et al. [41] also developed the PE-NPG binary phase diagram using calorimetry and x-ray diffraction but they did not notice the presence of an intermediate cubic phase as reported by Barrio et al. [42].

Table 3-1: Crystal structure, transition temperatures and thermal properties of NPG, AMPL and PE [14]

Compound	Low temp. phases	T <sub>TR</sub> (K)	ΔH <sub>TR</sub> (J/mol)	ΔS <sub>TR</sub> (J/mol K)	High temp. phases	T <sub>F</sub> (K)	ΔH <sub>F</sub> (J/mol)	ΔS <sub>F</sub> (J/mol K)
PG	Tetragonal	354	23120	65.29	FCC	471	5430	11.54
NPG	Monoclinic	313	13630	43.22	FCC	399	4600	11.83
PE	Tetragonal	461	41260	90.25	FCC	533	5020	9.45

Barrio et al. [42] have reported the presence of five invariant lines and the existence of an intermediate cubic phase, in a narrow concentration region. The intermediate cubic phase was reported as FCC ( $a=8.871$  at 353K) and the appearance of the five domains at 353K accounted for the existence of a peritectic invariant temperature. Due to uncertainties the PE-NPG binary in the present work has been calculated and optimized using experimental data from Chandra et al. [40]. A PG-NPG binary phase diagram has been proposed by Barrio et al. [37] in 1990, as well as Chandra et al. [34] in 1989. Chandra et al. [34] reported the solid-solid transformation occurs at 89°C (362K) in pure PG, at 40°C (313K) in pure NPG which lowered to 24°C (297K) due to eutectoidal transformation from the  $\gamma \rightarrow \alpha + \beta$ , at 75 mol% NPG in PG-NPG system. Barrio et al. [36] also reported similar results with a eutectoid invariant at 25°C (298K), at composition of 71 mole% NPG. They observed solid-liquid Gibbs minimum at 106.6°C (379.6K) at 0.21 molar fraction of PG. For optimizing the calculated PG-NPG binary in the present work experimental data from Barrio et al. [37] has been used. Both the above mentioned published phase diagrams were produced from thermal and x-ray diffraction analyses. Optimization of the PE-PG binary was carried out based on experimental data of Barrio et al. [37]. It should be noted that experimental data here imply invariant equilibria, tie-lines, phase transformation temperatures etc. and not activities of the systems.

### **3.3. Thermodynamic Modeling**

To facilitate reading the symbols used to denote the phases in the PE-PG-NPG system are listed in Table 3-2. For the present purpose only the significant features of the thermodynamic parameters are described. PE is represented by “A”, PG is represented

by “B” and NPG is represented by “C” for simplification. The low temperature phases are characterized by  $\alpha$ , or  $\beta$ , the high temperature phases are designated as  $\gamma'$  or  $\gamma$ . The FCC  $\gamma'$  denotes the high temperature PE rich phase, the high temperature PE-PG solid solution and the high temperature PG-NPG solid solution. Whereas, FCC  $\gamma$  denotes the high temperature NPG rich phase. If the reference state for each phase is taken to be that of the pure components in that phase, then the Gibbs energy of a solution phase  $\phi$  ( $\phi = \alpha, \beta, \gamma', \gamma, L$ ) can be represented as follows (unit of Gibbs energy is  $\text{J mol}^{-1}$  throughout this work, where mol is a mole of formula unit):

$$G^\phi = x_A {}^0G_A^\phi + x_B {}^0G_B^\phi + x_C {}^0G_C^\phi + RT(\ln x_A + \ln x_B + \ln x_C) + G^{EX,\phi} \quad (1)$$

Where  $\phi = \alpha, \beta, \gamma, \gamma', L$ ,  $R = 8.314 \text{ J mol}^{-1} \text{ K}^{-1}$ ,  $x_A$  is the mole fraction of “A”,  $x_B$  is the mole fraction of “B” and  $x_C$  is the mole fraction of “C”.  ${}^0G_A^\phi$ ,  ${}^0G_B^\phi$  and  ${}^0G_C^\phi$  are the pure component Gibbs energies in  $\phi$ .

Table 3-2: List of symbols to denote the phases in the ternary PE-PG-NPG system.

Symbol	Phase
Liq or L	Liquid
$\alpha$	Low temperature PE phase, low temperature PE-PG (solid solution) phase
$\beta$	Low temperature NPG phase
$\gamma'$	High temperature PE rich phase(PE-NPG), high temperature PE-PG phase (PE-PG solid solution)
$\gamma$	High temperature NPG rich phase(PE-NPG)

The binary interaction parameter  $L_{i,j}^{\phi}$  can be expressed as follows:

$$L_{i,j}^{\phi} = \sum_{n=0}^m {}^n L_{i,j}^{\phi} (x_i - x_j) \quad (2)$$

The ternary excess Gibbs free energy is written as follows:

$$G^{EX,\phi} = x_A^{\phi} x_B^{\phi} x_C^{\phi} (x_A^{\phi 0} L_{A,B,C}^{\phi} + x_B^{\phi 0} L_{A,B,C}^{\phi} + x_C^{\phi 0} L_{A,B,C}^{\phi}) \quad (3)$$

The binary and the ternary interaction parameters  ${}^n L_{i,j}^{\phi}$  and  ${}^n L_{i,j,k}^{\phi}$  take the following form of a power series:

$${}^n L_m^{\phi} = a + bT + cT \ln(T) + dT^2 + eT^{-1} + fT^3 + gT^7 + hT^9 \quad (4)$$

where  $a, b, c, d, e, f, g$  and  $h$  are the excess Gibbs energy parameters. In most cases only the first two terms of the above equation are used.

### ***Reference States***

For a phase  $\phi$  ( $\phi = \alpha, \beta, \gamma, \gamma', L$ ),  ${}^0 G_A^{\phi}$ ,  ${}^0 G_B^{\phi}$  and  ${}^0 G_C^{\phi}$  are the reference states of pure “A”, “B” and “C”, same as  $\phi$ . A single reference phase is chosen for each component and expressed the pure component Gibbs energies of other phases as changes from this reference phase. We chose  $\alpha$  for “A”,  $\beta$  for “B” and  $\alpha$  for “C” and set them equal to zero. This assumption is made only for the calculation of metastable phases. The enthalpy of formation of the polyalcohols has been calculated using Joback’s group contribution method and is accounted for while entering data of the respective compounds. The low temperature phase is considered as  $\alpha$  for the PE rich region in PE-NPG binary as well as

PE-PG solid solution (low-temperature) in PE-PG binary, as it is assumed that they will form a single phase when extrapolated into a ternary system. This assumption was made on the basis of the binaries and the crystal structure of the respective polyalcohols (tetragonal at low temperatures: PE and PG). Similar assumptions were also made for the high temperature phases depending on the crystal structure. NPG is denoted as a separate  $\beta$  phase as it forms a separate low temperature phase in case of the PE-NPG binary. The high temperature phases are denoted by  $\gamma$  and  $\gamma'$  as the crystal structure of PE, PG and NPG are face centered cubic (FCC) at high temperatures. So, it is predicted that the solid solution (high temperature) of PE-PG, PG-NPG and high temperature phase for PE-NPG (PE rich) forms a single phase.

Thus,

$${}^0G_A^\alpha = 0, {}^0G_B^\beta = 0 \text{ and } {}^0G_C^\alpha = 0 \quad (5)$$

The binary phase diagrams are calculated first and the ternary diagram is predicted using the Gibbs energy equations of the binary phases. For system A-B (PE-NPG), the Gibbs energies of the other phases in terms of the reference phases can be represented as:

$${}^0G_A^{\gamma'} = {}^0G_A^\alpha + \Delta {}^0G_A^{\alpha \rightarrow \gamma'} = \Delta {}^0G_A^{\alpha \rightarrow \gamma'} \quad (6)$$

$${}^0G_A^L = {}^0G_A^\alpha + \Delta {}^0G_A^{\alpha \rightarrow L} = \Delta {}^0G_A^{\alpha \rightarrow \gamma'} + \Delta {}^0G_A^{\alpha \rightarrow L} \quad (7)$$

$${}^0G_B^{\gamma'} = {}^0G_B^\beta + \Delta {}^0G_B^{\beta \rightarrow \gamma'} = \Delta {}^0G_B^{\beta \rightarrow \gamma'} \quad (8)$$

$${}^0G_B^L = {}^0G_B^\beta + \Delta {}^0G_B^{\beta \rightarrow L} = \Delta {}^0G_A^{\beta \rightarrow \gamma'} + \Delta {}^0G_B^{\beta \rightarrow L} \quad (9)$$

For component ‘‘A’’ the Gibbs energies of the stable phases are:

$${}^0G_A^{\gamma} = {}^0G_A^{\alpha} + \Delta {}^0G_A^{\alpha \rightarrow \gamma} = \Delta {}^0G_A^{\alpha \rightarrow \gamma} \quad (10)$$

$${}^0G_A^{\gamma} = \Delta H_{TR} - T\Delta S_{TR} + \int_{T_{TR}}^T \Delta C_P^{\alpha \rightarrow \gamma} dT - T \int_{T_{TR}}^T \frac{\Delta C_P^{\alpha \rightarrow \gamma}}{T} dT + \Delta H_F - T\Delta S_F + \int_{T_F}^T \Delta C_P^{\gamma \rightarrow L} dT - T \int_{T_F}^T \frac{\Delta C_P^{\gamma \rightarrow L}}{T} dT \quad (11)$$

$${}^0G_A^L = {}^0G_A^{\alpha} + \Delta {}^0G_A^{\alpha \rightarrow L} = \Delta {}^0G_A^{\alpha \rightarrow \gamma} + \Delta {}^0G_A^{\alpha \rightarrow L}$$

$${}^0G_A^L = \Delta H_{TR} - T\Delta S_{TR} + \int_{T_{TR}}^T \Delta C_P^{\alpha \rightarrow \gamma} dT - T \int_{T_{TR}}^T \frac{\Delta C_P^{\alpha \rightarrow \gamma}}{T} dT \quad (12)$$

Similar expressions can be obtained for Gibbs energies of stable phases of ‘‘B’’ and ‘‘C’’.

The Gibbs energies for metastable phases in binary systems are calculated using the stable phases as seen in previous calculations by Chellappa et al. [43]. For example, for ‘‘B’’ in  $\alpha$  phase (B-C system), the difference,  ${}^0G_B^{\alpha} - {}^0G_B^{\beta}$  is determined such that the following equation can be expressed to calculate the metastable phases ( $M_A^{\beta}$ ,  $M_B^{\alpha}$  etc.),

$${}^0G_B^{\alpha} = {}^0G_B^{\beta} + M_B^{\alpha} \quad (13)$$

The Gibbs energy of the  $\alpha$  phase,  $G_m^{\alpha}$ , can now be written as:

$$G_m^{\alpha} = x_B ({}^0G_B^{\beta} + M_B^{\alpha}) + x_C {}^0G_C^{\alpha} + RT(x_B \ln x_B + x_C \ln x_C) + G^{EX,\alpha}$$

$$G_m^{\alpha} = x_B M_B^{\alpha} + RT(x_B \ln x_B + x_C \ln x_C) + G^{EX,\alpha} \quad (14)$$

To estimate  $M_A^{\beta}$ ,  $M_B^{\alpha}$  etc., we assume that  $\alpha$  and  $\beta$  phases are ideal solutions. Therefore,

the partial molar Gibbs free energies can be written as:

$$\begin{aligned} G_B^\beta &= {}^0G_B^\beta + RT \ln(x_B^\beta) \\ G_B^\alpha &= {}^0G_B^\alpha + RT \ln(x_B^\alpha) \end{aligned} \quad (15)$$

Where,  $G_B^\beta$  and  $G_B^\alpha$  are the Gibbs energies of “B” in the  $\beta$  and  $\alpha$  phases respectively. At equilibrium,  $G_B^\beta = G_B^\alpha$ , it is reasonable to assume that at the temperature of maximum solubility,  $T=T_{\max}$ ,

$$\begin{aligned} {}^0G_B^\alpha &= {}^0G_B^\beta + RT_{\max} \ln\left(\frac{x_{B(\max)}^\beta}{x_{B(\max)}^\alpha}\right) \\ {}^0G_B^\alpha &= RT_{\max} \ln\left(\frac{x_{B(\max)}^\beta}{x_{B(\max)}^\alpha}\right) \\ M_B^\alpha &= RT_{\max} \ln\left(\frac{x_{B(\max)}^\beta}{x_{B(\max)}^\alpha}\right) \\ &= 8.314 \times 298 \times \ln\left(\frac{0.899}{0.601}\right) \\ &= 997.68J / mol \end{aligned}$$

A similar estimation can be made for  $M_C^\beta$  and is given by,

$$\begin{aligned} M_C^\beta &= RT_{\max} \ln\left(\frac{x_{C(\max)}^\alpha}{x_{C(\max)}^\beta}\right) \\ M_B^{\gamma'} &= RT_{\max} \ln\left(\frac{x_{B(\max)}^{\gamma'}}{x_{B(\max)}^{\gamma}}\right) \\ &= 8.314 \times 462.7 \times \ln\left(\frac{0.51}{0.36}\right) = 1340J / mol \end{aligned}$$

Similarly,

$$\begin{aligned}
M_B^{\gamma} &= RT_{\max} \ln \left( \frac{x_{A(\max)}^{\gamma}}{x_{A(\max)}^{\beta}} \right) \\
&= 8.314 \times 462.7 \times \ln \left( \frac{0.64}{0.49} \right) \\
&= 1028J / mol \\
M_c^{\beta} &= RT_{\max} \ln \left( \frac{x_{A(\max)}^{\beta}}{x_{A(\max)}^{\alpha}} \right) \\
&= 8.314 \times 298 \times \ln \left( \frac{0.399}{0.101} \right) = 3403.78J / mol
\end{aligned}$$

Table 3-3 shows the Gibbs energy expressions for the PE-PG-NPG ternary system. The assumption that  $\alpha$  and  $\beta$  phases are ideal solutions is used only to describe the metastable pure Gibbs energies  ${}^0G_B^{\alpha}$  and  ${}^0G_C^{\beta}$ .

The nature of non-ideality of  $\alpha$  phase can still be expressed using a sub-regular solution model for  $G^{EX,\alpha}$ .

### **3.4. Optimization of Binary Phase Diagrams**

Optimization is carried out where experimental data is fitted in the phase diagram using models. Table 2 shows the thermodynamic properties of pure phases of pure PE, PG and NPG [14]. For PE-NPG binary the maximum solubility of NPG in PE is assumed to be 1.5 mol%. In case of PE-PG, the experimental data suggest that the solution phases are

Table 3-3: Expressions of Gibbs energy equations for PE-PG-NPG ternary system

all ideal and phases formed are mostly solid solutions [37]. PG-NPG follows the same

No.	Gibbs energy expression
1	${}^0G_{PE}^{\alpha} = 0$
2	${}^0G_{NPG}^{\beta} = 0$
3	${}^0G_{PG}^{\alpha} = 0$
4	${}^0G_{PG}^{\beta} = 3403.78$
5	${}^0G_{NPG}^{\alpha} = 986.640$
6	${}^0G_{NPG}^{\alpha} = 20000 - 40T$
7	${}^0G_{PE}^{\beta} = 25000 - 10T$
8	${}^0G_{PG}^{\gamma} = 23120 - 65.29T - 0.236T^2 + 1115.333T - 78441.09 - 138.041T \ln(T)$
9	${}^0G_{PE}^{\gamma} = 41260 - 89.501T + 1.0895T^2 + 6794.78175T - 272492.7205 - 1093.350T \ln(T)$
10	${}^0G_{PE}^{\gamma} = 41260 - 89.501T + 1.0895T^2 + 6794.781T - 272492.72 - 1093.35T \ln(T) + 1341$
11	${}^0G_{NPG}^{\gamma} = 13630 - 43.22T + 0.351T^2 + 1621.98T - 51061.568 - 272.999T \ln(T)$
12	${}^0G_{NPG}^{\gamma} = 13630 - 43.22T + 0.351T^2 + 1621.98T - 51061.568 - 272.999T \ln(T) + 1028$
13	${}^0G_{PE}^L = 46280 - 98.919T + 1.3765T^2 + 7119.63T - 237151.6225 - 1180.015T \ln(T)$
14	${}^0G_{NPG}^L = 28550 - 76.83T - 0.175T^2 + 1161.791T + 6611.1915 - 152.5T \ln(T)$
15	${}^0G_{PG}^L = 18315 - 55.2T + 0.425T^2 + 2098.38T - 69849.68 - 349.613T \ln(T)$

pattern in terms of ideality where the high temperature  $\gamma^{\wedge}$  phase forms a completely miscible solid solution.

Interaction parameters for the binary systems are determined by using experimental data available in the literature. In order to determine the interaction parameters which can be then used to calculate the excess Gibbs free energy, an optimization procedure is used which requires all available experimental data to be compiled and creation of a work file (PARROT file). The optimization procedure is carried out in the PARROT module of the thermocalc software package and the details of the procedure have been explained in earlier publications [44].

In parametric form, the excess Gibbs energies of a binary system are of the following form:

For  $\varphi$  ( $\varphi = \alpha, \beta$ , etc.),  $G^{EX,\varphi} = x_A x_B (L_0^\varphi + L_1^\varphi (x_A - x_B))$ ,  $L_0^\varphi$  and  $L_1^\varphi$  are constants which have to be optimized.

For the PE-NPG system the interaction parameters were determined assuming the solution phases to be Henrian. The Henrian solution assumption was made based on the fact that PE and NPG form a dilute alloy, where the solubility of NPG in PE is much greater than the solubility of PE in NPG. The interaction parameters obtained by carrying out the optimization procedure were used to plot an optimized phase diagram for PE-NPG.

The unoptimized PG-NPG system showed the invariant equilibria at 308K. Experimental data from Barrio et al. [36] was used for optimization of PG-NPG. The low temperature phases were modeled using regular solution model with temperature dependence, but the resulting phase diagram was not a good fit with the experimental data, so a sub-regular solution model was used. The high temperature solid solution was modeled assuming regular solution model with a temperature dependency, and the liquid phase was modeled as a sub-regular solution model.

The optimization of the PE-PG binary was simpler, compared to PG-NPG or PE-NPG. For the optimization of the PE-PG binary, regular solution model was used with no temperature dependence. The interactions parameters are predicted to be small as the behavior of this binary system is almost ideal because of limited miscibility.

### **3.5. Results and Discussion**

The estimation of metastable Gibbs energies of pure components is first calculated by assuming ideal solution behavior. The ideal solution behavior is used only for the metastable estimations and the non-ideal behavior in high temperature phases is accounted for by assuming Henrian, sub-regular and regular solution behavior (low temperature phases and the liquid phases are assumed to be ideal).

The interaction parameters for PE-PG are given below:

$$G^{EX,\alpha}=0$$

$$G^{EX,L}=0$$

$$G^{EX,\gamma} = x_C x_B (72.3 - 522.7(x_B - x_C))$$

The calculated PE-PG binary system is shown in Figure 3-2, with superimposed experimental data points from Barrio et al. [37]. The magnitudes of the excess parameters are very small in case of the PE-PG system suggesting that all the solution phases are mostly ideal solutions. No de-mixing region at room temperature was noticed in the phase diagram indicating complete miscibility.

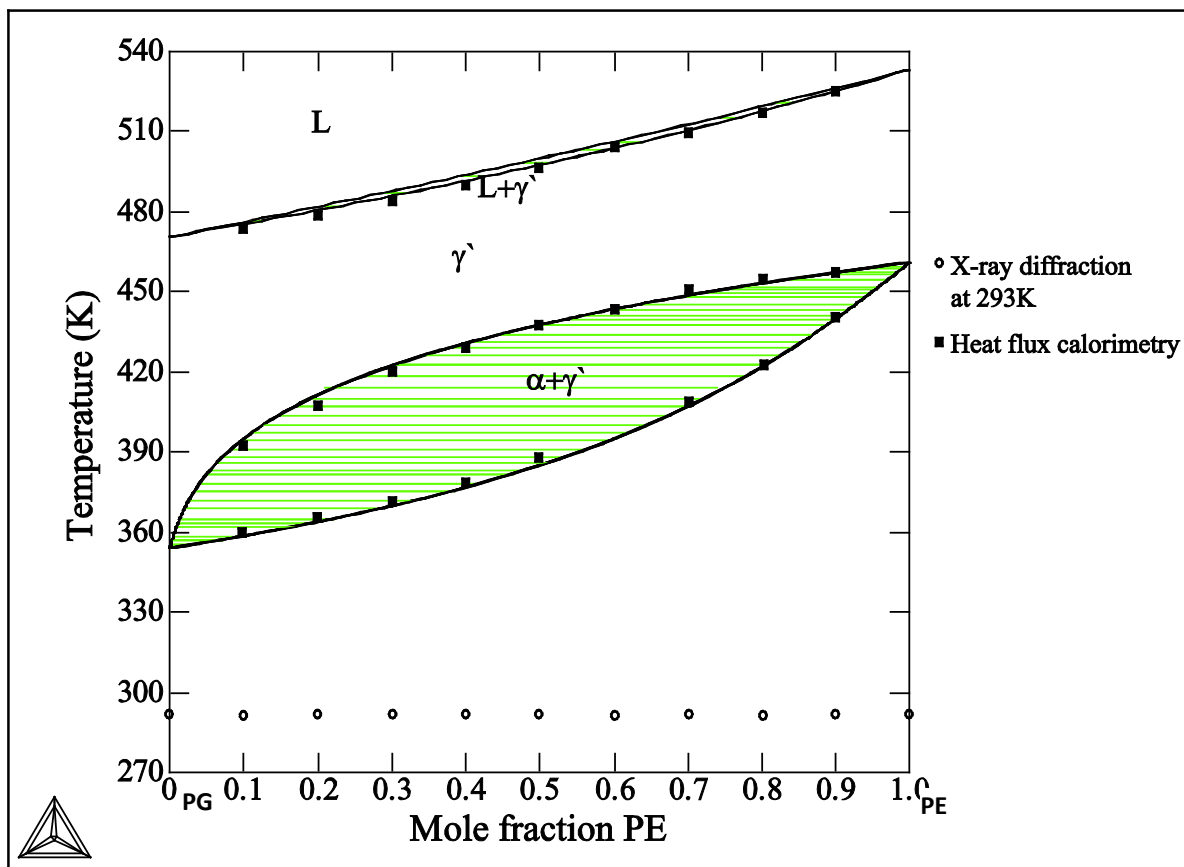


Figure 3-2 Calculated PE-PG phase diagram from this study (data points from Barrio et al. [37])

This is due to the fact that both pure PE and PG are isomorphous at low temperature as well as high temperature. The high temperature phase also indicates complete miscibility. There is a very narrow plastic  $\gamma'$  phase and liquid phase region. The excess Gibbs energies were initially considered to be zero in this work, but it was observed that the absence of the parameters made no difference in the calculations. The low temperature phases and the liquid phase were assumed to be ideal.

The PE-NPG system was optimized using Henrian solution model with temperature dependence. The optimized parameters for the binary system are given below;

$$G^{EX,\alpha} = x_A x_B (20000 - 40T)$$

$$G^{EX,\beta} = x_A x_B (25000 - 10T)$$

$$G^{EX,\gamma} = x_A x_B (1341)$$

$$G^{EX,\gamma'} = x_A x_B (1028)$$

$$G^{EX,L} = x_A x_B (2471.8)$$

The calculated PE-NPG system resulted in a complex phase diagram depicted in figure 3-3. Tesseire et al. [41] noted a solid-liquid phase at 165°C (438K) in the PE-NPG system, whereas Chandra et al. [22] showed a two phase region consisting of two individual high temperature phase regions. Barrio et al. [17] proposed a PE-NPG phase in the temperature range from room temperature to 393K. They observed invariant equilibria at 343.6K which does not correspond to the phase diagrams proposed by Tesseire et al. and Chandra et al. [34, 41]. The PE-NPG phase diagram by Chandra et al. [34] was calculated using the FACT Sage program.

There is good agreement between the phase diagrams calculated by Chandra et al. and proposed by Tesseire et al. [34,41]. According to Tesseire et al. a two phase region exists from room temperature to 36°C (309K), and a small region on the NPG rich side consisting of a low temperature NPG single phase and a high temperature NPG phase [41]. Table 3-4 shows the invariant reactions in the PE-NPG system (this work). The major difference between the two above mentioned phase diagrams is that Tesseire et al.

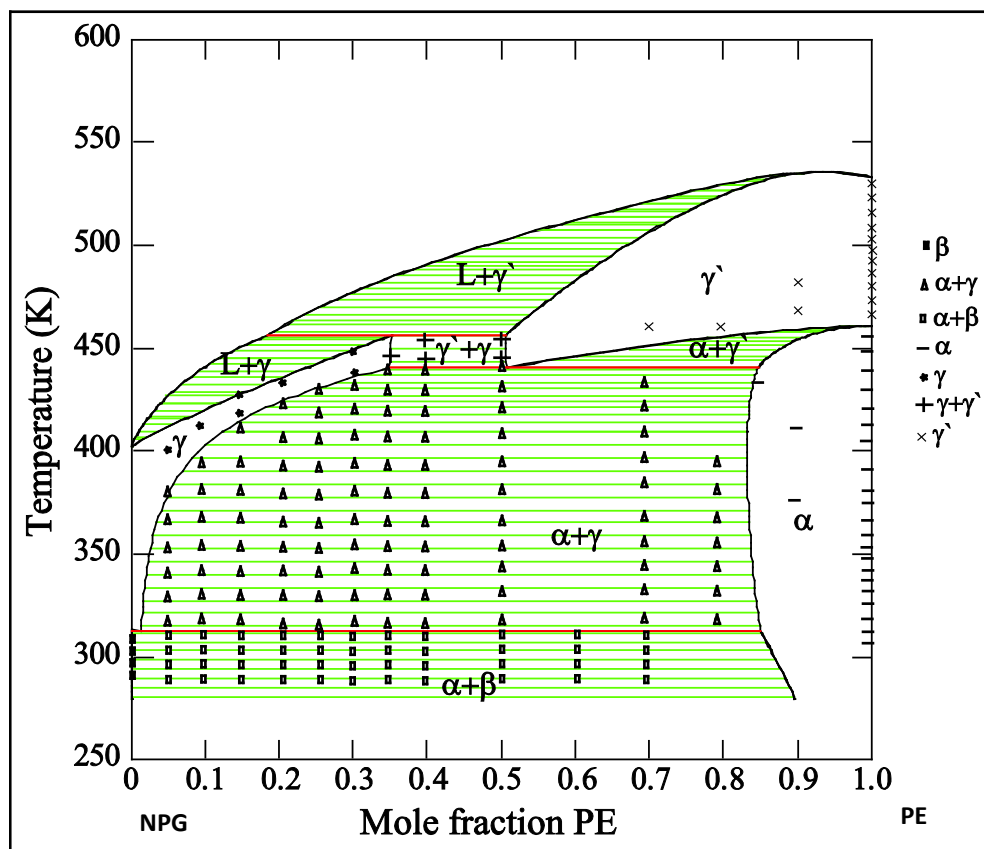


Figure 3-3 Calculated PE-NPG phase diagram from this study (data points from Chandra et al. [18, 35])

[41] predicted a two phase (solid-liquid) region at about 163°C (436K), whereas Chandra et al. predicted the presence of a two phase region consisting of two high temperature solid phases belonging to PE and NPG each at the same temperature. Barrio et al. pointed out that since the two substances are isomorphic at high temperatures a new phase might appear. The enthalpy of mixing for PE-NPG in PE-NPG liquid at 177°C (450K) was also calculated and is depicted in figure 3-5(a). The activities were calculated using the excess Gibbs energy parameters. Figure 3-6(a) shows the calculated activity of PE and NPG in PE-NPG liquid at 177°C (440K).

Table 3-4. Invariant equilibria for PE-NPG binary system (this work)

Invariant equilibria	X <sub>B</sub> (mole fraction NPG)			Temp. (K)
	$\alpha$	$\beta$	$\gamma^{\wedge}$	
$\alpha + \gamma^{\wedge} \rightarrow \beta$ (Peritectoid)	0.15	1.0	0.986	312
$\gamma^{\wedge} \rightarrow \alpha + \gamma$ (Eutectoid)	0.155	0.65	0.49	440
$\gamma^{\wedge} + L \rightarrow \gamma$ (Peritectic)	0.494	0.647	0.815	456

The solution phases for the PG-NPG binary were modeled using regular and sub-regular solution models. The PG-NPG system shows a demixing region in the solid state. This is attributed to the low-temperature forms of pure PG (tetragonal) and NPG (monoclinic). Chandra et al. [34] noticed similar behaviors, but the solid solution boundaries are slightly different than Barrio's phase diagram [36]. Both phase diagrams show a Gibbs minimum at the solid-liquid transition, but once again, there is a difference in the compositions at which the minimum is located. Figure 3-4 shows the calculated PG-NPG phase diagram, superimposed with experimental data from Barrio et al. [36].

The following are the optimized parameters for PG-NPG

$$G^{EX,\beta} = x_B x_C (16600 - 49.9T)$$

$$G^{EX,\alpha} = x_B x_C ((25300 - 77.8T) - 1495(x_C - x_B))$$

$$G^{EX,\gamma} = x_B x_C (-13200 + 36.2T)$$

$$G^{EX,L} = x_B x_C ((-1940 + 7.52T))$$

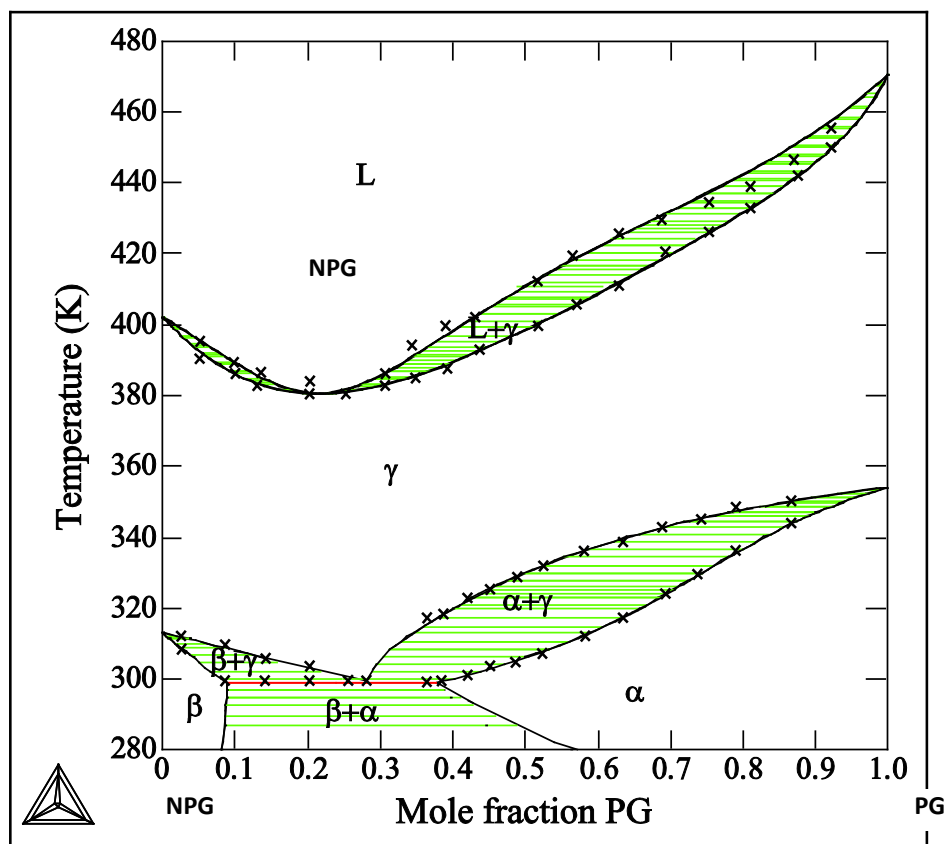


Figure 3-4 Calculated PG-NPG phase diagram from this study (data points from Barrio et al. [36])

Experimental data from Barrio et al. [36] has been used since it is the latest and most updated data to have been published. The high temperature solid phase forms a solid solution (total miscibility), since both high temperature phases of pure PG and NPG are the same (FCC). It can be hence assumed that this phase does not vary considerably from ideality. The enthalpy of mixing for PG-NPG in PG-NPG liquid at 177°C (450K) was also calculated and is depicted in Figure 3-5(b). Figure 3-6(b) shows the calculated activity of PG and NPG in PG-NPG liquid at 167°C (440K).

It should be noted that the binary phases project in to the ternary phases and that no separate ternary phase as such exists in the system. Figure 3-7 shows an example of how the binary phases project on to the ternary phase diagram. The binary phase diagrams have been reconstructed and optimized using available experimental data. The experimental data corresponds to tie-lines and invariant temperatures and not to the activities of the polyalcohols. The isotherms of the ternary PE-PG-NPG system are presented in figure 3-8. The isothermal sections are presented for a range of temperatures which show significant phase changes. The  $\alpha+\beta$  two phase region transforms into  $\alpha+\gamma$  where the  $\beta$  phase (low temperature NPG) undergoes a phase transformation and becomes high temperature  $\gamma$  solid solution at 298K. At room temperature there is a predominantly large two phase region are formed by PE and NPG ( $\alpha+\beta$  region). But at 25°C (298K) new two phase regions appear owing to the formation of high temperature  $\gamma$ , and the  $\alpha+\beta$  phase field decreases. At 30°C (313K), the  $\beta$  phase (low temperature NPG), disappears and is transformed into  $\gamma$ , and a large two phase region  $\alpha+\gamma$  exists along the NPG rich side. At 108°C (381K) the presence of a liquid phase is seen in the PG-NPG side. This is attributed to the gibbs minimum formed at 381K on the PG-NPG binary system. The inclusion of this liquid phase leads to the formation of two phase and three phase regions. It should be noted that  $\alpha$  phase corresponds to the low temperature PE phase as well as solid solution of PE-PG at low temperature. After 381K the  $\gamma'$  regions starts dominating the  $\alpha$  region and eventually all  $\alpha$  corresponding to PE-PG low temperature solid solution transforms into  $\gamma'$ . The  $\alpha$  phase field gradually decreases, and at about 190°C (463K) is transformed into  $\gamma'$ . The  $\gamma$  phase exists as a complete solid solution on the PG-NPG and PE-NPG (NPG rich) corner as the FCC orientationally

disordered  $\gamma$  phases are completely soluble, at these compositions. The reason that PE and NPG do not form a completely miscible solid solution in the high temperature region, unlike PE-PG and PG-NPG in spite of having the same crystal structure (FCC) is because of the nature of molecular bonding of the two O-H...O bonds of NPG with PE.

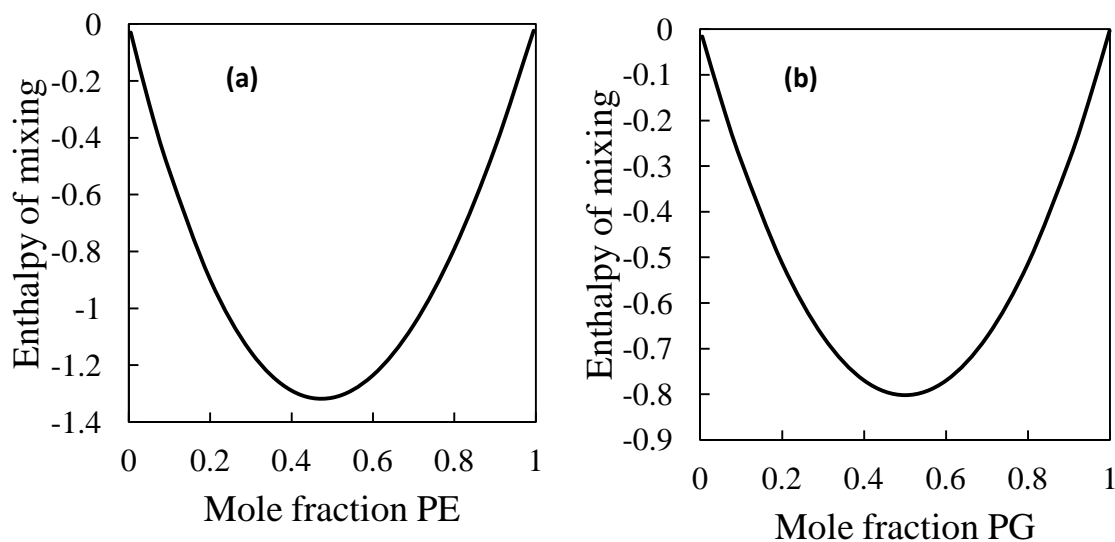


Figure 3-5 Enthalpy of mixing of (a) PG-NPG and (b) PE-NPG liquid at 450K (calculated, this work)

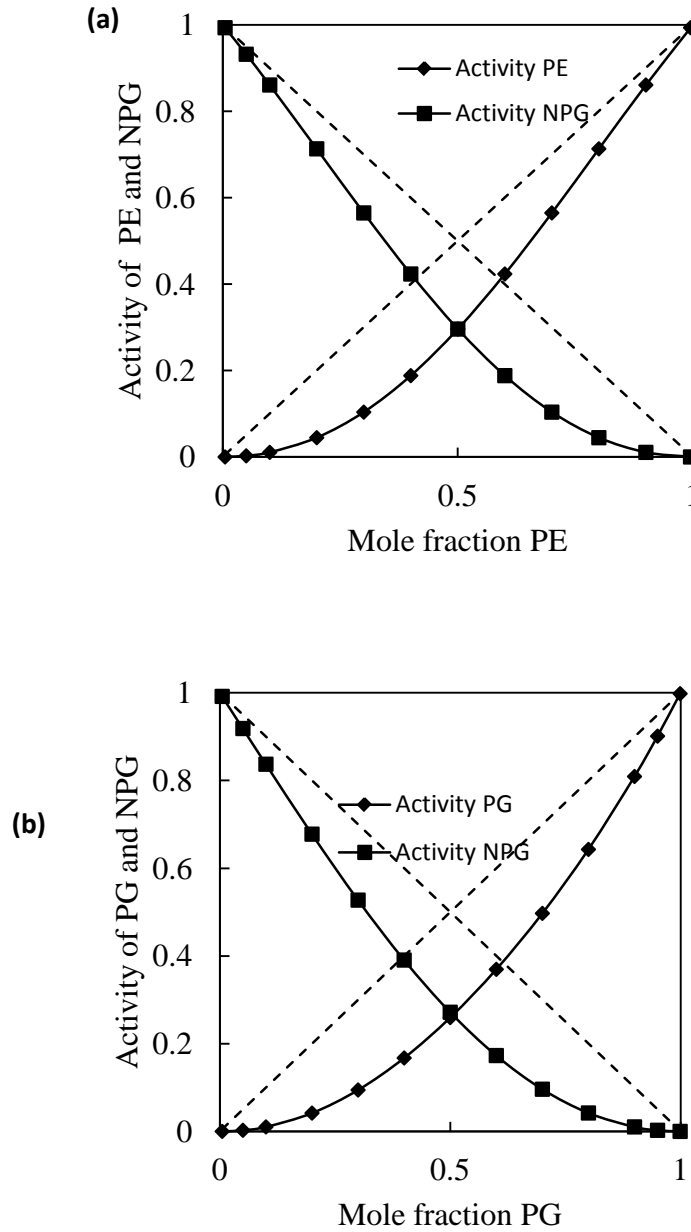


Figure 3-6 Activity of (a) PE and NPG in PE-NPG liquid and, (b) PG and NPG in PG-NPG liquid at 440K (calculated, this work)

If we consider a case of a 40% PE-60% NPG binary alloy, in which we have 90 weight%  $\gamma$  and 10 weight %  $\alpha$  at the eutectoid temperature of  $\sim 40^{\circ}\text{C}$  (313K). The composition of

$\gamma$ -phase is 35 % PE and that of the  $\alpha$ -phase is 84% PE. As we increase the temperature above the eutectoid temperature of 167°C (440K), say to 177°C (450K), the  $\gamma$  phase continues to be stable, and all of  $\alpha$  phase has transforms to  $\gamma'$ . The composition of the  $\gamma$ -phase is still remains at 35% PE, but the composition of new  $\gamma'$ -phase is now 50% PE. Thus at 177°C we will have 30 wt.% of  $\gamma'$  and 70 wt.% of  $\gamma$  (by the lever rule). Thus, the original 10 weight% of  $\alpha$  phase (that was below the eutectoid line) converts to 30 weight%  $\gamma'$  phase; the composition of  $\gamma'$  decreases from 90 weight% to 70 weight%, and in addition (20 weight% of  $\gamma$  phase also converts to  $\gamma'$  phase). The molecular structure of NPG has 2 –OH and 2 –CH<sub>3</sub> groups, as compared to PE that has 4 –OH groups. When PE and NPG molecules bond in the high temperature phases, there is an increase in the –CH<sub>3</sub> dangling bonds, and the differences in the vibrational motions of the PE and NPG solid solution phases [34] results in limited miscibility and the formation of a two,  $\gamma+\gamma'$ , phase region is observed.

As mentioned earlier no separate ternary phase exists in the system. To study and understand the effect of adding a third polyalcohol into a binary and how it affects the phases to undergo changes is represented by the isopleth sections of the ternary system (Figure 3-9). The ternary phases portrayed in the phase diagrams are the extension of the binary phases in to ternary phases. Ternary interaction parameters were not calculated because of the absence of experimental data, and also because the ternary interaction parameters are predicted to be very small, as the isothermal sections agree with the extrapolated binaries.

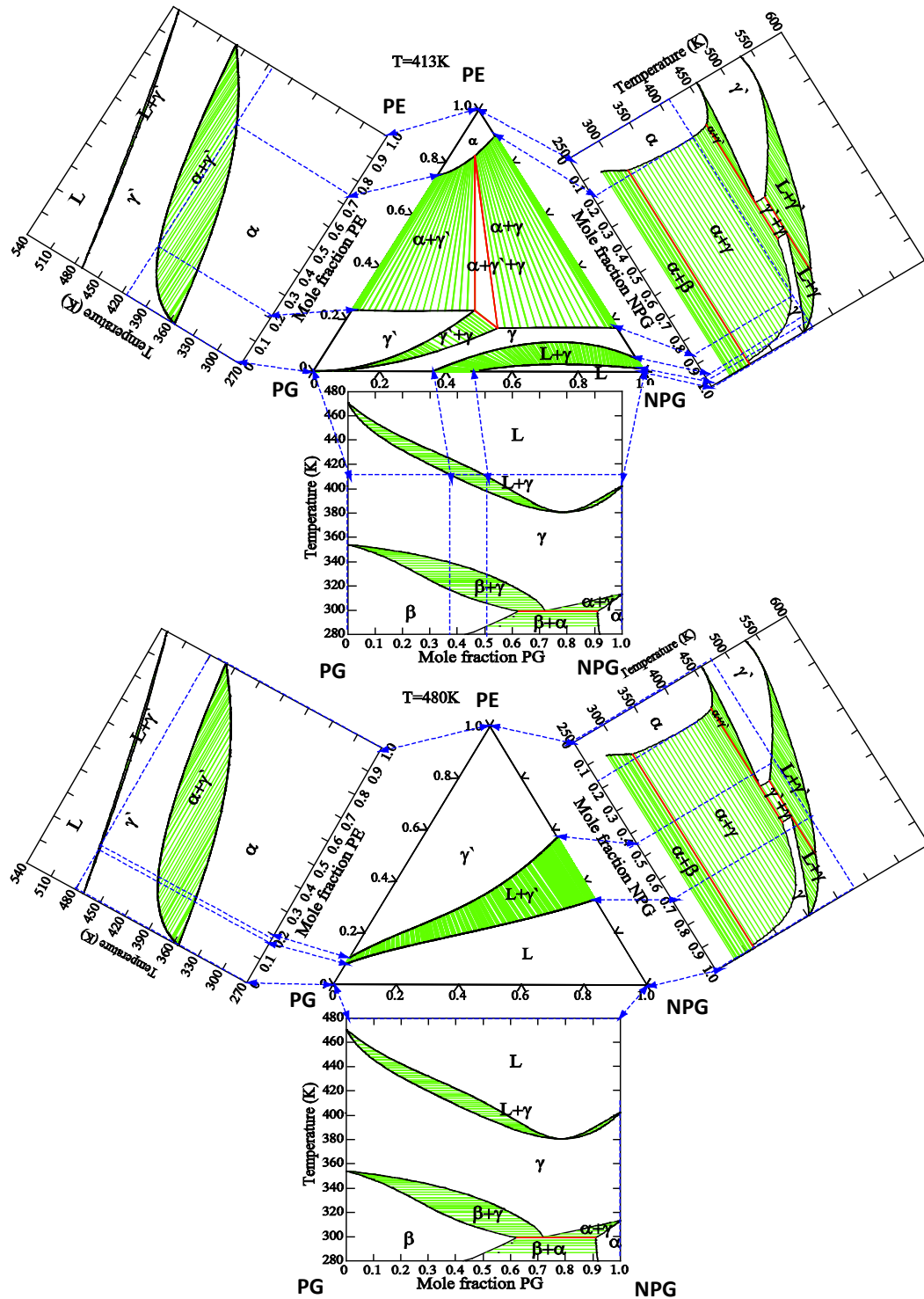


Figure 3-7 Binary phases projecting into PE-PG-NPG ternary. Two-phase regions are shown hatched by tie-lines (green in color); Red (in color) lines represent invariant equilibria.

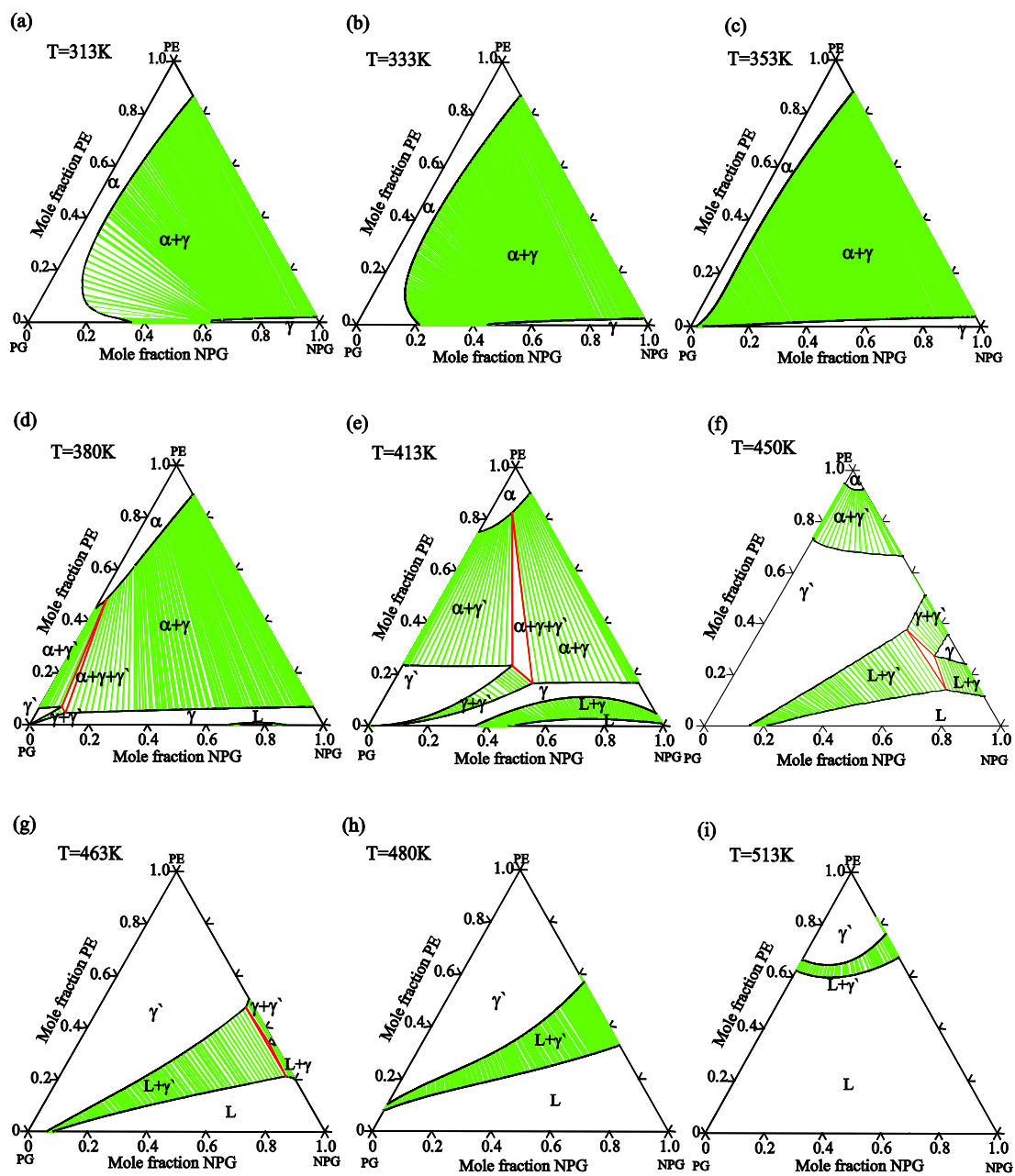


Figure 3-8 Isotherms for ternary PE-PG-NPG (a) 313K, (b) 333K, (c) 353K, (d) 380K, (e), 413K, (f) 450K, (g) 463K, (h) 480K and (i) 513K.

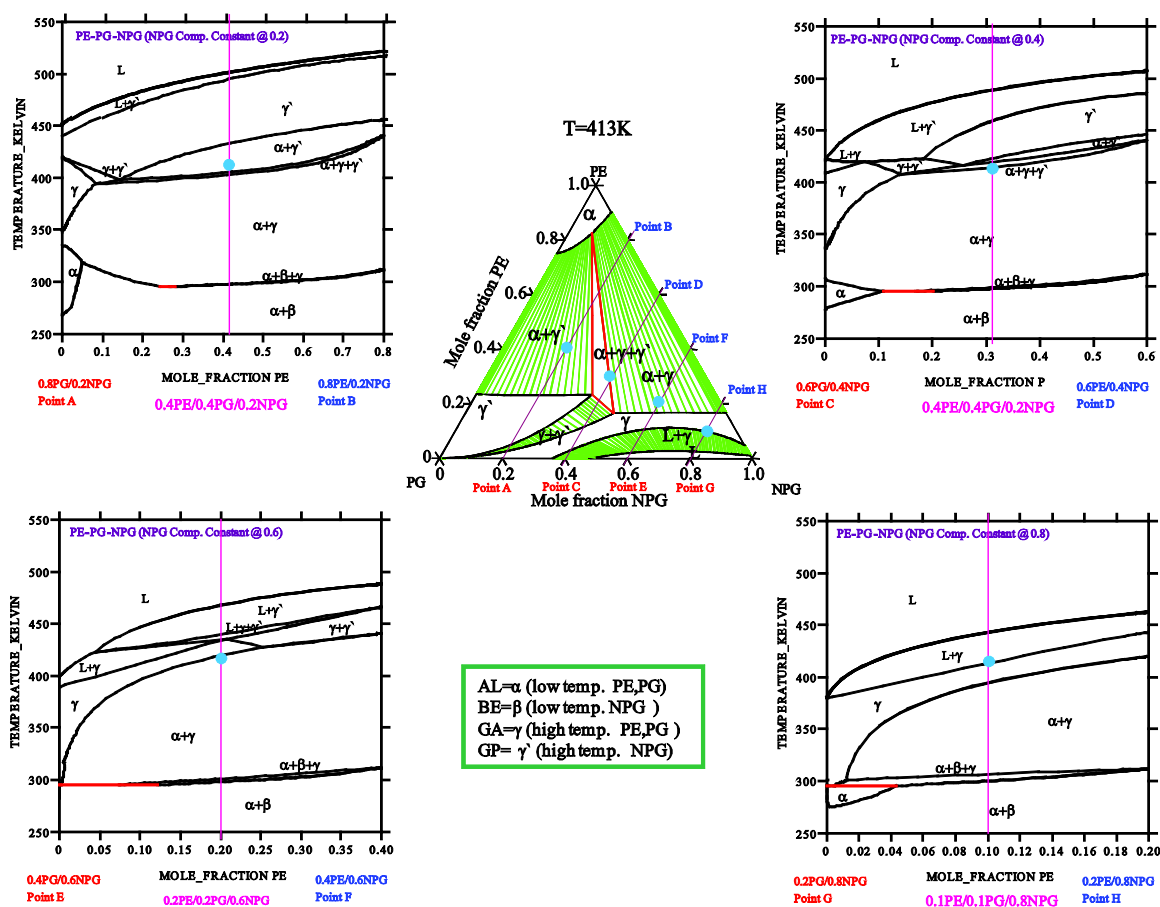


Figure 3-9 Isoleths along the line on the PE-PG-NPG isotherm at 413K.

Isoleths provide valuable information about phase transitions at various temperatures, whereas, isotherms are projected at a constant temperature. In order to study and analyze phase transitions, isopleths are preferred over isotherms, as several isotherms would have to be plotted at very small intervals. The isopleths are plotted between two components keeping the composition of the third component constant, over a desired temperature range. In figure 3-9, the isopleths or pseudo-binary sections are presented for the PE-PG-NPG system. The composition of NPG was kept constant and the isopleths were plotted

between PG and PE from 250K to 550K. An isotherm is also depicted in figure 3-9 (at 413K), so as to compare the compositions and temperature chosen, with an isotherm. At Isopleths along the line x-y on the PE-PG-AMPL ternary diagram (right). A small circle drawn (at 390K) on the line along the composition 0.1PE/0.45PG/0.45AMPL on the isopleth shows the  $\gamma$  phase is stable; these correspond with the phase marked small circle along the line x-y on the ternary diagram (right).

NPG is kept constant at 0.2 mole fraction in one of the isopleths, and a composition between PG and PE is chosen, so that the overall composition distribution of the chosen point is 0.2NPG/0.4PE/0.4PG. At the specified composition a vertical line is drawn to determine the phase transitions between room temperature and 550K. At 0.2NPG/0.4PE/0.4PG, the two phase region  $\alpha+\beta$  is transformed in to  $\alpha+\gamma$  phase at 303K. at 400K  $\alpha+\gamma$  is transformed in to a three phase region ( $\alpha+\gamma+\gamma'$ ), with the appearance of  $\gamma'$  phase. The three phase region exists for a very small temperature range, and after 3K, transforms in to a two phase region ( $\alpha+\gamma'$ ), as the  $\gamma$  phase disappears at this particular composition and beyond this temperature. The  $\alpha+\gamma'$  phase is stable till up to 429K, and then the  $\alpha$  phase is completely transformed in to  $\gamma'$ . This can be attributed to the transition temperatures of PE, where low temperature PE undergoes solid-solid phase transition to form high temperature FCC phase. The liquid phase starts appearing as a two phase region ( $\gamma'+L$ ) at 483K. And completely transforms into liquid 490K.

At 0.4NPG/0.3PE/0.3PG, a three phase region starts forming, which was not seen in case of 0.2NPG/0.4PE/0.4PG. This three phase region ( $\alpha+\beta+\gamma$ ) starts appearing at 302K, and the  $\beta$  is transformed in to  $\gamma$  at 304K. At 0.15PG/0.45PE/0.4NPG, the  $\alpha+\beta$  changes to  $\alpha+\gamma$

and 298K. This transformation is due to the invariant equilibria seen in PG-NPG at 298K, where  $\alpha+\beta$  is transformed to a completely miscible solution of  $\gamma$ . The existence of  $\alpha$  phase beyond 298K is mostly due to PE.

Table 3-5 shows the phase transitions occurring in the PE-PG-NPG ternary system at different compositions and temperatures. Binary alloys of these polyalcohols help in lowering the transition temperatures, but adding a third component creates more phase transitions to occur at different compositions. For example, in PE-NPG binary system, the first transition takes place at 312K, but adding PG, makes the operation range wider (298-308K). Solid-solid phase transitions can occur at a bigger temperature range, and any composition contributing to a desired phase transition temperature can be chosen for required application.

Table 3-5 Phase transitions in PE-PG-NPG system

$X_{PE}$	$X_{PG}$	Temp. (K)
0.5	0.3	$\alpha + \beta \xrightarrow{299K} \alpha + \gamma \xrightarrow{408K} \alpha + \gamma + \gamma'$ $\xrightarrow{410K} \alpha + \gamma' \xrightarrow{438K} \gamma' \xrightarrow{501K} L + \gamma' \xrightarrow{510K} L$
0.15	0.45	$\alpha + \beta \xrightarrow{298K} \alpha + \gamma \xrightarrow{411K} \gamma + \gamma' \xrightarrow{410K} \alpha + \gamma'$ $\xrightarrow{423K} L + \gamma' \xrightarrow{468K} L$
0.4	0.2	$\alpha + \beta \xrightarrow{301K} \alpha + \beta + \gamma \xrightarrow{302.5K} \alpha + \gamma \xrightarrow{410K} \alpha + \gamma'$ $\xrightarrow{419K} \alpha + \gamma + \gamma' \xrightarrow{426K} \alpha + \gamma' \xrightarrow{431K} \gamma' \xrightarrow{471K} L + \gamma'$
0.35	0.05	$\alpha + \beta \xrightarrow{305K} \alpha + \beta + \gamma \xrightarrow{308K} \alpha + \gamma \xrightarrow{440K} \gamma + \gamma'$ $\xrightarrow{458K} L + \gamma + \gamma' \xrightarrow{459K} L + \gamma' \xrightarrow{482K} L$

## 5. Conclusions

Based on the previous assessments of PE-NPG, PE-PG and PG-NPG systems the phase diagram for the PE-PG–NPG system has been calculated by employing a straightforward estimation for metastable Gibbs energies, in combination with thermodynamic optimization using the PARROT program in the Thermo-Calc software package. An initial assumption of ideality in the high-temperature phases is used only to estimate the metastable Gibbs energies of the binary systems (PE-NPG, PE-PG and PG-NPG). The non-ideality of the solution phases have been compensated by assuming various solution models. The optimization using Thermo-Calc software included available published experimental data from the binary phase diagrams (tie lines and invariant equilibria composition and temperatures). The PE-NPG system has been subject to incoherency in terms of experimental data. Although the high temperature phases in PE and NPG are isomorphic, the complex nature of the binary phase diagram (PE-NPG) can be attributed to syncrystallization. Also the solid-plastic phase transition temperatures in both PE and NPG are vastly different. The PG-NPG phase diagram shows invariant equilibria at 298 K and a Gibbs minimum at the melting curves. PE-PG system is almost ideal because of limited miscibility and both structures being isomorphic at both high and low temperature. The selected isothermal and isopleth sections of the system are calculated over an entire composition range. There is good agreement between the calculated and experimental phase boundaries and invariant equilibria of the binary phase diagrams. The ternary system for PE-PG–NPG system has been created for the first time, which may be of interest for various applications as well as to materials researchers. Further experimental data is required for optimization of the ternary system (PE-PG-NPG).

## References:

1. Ruan D, Zhang T, Zhang D, Liang S, Hu Q. *Acta Energiæ Solaris Sinica* 15(1) 1994 19.
2. Xing D, Shi G, Ruan D, Huo L, Li D, Zhang T, Zhang D. *Acta Energiæ Solaris Sinica* 16(2) 1994 131.
3. Benson DK, Burrows RW, Webb JD. *Solar Energy Materials* 13 (1986) 133.
4. Benson DK, Chandra D. Solid-state phase change materials for thermal energy storage. US DOE Contract No. DE-AC02-83CH10093, 1985.
5. Son CH. Solid±solid phase change materials as a space-suit battery heat storage medium. Ph.D. thesis, University of South Carolina, 1989.
6. Son CH, Morehouse JH. *ASME Journal of Solar Energy Engineering* 113 (1991) 244.
7. Zhang ZY, Yang ML. *Thermochimica Acta* 169 (1990) 263.
8. Murrill E, Breed L. *Thermochimica Acta* 1 (1970) 239.
9. Zhang ZY. *Thermochimica Acta* 202 (1992) 105.
10. J. Timmermanns. *J. Phys. Chem. Solids* 18 (1961) 1.
11. N.G. Parsonage, L.A.K. Staveley, *Disorder in Crystals*, Oxford University Press, 1976.
12. Y. Haget, *J. Chim. Phys.* 90(2) (1993) 313.
13. I. Nitta and T. Watanabe. *Bull. Chem. Soc. Japan* 13(1) (1938) 28.
14. D. Eilerman, R. Lippman and R. Rudman *Acta Cryst.* B39 (1983) 263.
15. D. Chandra and J.J. Fitzpatrick. In: C.S. Barrett, P.K. Fredecki and D.E. Levdén, Editors, *Advances in X-Ray Analysis* 28 (1985) 353.
16. D. Chandra, C.S. Day and C.S. Barrett. *Powder Diffr.* 8(2) (1993) 109.
17. M. Barrio, J. Font, J. Muntasell, J. Navarro, J.Ll. Tamarit, *Sol. Energy Mater.* 18 (1–2) (1998) 109.
18. D. Chandra, C.S. Barrett, Final Report to the DOE Contract No. DE-AC03-84SF12205, 1986.
19. D. Chandra, C.S. Barrett and D.K. Benson. *Advances in X-Ray Analysis* vol. 29, Plenum Publishing (1986) 305–313.
20. E. Murrill, L. Breed, *Thermochim. Acta* 1 (1970) 239.
21. D.K. Benson, R.W. Burrows, J.D. Webb, *Sol. Energy Mater.* 13 (1986) 133.
22. D. Chandra, C.S. Barrett, Final Report to DOE, Contract No. DEAC03-84SF12205, January, 1986.
23. J. Font, J. Muntasell, J. Navarro, J.Ll. Tamarit, J. Lloveras, *Sol. Energy Mater.* 15 (1987) 299.
24. J. Font, J. Muntasell, J. Navarro, J.Ll. Tamarit, *Thermochim. Acta* 118 (1987) 287.
25. J. Font, J. Muntasell, J. Navarro, J.Ll. Tamarit, *Sol. Energy Mater.* 15 (1987) 403.
26. J. Font, J. Muntasell, J. Navarro, J.Ll. Tamarit, *Thermochim. Acta* 136 (1988) 55.
27. J. Salud, D.O. Lopez, M. Barrio, J.Ll. Tamarit, H.A.J. Oonk, P. Negrier and Y. Haget. *J. Solid State Chem.* 133 (1997) 536.
28. M. Barrio, D.O. Lopez, J.Ll. Tamarit, P. Negrier and Y. Haget. *J. Mat. Chem.* 5(3) (1995) 431.
29. M. Barrio, D.O. Lopez, J.Ll. Tamarit, P. Negrier and Y. Haget. *J. Solid State Chem.* 124 (1996) 29.
30. D.O. Lopez, J. Van Braak, J.Ll. Tamarit and H.A.J. Oonk. *Calphad* 18(4) (1994) 387.

31. D.O. Lopez, J. Van Braak, J.Ll. Tamarit and H.A.J. Oonk. *Calphad* 19(1) (1995) 37.
32. J. Salud, D.O. Lopez, M. Barrio, J.Ll. Tamarit and H.A.J. Oonk. *J. Mat. Chem.* 9 (1999) 917.
33. D. O. Lopez, J. Salud, J. Ll. Tamarit, M. Barrio and H.A.J. Oonk. *Chem. Mater.* 12 (2000) 1108.
34. D. Chandra, C.S. Barrett and D.K.Benson *Advances in X-ray Analysis.* 32 (1989) 609.
35. H. Singh, An Experimental Phase Diagram Study of Ternary Pentaerythritol-Pentaglycerine-Neopentylglycol Orientationally Disordered Plastic Crystals, Ph.D. dissertation, Univ. of Nevada, Reno, August 2011.
36. M. Barrio, J. Font, J. Muntasell, J.Ll. Tamarit, N.B. Chanh and Y. Haget. *J. Chim. Phys.* 87 (1990) 255.
37. M. Barrio, J. Font, D.O. Lopez, J. Muntasell, J.Ll. Tamarit, N.B. Chanh and Y. Haget. *J. Chim. Phys.* 87 (1990) 1835.
38. W. Ding, M.S. Thesis, University of Nevada, Reno, 1991
39. J. Salud, D.O. Lopez, M. Barrio, J.Ll. Tamarit, H.A.J. Oonk, P. Negrier and Y. Haget. *J. Solid State Chem.* 133 (1997) 536.
40. D. Chandra, Crystal Structure and Thermal Studies On solid –State Energy Storage Materials, Final Report, Contract number:19X-SC644V/DE-AC05-84 OR21400, 1990.
41. M.Teisseire, N.B. Chanh, M.A. Cuevas-Diarte, J. Guion, Y. Haget, D. Lopez and J. Muntasell *Thermochnica Acta* 181 (1991) 1.
42. M. Barrio, J. Font, D.O. Lopez, J. Muntasell, J. Ll. Tamarit, N.B. Chanh and Y. Haget, *J. Phys. Chem. Solids* 52 (1991) 665.
43. R. Chellappa and D. Chandra, *CALPHAD* 27 (2003) 133.
44. N. Saunders and A.P. Miodownik. In: *CALPHAD (Calculation of Phase Diagrams): A Comprehensive Guide* Pergamon Materials Series, Elsevier Science Ltd. (1998).

## Chapter IV Thermodynamic assessment of pentaerythritol-neopentylglycol-2-amino-2methyl-1,3, propanediol (PE-NPG-AMPL) ternary phase diagram

---

### *Summary*

A thermodynamic analysis of the pentaerythritol-neopentylglycol-2-amino-2methyl-1,3, propanediol ternary system has been performed by using the CALPHAD approach. Because of the lack of experimental information available for the ternary system, binary phase diagrams of PE-NPG, PE-AMPL and AMPL-NPG were calculated using the CALPHAD method and optimized using the PARROT program in Thermo-Calc. Available experimental was used for the optimization method and estimation of excess energies for the binaries. The calculated phase diagrams were in good accordance with previous experimental results. The ternary PE-NPG-AMPL as well as the binaries was calculated from room temperature to the liquid phase. Substitutional solution model was assumed for optimization of interaction parameters.

### **4.1. Introduction**

The driving force behind the development of renewable energy source is the emission of greenhouse gases and increasing fuel prices. Direct solar radiation is considered to be one of the most promising sources of energy. Researchers are continually in search of new and alternative energy solutions. One of the options can be the development of

energy storage devices, which are equally important as developing new energy sources. Thermal energy can be stored during the day from solar radiation and utilized at later periods of time. For this purpose the development of thermal energy storage materials is important. Thermal energy can be stored as latent heat or sensible heat. In sensible heat storage, the heat capacity of the material is used for storage. In case of latent heat energy storage heat is stored and released when the material undergoes a phase change. These materials are known as phase change materials. Phase change materials can be solid-liquid, liquid-gas or solid-solid. Solid-solid phase change materials are of importance as the phase changes do not undergo large volume changes and also the problem of leakage in a thermal energy storage incorporating solid-solid phase change materials, is eliminated. Amongst solid-solid phase change materials, organic molecular materials are of great importance as they undergo solid-solid phase transitions, which results in a new (plastic) phase.

These crystalline organic molecular materials are classified as “plastic crystals”. Plastic crystals are molecular crystals in which the molecules can rotate around one or several axes [1]. The formation of plastic crystals is attributed to the ability of the pseudospherical molecules over a particular range of temperature to arrange themselves in a cubic array (FCC /BCC) [2]. They also undergo thermal rotatory displacements at the same time, so that there is no long range orientational order between the molecules [3,4]. This phase is also referred to as ODIC (orientationally disordered crystalline phase) [5]. At the upper temperature limit of this orientational disordered phase the liquefaction occurs with breakdown of the long range positional order with only a small entropy variation, generally smaller than  $21 \text{ Jmol}^{-1}\text{K}^{-1}$  a characteristic value to classify these

compounds and plastic crystal from a thermodynamic point of view [6]. Figure 4-1 shows the structure of PE, NPG and AMPL.

The focus of this research is the characterization of mixed crystals between organic compounds showing a plastic phase, as well as the potential use of these materials in thermal energy storage and systems for solar and other applications, owing to the large entropy variation in the phase transitions.

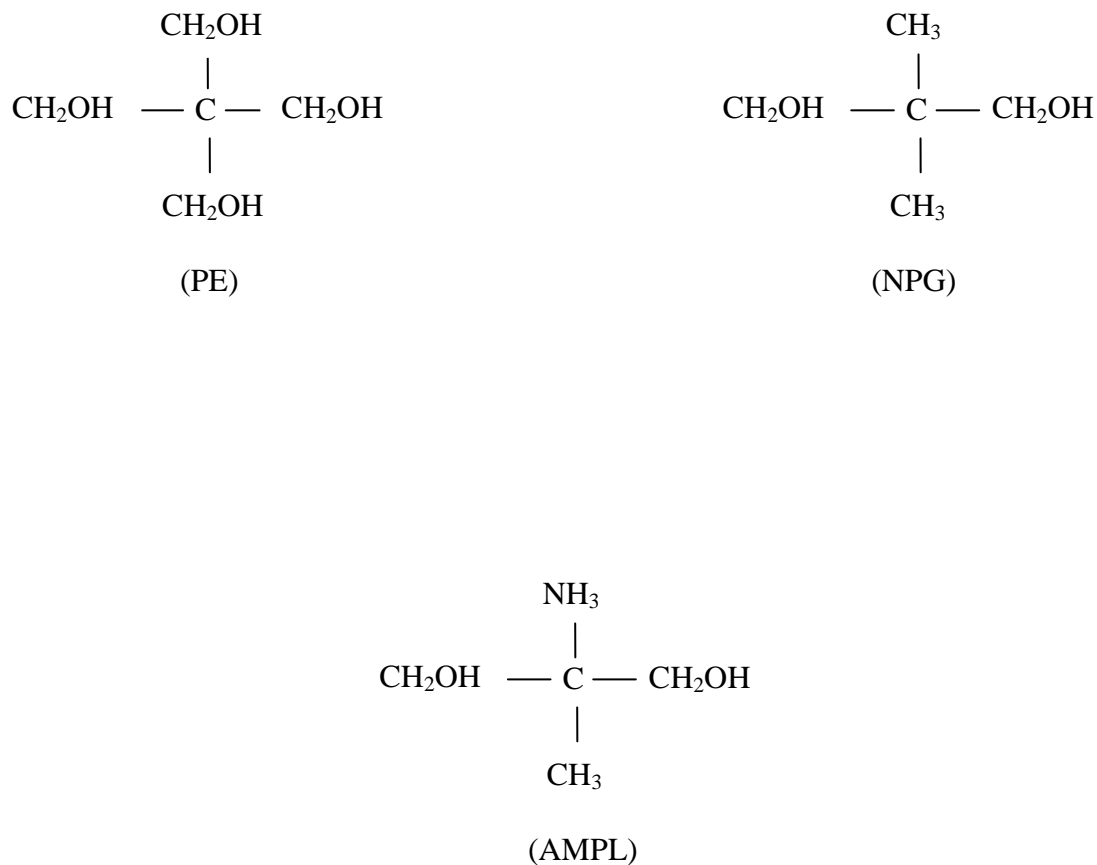


Figure 4-1 Structure of PE, NPG and AMPL

Pentaerythritol and related organic crystals undergo solid-solid phase transformations, from low temperature  $\alpha$  or  $\beta$  layered or chained structures (tetragonal, monoclinic, orthorhombic) to isotropic disordered high temperature cubic phases (FCC or BCC). This high temperature phase is alternatively referred to as orientally disordered crystal (ODIC) or plastic crystal phase. Examples of these 'plastic crystals' include PE, AMPL, pentaglycetine [PG:  $(\text{CH}_3)_2\text{C}(\text{CH}_2\text{OH})_3$ ], neopentylglycol [NPG:  $(\text{CH}_3)_2\text{C}(\text{CH}_2\text{OH})_2$ ], and tris(hydroxymethyl)aminomethane [TRIS:  $(\text{NH}_2)\text{C}(\text{CH}_2\text{OH})_3$ ]. The thermodynamic parameters and crystallographic details for a number of such pure compounds and their binary system have been reported in the literature are of PE-PG, PE-NPG, PG-NPG, PG-AMPL, NPG-AMPL, TRIS-AMPL, NPG-TRIS, PG-TRIS, and PE-TRIS. Calculated phase diagrams for most of the systems have been reported by various investigators. To our knowledge, no ternary phase diagrams have been reported in these types of systems. This work aims at creating a calculated PE-NPG-AMPL ternary phase diagram. Nita and Watanabe [7] reported crystallographic properties of PE. Chandra et al used high resolution Guinier diffraction and reported high temperature structural details of PE [8] and NPG. These polyalcohols when combined to form solid solutions show a variation in the phase transition temperatures. The solid solutions can then be used to suit particular applications [9]. To study the alloying effect on the solid-solid phase transitions, Benson et al. [10] investigated binary systems such as PE-PG, PE-NPG, and PG-NPG for thermal energy storage in solar buildings. Font et al. [11] carried out calorimetric studies of the mixtures of PE-NPG and PG-NPG and Barrio et al. [12] conducted an investigation of heat storage applicability of PE-PG, PG-NPG, and PE-NPG binary systems. Chandra et

al. [13,14] reported a reduction in the transition temperature of PE by alloying it with PG and NPG. Several research groups have reported partial and complete phase diagrams of PG-NPG [15,16], PE-NPG [17,18,19,20,21,22], TRIS-NPG [23,24], PE-PG [25], TRIS-PG [26], TRIS-PE [27], TRIS-AMPL [28], and PE-AMPL [29].

Chandra et al. [30] determined the complete phase diagram for the AMPL-NPG binary. Barrio et al. [31] also reported on the AMPL-NPG binary, but there were significant differences between these two phase diagrams of Chandra et al. and Barrio et al. Salud et al. [32] performed further experimental studies on the AMPL-NPG system in 1997 including a calculated phase diagram. Chellappa et al. also published calculated phase diagrams for AMPL-NPG [33] and PE-AMPL [34].

This work involves thermodynamic assessments of the PE-NPG, AMPL-NPG and PE-AMPL binary systems utilizing the CALPHAD method. These calculated binary phase diagrams are then used to compute the PE-NPG-AMPL ternary system. So far we haven't seen any published record of ternary phase diagrams of plastic disordered crystals of PE, NPG and AMPL.

#### **4.2. Computational Procedure**

In order to compute phase equilibria and calculate the phase diagrams, certain thermodynamic parameters need to be calculated. This section describes the determination of thermodynamic properties (enthalpies and entropies of formation for PE, NPG and AMPL, Gibbs free energies of the stable and metastable phases, etc.).

#### 4.2.1. Calculation of thermodynamic properties

Joback's group contribution method is used to calculate the enthalpy and entropy of formation. Since, the organic plastic crystals (e.g. PE, NPG, AMPL, etc.) are not pure elements; their enthalpy of formation is not zero. These thermophysical quantities can be calculated using group contribution methods, which takes into account the smallest constituents (atoms/groups), and in this case, the functional groups (which may be composed of few atoms and bonds). Data for the functional groups is taken from Marrero and Gani [35]

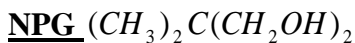


$$\Delta H_{AMPL} = \begin{pmatrix} -22.01 \\ -76.5 \\ 82.23 \\ -20.64 \\ -208.4 \end{pmatrix} \quad k = (1 \quad 1 \quad 1 \quad 1 \quad 2) \quad \Delta G_{AMPL} = \begin{pmatrix} 14.07 \\ -43.96 \\ 116.02 \\ 8.42 \\ -189.2 \end{pmatrix}$$

$$\Delta H_{0_{AMPL}} = (68.29 + k \cdot \Delta H_{AMPL}) \cdot 10^3 = 406030 \text{ kJ / mol}$$

$$\Delta G_{0_{AMPL}} = (53.88 + k \cdot \Delta G_{AMPL}) \cdot 10^3 = -221550 \text{ kJ / mol}$$

$$S_{0_{AMPL}} = \frac{\Delta H_{0_{AMPL}} - \Delta G_{0_{AMPL}}}{298} = -619.06 \text{ kJ / mol.K}$$



$$\Delta H_{NPG} = \begin{pmatrix} -76.45 \\ 82.2 \\ -20.64 \\ -208.04 \end{pmatrix} \quad k = (2 \quad 1 \quad 2 \quad 2)$$

$$\Delta H_{0_{NPG}} = (68.29 + k \cdot \Delta H_{NPG}) \cdot 10^3 = -459770 \text{ kJ / mol}$$

$$\Delta G_{0_{NPG}} = (53.88 + k \cdot \Delta G_{NPG}) \cdot 10^3 = -279580 \text{ kJ / mol}$$

$$S_{0_{AMPL}} = \frac{\Delta H_{0_{NPG}} - \Delta G_{0_{NPG}}}{298} = -604.66 \text{ kJ / mol.K}$$

#### 4.2.2. Thermodynamic Modeling of Solution Phases

The most relevant features of the description of the thermodynamic parameters are discussed for the present purpose. The low temperature phases are characterized by  $\alpha$ ,  $\beta$  or  $\delta$ , the high temperature phases are designated as  $\gamma$ ,  $\epsilon$  or  $\eta$ , and the liquid phase as L. For simplicity PE is represented by A, NPG as B and AMPL as C. Table 4-1 shows the list of symbols used to describe the various phases in the PE-NPG-AMPL ternary system.

A CALPHAD type optimization using regular and subregular solution model is considered to be adequate to describe the Gibbs energies of different phases. The low temperature “Phase II” are represented by “ $\alpha$ ”, “ $\beta$ ” or “ $\delta$ ” and the high temperature phases are represented as  $\gamma$ ,  $\epsilon$ ,  $\eta$ . The liquid phase is designated as “L”.

Table 4-1 List of symbols denoting phases in PE-NPG-AMPL system

Symbol	Phase
Liq or L	Liquid
$\alpha$	Low temperature PE phase
$\beta$	Low temperature NPG phase
$\delta$	Low temperature AMPL phase
$\gamma$	High temperature PE phase
$\varepsilon$	High temperature NPG phase
$\eta$	High temperature AMPL phase

If the reference state for each phase is taken to be that of the pure components in that phase, then the Gibbs energy of a solution phase  $\phi$  ( $\phi = \alpha, \beta, \delta, \gamma, \varepsilon, \theta, \eta, L$ ) can be represented as follows (unit of Gibbs energy is  $\text{J mol}^{-1}$  throughout this work, where a mol is a mole of formula unit):

$$G^\phi = x_A {}^0G_A^\phi + x_B {}^0G_B^\phi + x_C {}^0G_C^\phi + RT(\ln x_A + \ln x_B + \ln x_C) + G^{EX,\phi} \quad (1)$$

Where  $\phi = \alpha, \beta, \delta, \gamma, \varepsilon, \theta, \eta, L$ ,  $R = 8.314 \text{ J mol}^{-1} \text{ K}^{-1}$ ,  $x_A$  is the mole fraction of "A",  $x_B$  is the mole fraction of "B" and  $x_C$  is the mole fraction of "C".  ${}^0G_A^\phi$ ,  ${}^0G_B^\phi$  and  ${}^0G_C^\phi$  are the pure component Gibbs energies in  $\phi$ .

The excess Gibbs energy for a binary system A-B, can be demoted as;

$$G_{mix}^{xs} = x_A x_B (L_{AB}^0 + L_{AB}^1 (x_A - x_B)) \quad (2)$$

The binary interaction parameters for excess Gibbs energies,  $L_{i,j}^\phi$  can be expressed as follows:

$$L_{i,j}^\phi = \sum_{n=0}^m {}^n L_{i,j}^\phi (x_i - x_j)$$

The ternary excess Gibbs free energy is written as follows:

$$\begin{aligned} G_{mix}^{xs} = & x_A x_B (L_{AB}^0 + L_{AB}^1 (x_A - x_B)) + x_B x_C (L_{BC}^0 + L_{BC}^1 (x_B - x_C)) \\ & + x_A x_C (L_{AC}^0 + L_{AC}^1 (x_A - x_C)) \end{aligned} \quad (3)$$

The binary and the ternary interaction parameters  ${}^n L_{i,j}^\phi$  and  ${}^n L_{i,j,k}^\phi$  take the following form:

$${}^n L_m^\phi = a + bT + cT \ln(T) + dT^2 + eT^{-1} + fT^3 + gT^7 + hT^9$$

where  $a, b, c, d, e, f, g$  and  $h$  are the excess Gibbs energy parameters. In most cases only the first two terms of the above equation are used.

For a phase  $\phi$  ( $\phi = \alpha, \beta, \delta, \gamma, \varepsilon, \eta, L$ ),  ${}^0 G_A^\phi$ ,  ${}^0 G_B^\phi$  and  ${}^0 G_C^\phi$  are the reference states of pure “A”, “B” and “C”, same as  $\phi$ . A single reference phase is chosen for each component.

The reference phases were chosen and denoted as:  $\alpha$  for “A”,  $\beta$  for “B” and  $\delta$  for “C” and set to zero.

Therefore,

$${}^0 G_A^\alpha = 0, {}^0 G_B^\beta = 0 \text{ and } {}^0 G_C^\delta = 0 \quad (4)$$

The binary phase diagrams are calculated first and extrapolated to a ternary system.

The stable phases for “A” are  $\alpha$ , and  $\gamma$ ,  $\varepsilon$  and  $\beta$  for “B” and  $\theta$  and  $\delta$  for “C”. Gibbs energies of the other phases in terms of these reference states can be represented as:

For system A-B (PE-NPG), the Gibbs energies of the other phases in terms of the reference phases can be represented as:

$${}^0G_A^\gamma = {}^0G_A^\alpha + \Delta^0G_A^{\alpha \rightarrow \gamma} = \Delta^0G_A^{\alpha \rightarrow \gamma} \quad (5)$$

$${}^0G_A^L = {}^0G_A^\alpha + \Delta^0G_A^{\alpha \rightarrow L} = \Delta^0G_A^{\alpha \rightarrow \gamma} + \Delta^0G_A^{\alpha \rightarrow L} \quad (6)$$

$${}^0G_B^\varepsilon = {}^0G_B^\beta + \Delta^0G_B^{\beta \rightarrow \varepsilon} = \Delta^0G_B^{\beta \rightarrow \gamma} \quad (7)$$

$${}^0G_B^L = {}^0G_B^\beta + \Delta^0G_B^{\beta \rightarrow L} = \Delta^0G_A^{\beta \rightarrow \varepsilon} + \Delta^0G_B^{\beta \rightarrow L} \quad (8)$$

The pure Gibbs energies were determined using the heat capacity data. So, for component “A” the Gibbs energies of the stable phases are:

$${}^0G_A^\gamma = {}^0G_A^\alpha + \Delta^0G_A^{\alpha \rightarrow \gamma} = \Delta^0G_A^{\alpha \rightarrow \gamma}$$

$${}^0G_A^\gamma = \Delta H_{TR} - T\Delta S_{TR} + \int_{T_{TR}}^T \Delta C_P^{\alpha \rightarrow \gamma} dT - T \int_{T_{TR}}^T \frac{\Delta C_P^{\alpha \rightarrow \gamma}}{T} dT$$

$${}^0G_A^L = {}^0G_A^\alpha + \Delta^0G_A^{\alpha \rightarrow L} = \Delta^0G_A^{\alpha \rightarrow \gamma} + \Delta^0G_A^{\alpha \rightarrow L}$$

$${}^0G_A^L = \Delta H_{TR} - T\Delta S_{TR} + \int_{T_{TR}}^T \Delta C_P^{\alpha \rightarrow \gamma} dT - T \int_{T_{TR}}^T \frac{\Delta C_P^{\alpha \rightarrow \gamma}}{T} dT + \Delta H_F - T\Delta S_F + \int_{T_F}^T \Delta C_P^{\gamma \rightarrow L} dT - T \int_{T_F}^T \frac{\Delta C_P^{\gamma \rightarrow L}}{T} dT$$

Similar expressions can be obtained for Gibbs energies of stable phases of “B” and “C”.

### 4.2.3. Metastable Phase Calculations

The Gibbs energies for metastable phases are estimated by modifications to the stable phases. For example, for “ A” in  $\beta$  phase, we are interested in determining the difference,  ${}^0G_A^\beta - {}^0G_A^\alpha$ , such that we can express,

$${}^0G_A^\beta = {}^0G_A^\alpha + M_A^\beta$$

The Gibbs energy of the  $\beta$  phase,  $G_m^\beta$ , can now be written as:

$$\begin{aligned} G_m^\beta &= x_A ({}^0G_A^\alpha + M_A^\beta) + x_B {}^0G_B^\beta + RT \times (x_A \ln x_A + x_B \ln x_B) + G^{EX,\beta} \\ G_m^\beta &= x_A M_A^\beta + RT \times (x_A \ln x_A + x_B \ln x_B) + G^{EX,\beta} \end{aligned}$$

Similarly for the  $\alpha$  phase, we can write the Gibbs free energy,  $G_m^\alpha$ , as:

$$\begin{aligned} G_m^\alpha &= x_A {}^0G_A^\alpha + x_B ({}^0G_B^\beta + M_B^\alpha) + RT \times (x_A \ln x_A + x_B \ln x_B) + G^{EX,\alpha} \\ G_m^\alpha &= x_B M_B^\alpha + RT \times (x_A \ln x_A + x_B \ln x_B) + G^{EX,\alpha} \end{aligned}$$

To estimate  $M_A^\beta$  and  $M_B^\alpha$ ,  $\alpha$  and  $\beta$  phases are assumed to be ideal solutions. It should be noted that this assumption is based only for the purpose of calculating the metastable phases.

Therefore, the partial molar Gibbs free energies can be written as:

$$\begin{aligned} G_B^\beta &= {}^0G_B^\beta + RT \ln(x_B^\beta) \\ G_B^\alpha &= {}^0G_B^\alpha + RT \ln(x_B^\alpha) \end{aligned}$$

Where,  $G_B^\beta$  and  $G_B^\alpha$  are the Gibbs energies of “B” in the  $\beta$  and  $\alpha$  phases respectively. At equilibrium,  $G_B^\beta = G_B^\alpha$ , the following estimation can be made at the temperature of maximum solubility,  $T = T_{\max}$ ,

$$\begin{aligned} {}^0G_B^\alpha &= {}^0G_B^\beta + RT_{\max} \ln \left( \frac{x_{B(\max)}^\beta}{x_{B(\max)}^\alpha} \right) \\ {}^0G_B^\alpha &= RT_{\max} \ln \left( \frac{x_{B(\max)}^\beta}{x_{B(\max)}^\alpha} \right) \\ M_B^\alpha &= RT_{\max} \ln \left( \frac{x_{B(\max)}^\beta}{x_{B(\max)}^\alpha} \right) \\ &= 8.314 \times 283.15 \times \ln \left( \frac{0.96}{0.03} \right) \\ &= 8158.7 \text{ Jmol}^{-1} \end{aligned}$$

A similar estimation can be made for  $M_A^\beta$  and is given by,

$$\begin{aligned} M_A^\beta &= RT_{\max} \ln \left( \frac{x_{A(\max)}^\alpha}{x_{A(\max)}^\beta} \right) \\ &= 8.314 \times 283.15 \times \ln \left( \frac{0.97}{0.04} \right) \end{aligned}$$

The assumption that  $\alpha$  and  $\beta$  phases are ideal solutions is used only to describe the metastable pure Gibbs energies  ${}^0G_B^\alpha$  and  ${}^0G_A^\beta$ . The nature of non-ideality of  $\alpha$  phase can still be expressed using a subregular solution model for  $G^{EX,\alpha}$ .

To estimate the metastable  ${}^0G_A^\varepsilon$  and  ${}^0G_B^\gamma$ , we again assume ideal solutions and thus we can make the following estimations:

$$\begin{aligned} {}^0G_A^\varepsilon &= {}^0G_A^\gamma + RT_{\max} \ln\left(\frac{x_{A(\max)}^\gamma}{x_{A(\max)}^\varepsilon}\right) \\ &= \Delta^0G_A^{\alpha\rightarrow\gamma} + RT_{\max} \ln\left(\frac{x_{A(\max)}^\gamma}{x_{A(\max)}^\varepsilon}\right) \end{aligned}$$

$$\begin{aligned} M_A^\gamma &= RT_{\max} \ln\left(\frac{x_{A(\max)}^\gamma}{x_{A(\max)}^\varepsilon}\right) \\ &= 8.314 \times 325.15 \times \ln\left(\frac{0.57}{0.48}\right) \\ &= 404.5 \text{ Jmol}^{-1} \end{aligned}$$

Similarly,

$$\begin{aligned} M_B^\varepsilon &= RT_{\max} \ln\left(\frac{x_{B(\max)}^\varepsilon}{x_{B(\max)}^\gamma}\right) \\ &= 8.314 \times 325.15 \times \ln\left(\frac{0.51}{0.43}\right) \\ &= 461.25 \text{ Jmol}^{-1} \end{aligned}$$

### 4.3. Experimental Data

#### 4.3.1. *Phase Equilibria*

A brief outline of the thermodynamic strategy used in this work is presented in this section. Most of the descriptions of the enthalpies and transition temperatures were obtained from Murrill and Breed [36] and are shown in Table 4-2. The enthalpies and the phase transition temperatures for AMPL were taken from Murrill and Breed [42]. Data for AMPL reported by Ding [37] is higher than the data available in literature. The compound used by Salud et al. [38] was higher than that used in earlier works [39,40]. The reason for the difference in the data can be attributed to this fact. The melting temperature of NPG reported by Ding [44] was 399K. This value is lower than that reported in literature (402.8K) but is closer to the one reported in previous works [36] and also to the values reported by Sigma-Aldrich. This data has been used for the calculations in this work. Pure PE data has been used from Chandra et al. Enthalpies and phase transition temperatures for pure PE and NPG used for calculations were taken from Eilerman et al. [41]

Table 4-2 Crystal structure, transition temperatures and thermal properties of NPG, AMPL and PE [42]

Compound	Low temp. phases	T <sub>TR</sub> (K)	ΔH <sub>TR</sub> (J/mol)	ΔS <sub>TR</sub> (J/mol K)	High temp. phases	T <sub>F</sub> (K)	ΔH <sub>F</sub> (J/mol)	ΔS <sub>F</sub> (J/mol K)
AMPL	Monoclinic	353	23330	66.01	BCC	471	5430	11.54
NPG	Monoclinic	313	13630	43.22	FCC	399	4600	11.83
PE	Tetragonal	461	41260	90.25	FCC	533	5020	9.45

### ***4.3.2. AMPL-NPG binary phase diagram***

The data that is available for these kinds of organic systems are essentially the tie lines and invariant equilibria determined by using DSC and x-ray diffraction. For the AMPL–NPG system, there are no reported experimental data on activities or heat of mixing etc. In this work, we have only used the data from the works by Chandra et al. [43] and Ding [44] for optimization. Chandra et al. [43] and Ding [44] developed the experimental phase diagram of AMPL–NPG in 1991, subsequently by Barrio et al. [45] in 1994 and again by Salud et al. [46] in 1997. Although the global features of the phase diagram were reproduced in all the previous works [43] [44] [45] and [46], there were some significant differences between them. A comparison of the various invariant equilibria reported is shown in Table 5. Comparing the data of Salud et al. [46], Chandra et al. and Ding [43] and [44], in Table 5 a 12 K difference in the eutectic temperature was found. In part, this difference in temperature can be attributed to the fact that Salud et al. [46] used 99.9% pure AMPL while all other works used 99% pure AMPL. For the present work experimental data from Chandra et al. [43] and Ding [44] were used for optimization.

### ***4.3.3. PE-AMPL binary phase diagram***

The PE-AMPL system has been calculated previously by Chellappa et al. [34] using the CALPHAD method. Chellappa et al. used pure PE data from Chandra et al. [47] and pure AMPL data from Barrio et al. [48] as well as Murrill and Breed [42]. These values are listed in Table 4-2.

The calculated slopes for the liquidus and solidus boundaries for the two-phase  $\gamma+L$  and  $\eta+L$  systems were tested for thermodynamic consistency using the equation given in Pelton [49]. Pelton [49] provides an exposition for checking the thermodynamic consistency of the slopes of phase boundaries in the liquidus region by determining the enthalpies of fusion from the slopes as follows:

$$(dT/dX_A^L)_{x_A=1}^{-1} - (dT/dX_A^S)_{x_A=1}^{-1} = \Delta H_{F(A)}^0 / R(T_{F(A)}^0)^2$$

#### ***4.3.4. PE-NPG binary phase diagram***

The PE-NPG binary phase diagram is reported by different groups with significant differences in their observations [50, 51, 52]. Barrio et al. [50] reported the existence of an intermediate cubic phase. They reported an invariant temperature as 70.6°C (343.6K), produced by the presence of a new phase. Teisseire et al. [52] also developed the PE-NPG binary phase diagram using calorimetry and x-ray diffraction but they did not notice the presence of an intermediate cubic phase as reported by Barrio et al. [50]. Tesseire et al. [52] noted a solid-liquid phase at 165°C (438K) in the PE-NPG system, whereas Chandra et al. [53] showed a two phase region consisting of two individual high temperature phase regions. Barrio et al. [50] proposed a PE-NPG phase in the temperature range from room temperature to 393K. They observed invariant equilibria at 343.6K which does not correspond to the phase diagrams proposed by Tesseire et al. and Chandra et al. [52,53]. The PE-NPG phase diagram by Chandra et al. [54] was calculated using the FACT Sage program. There is good agreement between the phase diagrams calculated by Chandra et al. and proposed by Tesseire et al. [54,52]. According to Tesseire et al. a two phase region exists from room temperature to 36°C (309K), and a

small region on the NPG rich side consisting of a low temperature NPG single phase and a high temperature NPG phase [52]. The major difference between the two above mentioned phase diagrams are that Tesseire et al.[52] predicted a two phase (solid-liquid) region at about 163°C (436K), whereas Chandra et al. predicted the presence of a two phase region consisting of two high temperature solid phases belonging to PE and NPG each at the same temperature. Barrio et al. pointed out that since the two substances are isomorphic at high temperatures a new phase might appear

#### **4.4. Results and Discussion**

##### ***4.4.1. Thermodynamic Analysis***

The binary systems were calculated first using ideal solution assumption with the inclusion of heat capacity. However, these results proved not to be satisfactory in the analysis. Therefore, the excess parameters were calculated using experimental data. To determine the excess Gibbs energy parameters, a thermodynamic optimization utilizing all available experimental data is desired [55]. The optimization to determine the excess Gibbs energy parameters was carried out using the PARROT module of the Thermo-Calc software [56,57]. Henrian, regular and sub-regular solution models were used to evaluate the excess parameters for the various phases. The details are summarized in this section.

##### ***4.4.2. AMPL–NPG binary system***

The AMPL-NPG system shows limited miscibility, and the  $\beta$  and  $\delta$  phases were assumed to be ideal ( $G^{EX,\beta} = 0$  and  $G^{EX,\delta} = 0$ ). The  $\epsilon$  and  $\theta$  phase were modeled as sub-regular

solution without temperature dependence. The liquid phase was also assumed to be ideal.

Table 4-3 lists the Gibbs energy equations for AMPL-NPG binary system.

Table 4-3 Expressions for Gibbs energies of pure components (NPG-AMPL)

No.	Gibbs energy expression
NPG-AMPL	
1	${}^0G_{NPG}^{\beta} = 0$
2	${}^0G_{AMPL}^{\delta} = 0$
3	${}^0G_{NPG}^{\delta} = 8158.7$
4	${}^0G_{AMPL}^{\beta} = 7505.88$
5	${}^0G_{NPG}^{\varepsilon} = 13630 - 43.55T + 0.351T^2 + 1621.98T - 51061.57 - 272.99T \ln(T)$
6	${}^0G_{AMPL}^{\eta} = 23300 - 66.01T - 0.275T^2 + 949.46T - 73097.48 - 110T \ln(T)$
7	${}^0G_{NPG}^{\eta} = 13630 - 43.55T + 0.351T^2 + 1621.98T - 51061.57 - 272.99T \ln(T) + 461.25$
8	${}^0G_{AMPL}^{\varepsilon} = 23300 - 66.01T - 0.275T^2 + 949.46T - 73097.48 - 110T \ln(T) + 404.55$
9	${}^0G_{NPG}^L = 18315 - 55.2T + 0.425T^2 + 2098.38T - 69849.68 - 349.613T \ln(T)$
10	${}^0G_{AMPL}^L = 26291.4 - 73.77T - 0.29T^2 + 1026.62T - 78953.7 - 119.44T \ln(T)$

For  $\varphi(\varphi=\varepsilon,\eta)$ ,  $G^{EX,\varphi}=x_Ax_B(L_0^{\varphi}+L_1^{\varphi}(x_A-x_B))$ ,  $L_0^{\varphi}$  and  $L_1^{\varphi}$  are constants which have to be optimized for.

Figure 4-2 shows the optimized phase diagram of AMPL-NPG. The optimization was carried out using the PARROT module of Thermo-Calc software. The expressions determined for the excess Gibbs energies are given below:

$$G^{EX,\delta}=0$$

$$G^{EX,\theta}=0$$

$$G^{EX,L}=0$$

$$G^{EX,\varepsilon}=x_Ax_B(75.6-528.2(x_A-x_B))$$

$$G^{EX,\eta}=x_Ax_B(162.5+598.7(x_A-x_B)).$$

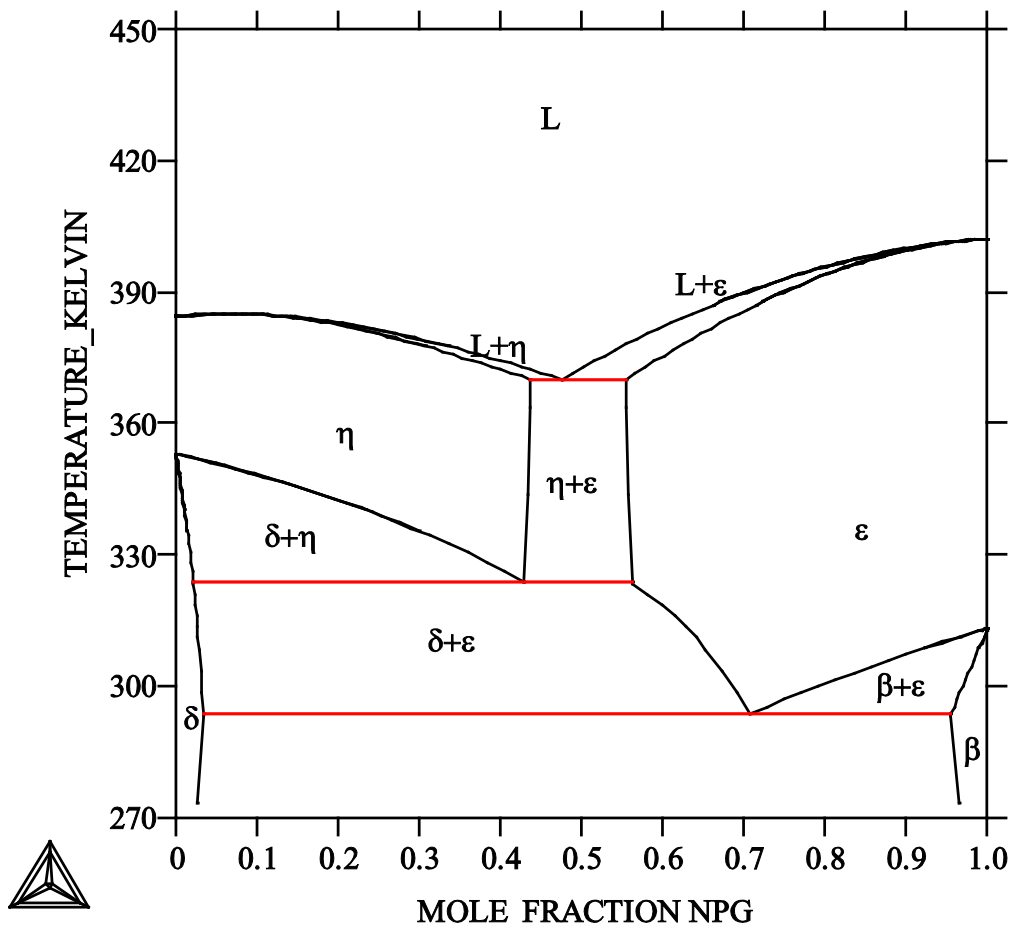


Figure 4-2 Optimized binary phase diagram of AMPL-NPG

The AMPL-NPG phase diagram reported earlier [33], agrees mostly with the experimental phase diagram, but invariant equilibria temperatures differed by 3-7K. Salud et al. re-determined the AMPL-NPG system because of incoherencies in earlier reported works [32]. Chellappa et al. [33] have reported interesting comparisons between the excess parameters reported in their work, with that reported by Salud et al. [32]. The low temperature phases were assumed to be ideal in both cases as well as this

work. This assumption was made because of limited miscibility of the low temperature phases. Temperature dependence has not been taken in to account for the determination of excess Gibbs energy parameters. The calculation of the AMPL-NPG binary phase diagram in this work, involved the use of the calculated phase diagram reported by Chellappa et al. [33]. Table 4-4 lists the invariant equilibria in the AMPL-NPG system. The binary phase diagram in this work was calculated for the assessment of the ternary system (PE-NPG-AMPL).

Table 4-4 Comparison of calculated and experimental invariant equilibria

Invariant equilibria $X_B$ (Mole fraction of NPG) Temperature				
	$\alpha$	$\gamma$	$\beta$	
$\alpha+\beta\rightarrow\gamma$	(E) 0.03	0.70	0.95	293.15 [43] and [44]
(Eutectoid 1)	(C) 0.03	0.71	0.96	290.96
	(E) 0.05	0.75	0.92	293.7 [46]
	(C) 0.09	0.79	0.98	300.5 [46]
	(E) 0.06	0.54	0.92	293.7±1.0 [45]
	$\alpha$	$\gamma'$	$\gamma$	
$\alpha+\gamma\rightarrow\gamma'$	(E) 0.05	0.43	0.51	323.15 [43] and [44]
(Eutectoid 2)	(C) 0.02	0.43	0.56	323.63
	(E) 0.06	0.46	0.51	325.0 [46]
	(C) 0.04	0.40	0.42	332.5 [46]
	(E) 0.07	0.46	0.51	325.0±1.2 [45]
	$\gamma'$	L	$\gamma$	
$\gamma+\gamma'\rightarrow L$	(E) 0.45	0.47	0.49	365.15 [43] and [44]
(Eutectic)	(C) 0.44	0.48	0.55	367.74
	(E) 0.38	0.42	0.44	377.5 [46]
	(C) 0.41	0.42	0.44	380.8 [46]
	(E) 0.39	0.42	0.44	363.9±1.4 [45]

E: Experiment, C: Calculation.

The activity of the AMPL-NPG mixture has been calculated from the excess Gibbs energy parameters.

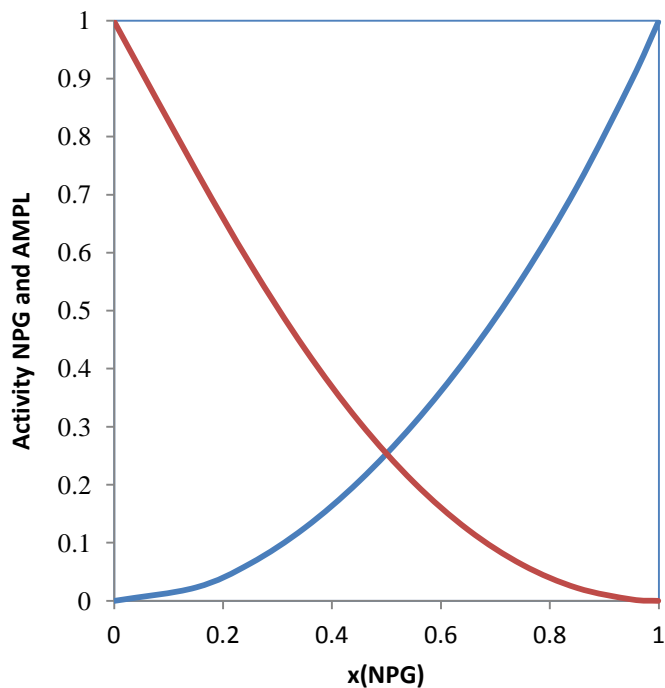


Figure 4-3 Activities of AMPL and NPG at 340K

#### ***4.3.2. PE-AMPL binary system***

The optimization of the PE-AMPL binary phase diagram was carried out using sub-regular solution models for the high temperature phases ( $\gamma$  and  $\eta$ ). Regular solution model was assumed for the low temperature phases ( $\alpha$  and  $\delta$ ), and the liquid solution was assumed to be ideal. In fact, most phase diagram calculations for these binary organic

systems utilize temperature dependent sub-regular solution for high temperature phases [38,39 and 40]. The optimized phase diagram is presented in figure 4-4a.

The ideal solution assumption is used for estimation of the Gibbs energies of the metastable phases. The following are the final optimized parameters for the PE-AMPL binary system:

$$G^{EX,\alpha} = x_A x_B (28\,452 - 91T)$$

$$G^{EX,\delta} = x_A x_B (45\,753 - 138T)$$

$$G^{EX,\gamma} = x_A x_B ((-13\,415 + 28T) - 1513(x_A - x_B))$$

$$G^{EX,\eta} = x_A x_B ((1109 - 5T) - 235(x_A - x_B))$$

$$G^{EX,L} = 0$$

The interaction parameters were very close to the ones reported by Chellappa et al. for the calculation of the PE-AMPL system using the CALPHAD method and Thermo-Calc software [34]. Table 4-5 shows experimental invariant equilibria for the PE-AMPL system.

Table 4-5 Experimental invariant equilibria

Invariant equilibria	X (mole fraction AMPL)			Temperature (K)
	$\alpha$	$\delta$	$\eta$	
$\alpha + \eta \rightarrow \delta$ (Peritectoid)	0.35	0.9	0.95	357
$\gamma \rightarrow \alpha + \eta$ (Eutectoid)	0.2	0.6	0.65	423
$\gamma + L \rightarrow \eta$ (Peritectic)	0.5	0.53	0.55	457

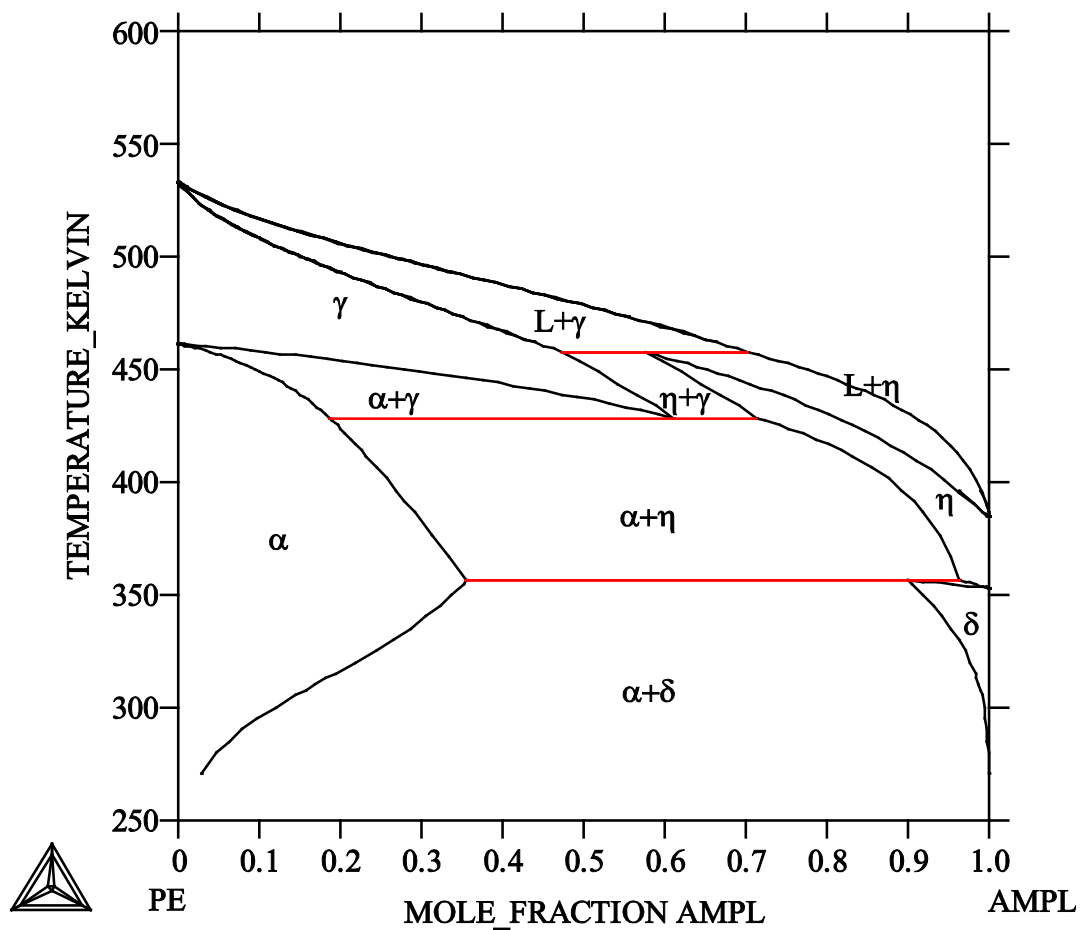


Figure 4-4a Binary phase diagram of PE-AMPL (optimized)

The low temperature peritectoid was not shown by Russell [29]. Chellappa et al. [33] attributed this to the use of incorrect pure AMPL transition temperature (357K) by Ding [44]. The use of the correct transition temperature (353K) provided by Sigma-Aldrich company, shows the existence of a peritectoid. Table 4-6 lists the Gibbs energy equations for the PE-AMPL binary system. The calculated PE-AMPL phase diagram agrees with that calculated by Chellappa et al. using CALPHAD method, that the two phase region  $\delta+\eta$  (in this case), cannot exist above the invariant temperature.

This two phase region has to be below the invariant temperature, in order to agree with Gibbs phase rule. Table 4-5 shows the Gibbs energy equations used for the calculation of PE-AMPL binary phase diagram.

Russell [29] did not report the low temperature peritectoid; this is attributed to using the incorrect pure AMPL transition temperature of 357 K reported in Ding [58]. This value is the same as the invariant temperature that she determined using DSC and x-ray analysis. A careful survey would have revealed that the value reported in the literature as well given by Sigma-Aldrich is 353 K. In this work, we have used this value to show the existence of a peritectoid. Also, the two-phase region of  $\beta+\eta$  reported by Russell [29] above the invariant temperature is not possible, since it violates the Gibbs phase rule; this two-phase region has to be below the invariant temperature. The global features of the experimental PE-AMPL binary phase diagram are not well represented using the ideal solution assumption as compared to the NPG-AMPL [59] binary system.

Table 4-6 Expressions for Gibbs energies of pure components (PE -AMPL)

No.	Gibbs energy expression
1	${}^0G_{PE}^{\alpha} = 0$
2	${}^0G_{AMPL}^{\delta} = 0$
3	${}^0G_{AMPL}^{\alpha} = 4381$
4	${}^0G_{PE}^{\delta} = 7795$
5	${}^0G_{PE}^{\gamma} = 41260 - 89.5T + 1.089T^2 + 6794.78T - 272492.72 - 1093.35T \ln(T)$
6	${}^0G_{AMPL}^{\eta} = 23300 - 66.01T - 0.275T^2 + 949.46T - 73097.48 - 110T \ln(T)$
7	${}^0G_{PE}^{\eta} = 41260 - 89.5T + 1.089T^2 + 6794.78T - 272492.7 - 1093.35T \ln(T) + 439$
8	${}^0G_{AMPL}^{\gamma} = 23300 - 66.01T - 0.275T^2 + 949.46T - 73097.48 - 110T \ln(T) + 324.2$
9	${}^0G_{PE}^L = 46280 - 98.92T + 1.3765T^2 + 7119.4T - 237151.62 - 1180.015T \ln(T)$
10	${}^0G_{AMPL}^L = 26291.4 - 73.33T - 0.29T^2 + 1026.62T - 78953.7 - 119.44T \ln(T)$

This preliminary calculated phase diagram with the ideal solution assumption showed that there is no  $\gamma+\eta$  two-phase region and the liquid phase penetrates into the low temperature  $\alpha$  phase. But this calculation gave us important clues regarding the behavior of high temperature phases. Pelton [60] systematically explained the influence of regular solution parameters on phase boundaries. It was clear that, at least, using positive regular parameters for  $\gamma$  and  $\eta$ , we can make the liquid phase ‘not penetrate’ into the low temperature  $\alpha$  phase; thus representing the true behavior of the system. In the same paper [60], Pelton describes the need for sub-regular parameters when the behavior of system is not symmetric with respect to concentration. This is indeed the case with PE–AMPL which does not exhibit symmetrical behavior like NPG–AMPL. Therefore, it was decided to use to sub-regular parameters for the high temperature  $\gamma$  and  $\eta$  phases.

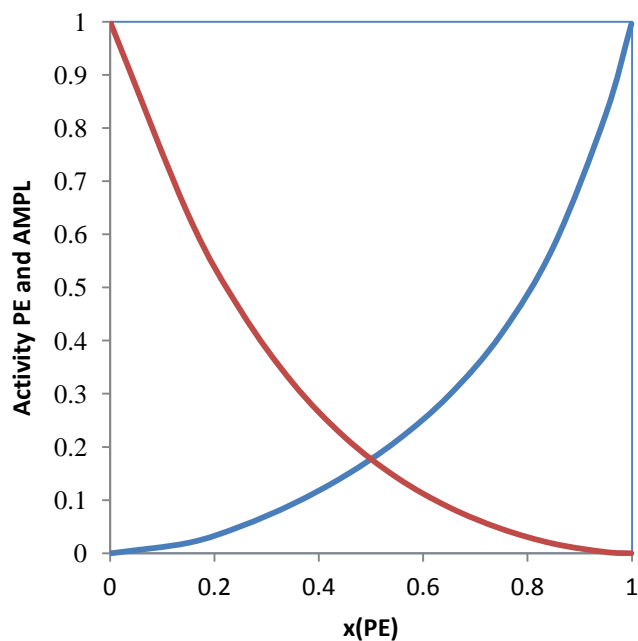


Figure 4-4b Activities of PE and AMPL at 340K

Russell [29] did not report the low temperature peritectoid; this is attributed to using the incorrect pure AMPL transition temperature of 357 K reported in Ding [44]. This value is the same as the invariant temperature that she determined using DSC and x-ray analysis. A careful survey would have revealed that the value reported in the literature as well given by Sigma-Aldrich is 353 K. In this work, we have used this value to show the existence of a peritectoid. Also, the two-phase region of  $\beta+\gamma$  reported by Russell [29] above the invariant temperature is not possible, since it violates the Gibbs phase rule; this two-phase region has to be below the invariant temperature. The calculated activities for the for the PE-AMPL system are shown in Figure 4-4b.

#### **4.3.3. PE–NPG binary system**

The PE-NPG system was optimized using Henrian solution model with temperature dependence. The optimized parameters for the binary system are given below;

$$G^{EX,\alpha} = x_A x_B (20000 - 40T)$$

$$G^{EX,\beta} = x_A x_B (25000 - 10T)$$

$$G^{EX,\varepsilon} = x_A x_B (1341)$$

$$G^{EX,\gamma} = x_A x_B (1028)$$

$$G^{EX,L} = x_A x_B (2471.8)$$

The calculated PE-NPG system resulted in a complex phase diagram depicted in Figure 4-4a Tesseire et al. [44] noticed a solid-liquid phase at 165°C (438K), whereas Chandra et al. [22] noticed a two phase region consisting of two individual high temperature phase regions. Barrio et al. [17] proposed a PE-NPG phase in the temperature range from room

temperature to 393K. They observed invariant equilibria at 343.6K which does not correspond to the phase diagrams proposed by Tesseire et al. and Chandra et al. [35, 44]. The PE-NPG phase diagram by Chandra et al. was calculated using the FACT Sage program. There is good agreement between the phase diagrams calculated by Chandra et al. and proposed by Tesseire et al. According to Tesseire et al. a two phase region exists from room temperature to 36°C, and a small region on the NPG rich side consisting of a low temperature NPG single phase and a high temperature NPG phase [44]. Table 4-7 shows the Gibbs energy expressions for the PE-NPG system.

Table 4-7 Expressions for Gibbs energies of pure components (PE-NPG)

No.	Gibbs energy expression
	PE-NPG
1	${}^0G_{PE}^{\alpha} = 0$
2	${}^0G_{NPG}^{\beta} = 0$
3	${}^0G_{PE}^{\beta} = 25000 - 10T$
4	${}^0G_{NPG}^{\alpha} = 20000 - 40T$
5	${}^0G_{PE}^{\gamma} = 41260 - 89.5T + 1.089T^2 + 6794.7T - 272492.7 - 1093.35T \ln(T)$
6	${}^0G_{NPG}^{\gamma} = 41260 - 89.5T + 1.089T^2 + 6794.7T - 272492.7 - 1093.35T \ln(T) + 1341$
7	${}^0G_{PE}^{\varepsilon} = 13630 - 43.54T + 0.35T^2 + 1621.98T - 51061.5 - 272.9T \ln(T) + 1028$
8	${}^0G_{NPG}^{\varepsilon} = 13630 - 43.54T + 0.35T^2 + 1621.98T - 51061.5 - 272.9T \ln(T)$
9	${}^0G_{NPG}^L = 18315 - 55.2T + 0.425T^2 + 2098.38T - 69849.69 - 349.613T \ln(T)$
10	${}^0G_{PE}^L = 46280. - 98.92T + 1.3765T^2 + 7119.64T - 237151.63 - 118.015T \ln(T)$

The calculated binary phase diagram for PE-NPG is shown in Figure 4-5a. The major difference between the two above mentioned phase diagrams are that Tesseire et al. [44] predicted a two phase (solid-liquid) region at about 163°C, whereas Chandra et al. predicted the presence of a two phase region consisting of two high temperature solid

phases belonging to PE and NPG each at the same temperature. Barrio et al. pointed out that since the two substances are isomorphous at high temperatures a new phase might appear. The reason that PE and NPG do not form a completely miscible solid solution in

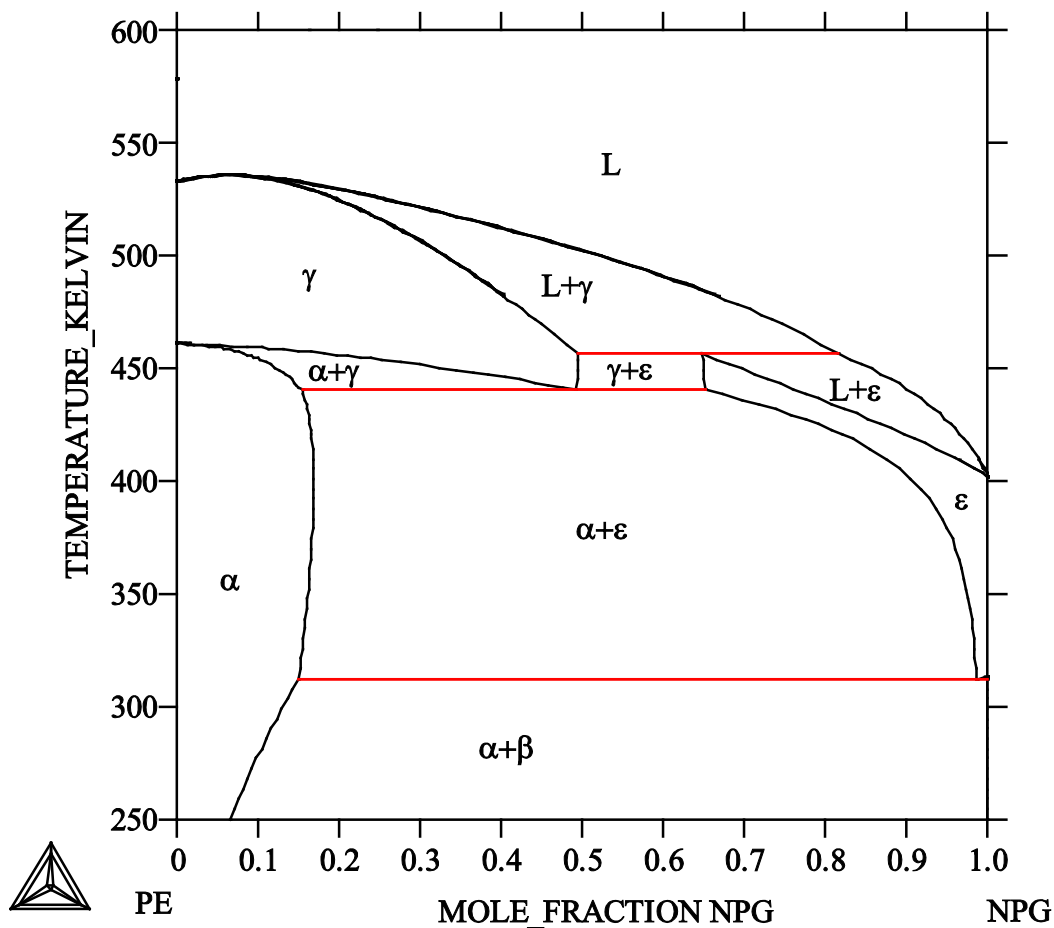


Figure 4-5a Optimized binary phase diagram for PE-NPG system

the high temperature region, unlike PE-PG and PG-NPG in spite of having the same crystal structure (FCC) is because of the nature of molecular bonding of the two O-H...O bonds of NPG with the PE. Let us consider a case of a 40% PE-60% NPG binary alloy, in which we have 90 weight%  $\gamma$  and 10 weight %  $\alpha$  at the eutectoid temperature of  $\sim 40^{\circ}\text{C}$  (313K). The composition of  $\gamma$ -phase is 35 % PE and that of the  $\alpha$ -phase is 84% PE. As

we increase the temperature above the eutectoid temperature of  $167^{\circ}\text{C}$  ( $440\text{K}$ ), say to  $177^{\circ}\text{C}$  ( $450\text{K}$ ), the  $\gamma$  phase continues to be stable, and all of  $\alpha$  phase has transforms to  $\varepsilon$ . The composition of the  $\gamma$ -phase is still remains at 35% PE, but the composition of new  $\varepsilon$ -phase is now 50% PE. Thus at  $177^{\circ}\text{C}$  we will have 30 wt.% of  $\varepsilon$  and 70 wt.% of  $\gamma$  (by the lever rule). Thus, the original 10 weight% of  $\alpha$  phase (that was below the eutectoid line) converts to 30 weight%  $\varepsilon$  phase; the composition of  $\varepsilon$  decreases from 90 weight% to 70 weight%, and in addition (20 weight% of  $\gamma$  phase also converts to  $\varepsilon$  phase). The molecular structure of NPG has 2  $-\text{OH}$  and 2  $-\text{CH}_3$  groups, as compared to PE that has 4  $-\text{OH}$  groups. When PE and NPG molecules bond in the high temperature phases, there is an increase in the  $-\text{CH}_3$  dangling bonds, and the differences in the in the vibrational motions of the PE and NPG solid solution phases [34] results in limited miscibility and the formation of a two,  $\gamma+\varepsilon$ , phase region is observed. Figure 4-5b shows the activity plot for PE and NPG, calculated from the interaction parameters.

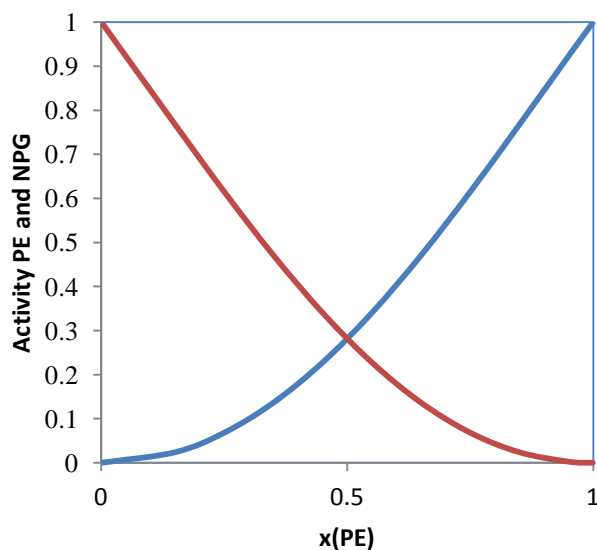


Figure 4-5b Activities of PE and NPG at 340K

#### 4.3.4. Ternary PE-NPG-AMPL

The binary phase diagrams have been calculated using a straight forward assessment of the metastable Gibbs energies along with optimization and estimation of interaction parameters. The binary phase diagrams are then used to calculate the ternary system (PE-NPG-AMPL). The following assumptions were made in order to estimate the number of phases present in the system:

- Low temperature PE has tetragonal crystal structure, NPG has monoclinic and AMPL also has monoclinic structure for the low temperature phases. In spite of AMPL and NPG being monoclinic, there is very limited solubility between the two compounds as can be seen from the AMPL-NPG phase diagram. So, it is a reasonable assumption that that the low temperature for the ternary phases consist of three phases (which are predominantly PE, NPG and AMPL depending upon composition), since there is limited solubility among the phases (i.e. no completely miscible solid solution as in PE-PG and high temperature PG-NPG).
- Crystal structures for high temperature PE, NPG and AMPL are FCC, FCC and BCC respectively. Although PE and NPG are both FCC at high temperatures, they do not form a completely miscible solid solution, and there is a small two phase region  $\gamma+\epsilon$ . This can be attributed to syncrystallization effect and the number of OH and CH<sub>3</sub> bonds in the compounds (this has been described in the PE-NPG binary phase diagram section). PE-AMPL binary system has two distinct high temperatures and the same pattern is also see in AMPL-NPG. Hence, it is assumed that there are three high temperature phases in the PE-NPG-

AMPL system. Figure 4-5c depicts the projection of phases of the binary phase diagrams on to a ternary isotherm.

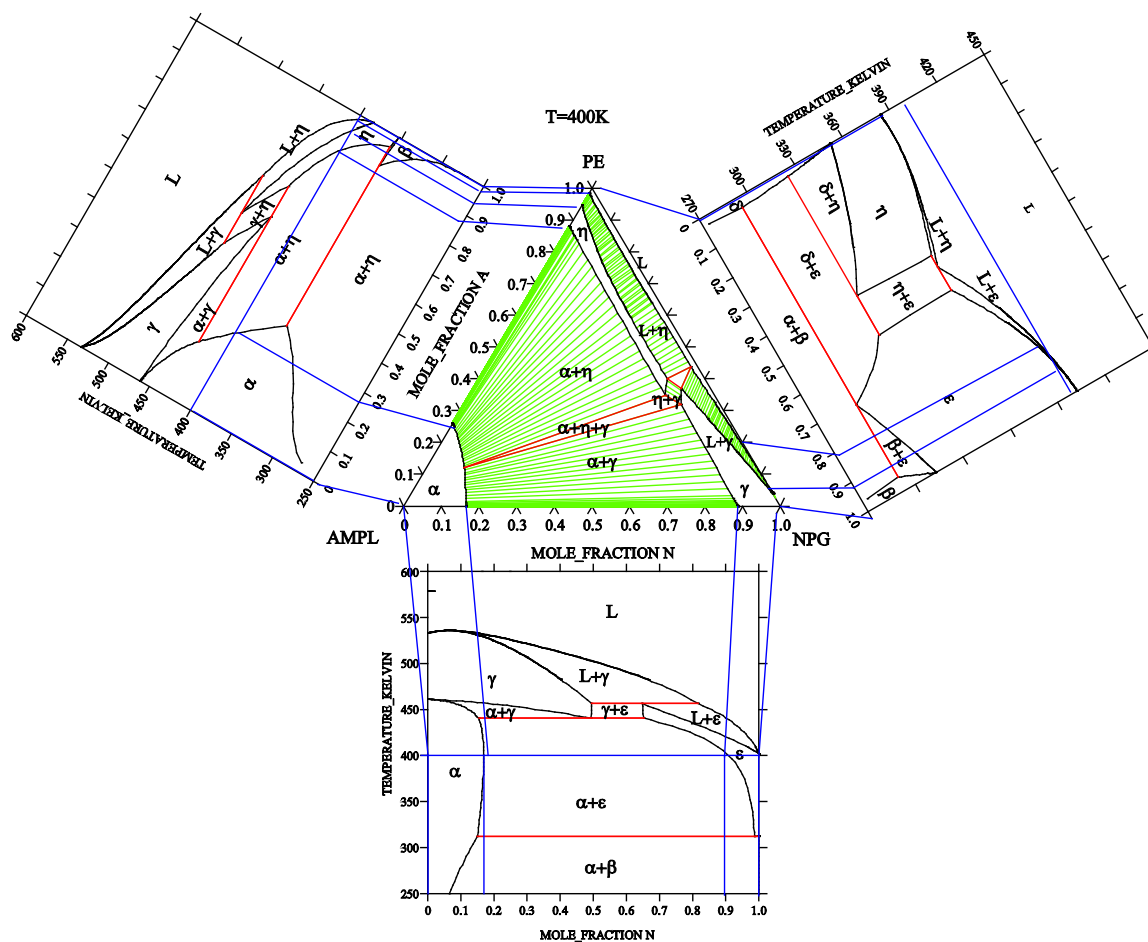


Figure 4-5c Binary phases projecting on to ternary isotherm at 400K

Figure 4-6 shows the isotherms for PE-NPG-AMPL at various temperatures. Isoleths or pseudobinary phase diagrams are plotted to determine continuous phase transitions in the

PE-NPG-AMPL ternary system, at constant composition. Figure 4-7 shows two isopleths and a corresponding isotherm at 300K. In both isopleths AMPL composition is kept constant (0.5 and 0.2 mole fraction). A composition is picked (0.5AMPL/0.25PE/0.25NPG) at 300K. at that specific composition and temperature, the isopleth as well as the isotherm shows a three phase region ( $\alpha+\delta+\epsilon$ ).

Similarly, at 0.2AMPL/0.4PE/0.4NPG and 300K, the point lies in a two phase region ( $\alpha+\epsilon$ ). The isopleths are pseudobinaries where composition is plotted against temperature. Keeping the composition fixed and increasing the temperature can show the continuous phase transitions taking place for that particular composition. For example, at 0.5AMPL/0.1NPG/0.4PE, a three phase region ( $\alpha+\beta+\delta$ ) exists at room until room temperature. This three phase region then transforms from  $\alpha+\beta+\delta$  to  $\alpha+\delta+\epsilon$ , where the  $\beta$  phase transitions in to  $\epsilon$  (low temperature NPG to high temperature NPG) at 296K. This can be explained as the contribution of the AMPL-NPG binary system to the ternary. The  $\alpha+\delta+\epsilon$  the transforms in to  $\alpha+\gamma$  at 348K. At 357K,  $\alpha+\gamma$  is becomes  $L+\alpha+\gamma$ , as liquid phase starts to appear at this temperature. This is due to the low melting point of AMPL. The  $L+\alpha+\gamma$  three phase region exists as a small sliver and then becomes  $L+\alpha$ , when the  $\gamma$  phase completely melts. At 422K  $L+\alpha$  transforms in to  $\eta+\gamma$ , and then to  $\gamma$  at 453K.  $\gamma$  phase is stable until 478K, and then becomes liquid. Similarly, at 0.2AMPL/0.4PE/0.4NPG,  $\alpha+\beta+\delta$  three phase region is stable till 297K, and then transforms on to  $\alpha+\delta$  two phase region. This two phase region then converts to  $\alpha+\epsilon$  at 312K.

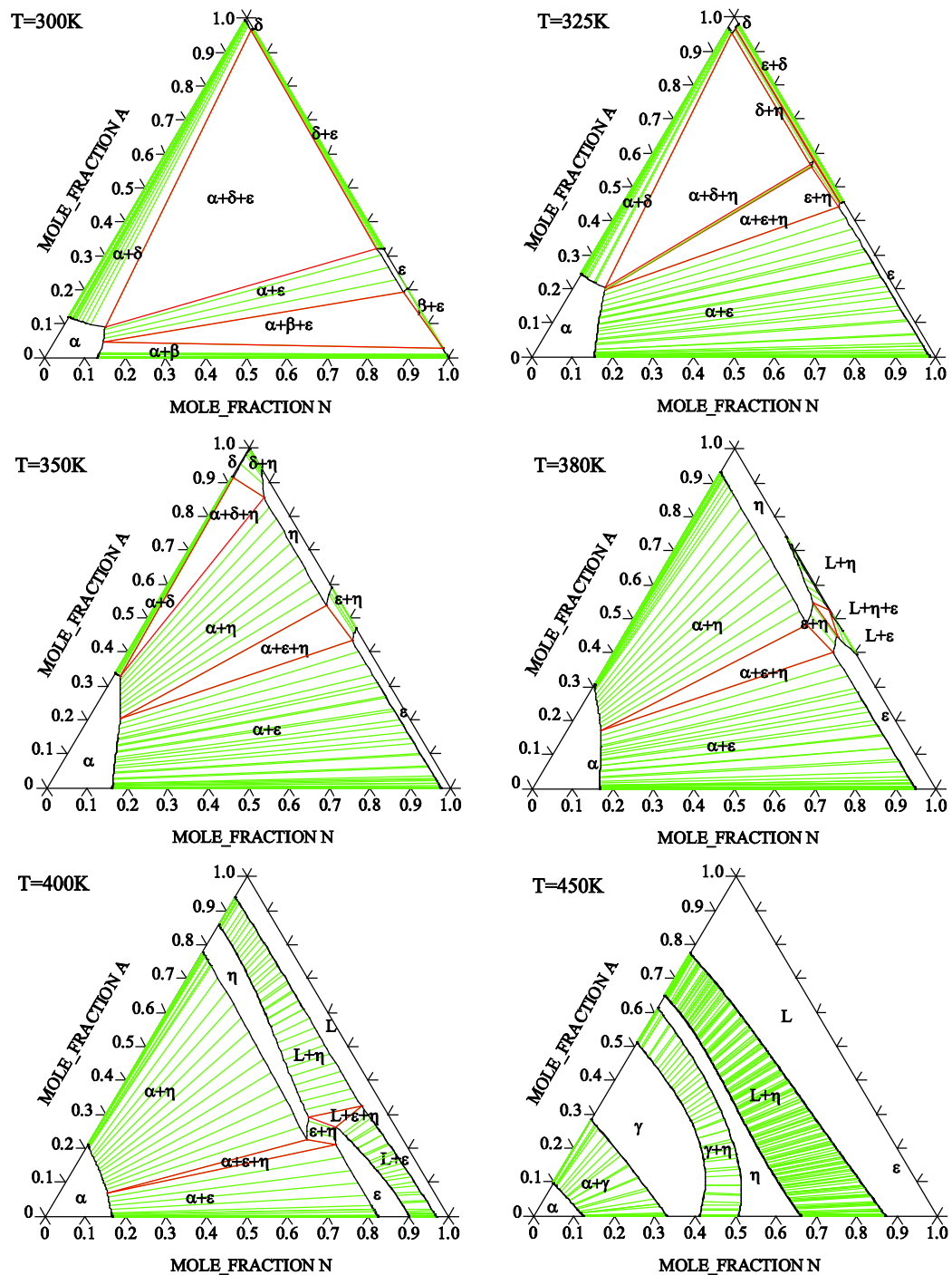


Figure 4-6 Isotherms for PE-NPG-AMPL ternary system

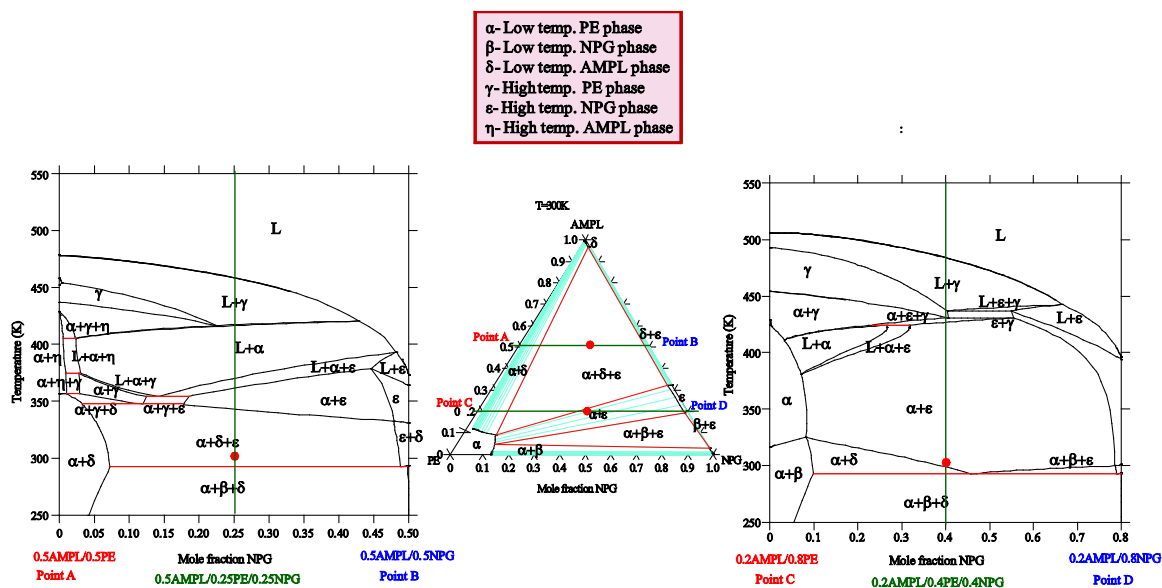


Figure 4-7 Isopleths at 0.5AMPL/0.5PE-NPG and 0.2AMPL/0.8PE-NPG and isotherm at 300K

The  $\alpha+\epsilon$  two phase fraction region is stable for a wide temperature range (312-426K). Then it transforms into  $\alpha+\epsilon+\gamma$ , which is stable up to 429K, and then becomes  $\gamma$  until 447K and then liquid phase starts appearing as  $L+\gamma$ . The  $L+\gamma$  is stable till 495K and then becomes completely liquid. Table 4-8 shows the phase transitions occurring in the PE-NPG-AMPL ternary system

Table 4-8 Phase transitions occurring in the PE-NPG-AMPL ternary system.

$X_{PE}$	$X_{NPG}$	Phase transitions
0.7	0.1	$\alpha + \beta + \delta \xrightarrow{297K} \alpha + \delta \xrightarrow{323K} \alpha + \epsilon \xrightarrow{382K} L + \alpha + \epsilon \xrightarrow{384K} L$ $L + \alpha \xrightarrow{421K} \alpha + \gamma \xrightarrow{450K} \gamma \xrightarrow{494K} L + \gamma \xrightarrow{505K} L$
0.6	0.2	$\alpha + \beta + \delta \xrightarrow{237K} \alpha + \delta \xrightarrow{318K} \alpha + \epsilon \xrightarrow{398K} L + \alpha + \epsilon \xrightarrow{403K} L$ $L + \alpha \xrightarrow{422K} \alpha + \epsilon + \gamma \xrightarrow{422.8K} \alpha + \gamma \xrightarrow{448K} \gamma \xrightarrow{479K} L + \gamma$ $\xrightarrow{502K} L$

0.35	0.15	$\alpha + \beta + \delta \xrightarrow{297K} \alpha + \delta + \varepsilon \xrightarrow{348K} \alpha + \gamma + \varepsilon \xrightarrow{353K} L + \alpha \xrightarrow{415K}$ $L + \eta + \gamma \xrightarrow{423K} \gamma \xrightarrow{438K} L + \gamma \xrightarrow{477K} L$
0.1	0.4	$\alpha + \beta + \delta \xrightarrow{297K} \alpha + \delta + \varepsilon \xrightarrow{338K} \alpha + \varepsilon \xrightarrow{3376K} L + \alpha + \varepsilon \xrightarrow{381K}$ $L + \alpha \xrightarrow{420K} L + \gamma \xrightarrow{431K} L$
0.2	0.6	$\alpha + \beta + \delta \xrightarrow{297K} \alpha + \beta + \varepsilon \xrightarrow{299K} \alpha + \varepsilon \xrightarrow{427K} \varepsilon \xrightarrow{432K}$ $L + \varepsilon \xrightarrow{447K} L + \varepsilon + \gamma \xrightarrow{448K} L + \gamma \xrightarrow{452K} L$

#### 4.3.5. Activity Calculations

Interaction parameters are numerical coefficients introduced by Wagner [61], to allow a limiting expression of activity coefficient in terms of solute concentrations. For a ternary system, this can take the form

$$\ln \gamma_i = \ln \gamma_i^0 + \varepsilon_i^i X_i + \varepsilon_i^j X_j$$

Where  $\varepsilon$ 's are the interaction parameters, the X's are the mole fractions of the two solutes, and  $\gamma_i^0$  is the activity coefficient of the i-th component. In a sense, the interaction parameters define the strength between the solute species. Numerical values for interaction parameters can be evaluated from electromotive force measurements. But in this work, interaction parameters are calculated using the PARROT module in the Thermo-Calc software.

#### Application of Krupkowski's formalism

Krupkowski's formalism [62] can be applied to evaluating activity coefficients in multicomponent systems from data for the pertinent binary systems. This method is used

for the calculation of ternary activity coefficients from binary data, since no ternary experimental data is available for PE-NPG-AMPL system and the ternary interaction parameter is considered zero. For binary solutions the following equations are used;

$$\ln \gamma_j = \omega_{jk}(T) \left[ (1 - X_k)^{m_{jk}} - \frac{m_{jk}}{m_{jk} - 1} (1 - X_k)^{m_{jk} - 1} + \frac{1}{m_{jk} - 1} \right]$$

$$\ln \gamma_k = \omega_{jk}(T)(1 - X_k)^{m_{jk}}$$

where:

$\gamma_j, \gamma_k$  = activity coefficients of the component  $j$  and  $k$

$\omega_{jk}$  = function of binary solutions dependent on temperature

$m_{jk}$  = experimental asymmetry coefficient independent of temperature

Since, this work provides only calculated values of activity, the experimental asymmetric coefficient ( $m_{jk}$ ) is assumed to be unity. It should be noted that while using this data for comparison with experiments  $m_{jk}$  should be accounted for.

According to Krupkowski's formalism the equation for activity in coefficient in multicomponent system takes the form,

$$\ln \gamma_i = \sum_{\substack{j,k=1 \\ j \neq k}}^n [\ln \gamma_i]_{j,k}$$

where,  $[\ln \gamma_i]_{j,k}$  is the partial contribution of binary solutions.

The procedure for calculating ternary activity from binary data has been previously described in literature [63], and allows operation of  $\ln \gamma_i$  at any chosen composition. The relation for  $\ln \gamma_{PE}$  can be described as:

$$\begin{aligned} \ln \gamma_{PE} = & -\omega_{PE-NPG}(1-X_{PE})X_{PE}X_{NPG} + \omega_{PE-NPG}(1-X_{PE})X_{NPG} \\ & - \omega_{PE-AMPL}(1-X_{PE})X_{PE}X_{AMPL} + \omega_{PE-AMPL}(1-X_{PE})X_{AMPL} \\ & - \omega_{NPG-AMPL}(1-X_{PE})X_{NPG}X_{AMPL} \end{aligned}$$

Table 4-9 Activity of PE (at 0.06  $X_{PE}$ ) at 460, 500 and 640K

$X_{NPG}$	$X_{AMPL}$	$\ln \gamma(PE)$		
		460K	500K	640K
0.01	0.94	2.168398	2.261424	2.587013
0.15	0.84	1.94679	2.029919	2.32087
0.25	0.74	1.724401	1.797634	2.053949
0.35	0.64	1.503497	1.566834	1.788511
0.45	0.54	1.283719	1.337159	1.5242
0.55	0.44	1.064708	1.108251	1.260655
0.65	0.34	0.846103	0.87975	0.997517
0.75	0.24	0.627546	0.651297	0.734426
0.85	0.14	0.408678	0.422533	0.471025
0.95	0.04	0.18914	0.193098	0.206953
0.94	0.01	0.118332	0.119321	0.122785

## 4.5. Conclusions

The phase diagram for the AMPL–NPG system was calculated utilizing a simple estimation for metastable Gibbs energies, in combination with thermodynamic optimization. The low-temperature  $\alpha$  and  $\beta$  phases and the liquid phase were assumed to be ideal. An initial assumption of ideality in the high-temperature phases is used only to estimate the metastable Gibbs energies. The nonideality of the high temperature solution phases have been modeled as subregular solutions. The optimization using Thermo-Calc software included data from the phase diagram only (tie lines and invariant equilibria composition and temperatures). There is good agreement between the calculated and experimental phase boundaries and invariant equilibria. The agreement between the calculated and measured values of the enthalpies of fusion is not very good but reasonable especially since the measured values were not used in the thermodynamic optimization.

The magnitude of heat capacities ( $245\text{--}475\text{ J mol}^{-1}\text{ K}^{-1}$ ) for these organic plastic crystals is relatively high and they result from sharp increases during the solid–solid phase transitions. Such changes become significant since they also have low melting temperatures ( $400\text{--}500\text{ K}$ ). These effects can become important when making an initial phase diagram calculation in the absence of any experimental phase diagram data and help us narrow down the expected phase diagram behavior.

The metastable Gibbs energies of pure components were determined assuming ideal solutions. The regular and sub-regular excess Gibbs energy parameters were optimized for using the PARROT module of Thermo-Calc. The liquid phase was assumed to be

ideal. The calculated invariant equilibria and tie-line temperature and compositions from the optimized phase diagram are in good agreement with the experimental values. The enthalpies of fusion are also in reasonable agreement with the experimental values.

In contrast to the case for the NPG–AMPL binary system, the heat capacities did not play a significant role in the calculated binary phase diagram assuming ideal solution for all phases. This can be attributed to the fact that the solution phases of PE–AMPL are highly non-ideal and this non-ideality has a dominating effect rather than inclusion of heat capacities. Nevertheless, the knowledge of the heat capacities has been included in determining the Gibbs energies of the pure components. The PE-NPG-AMPL ternary system has been calculated using the CALPHAD method using available experimental binary phase diagram data. The activity of PE in liquid PE-NPG-AMPL is calculated using Krupkowski's formalism. The isopleths provide important information on the phase transitions happening in the system. There is no record of any experimental data published for this particular ternary system. The calculated PE-NPG-AMPL ternary phase diagram might be useful to provide valuable information regarding phase transitions and microstructure evaluation for this alloy.

## References:

- 
- 1 W.J. Dunning, *J. Phys. Chem. Solids*, (1961), 18, 21.
  - 2 J. Timmermans, *J. Phys. Chem. Solids*, (1961), 18, 1.
  - 3 G. W. Gray and P. A. Winsor, "Liquid Crystals and Plastic Crystals", Ed. Ellis Horwood Limited, Chichester, Great Britain, 1974.
  - 4 L. A. K. Staveley, *J. Phys. Chem. Solids*, (1961) 18 46.
  - 5 R. Rudman, *Solid State Communication*, (1979) 29 765.
  - 6 J. Timmermans, *J. Chim. Phys.*, (1938) 35 331.
  - 7 I. Nitta and T. Watanabe. *Bull. Chem. Soc. Japan*, **13** 1 (1938), pp. 28–35.
  - 8 D. Chandra and J.J. Fitzpatrick, *Advances in X-Ray Analysis*, **vol. 28**, in: C.S. Barrett, P.K. Fredecki, D.E. Levdin, Editors (1985), pp. 353–360.
  - 9 E. Murrill and L. Breed. *Thermochim. Acta*, **1** (1970), pp. 239–246.
  - 10 D.K. Benson, R.W. Burrows and J.D. Webb. *Solar Energy Mater.*, **13** (1986), pp. 133–152.
  - 11 J. Font, J. Muntasell, J. Navarro, J.Ll. Tamarit and J. Lloveras. *Solar Energy Mater.*, **15** (1987), pp. 209–310.
  - 12 M. Barrio, J. Font, J. Muntasell, J. Navarro and J.Ll Tamarit. *Solar Energy Mater.*, **18** (1988), pp. 109–115.
  - 13 D. Chandra, C.S. Barrett, Final Report to the DOE Contract No. DE-AC03-84SF12205, 1986.
  - 14 D. Chandra, C.S. Barrett and D.K. Benson, Plenum Publishing (1986), pp. 305–313.
  - 15 D. Chandra, C.S. Barrett and D.K. Benson, Plenum Publishing (1986), pp. 609–616.
  - 16 M. Barrio, J. Font, D.O. Lopez, J. Muntasell, J.Ll. Tamarit, N.B. Chanh and Y. Haget. *J. Chim. Phys.*, **87** (1990), pp. 1835–1851.
  - 17 D. Chandra, R.A. Lynch, W. Ding and J.J. Tomlinson. *Adv. in X-Ray Anal.*, **33** (1990), pp. 445–452.
  - 18 D. Chandra, Final Report to Oakridge National Laboratory Contract No. 19X-SC644V/DE-AC05-84 OR21400, 1990.
  - 19 J. Font, D.O. Lopez, J. Muntasell and J.Ll. Tamarit. *Mat. Res. Bull.*, **24** (1989), pp. 1251–1259.
  - 20 M. Barrio, J. Font, D.O. Lopez, J. Muntasell, J.Ll. Tamarit, N.B. Chanh and Y. Haget. *J. Phys. Chem. Solids*, **52** 5 (1991), pp. 665–672.
  - 21 M. Teisseire, N.B. Chanh, M.A. Cuevas-Diarte, J. Guion, Y. Haget, D.O. Lopez and J. Muntasell. *Thermochim. Acta*, **181** (1991), pp. 1–11.
  - 22 M. Barrio, J. Font, D.O. Lopez, J. Muntasell, J.Ll Tamarit, N.B. Chanh, Y. Haget, M. Teisseire, J. Guion and X. Alcobe. *J. Chim. Phys.*, **89** (1992), pp. 695–705.
  - 23 J. Hansen, M.S. Thesis, University of Nevada, Reno, 1997.
  - 24 M. Barrio, D.O. Lopez, J.Ll. Tamarit, P. Negrier and Y. Haget. *J. Mater. Chem.*, **5** 3 (1995), pp. 431–439.
  - 25 M. Barrio, J. Font, J. Muntasell, J.Ll. Tamarit, N.B. Chanh and Y. Haget. *J. Chim Phys.*, **87** (1990), pp. 2455–2470.
  - 26 M. Barrio, J. Font, D.O. Lopez, J. Muntasell, J.Ll. Tamarit, P. Negrier, N.B. Chanh and Y. Haget. *J. Phys. Chem. Solids*, **54** 2 (1993), pp. 171–181.

- 
- 27 M. Barrio, D.O. Lopez, J.Ll. Tamarit, P. Negrier and Y. Haget. *J. Solid State Chem.*, **124** (1996), pp. 29–38.
- 28 M. Barrio, J. Font, D.O. Lopez, J. Muntasell, J.Ll. Tamarit and Y. Haget. *J. Chim. Phys.*, **91** (1994), pp. 189–202.
- 29 R. Russell, M.S. Thesis, University of Nevada, Reno, 1995.
- 30 D. Chandra, W. Ding and R.A. Lynch. *J. Less-Common Metals*, **168** (1991), pp. 159–167.
- 31 M. Barrio, J. Font, D.O. Lopez, J. Muntasell, J.Ll. Tamarit, P. Negrier and Y. Haget. *J. Phys. Chem. Solids*, **55** 11 (1994), pp. 1295–1302.
- 32 J. Salud, D.O. Lopez, M. Barrio, J.Ll. Tamarit, H.A.J. Oonk, P. Negrier and Y. Haget. *J. Solid State Chem.*, **133** (1997), pp. 536–544.
- 33 Raja Chellappa, Dhanesh Chandra, CALPHAD, **27** (2003) 133-140.
- 34 Raja Chellappa, Renee Russell, Dhanesh Chandra, CALPHAD, **28** (2004) 3-8.
- 35 J. Marrero and R. Gani, Fluid Phase Equilibria, **183**, 2001, 183-208
- 36 E. Murrill and L. Breed. *Thermochim. Acta*, **1** (1970), pp. 239–246.
- 37 D. Chandra, W. Ding and R.A. Lynch. *J. Less-Common Metals*, **168** (1991), pp. 159–167.
- 38 J. Salud, D.O. Lopez, M. Barrio, J.Ll. Tamarit, H.A.J. Oonk, P. Negrier and Y. Haget. *J. Solid State Chem.*, **133** (1997), pp. 536–544.
- 39 D.O. Lopez, J. Van Braak, J.Ll. Tamarit and H.A.J. Oonk. *Calphad*, **18** 4 (1994), pp. 387–396.
- 40 D.O. Lopez, J. Van Braak, J.Ll. Tamarit and H.A.J. Oonk. *Calphad*, **19** 1 (1995), pp. 37–47
- 41 D. Eilerman, R. Lippman and R. Rudman. *Acta Cryst.* **B39** (1983), pp. 263–266.
- 42 E Murrill and L Breed. *Thermochim. Acta*, **1** (1970), pp. 239–246.
- 43 D. Chandra, W. Ding and R.A. Lynch. *J. Less-Common Metals*, **168** (1991), pp. 159–167.
- 44 W. Ding, M.S. Thesis, University of Nevada, Reno, 1991.
- 45 M. Barrio, J. Font, D.O. Lopez, J. Muntasell, J.Ll. Tamarit, P. Negrier and Y. Haget. *J. Phys. Chem. Solids*, **55** 11 (1994), pp. 1295–1302.
- 46 J. Salud, D.O. Lopez, M. Barrio, J.Ll. Tamarit, H.A.J. Oonk, P. Negrier and Y. Haget. *J. Solid State Chem.*, **133** (1997), pp. 536–544.
- 47 D Chandra, W.-M Chien, V Gandikotta and D.W Lindle. *Z. Phys. Chem.*, **216** (2002).
- 48 M Barrio, J Font, D.O Lopez, J Muntasell, J.Ll Tamarit and Y Haget. *J. Chim. Phys.*, **91** (1994), pp. 189–202.
- 49 A.D Pelton. *Met. Trans. A*, **19A** (1988), pp. 1819–1825.
- 50 M. Barrio, J. Font, J. Muntasell, J. Navarro, J.Ll. Tamarit, Sol. Energy Mater. **18** (1–2) (1998) 109.
- 51 D. Chandra, Crystal Structure and Thermal Studies On solid –State Energy Storage Materials, Final Report, Contract number:19X-SC644V/DE-AC05-84 OR21400, 1990
- 52 M.Teisseire, N.B. Chanh, M.A. Cuevas-Diarte, J. Guion, Y. Haget, D. Lopez and J. Muntasell *Thermochimica Acta* **181** (1991) 1.
- 53 D. Chandra, C.S. Barrett, Final Report to DOE, Contract No. DEAC03- 84SF12205, January, 1986.

- 
- 54 Chandra, C.S. Barrett and D.K. Benson *Advances in X-ray Analysis*. 32 (1989) 609.
- 55 N. Saunders and A.P. Miodownik, *CALPHAD :A Comprehensive Guide*, Elsevier Science Ltd (1998).
- 56 N Saunders and A.P Miodownik, *Pergamon Materials Series, CALPHAD (Calculation of Phase Diagrams): A Comprehensive Guide*, Elsevier Science Ltd (1998)
- 57 Thermo-Calc® User's Guide, Version N, Thermo-Calc Software AB, Stockholm, Sweden, 2000. [SD-008]
- 58 W. Ding, M.S. Thesis, University of Nevada, Reno, 1991.
- 59 R Chellappa and D Chandra. *Calphad*, **27** (2003), pp. 133–140.
- 60 A.D Pelton and W.T Thompson. *Prog. Solid State Chem.*, **10** 3 (1975), p. 119.
- 61 C. Wagner: *Thermodynamics of Alloys*, Addison-Wesley Publ. Co., Cambridge, Mass., 1952.
- 62 A. Krupkowski: *BUl. Acad. Pol. Sci. Lett.*, 1951, vol. 1, 15-45.
- 63 W. Ptak and Z. Moser: *Arch. Hutnictwa*, 1996, 11, 289-324

## Chapter V *∞* Phase diagram calculations of pentaglycerine-neopentylglycol-2-amino-2methyl-1,3, propanediol (PG-NPG-AMPL) ternary system

---

A thermodynamic analysis of the pentaglycerine-neopentylglycol-2-amino-2methyl-1,3, propanediol ternary system has been performed by using the CALPHAD approach. Because of the lack of experimental information available for the ternary system, binary phase diagrams of PG-NPG, PG-AMPL and AMPL-NPG were calculated using the CALPHAD method and optimized using the PARROT program in Thermo-Calc. Available experimental was used for the optimization method and estimation of excess energies for the binaries. The calculated phase diagrams were in good accordance with previous experimental results. The ternary PG-NPG-AMPL as well as the binaries was calculated from room temperature to the liquid phase. Substitutional solution model was assumed for optimization of interaction parameters.

The calculation of the PG-NPG-AMPL system involved PG-AMPL, NPG-AMPL and PG-NPG binaries. The PG-NPG binary phase diagram has been calculated and discussed in chapter 3, whereas, the AMPL-NPG phase diagram has been described in detail in chapter 4. In this chapter, the PG-AMPL binary phase diagram is calculated and then extrapolated in to the ternary (PG-NPG-AMPL system)

The calculation procedure is similar to the ones used for the other binary systems; and involves the calculation of metastable phases.

## 5.1. Computational Procedure

### 5.1.1. *Thermodynamic Modeling of Solution Phases*

The most relevant features of the description of the thermodynamic parameters are discussed for the present purpose. The low temperature phases are characterized by  $\alpha$  or  $\beta$ , the high temperature phases are designated as  $\gamma$ ,  $\gamma'$ , and the liquid phase as L. For simplicity PG is represented by A, NPG as B and AMPL as C. Table 5-1 shows the list of symbols used to describe the phases on the PG-NPG-AMPL ternary phase diagram.

Table 5-1 List of symbols for PG-NPG-AMPL ternary system

Symbol	Phase
Liq or L	Liquid
$\alpha$	Low temperature PG phase
$\beta$	Low temperature NPG phase
$\delta$	Low temperature AMPL phase
$\gamma$	High temperature PG, NPG phase
$\gamma'$	High temperature AMPL phase
L	Liquid phase

A CALPHAD type optimization using regular and subregular solution model is considered to be adequate to describe the Gibbs energies of different phases. The low temperature “Phase II” are represented by  $\alpha$  or  $\beta$  and the high temperature phases are represented as  $\gamma$  or  $\gamma'$ . The liquid phase is designated as “L”.

If the reference state for each phase is taken to be that of the pure components in that phase, then the Gibbs energy of a solution phase  $\phi$  ( $\phi = \alpha, \beta, \gamma, \gamma', L$ ) can be represented

as follows (unit of Gibbs energy is  $\text{J mol}^{-1}$  throughout this work, where a mol is a mole of formula unit):

$$G^\phi = x_A {}^0G_A^\phi + x_B {}^0G_B^\phi + x_C {}^0G_C^\phi + RT(\ln x_A + \ln x_B + \ln x_C) + G^{EX,\phi} \quad (1)$$

Where  $\phi = \alpha, \beta, \gamma, \gamma', L, R$ ,  $R = 8.314 \text{ J mol}^{-1} \text{ K}^{-1}$ ,  $x_A$  is the mole fraction of "A",  $x_B$  is the mole fraction of "B" and  $x_C$  is the mole fraction of "C".  ${}^0G_A^\phi$ ,  ${}^0G_B^\phi$  and  ${}^0G_C^\phi$  are the pure component Gibbs energies in  $\phi$ .

The excess Gibbs energy for a binary system A-B, can be demoted as;

$$G_{mix}^{xs} = x_A x_B (L_{AB}^0 + L_{AB}^1 (x_A - x_B)) \quad (2)$$

The binary interaction parameters for excess Gibbs energies,  $L_{i,j}^\phi$  can be expressed as follows:

$$L_{i,j}^\phi = \sum_{n=0}^m {}^n L_{i,j}^\phi (x_i - x_j)$$

The ternary excess Gibbs free energy is written as follows:

$$G_{mix}^{xs} = x_A x_B (L_{AB}^0 + L_{AB}^1 (x_A - x_B)) + x_B x_C (L_{BC}^0 + L_{BC}^1 (x_B - x_C)) + x_A x_C (L_{AC}^0 + L_{AC}^1 (x_A - x_C)) \quad (3)$$

The binary and the ternary interaction parameters  ${}^n L_{i,j}^\phi$  and  ${}^n L_{i,j,k}^\phi$  take the following form:

$${}^n L_m^\phi = a + bT + cT \ln(T) + dT^2 + eT^{-1} + fT^3 + gT^7 + hT^9$$

where  $a, b, c, d, e, f, g$  and  $h$  are the excess Gibbs energy parameters. In most cases only the first two terms of the above equation are used.

For a phase  $\phi$  ( $\phi = \alpha, \beta, \delta, \gamma, \varepsilon, \eta, L$ ),  ${}^0G_A^\phi$ ,  ${}^0G_B^\phi$  and  ${}^0G_C^\phi$  are the reference states of pure “A”, “B” and “C”, same as  $\phi$ . A single reference phase is chosen for each component.

The reference phases were chosen and denoted as:  $\alpha$  for “A”,  $\beta$  for “B” and  $\delta$  for “C” and set to zero.

Therefore,

$${}^0G_A^\alpha = 0, {}^0G_B^\beta = 0 \text{ and } {}^0G_C^\delta = 0 \quad (4)$$

The binary phase diagrams are calculated first and extrapolated to a ternary system.

The stable phases for “A” and B are  $\alpha$ , and  $\gamma$ , and  $\beta$  and  $\gamma'$  for “C”. Gibbs energies of the other phases in terms of these reference states can be represented as:

For system A-B (PE-PG), the Gibbs energies of the other phases in terms of the reference phases can be represented as:

$${}^0G_A^\gamma = {}^0G_A^\alpha + \Delta {}^0G_A^{\alpha \rightarrow \gamma} = \Delta {}^0G_A^{\alpha \rightarrow \gamma} \quad (5)$$

$${}^0G_A^L = {}^0G_A^\alpha + \Delta {}^0G_A^{\alpha \rightarrow L} = \Delta {}^0G_A^{\alpha \rightarrow \gamma} + \Delta {}^0G_A^{\alpha \rightarrow L} \quad (6)$$

$${}^0G_B^\varepsilon = {}^0G_B^\beta + \Delta {}^0G_B^{\beta \rightarrow \varepsilon} = \Delta {}^0G_B^{\beta \rightarrow \gamma} \quad (7)$$

$${}^0G_B^L = {}^0G_B^\beta + \Delta {}^0G_B^{\beta \rightarrow L} = \Delta {}^0G_A^{\beta \rightarrow \varepsilon} + \Delta {}^0G_B^{\beta \rightarrow L} \quad (8)$$

The pure Gibbs energies were determined using the heat capacity data. So, for component “A” the Gibbs energies of the stable phases are:

$${}^0G_A^\gamma = {}^0G_A^\alpha + \Delta {}^0G_A^{\alpha \rightarrow \gamma} = \Delta {}^0G_A^{\alpha \rightarrow \gamma}$$

$${}^0G_A^\gamma = \Delta H_{TR} - T\Delta S_{TR} + \int_{T_{TR}}^T \Delta C_P^{\alpha \rightarrow \gamma} dT - T \int_{T_{TR}}^T \frac{\Delta C_P^{\alpha \rightarrow \gamma}}{T} dT$$

$${}^0G_A^L = {}^0G_A^\alpha + \Delta {}^0G_A^{\alpha \rightarrow L} = \Delta {}^0G_A^{\alpha \rightarrow \gamma} + \Delta {}^0G_A^{\alpha \rightarrow L}$$

$${}^0G_A^L = \Delta H_{TR} - T\Delta S_{TR} + \int_{T_{TR}}^T \Delta C_P^{\alpha \rightarrow \gamma} dT - T \int_{T_{TR}}^T \frac{\Delta C_P^{\alpha \rightarrow \gamma}}{T} dT + \Delta H_F - T\Delta S_F + \int_{T_F}^T \Delta C_P^{\gamma \rightarrow L} dT - T \int_{T_F}^T \frac{\Delta C_P^{\gamma \rightarrow L}}{T} dT$$

Similar expressions can be obtained for Gibbs energies of stable phases of “B” and “C”.

### 5.1.2. Metastable Phase Calculations

Metastable phases are only calculated for the PE-AMPL system and PG-NPG system.

The PE-PG shows complete miscibility for both low and high temperature phases. The

Gibbs energies for metastable phases are estimated by modifications to the stable phases.

For example, for “ A” in  $\beta$  phase, we are interested in determining the difference,

${}^0G_A^\beta - {}^0G_A^\alpha$ , such that we can express,

$${}^0G_A^\beta = {}^0G_A^\alpha + M_A^\beta$$

The Gibbs energy of the  $\beta$  phase,  $G_m^\beta$ , can now be written as:

$$G_m^\beta = x_A ({}^0G_A^\alpha + M_A^\beta) + x_C {}^0G_C^\beta + RT \times (x_A \ln x_A + x_C \ln x_C) + G^{EX,\beta}$$

$$G_m^\beta = x_A M_A^\beta + RT \times (x_A \ln x_A + x_C \ln x_C) + G^{EX,\beta}$$

Similarly for the  $\alpha$  phase, we can write the Gibbs free energy,  $G_m^\alpha$ , as:

$$G_m^\alpha = x_A {}^0G_A^\alpha + x_B ({}^0G_B^\beta + M_B^\alpha) + RT \times (x_A \ln x_A + x_B \ln x_B) + G^{EX,\alpha}$$

$$G_m^\alpha = x_B M_B^\alpha + RT \times (x_A \ln x_A + x_B \ln x_B) + G^{EX,\alpha}$$

To estimate  $M_A^\beta$  and  $M_C^\alpha$ ,  $\alpha$  and  $\beta$  phases are assumed to be ideal solutions. It should be noted that this assumption is based only for the purpose of calculating the metastable phases.

Therefore, the partial molar Gibbs free energies can be written as:

$$G_B^\beta = {}^0G_B^\beta + RT \ln(x_B^\beta)$$

$$G_B^\alpha = {}^0G_B^\alpha + RT \ln(x_B^\alpha)$$

Where,  $G_B^\beta$  and  $G_B^\alpha$  are the Gibbs energies of “B” in the  $\beta$  and  $\alpha$  phases respectively. At equilibrium,  $G_B^\beta = G_B^\alpha$ , the following estimation can be made at the temperature of maximum solubility,  $T=T_{\max}$ ,

The assumption that  $\alpha$  and  $\beta$  phases are ideal solutions is used only to describe the metastable pure Gibbs energies  ${}^0G_B^\alpha$  and  ${}^0G_A^\beta$ . The nature of non-ideality of  $\alpha$  phase can still be expressed using a subregular solution model for  $G^{EX,\alpha}$ .

## **5.2. PG-AMPL binary phase diagram**

The experimental PG-AMPL binary phase diagram was reported by Salud et al. in 1997 [1]. They established the phase diagram from room temperature to the liquid state using thermal analysis and X-ray powder diffraction techniques. They discussed the intermolecular interactions in the orientationally disordered mixed crystals by analyzing the evolution of the packing coefficient as a function of the composition. They analyzed the phase diagram thermodynamically using the enthalpy-entropy compensation theory.

From the Guinier-Simon patterns, they determined the existence of a two-phase domain  $[M_1+Q]$ , the disappearance of the cubic  $C_1$  phase, and giving rise to a  $[M_1 + C_1]$  domain. At 330K, they noticed the disappearance of the  $M_1$  phase. At  $X=0.55$  (mole fraction PG), as the temperature increased, they noticed the transition from  $[M_1+Q]$  to  $[Q+C_1]$  at 321K. At the same composition in the mixture the  $C_1$  phase disappeared and  $C_F$  appeared at 326-328K, giving rise to a  $[Q+C_F]$  two-phase domain. At higher temperatures, transformations of the  $[Q+C_F]$  domain to  $[C_F]$  on-phase domain (to an orientationally disordered molecular alloy). They were not able to make a proper determination of the transition from plastic crystalline solid to liquid. Salud et al. [1] attribute this to the large differences in vapor pressure. Determination of these characteristics of the phase diagram were made by diffraction as a function of temperature. They also did diffraction at constant temperature because, they wanted to determine the existence of close eutectoid invariants, and to delimit the range of the  $[M_1+Q]$  and  $[C_1+C_F]$  two-phase region.

Tamarit et al. [2] showed that the intermolecular interactions by hydrogen bonds play an important role in the orientationally disordered phases. Salud et al. [1] studied the packing coefficient evolution for PG-AMPL and observed that the total number of groups able to form hydrogen bonds are equal; two  $CH_2OH$  groups and one  $NH_2$  group in the AMPL molecule and three  $CH_2OH$  groups in the PG molecule. They also showed that the substitution of the molecules did not produce any significant changes in the intermolecular interaction scheme. They also emphasized the relatively high values of the packing parameter for the pure compounds as well as for their alloys, which ruled out incompatibility between high packing and the existence of orientational disorder [3]. Salud et al. [1] used the enthalpy-entropy compensation theory [4] to thermodynamically

analyze the phase diagram. Since excess enthalpy data are hard to obtain, they measured the heat of melting as a function of the mol fraction for the PG-AMPL system in each solid solution domain. They assumed temperature independent enthalpy form and nonexistence of excess values for the liquid solution. The excess enthalpy for each solid solution was obtained by fitting a second-order polynomial to the experimental data. They calculated the phase diagram using the Pro Phase program [5]. The calculated PG-AMPL phase diagram (this work) is shown in figure 5-1.

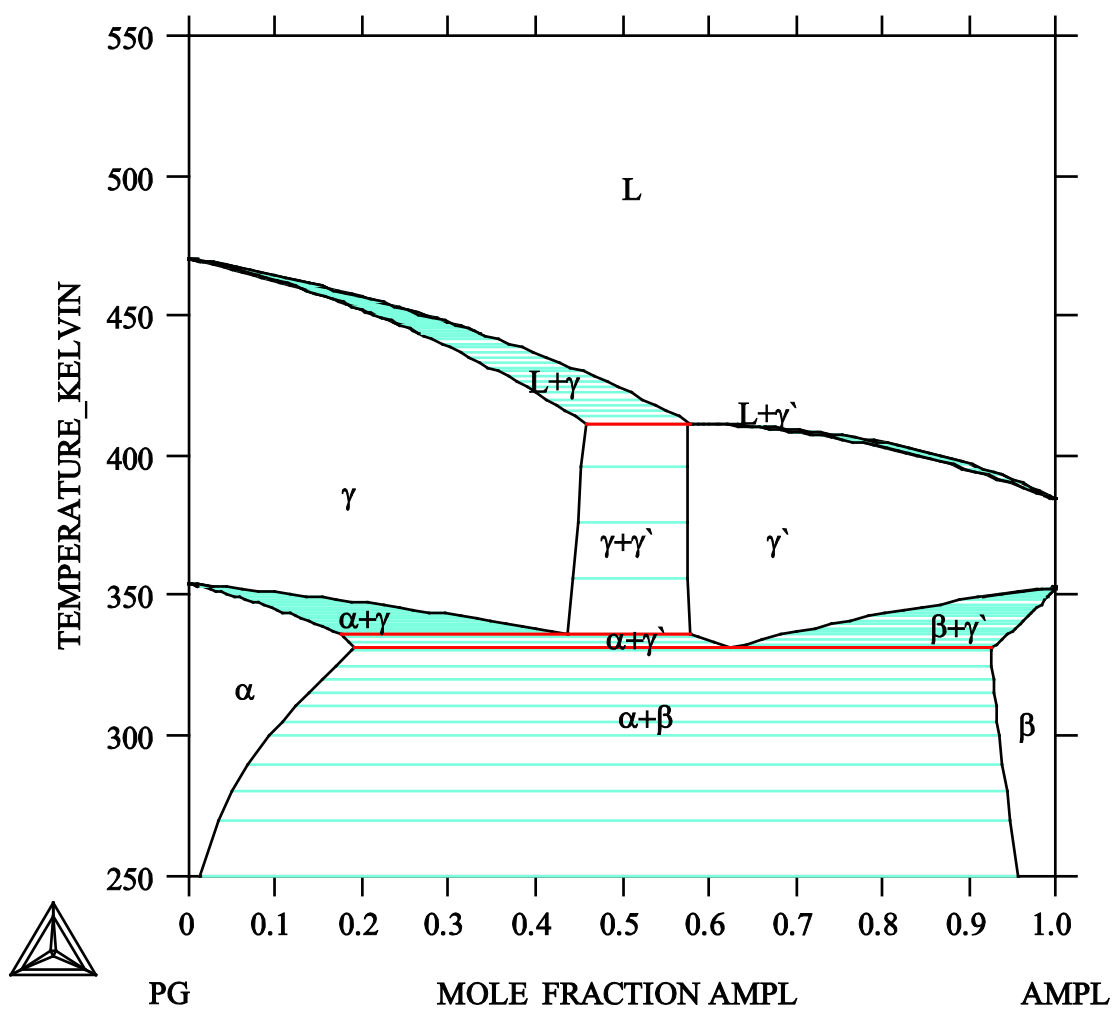


Figure5-1 PG-AMPL phase diagram (optimized)

### 5.3. AMPL-NPG binary phase diagram

The AMPL-NPG binary phase diagram has been described in chapter 4. It should be noted that the notation of the phases have been changed in order to show the binary phase projections on to the ternary. Figure 5-2 shows the AMPL-NPG binary phase diagram.

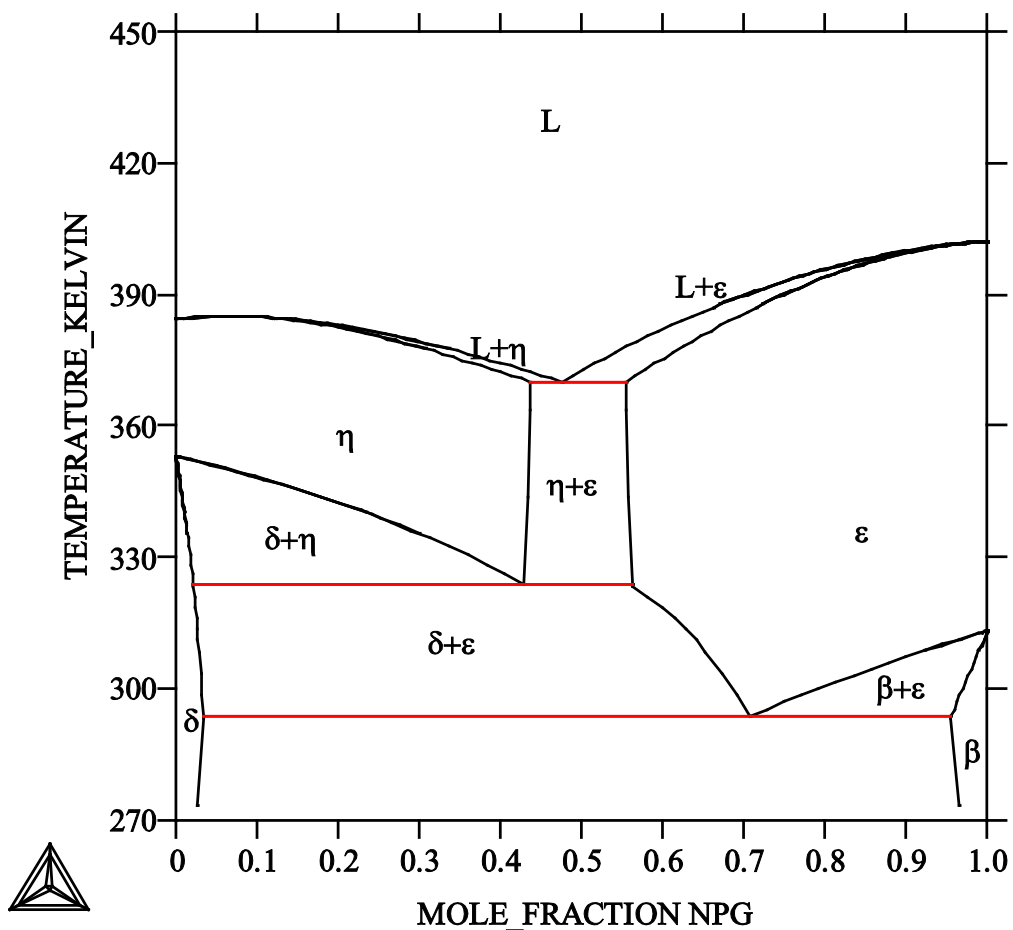


Figure 5-2 AMPL-NPG binary system (calculated, this work)

#### 5.4. PG-NPG binary phase diagram

The PG-NPG binary phase diagram has been calculated and optimized in chapter 3 and is depicted in figure 5-3.

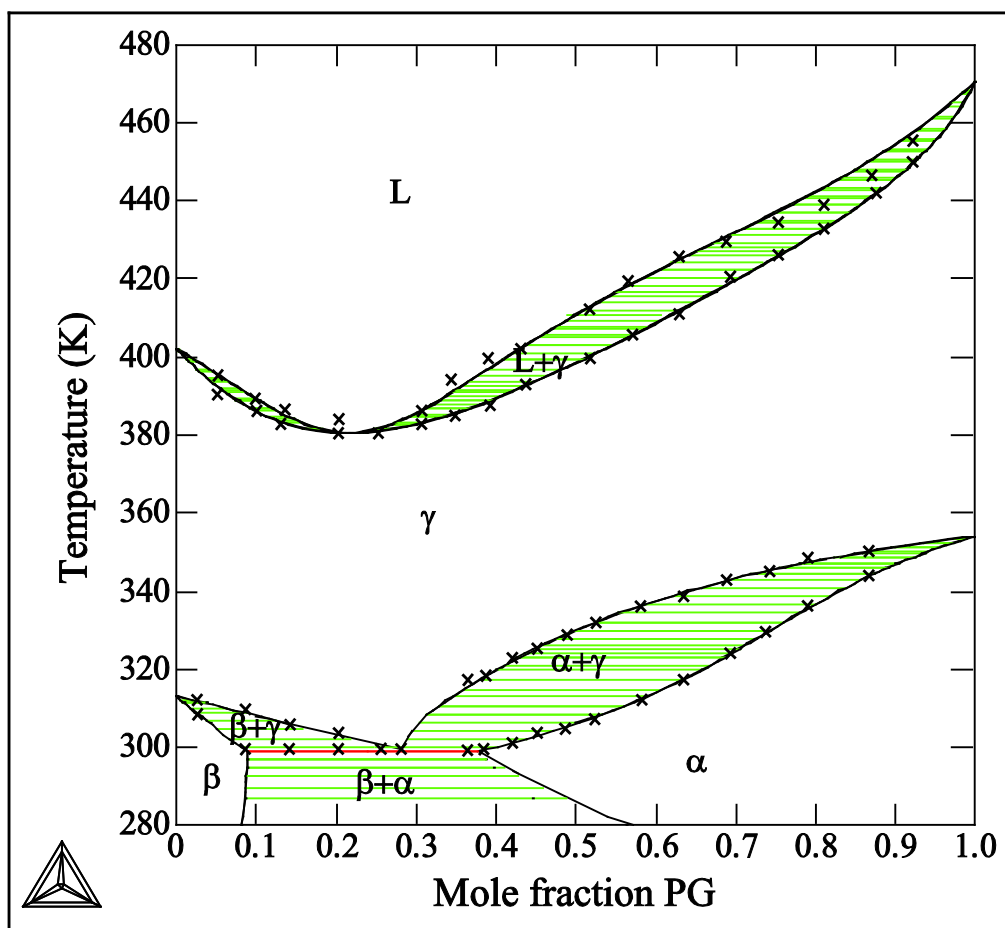


Figure 5-3 PG-NPG phase diagram

#### 5.4. PG-NPG-AMPL ternary phase diagram

The ternary phase diagram was calculated using Gibbs energy equations for the pure compounds. Table 5-2 lists the Gibbs energy equations used to calculate the PG-NPG-AMPL ternary phase diagram. It is predicted that three low temperature phases exist, and two high temperature phases. This assumption was based on the PG-NPG binary phase diagram (completely miscible solution of high temperature phase).

Table 5-2 Gibbs energy expressions for PG-NPG-AMPL

No.	Gibbs energy expressions
1	${}^0G_{PG}^{\alpha} = 0$
2	${}^0G_{NPG}^{\beta} = 0$
3	${}^0G_{AMPL}^{\delta} = 0$
4	${}^0G_{PG}^{\beta} = 3307.56$
5	${}^0G_{NPG}^{\alpha} = 986.64$
6	${}^0G_{NPG}^{\delta} = 8158.7$
7	${}^0G_{AMPL}^{\alpha} = 4660.86$
8	${}^0G_{PG}^{\delta} = 6535.12$
9	${}^0G_{AMPL}^{\beta} = 7505.8$
10	${}^0G_{NPG}^{\gamma} = 13630 - 43.55T + 0.351T^2 + 1621.98T - 51061.57 - 272.9T \ln(T)$
11	${}^0G_{NPG}^{\gamma} = 13630 - 43.55T + 0.351T^2 + 1621.98T - 51061.57 - 272.9T \ln(T) + 461.25$
12	${}^0G_{AMPL}^{\gamma} = 23300 - 66.01T - 0.275T^2 + 949.46T - 73097.48 - 110T \ln(T)$
13	${}^0G_{AMPL}^{\gamma} = 23300 - 66.01T - 0.275T^2 + 949.46T - 73097.48 - 110T \ln(T) + 404.55 + 830.45$
14	${}^0G_{AMPL}^{\gamma} = 23300 - 6.01T - 0.275T^2 + 949.46T - 73097.48 - 110T \ln(T) + 830.445$
15	${}^0G_{PG}^{\gamma} = 23120 - 65.29T$
16	${}^0G_{PG}^{\gamma} = 23120 - 65.29T + 1008.62$
17	${}^0G_{PG}^L = 28550 - 76.83T$
18	${}^0G_{NPG}^L = 18315 - 55.2T + 0.425T^2 + 2098.38T - 69849.68 - 349.613T \ln(T)$
19	${}^0G_{AMPL}^L = 26291.4 - 73.77T - 0.29T^2 + 1026.62T - 78953.7 - 119.44T \ln(T)$

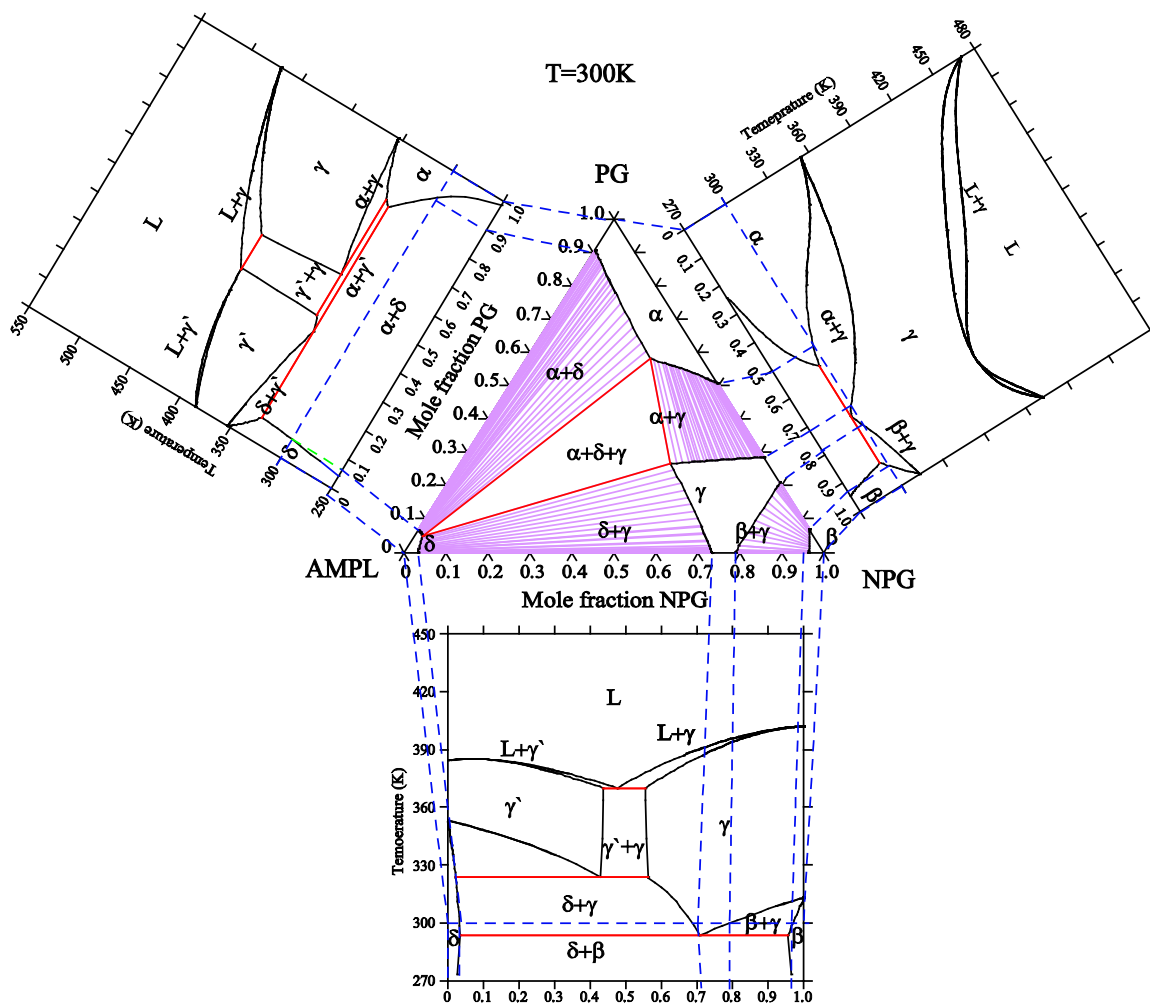


Figure 5-4 Binary phases projecting on to ternary (PG-NPG-AMPL) phase diagram

Figure 5-4 depicts how the three binary phase diagrams extrapolate in to ternary phase diagram. It can also be seen from the figure that the assumption (that there are only two high temperature phases) is reasonable. No separate new phase exists in the ternary phase diagram. All the phases are projections of the binary phase diagrams. Figure 5-5 shows several isotherms of the PG-NPG-AMPL ternary phase diagram over a

temperature range. The appearance of liquid phase at lower temperatures (compared to PE-PG-NPG) is due to the lower melting point of AMPL.

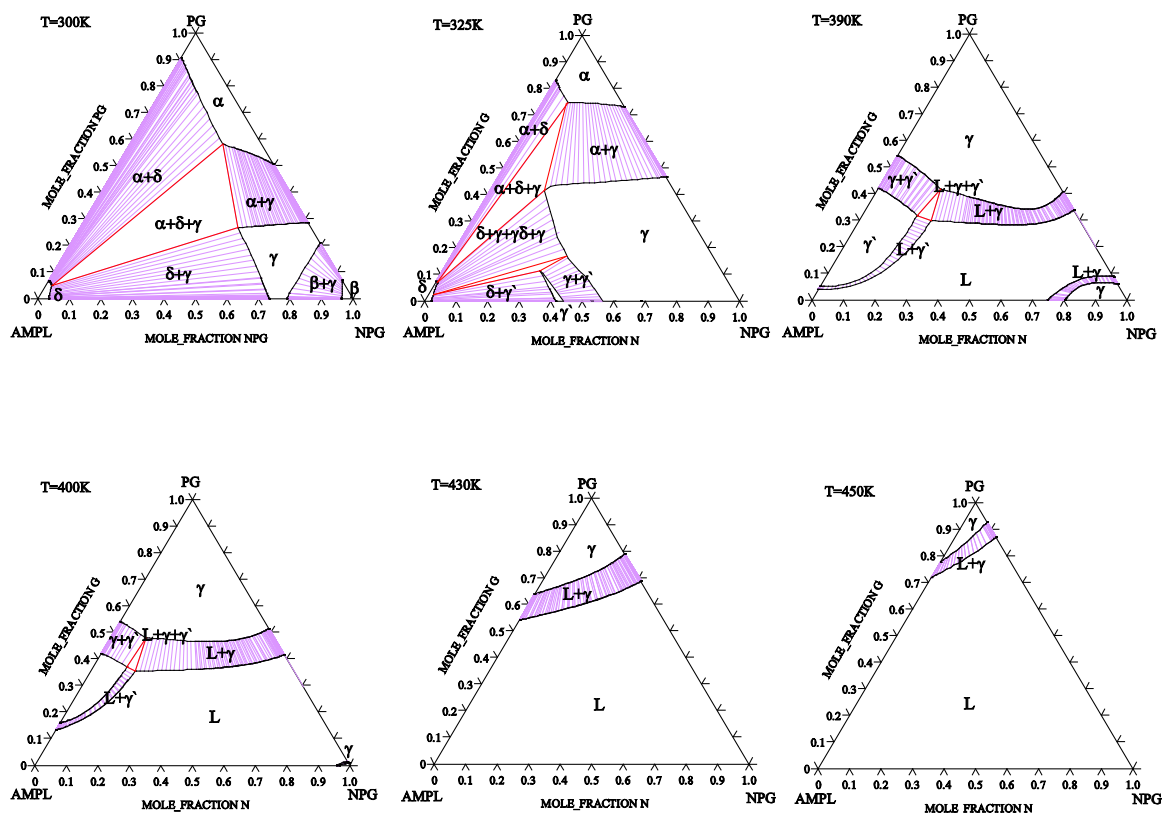


Figure 5-5 Isotherms of PG-NPG-AMPL over a temperature range showing phase transitions from room temperature to liquid phase

Figure 5-6 shows isopleths and an isotherm at 300K. Isopleths are pseudobinary phase diagrams, where one of the three compositions is kept constant and the diagram is plotted as composition against temperature. This makes studying continuous phase transitions easier.

At 0.8PG/0.1AMPL/0.1NPG, a three phase region ( $\alpha+\beta+\delta$ ) exists from 250K to 259K. After that the three phase region is transformed into a  $\alpha+\delta$  two phase region. This region

is stable up to 300K, and then is transformed in to a one phase region ( $\alpha$ ). At about 338K the  $\alpha$  phase is transformed to a very small sliver of  $\alpha+\gamma+\gamma'$ . This sliver exists for only 1-2K at that particular composition. After that the three phase region is converted in to  $\gamma$  single phase region. This phase is stable over a wide range of temperature up to 442K and then liquid phase starts to appear along with  $\gamma$  phase ( $L+\gamma$ ). At about 454K the  $\gamma$  completely melts and forms liquid single phase.

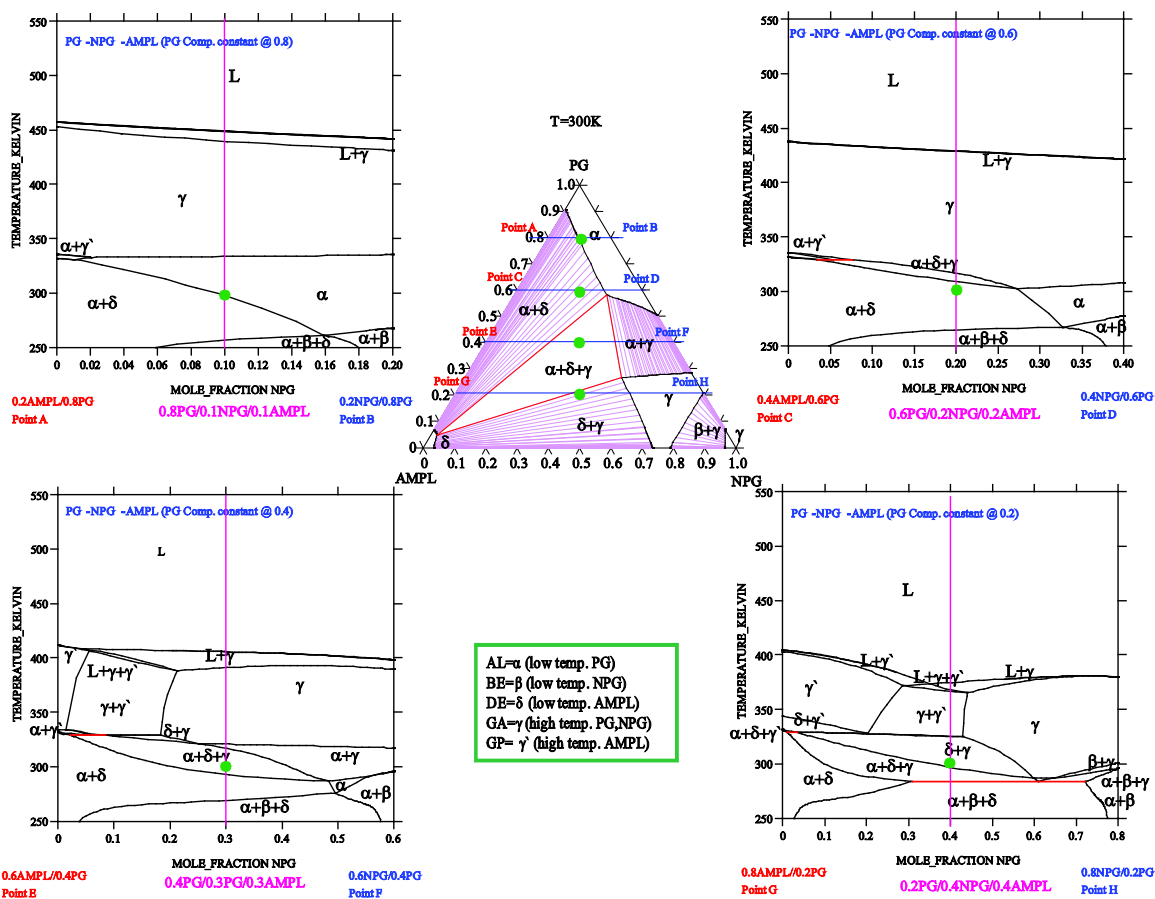


Figure 5-6 Isoleths of PG-NPG-AMPL and an isotherm at 300K

Similarly, at 0.4PG/0.3AMPL/0.3NPG, a three phase region ( $\alpha+\beta+\delta$ ) exists from 250K to 270K. At about 270K the three phase region is transformed to  $\alpha+\delta$  two phase region.

This two phase region is stable up to 299K and then transforms in to  $\alpha+\delta+\gamma$  three phase region. At 330K the three phase region is transformed in to  $\gamma$  single phase region. At 389K the single phase region starts converting to  $L+\gamma$ . After 410K this region becomes completely liquid. Table 5-3 lists the phase transition occurring at various compositions and temperatures.

Table 5-3 Phase transitions in PG-NPG-AMPL system

$X_{AMPL}$	$X_{NPG}$	Phase transitions
0.16	0.04	$\alpha + \beta + \delta \xrightarrow{277K} \alpha \xrightarrow{340K} \gamma \xrightarrow{435K} L + \gamma \xrightarrow{448K} L$
0.4	0.2	$\alpha + \beta + \delta \xrightarrow{280K} \alpha + \delta \xrightarrow{298K} \alpha + \delta + \gamma \xrightarrow{348K} \gamma \xrightarrow{389K} L + \gamma \xrightarrow{402K} L$
0.1	0.5	$\alpha + \beta + \delta \xrightarrow{272K} \alpha + \delta \xrightarrow{322K} \alpha + \delta + \gamma \xrightarrow{338K} \gamma + \gamma' \xrightarrow{408K} L + \gamma + \gamma' \xrightarrow{410K} L + \gamma \xrightarrow{413K} L$
0.2	0.2	$\alpha + \beta + \delta \xrightarrow{278K} \alpha + \delta \xrightarrow{318K} \alpha + \delta + \gamma \xrightarrow{326K} \gamma \xrightarrow{440K} L + \gamma \xrightarrow{444K} L$
0.4	0.4	$\alpha + \beta + \delta \xrightarrow{295K} \alpha + \delta + \gamma \xrightarrow{305K} \delta + \gamma \xrightarrow{338K} \gamma + \gamma' \xrightarrow{426K} L + \gamma + \gamma' \xrightarrow{428K} L + \gamma \xrightarrow{430K} L$

## References:

- 
1. J. Salud, D. O. Lopez, M. Barrio, J. Ll Tamarit, H. A. Oonk, P. Negrier and Y. Haget, *J. Solid State Chemistry* 133 (1997) 536-544.
  2. J. Ll Tamarit, M. Barrio, D.O. Lopez and Y. Haget, *J. Appl. Crystallogr.* 30, 118 (1997).
  3. S. Urban, J. Domsowski and Z. Tomkowiz, *Mater. Sci.*, IV/3, 91 (1978).
  4. H. M. Boots and P. K. de Bokx. *J. Phys. Chem.* 93, 8240 (1989).
  5. L. Robe ls-Beneyt, Doctoral thesis, Bordeaux, 1995.

## Chapter VI The equilibrium phase diagram of the pentaerythritol-pentaglycerine-2-amino-2methyl-1,3, propanediol (PE-PG-AMPL) system

---

### **6.1. Computational Procedure**

In order to compute phase equilibria and calculate the phase diagrams, certain thermodynamic parameters need to be calculated. This section describes the determination of thermodynamic properties (enthalpies and entropies of formation for PE, PG and AMPL, Gibbs free energies of the stable and metastable phases, etc.).

#### **6.1.1. Thermodynamic Modeling of Solution Phases**

The most relevant features of the description of the thermodynamic parameters are discussed for the present purpose. Table 6-1 shows the list of symbols used to describe the phases in PE-PG-AMPL system. The low temperature phases are characterized by  $\alpha$  or  $\beta$ , the high temperature phases are designated as  $\gamma$ ,  $\gamma'$ , and the liquid phase as L. For simplicity PE is represented by A, PG as B and AMPL as C.

A CALPHAD type optimization using regular and subregular solution model is considered to be adequate to describe the Gibbs energies of different phases. The low temperature "Phase II" are represented by  $\alpha$  or  $\beta$  and the high temperature phases are represented as  $\gamma$  or  $\gamma'$ . The liquid phase is designated as "L".

If the reference state for each phase is taken to be that of the pure components in that

Table 6-1 List of symbols for denoting phases in PE-PG-AMPL system

Symbol	Phase
Liq or L	Liquid
$\alpha$	Low temperature PE, PG phase
$\beta$	Low temperature AMPL phase
$\gamma$	High temperature PE, PG phase
$\gamma'$	High temperature AMPL phase
L	Liquid phase

phase, then the Gibbs energy of a solution phase  $\phi$  ( $\phi = \alpha, \beta, \gamma, \gamma', L$ ) can be represented as follows (unit of Gibbs energy is  $\text{J mol}^{-1}$  throughout this work, where a mol is a mole of formula unit):

$$G^\phi = x_A {}^0G_A^\phi + x_B {}^0G_B^\phi + x_C {}^0G_C^\phi + RT(\ln x_A + \ln x_B + \ln x_C) + G^{EX,\phi} \quad (1)$$

Where  $\phi = \alpha, \beta, \gamma, \gamma', L$ ,  $R = 8.314 \text{ J mol}^{-1} \text{ K}^{-1}$ ,  $x_A$  is the mole fraction of "A",  $x_B$  is the mole fraction of "B" and  $x_C$  is the mole fraction of "C".  ${}^0G_A^\phi$ ,  ${}^0G_B^\phi$  and  ${}^0G_C^\phi$  are the pure component Gibbs energies in  $\phi$ .

The excess Gibbs energy for a binary system A-B, can be demoted as;

$$G_{mix}^{xs} = x_A x_B (L_{AB}^0 + L_{AB}^1 (x_A - x_B)) \quad (2)$$

The binary interaction parameters for excess Gibbs energies,  $L_{i,j}^\phi$  can be expressed as follows:

$$L_{i,j}^{\phi} = \sum_{n=0}^m {}^n L_{i,j}^{\phi} (x_i - x_j)$$

The ternary excess Gibbs free energy is written as follows:

$$\begin{aligned} G_{mix}^{xs} = & x_A x_B (L_{AB}^0 + L_{AB}^1 (x_A - x_B)) + x_B x_C (L_{BC}^0 + L_{BC}^1 (x_B - x_C)) \\ & + x_A x_C (L_{AC}^0 + L_{AC}^1 (x_A - x_C)) \end{aligned} \quad (3)$$

The binary and the ternary interaction parameters  ${}^n L_{i,j}^{\phi}$  and  ${}^n L_{i,j,k}^{\phi}$  take the following form:

$${}^n L_m^{\phi} = a + bT + cT \ln(T) + dT^2 + eT^{-1} + fT^3 + gT^7 + hT^9$$

where  $a, b, c, d, e, f, g$  and  $h$  are the excess Gibbs energy parameters. In most cases only the first two terms of the above equation are used.

For a phase  $\phi$  ( $\phi = \alpha, \beta, \gamma, \gamma', L$ ),  ${}^0 G_A^{\phi}$ ,  ${}^0 G_B^{\phi}$  and  ${}^0 G_C^{\phi}$  are the reference states of pure “A”, “B” and “C”, same as  $\phi$ . A single reference phase is chosen for each component.

The reference phases were chosen and denoted as:  $\alpha$  for “A”,  $\beta$  for “B” and  $\alpha$  for “C” and set to zero.

Therefore,

$${}^0 G_A^{\alpha} = 0, {}^0 G_B^{\beta} = 0 \text{ and } {}^0 G_C^{\alpha} = 0 \quad (4)$$

The binary phase diagrams are calculated first and extrapolated to a ternary system.

The pure Gibbs energies were determined using the heat capacity data. So, for component “A” the Gibbs energies of the stable phases are:

$${}^0 G_A^{\gamma} = {}^0 G_A^{\alpha} + \Delta {}^0 G_A^{\alpha \rightarrow \gamma} = \Delta {}^0 G_A^{\alpha \rightarrow \gamma}$$

$${}^0G_A^\gamma = \Delta H_{TR} - T\Delta S_{TR} + \int_{T_{TR}}^T \Delta C_P^{\alpha \rightarrow \gamma} dT - T \int_{T_{TR}}^T \frac{\Delta C_P^{\alpha \rightarrow \gamma}}{T} dT$$

$${}^0G_A^L = {}^0G_A^\alpha + \Delta {}^0G_A^{\alpha \rightarrow L} = \Delta {}^0G_A^{\alpha \rightarrow \gamma} + \Delta {}^0G_A^{\alpha \rightarrow L}$$

$${}^0G_A^L = \Delta H_{TR} - T\Delta S_{TR} + \int_{T_{TR}}^T \Delta C_P^{\alpha \rightarrow \gamma} dT - T \int_{T_{TR}}^T \frac{\Delta C_P^{\alpha \rightarrow \gamma}}{T} dT + \Delta H_F - T\Delta S_F + \int_{T_F}^T \Delta C_P^{\gamma \rightarrow L} dT - T \int_{T_F}^T \frac{\Delta C_P^{\gamma \rightarrow L}}{T} dT$$

Similar expressions can be obtained for Gibbs energies of stable phases of “B” and “C”.

### 6.1.2. Metastable Phase Calculations

Metastable phases are only calculated for the PE-AMPL system and PG-NPG system.

The PE-PG shows complete miscibility for both low and high temperature phases. The

Gibbs energies for metastable phases are estimated by modifications to the stable phases.

For example, for “ A” in  $\beta$  phase, we are interested in determining the difference,

${}^0G_A^\beta - {}^0G_A^\alpha$ , such that we can express,

$${}^0G_A^\beta = {}^0G_A^\alpha + M_A^\beta$$

The Gibbs energy of the  $\beta$  phase,  $G_m^\beta$ , can now be written as:

$$G_m^\beta = x_A ({}^0G_A^\alpha + M_A^\beta) + x_C {}^0G_C^\beta + RT \times (x_A \ln x_A + x_C \ln x_C) + G^{EX,\beta}$$

$$G_m^\beta = x_A M_A^\beta + RT \times (x_A \ln x_A + x_C \ln x_C) + G^{EX,\beta}$$

Similarly for the  $\alpha$  phase, we can write the Gibbs free energy,  $G_m^\alpha$ , as:

$$G_m^\alpha = x_A {}^0G_A^\alpha + x_B ({}^0G_B^\beta + M_B^\alpha) + RT \times (x_A \ln x_A + x_B \ln x_B) + G^{EX,\alpha}$$

$$G_m^\alpha = x_B M_B^\alpha + RT \times (x_A \ln x_A + x_B \ln x_B) + G^{EX,\alpha}$$

To estimate  $M_A^\beta$  and  $M_C^\alpha$ ,  $\alpha$  and  $\beta$  phases are assumed to be ideal solutions. It should be noted that this assumption is based only for the purpose of calculating the metastable phases.

Therefore, the partial molar Gibbs free energies can be written as:

$$G_B^\beta = {}^0G_B^\beta + RT \ln(x_B^\beta)$$

$$G_B^\alpha = {}^0G_B^\alpha + RT \ln(x_B^\alpha)$$

## **6.2. Experimental Data**

### **6.2.1. Phase Equilibria**

A brief outline of the thermodynamic strategy used in this work is presented in this section. Most of the descriptions of the enthalpies and transition temperatures were obtained from Murrill and Breed [1] and are shown in Table 2. The enthalpies and the phase transition temperatures for AMPL were taken from Murrill and Breed [1]. Data for AMPL reported by Ding [2] is higher than the data available in literature. The compound used by Salud et al. [3] was higher than that used in earlier works [4,5]. The reason for the difference in the data can be attributed to this fact. The melting temperature of NPG reported by Ding [6] was 399K. This value is lower than that reported in literature (402.8K) but is closer to the one reported in previous works [1] and also to the values reported by Sigma-Aldrich. This data has been used for the calculations in this work. Pure PE data has been used from Chandra et al. Enthalpies and phase transition temperatures for pure PE and PG used for calculations were taken from Eilerman et al. [7]

Table 6-2 Crystal structure, transition temperatures and thermal properties of PG, AMPL and PE [8]

Compound	Low temp. phases	$T_{TR}(K)$	$\Delta H_{TR}(J/mol)$	$\Delta S_{TR}(J/mol K)$	High temp. phases	$T_F (K)$	$\Delta H_F(J/mol)$	$\Delta S_F(J/mol K)$
PG	Tetragonal	354	23120	65.29	FCC	471	5430	11.54
AMPL	Monoclinic	353	23330	66.01	BCC	471	5430	11.54
PE	Tetragonal	461	41260	90.25	FCC	533	5020	9.45

### 6.3. PE-PG-AMPL ternary phase diagram

The binary phase diagrams constituting the PE-PG-AMPL system have been described in previous chapters. In this chapter only the ternary phase diagram and phase transitions will be discussed. The ternary phase diagram was created using Gibbs energy equations and predicting the number of phases in the ternary. Table 6-3 shows the Gibbs energy expressions for the PE-PG-AMPL system. In this ternary two low temperature phases (one phase belonging to PE, PG and the other to PG-AMPL), and two high temperature phases. This assumption was made because, PE and PG form completely miscible solutions at both low and high temperature phases and hence are considered as one phase for each temperature region. Figure 6-1, 6-2 and 6-3 shows PE-PG-AMPL isotherms at several temperatures.

Table 6-3 Gibbs energy expressions for PE-PG-AMPL system

No.	Gibbs energy expressions
1	${}^0G_{PE}^{\alpha} = 0$
2	${}^0G_{PG}^{\alpha} = 0$
3	${}^0G_{AMPL}^{\beta} = 0$
4	${}^0G_{AMPL}^{\alpha} = 4660.886$
5	${}^0G_{PG}^{\beta} = 65365.12$
6	${}^0G_{AMPL}^{\alpha} = 4381$
7	${}^0G_{AMPL}^{\alpha} = 4660.886$
7	${}^0G_{PE}^{\beta} = 7795$
8	${}^0G_{AMPL}^{\alpha} = 4660.886$
9	${}^0G_{PE}^{\gamma} = 41260 - 89.501T + 1.08T^2 + 6794.78T - 272492.72 - 1093.35T \ln(T)$
10	${}^0G_{AMPL}^{\gamma} = 23300 - 6.01T - 0.275T^2 + 949.46T - 73097.48 - 110T \ln(T) + 324.2$
11	${}^0G_{AMPL}^{\gamma} = 23300 - 6.01T - 0.275T^2 + 949.46T - 73097.48 - 110T \ln(T) + 324.2$
12	${}^0G_{PE}^{\gamma} = 41260 - 89.5T + 1.08T^2 + 6794.78T - 272492.72 - 1093.35T \ln(T) + 439$
13	${}^0G_{PG}^{\gamma} = 23120 - 65.29T$
14	${}^0G_{AMPL}^{\gamma} = 23300 - 6.01T - 0.275T^2 + 949.46T - 73097.48 - 110T \ln(T) + 830.445$
15	${}^0G_{PG}^{\gamma} = 23120 - 65.29T + 1008.62$
16	${}^0G_{PG}^L = 28550 - 76.83T$
17	${}^0G_{PE}^L = 46280 - 98.92T + 1.376T^2 + 7119.63T - 237151.623 - 1180.015T \ln(T)$
18	${}^0G_{AMPL}^L = 26291.4 - 73.77T - 0.29T^2 + 1026.62T - 78953.7 - 119.44T \ln(T)$

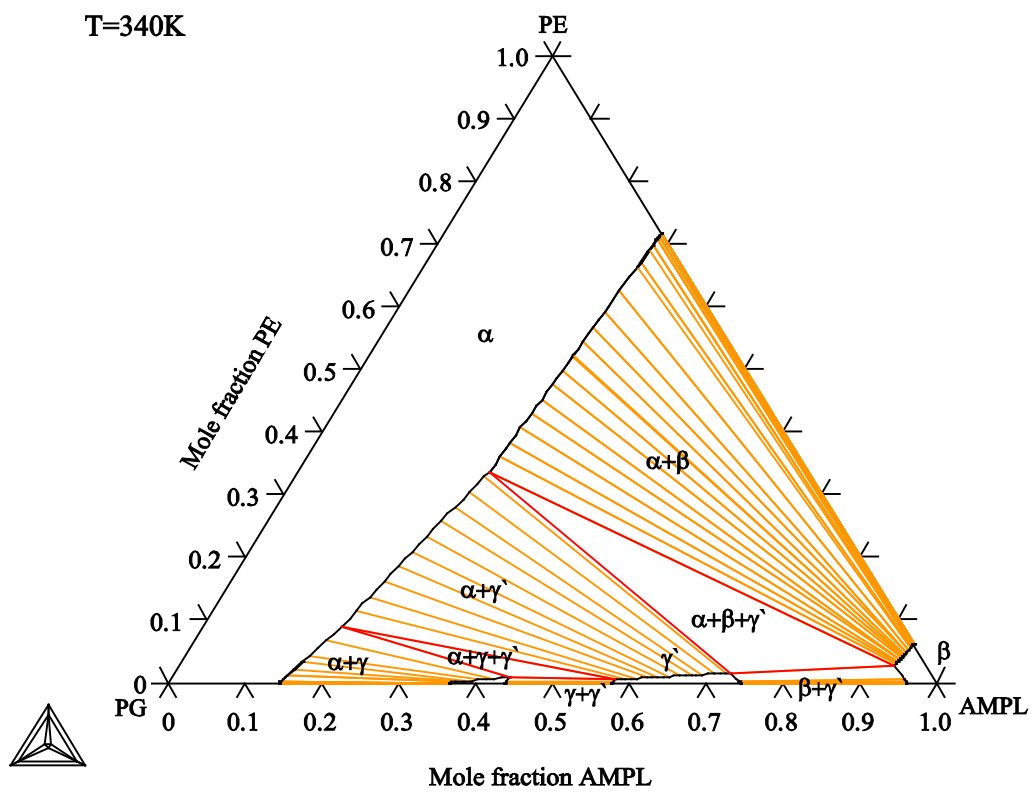
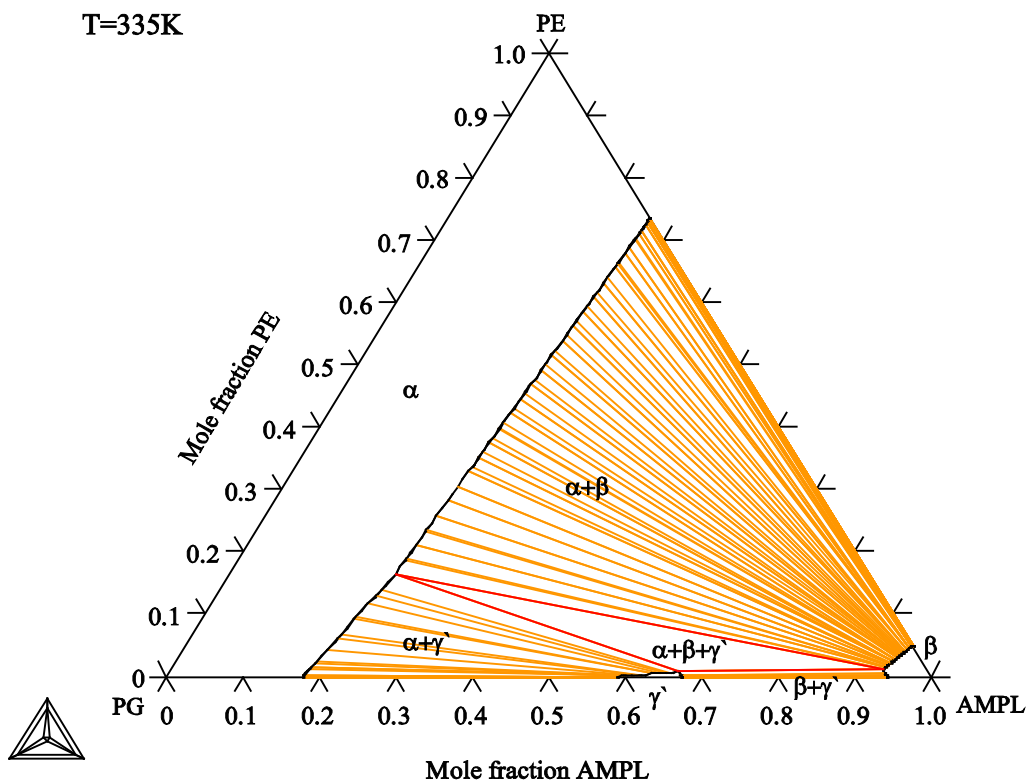


Figure 6-1 PE-PG-AMPL isotherms at 335K and 340K

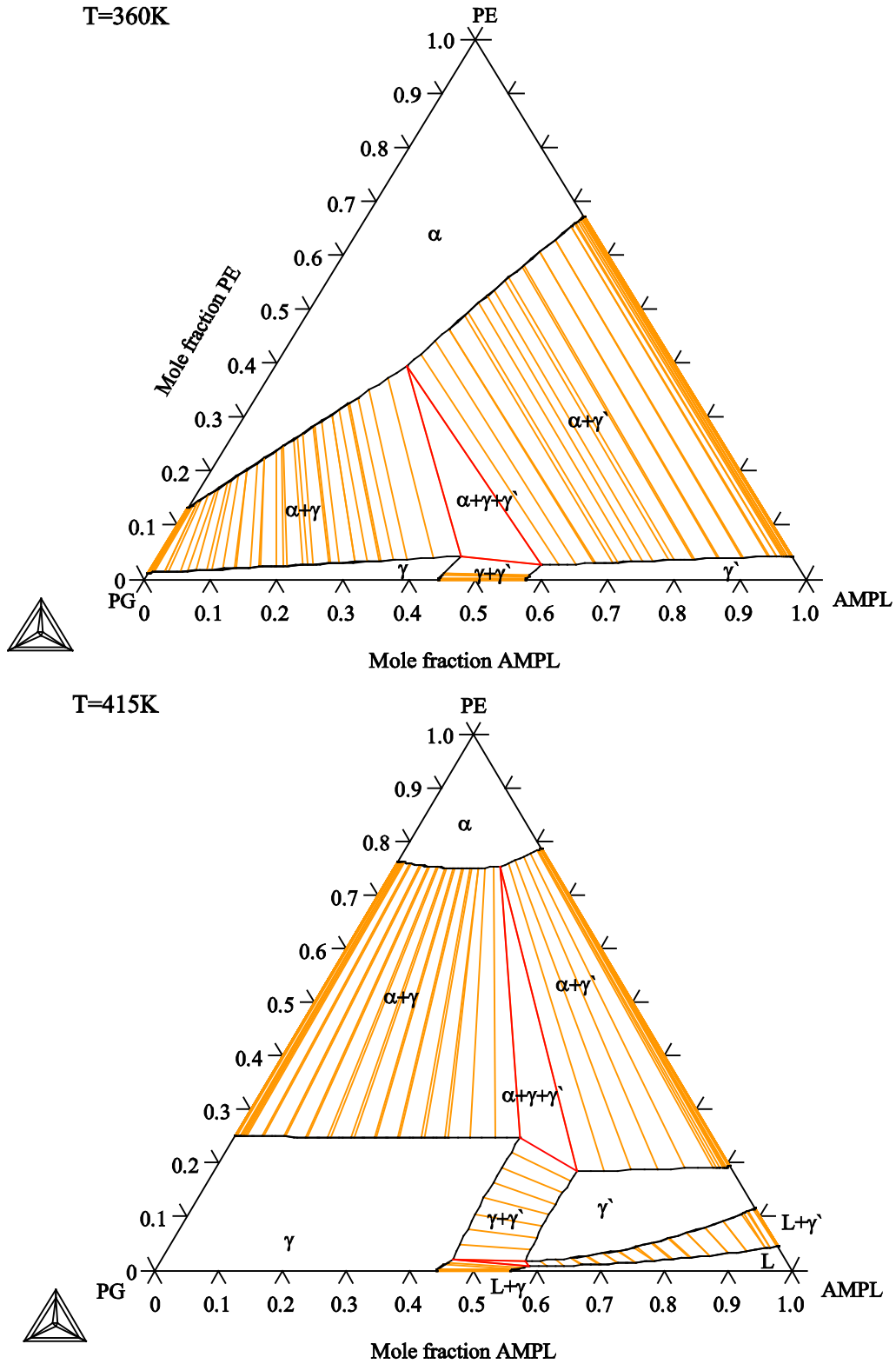


Figure 6-2 PE-PG-AMPL isotherms at 360K and 415K

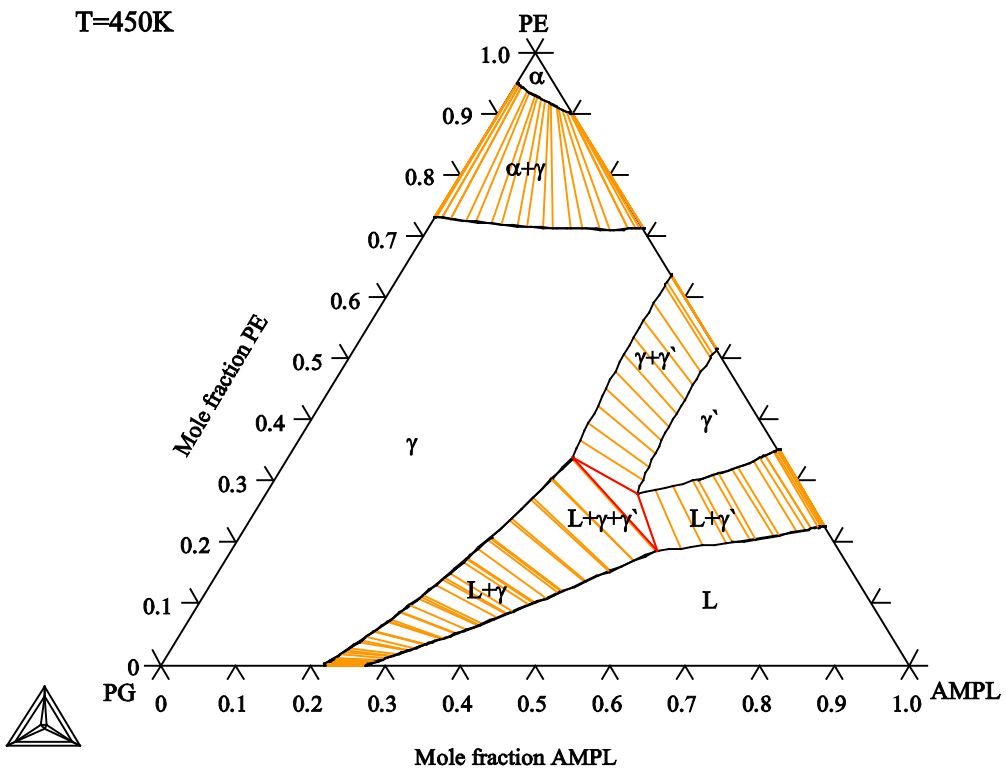
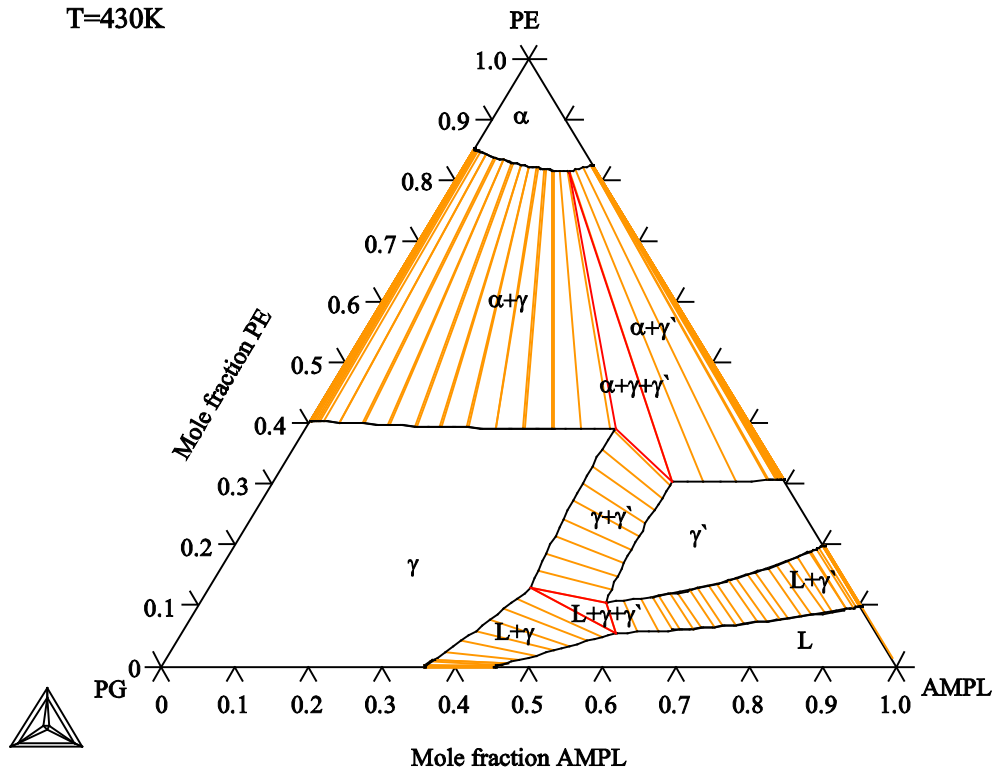


Figure 6-3 PE-PG-AMPL isotherms at 430K and 450K

Isopleths for PE-PG-AMPL are plotted in figure 6-4 along with an isotherm at 390K. The isotherm helps to depict the composition on the isopleths.

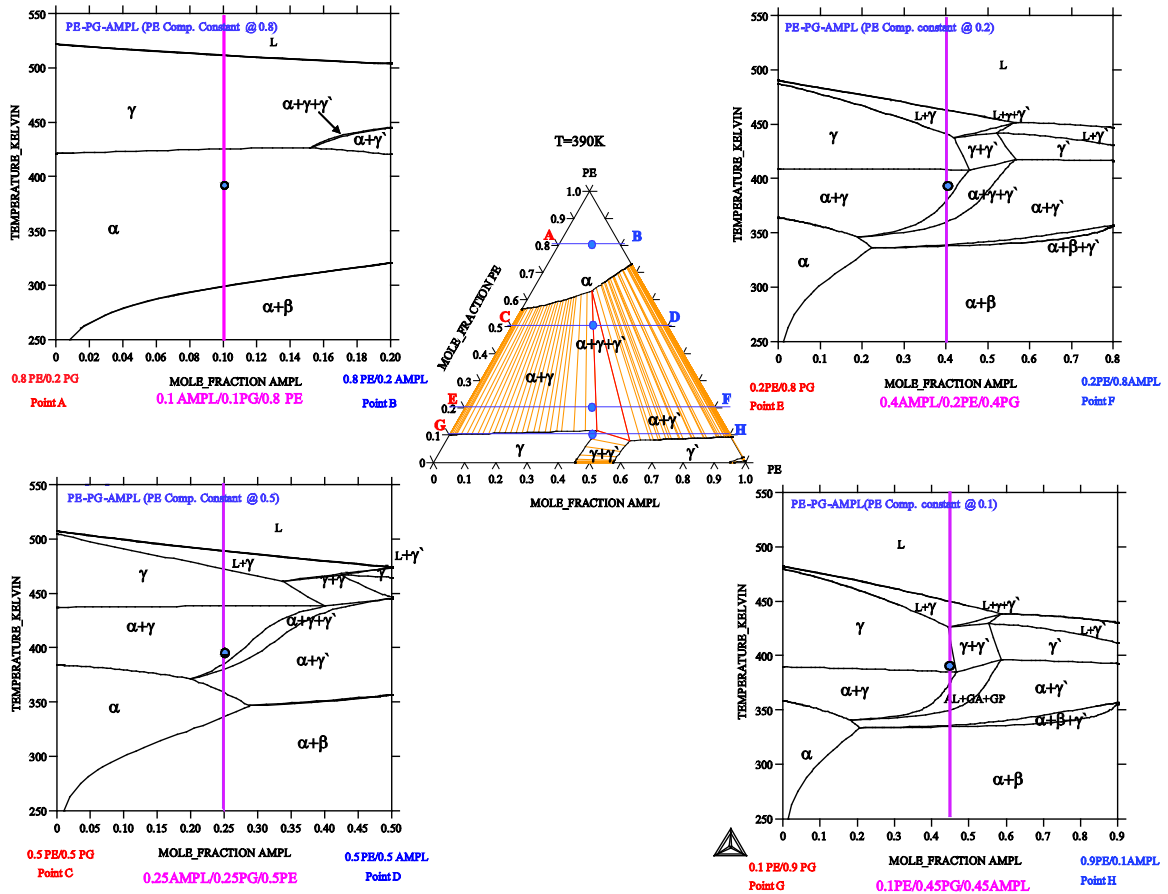


Figure 6-4 PE-PG-AMPL isopleths and an isotherm at 390K

At 0.8PE/0.1PG/0.1AMPL, a two phase  $\alpha+\beta$  region exists from 250K to 298K. After that the two phase region becomes single phase  $\alpha$ . The  $\alpha$  phase is stable up until 423K after which it is converted to  $\gamma$ . The  $\gamma$  phase is also stable for a wide temperature range. It melts in to liquid at 517K.

Similarly, at 0.2 PE/0.4PG/0.4AMPL, two phase region  $\alpha+\beta$  is stable till 335K after which it transforms in to a three phase  $\alpha+\beta+\gamma'$  reion. This three phase region exists as a very small sliver, and then transitions in to two phase  $\alpha+\gamma'$  region. This region is stable till 352K and the changes to  $\alpha+\gamma+\gamma'$  region. At 402K the three phase region is converted to single phase  $\gamma$ , which is stable till 448K and then transforms to  $L+\gamma$  with the appearance of liquid phase. The two phase region completely becomes liquid at 473K. Table 6-4 shows the phase transitions at various compositions and temperatures.

Table 6-4 Phase transitions in PE-PG-AMPL

$X_{AMPL}$	$X_{PG}$	Phase transitions
0.3	0.5	$\alpha + \beta \xrightarrow{331K} \alpha + \gamma' \xrightarrow{353K} \alpha + \gamma + \gamma' \xrightarrow{355K} \alpha + \gamma \xrightarrow{410K} L + \gamma$ $\xrightarrow{521K} L$
0.6	0.2	$\alpha + \beta \xrightarrow{347K} \alpha + \beta + \gamma' \xrightarrow{349K} \alpha + \gamma' \xrightarrow{418K} \gamma' \xrightarrow{448K} L + \gamma'$ $\xrightarrow{455K} L$
0.25	0.25	$\alpha + \beta \xrightarrow{346K} \alpha \xrightarrow{377K} \alpha + \gamma + \gamma' \xrightarrow{380} \alpha + \gamma \xrightarrow{444K} \rightarrow$ $\gamma \xrightarrow{423K} L + \gamma \xrightarrow{447K} L$

## References:

- 
- 1 E. Murrill and L. Breed. *Thermochim. Acta*, **1** (1970), pp. 239–246.
  - 2 D. Chandra, W. Ding and R.A. Lynch. *J. Less-Common Metals*, **168** (1991), pp. 159–167.
  - 3 J. Salud, D.O. Lopez, M. Barrio, J.Ll. Tamarit, H.A.J. Oonk, P. Negrier and Y. Haget. *J. Solid State Chem.*, **133** (1997), pp. 536–544.
  - 4 D.O. Lopez, J. Van Braak, J.Ll. Tamarit and H.A.J. Oonk. *Calphad*, **18** 4 (1994), pp. 387–396.
  - 5 D.O. Lopez, J. Van Braak, J.Ll. Tamarit and H.A.J. Oonk. *Calphad*, **19** 1 (1995), pp. 37–47.
  - 6 W. Ding, M.S. Thesis, University of Nevada, Reno, 1991.
  - 7 D. Eilerman, R. Lippman and R. Rudman. *Acta Cryst.* **B39** (1983), pp. 263–266.
  - 8 E Murrill and L Breed. *Thermochim. Acta*, **1** (1970), pp. 239–246.

## Chapter VII Condensed Summary and Conclusions

---

### A. Condensed Summary

**Binary Systems:** We calculated the binary Gibbs energy equations for the pure compounds and metastable phases for the PE-NPG, PE-PG, PG-NPG, AMPL-NPG, PE-AMPL and PG-AMPL. The experimental data available in the literature for the binary systems was used to optimize thermodynamic parameters to calculate the binary phase diagrams; these binary phase diagram calculated were fed into the Thermo-Calc program routines. Different substitutional solution models were used to determine the interaction parameters to determine Gibbs energy equations and metastable phase calculations to ultimately give the ternary isothermal section of phase diagrams. More importantly the relation between the compositions and temperature for the ternaries were determined from the isopleths generated from these ternary calculations. For optimization of the binary phase diagrams substitutional solution models were used; the PARROT module in the Thermo-Calc software was used to optimize the phase diagrams and calculate interaction parameters. The interaction parameters were used to calculate activities and enthalpies of mixing.

**Ternary Systems:** We computed four ternary systems :(1) PE-NPG-NPG, (2) PE-NPG-AMPL, (3) PG-NPG-AMPL, and (4) PE-PG-AMPL. We also calculated the isopleths form the ternary isotherms for all the system computed. Although we have data for several isopleths, we have selected isopleths for a few compositions and plotted composition vs. temperature pseudo binaries. Due to limited experimental data in the [Type text]

literature for the ternary phase diagrams of “Plastic Crystals,” the ternary interaction parameters have not been calculated. The PE-PG-NPG phase diagram was calculated using the binaries PE-NPG, PE-PG and PG-NPG; phase diagrams were computed from room temperature to the liquid phase. It should be noted that the PG-NPG was calculated from 280K to show the transition at 298K. Gibbs energy equations and metastable calculations were performed to compute the phase diagrams.

## **B. Conclusions**

In this study, four ternary, polyalcohol and amine, systems are developed with the CALPHAD methodology, using thermodynamically modeled binary PE-NPG, PE-PG, PG-NPG, and PG-AMPL systems. We also used some literature (computational) data of AMPL-NPG, and PE-AMPL binary systems. Ternary phase diagrams at various temperatures calculated for the PE-PG-NPG, PE-NPG-AMPL, PG-NPG-AMPL and PE-PG-AMPL and isopleths thereof from these ternary systems yielded more solid state or solid–liquid phase transitions allowing more heat storage (isothermal) temperatures. In the systems containing of AMPL with PG and NPG we observed low temperature transitions (as low as 253K) useful for cooling applications. Some of the important conclusions from this study are presented for all the four systems and are described below.

### **System No. 1: Polyalcohol PE-PG-NPG system**

For optimization of binaries, low temperature phases ( $\alpha$  and  $\beta$  in PE-NPG) a Henrian solution model had to be used because the NPG forms a dilute solution with PE, on the NPG side. For the high temperature (orientationally disordered phases- ODIC)  $\gamma$  phases,

[Type text]

in this case a regular solution model was used. For the PG-NPG system,  $\alpha$ ,  $\beta$ , and  $\gamma$  a sub-regular solution model was used, and for liquid phase a regular solution model was used. In the case of PE-PG binary, the low temperature and liquid phases were modeled as ideal solutions. Whereas the high temperature ODIC  $\gamma$  phase was modeled using regular solution; the interaction parameters derived for this were very small suggesting that the solution can be considered ideal.

In the ternary PE-PG-NPG system we designated  $\alpha$ ,  $\beta$ ,  $\gamma$ , and  $\gamma'$  solid phases, as *PE-PG* low temperature stability exhibited ideal solution behavior and has only one  $\alpha$  phase, with no de-mixing. The low temperature PE rich phase in *PE-NPG* when projected on ternary phase diagram combines with the phase that forms one large completely miscible solid solution. The four isopleths (or pseudo binaries) chosen; for example  $\alpha+\beta \rightarrow \alpha+\beta+\gamma \rightarrow \alpha+\gamma$ , that gives wide range of composition and temperature as compared to the binaries of these polyalcohol. In general there are more solid state phase transitions in the ternary system than those observed in the related binaries.

### **System No. 2 Polyalcohol-Amine PE-NPG-AMPL system**

The activities of PE-AMPL and AMPL-NPG and PE-NPG exhibits negative deviation from ideality (Raoult's law). This is the most complicated system; because we had to assign three low temperature and three ODIC phases of the binaries, as all the binaries constituting the ternaries have demixing regions in both the low and high temperature phase stability regions. From the binary interaction parameter we extracted the activity PE in liquid PE-NPG-AMPL at 460K, 500K, and 640K using Krupkowski's formalism.

[Type text]

The isopleths at 0.5 AMPL-0.25PE-0.25NPG show  $\alpha+\beta+\delta \rightarrow \alpha+\beta+\epsilon \rightarrow \alpha+\epsilon \rightarrow L+\alpha+\epsilon \rightarrow L+\alpha \rightarrow L+\gamma$ . These complex ternary phase transitions are extremely difficult to determine easily by experimental methods.

**System No. 3: Polyalcohol - Amine PG-NPG-AMPL system**

The optimized PG-AMPL system agrees with literature experimental phase diagram, using regular solution model, for all phases.

In the ternary we assigned three low temperature ( $\alpha$ ,  $\beta$ ,  $\delta$ ) and two high temperature ( $\gamma$  - FCC) and ( $\gamma'$ -BCC) phases. All phases projected in the ternary isotherms from the binaries do not show any new phases or compounds forming. Isotherms plotted from 280K to ~500K exhibit the liquid phase starts appearing at low temperatures (because of the low melting temperature of AMPL (380K), as compared to the other system discussed above. The isopleth at 0.2PG-0.4NPG-0.4 AMPL three phase region was found at low temperatures, and the following phase transitions were observed:  $\alpha+\beta+\delta$  (282K)  $\rightarrow$   $\alpha+\delta+\gamma$  (308K)  $\rightarrow$   $\delta+\gamma$  (335K)  $\rightarrow$   $\gamma+\gamma'$  (374K)  $\rightarrow$   $L+\gamma+\gamma'$  (375K)  $\rightarrow$   $L+\gamma$  (377K)  $\rightarrow$  L, showing low temperature transitions (from 250K to 300K) in the range of these composition.

**System No. 4 Polyalcohol-Amine PE-PG-AMPL system**

The ternary PE-PG-AMPL consisting of two low temperature ( $\alpha$ ,  $\beta$ ) and ( $\gamma$ ,  $\gamma'$ ) at 0.8PE-0.1PG-0.1AMPL a two phase region exists from 250K to 298K. The  $\alpha$  (423K)  $\rightarrow$   $\gamma$  (517K)  $\rightarrow$  L. At higher composition, 0.2PE-0.5PG-0.3AMPL, the situation is different;  $\alpha+\beta$  (331K)  $\rightarrow$   $\alpha+\gamma'$  (353K)  $\rightarrow$   $\alpha+\gamma+\gamma'$  (355K)  $\rightarrow$   $\alpha+\gamma$  (410K)  $\rightarrow$   $L+\gamma$  (521K)  $\rightarrow$  L. For the composition, 0.5PE-0.25PG-0.25AMPL, the  $\alpha+\beta$  (346K)  $\rightarrow$

[Type text]

$\alpha(377\text{K}) \rightarrow \alpha + \gamma + \gamma'$  (380K)  $\rightarrow \alpha + \gamma$  (444K)  $\rightarrow \gamma$  (423K)  $\rightarrow L + \gamma$  (447K)  $\rightarrow L$ ; thus complex phase transition sequence are observed.

[Type text]